Insights into the mechanisms controlling the dissolution of alumino-borosilicate glass and development of a new Monte Carlo model

Kamalesh Damodaran

THÈSE POUR OBTENIR LE GRADE DE DOCTEUR
DE L'UNIVERSITÉ DE MONTPELLIER

En Physique

École doctorale : Information, Structures, Systèmes

Unité de recherche CEA, DES, ISEC, DE2D, SEVT, LCLT

Insights into the mechanisms controlling the dissolution of alumino-borosilicate glass and development of a new Monte Carlo model

Présentée par Kamalesh DAMODARAN

Le 09 Décembre, 2022

Sous la direction de Stéphane GIN
et Andrey KALINICHEV

Devant le jury composé de

M. Damien DAVAL, Chargé de recherche CNRS, Laboratoire d'hydrologie et de géochimie de Strasbourg	Rapporteur
M. Mathieu SALANNE, Professeur, Sorbonne Université	Rapporteur
M. Sergey CHURAKOV, Full Professor, University of Bern	Examinateur
Mme. Lucyna FIRLEJ, Professeure, Université de Montpellier	Présidente du jury
Mme. Stephanie ROSSANO, Professeure, Université de Marne La Vallée	Examinatrice
M. Jean-Marc DELAYE, Directeur de recherche, CEA Marcoule	Encadrant CEA
M. Stéphane GIN, Directeur de recherche, CEA Marcoule	Directeur de thèse
M. Andrey KALINICHEV, Directeur de recherche, Subatech Nantes	Encadrant SUBATECH

cea

UNIVERSITÉ DE MONTPELLIER

U.S. DEPARTMENT OF ENERGY

WastePD Performance and Design

Résumé (Abstract French)

En France, les déchets nucléaires de haute activité sont vitrifiés. Ils seront à terme stockés en formation géologique profonde. Après corrosion des enveloppes métalliques, l'eau souterraine arrivera au contact du verre et interagira chimiquement avec ce dernier, conduisant à la mobilisation des radionucléides solubles. Il est donc important de définir des verres avec des compositions et des durabilités optimales pour limiter ce relâchement. L'aluminium est un constituant majeur des verres nucléaires. Mais son rôle sur l'altération est encore mal compris. Pendant la phase de régime initial, à faible concentration, il conduit à accroître la résistance du verre à l'hydrolyse, alors qu'à plus forte concentration, un effet opposé est observé. Pour comprendre ce phénomène, nous avons réalisé un grand nombre de simulations de dynamique moléculaire, couplées à la technique de "Potential Mean Force" (PMF) pour estimer les barrières d'activation pour l'hydrolyse dans la silice pure et dans des verres d'alumino-silicates. En parallèle, des expériences ont été faites pour valider les simulations. Cette étude a révélé que les liaisons Al-O sont aisément dissociables comparées aux liaisons Si-O. Cependant la présence de Al augmente significativement la durabilité du verre en renforçant les liaisons Si-O et en augmentant la connectivité du réseau vitreux.

Au contraire, à plus forte concentration, la dissolution préférentielle des Al affaiblit le réseau silicaté en raison de la percolation des liaisons faibles Al-O. La résistance du verre à l'altération s'affaiblit. Grâce à la technique PMF, nous avons évaluer à 0.49eV l'énergie d'activation moyenne pour l'hydrolyse des liaisons autour des Al, ce qui représente moins de la moitié de l'énergie nécessaire pour dissocier les liaisons autour des Si dans la silice pure (1.22eV) ou dans un verre alumino-silicaté (1.34eV). Nous avons montré que ces différences d'énergie sont statistiquement significatives. Cet effet est un processus principalement local. Des calculs de dynamique moléculaire par la méthode ReaxFF ont permis de valider les résultats. Nous avons poursuivi les investigations avec des verres contenant du Ca et du Na. Le mélange Ca/Na dans un verre alumino-silicaté conduit à rendre insignifiant le renforcement des liaisons Si-O par le Al du fait de la compensation de cet effet par l'accroissement du désordre structural.

Finalement, nous avons étudié le rôle du Al pendant la phase d'altération résiduelle, c'est-à-dire quand un gel passivant se forme. Pour cela, six verres d'alumino-borosilicate avec des teneurs variables en Al_2O_3 (de 0% à 9.6% massiques) ont été préparés. Trois verres contiennent une concentration en Al_2O_3 faible voire nulle et les trois autres ont des concentrations en Al_2O_3 plus élevées. Les verres avec de faibles quantités de Al_2O_3 relâchent rapidement une grande quantité de Si en solution. En revanche, les verres avec une quantité plus importante de Al_2O_3 relâchent moins de Si. Ceci confirme le contrôle du relâchement des Si en solution en conditions diluées par le Al. Au final, quand la

solution devient saturée en Si, une couche protectrice se forme à la surface du verre.

Un nouveau modèle Monte Carlo a été développé pour reproduire et mieux comprendre ces résultats expérimentaux. Les verres relâchant davantage de Si en solution forment une couche épaisse enrichie en Si à la surface du gel en contact avec l'eau. En analysant expérimentalement le couche d'altération de l'un des six verres par Tof-SIMS, nous avons observé que le B, élément soluble et généralement traceur de l'altération est partiellement retenu dans le gel formé après un mois de réaction. Cette rétention est corrélée à la décroissance de la vitesse d'altération. En couplant les simulations Monte Carlo et les expériences, il a été proposé que la formation d'une couche externe enrichie en Si conduit à la rétention du B dans le gel, ce qui, à son tour, pourrait limiter la poursuite de l'altération.

Abstract (English)

In France, High-level nuclear wastes are vitrified. The resulting packages will eventually be stored in a deep geological formation. After corrosion of the canister and overpack, the groundwater will interact with the glass, resulting in the mobilization of soluble radionuclides. Therefore, researchers must design the glass with an optimal composition and durability to limit the radionuclides release in the environment. Al is an important constituent of nuclear waste glasses; however, its role on glass durability remains somewhat of a mystery! During the initial dissolution regime, at low concentration in the glass, it increases the resistance to hydrolysis of the glass, whereas at high concentration, an opposite effect is observed. To understand this phenomenon, we performed a large number of Molecular Dynamics simulations coupled with the potential mean force technique (PMF) to estimate the activation barriers for hydrolysis of cation-oxygen bonds in pure silica and in alumino silicate glasses. In parallel, experiments were performed to validate the simulation results. This study revealed that the Al-O bonds are easier to dissociate than the Si-O bonds. However, Al increases the glass chemical durability by significantly increasing both the strength of the Si-O bonds and network connectivity in alumino silicate glass.

In contrast, at high Al concentration, preferential dissolution of Al weakens the silicate network because of the percolation of the weak Al-O bonds, so the glass resistance becomes poor. Through PMF calculations, we evaluated the activation barriers for dissociating bonds around Al as 0.49 eV, which is less than half of the energy to dissociate bonds around Si in pure silicate (1.22 eV) and around Si in aluminosilicate glass (1.34 eV). We have shown that these energy differences are statistically significant. Molecular structural investigation revealed that Si with Al as a second neighbor in the glass network has significantly higher activation energy for dissociation than Si in pure silicate glass. Then the strengthening of the Si-O bonds when Al is present in the glass is mainly a local effect. The role of Al in strengthening the Si is qualitatively validated by ReaxFF calculations, another molecular modelling technique but more precise. Then we have continued the investigations with glasses containing Ca or Na. Mixing both Ca and Na in aluminosilicate glass made the strengthening effect of Si by Al insignificant because the strengthening effect is compensated by an increase of the structural disorder.

Finally we have investigated the role of Al during the residual alteration rate. For this, we designed six sodium borosilicate glasses with varying concentrations of Al_2O_3 from 0% up to 9.6 wt%. Three glasses have small to no Al content, and the three other glasses have higher Al contents. It is observed that glasses with small quantities of Al_2O_3 quickly released a large amount of Si into the solution. On the other hand, glasses with a larger quantity of Al_2O_3 released less amount of Si. This is because the Al content controls Si

release into the solution under dilute conditions. Eventually, the solution is saturated with Si, and the glass develops a protective layer on its surface.

A new Monte Carlo model was developed to reproduce and better understand these experimental results. Glasses releasing more Si into the solution favored the formation of a thick Si-enriched layer on the gel surface in contact with water. By investigating experimentally the alteration layer of one of the six glasses by ToF-SIMS, we observed that B begins to be retained in the young gel developed during one month. This retention is correlated to the decrease of the residual alteration rate. By coupling Monte Carlo simulations and experiments, it is proposed that the formation of an external layer enriched in Si induces B retention in the gel, which in turn, could limit further glass alteration.

Contents

List of Figures

List of Tables

Introduction

Nuclear fission can produce a carbon-neutral form of electricity. However, handling the high-level radioactive nuclear wastes created as byproducts is challenging [Gin et al., 2013, Guo et al., 2020]. Many countries, including France, The United States, Japan, The United Kingdom, and Germany, immobilize these wastes in borosilicate glass. These materials are developed by melting the calcinated wastes and additives at high temperature ($> 1000°C$). The resulting homogenous melt is poured into stainless steel canisters. They aimed to be disposed of in geological repositories [Frankel et al., 2021, Majérus et al., 2020, Guo et al., 2020]. In such a scenario, groundwater will react with the glass after the corrosion of metallic envelopes to make irreversible chemical reactions [Gin et al., 2013, Grambow, 2006], leading to the release of soluble radionuclides into the environment over a geological timescale. The glass alteration mechanisms have been studied for decades to develop models used to assess the safety of nuclear waste disposal [Frankel et al., 2021, Thorpe et al., 2021]. Recent reviews provide the current state of knowledge in this field [Frankel et al., 2021, Thorpe et al., 2021, Gin et al., 2021a, Frankel, 2018]. Briefly, glass dissolution takes place in three stages [Vienna et al., 2018, Aréna et al., 2019, Farid et al., 2019, Piovesan et al., 2018], (i) Forward dissolution rate (r_0), where the glass dissolves in dilute solution without a feedback mechanism. (ii) Residual rate, where the glass dissolves several orders of magnitude slower than r_0 due to the saturation of the solution and the formation of a passivating layer [Thorpe et al., 2021], and (iii) Possible resumption of alteration when, at some specific conditions, secondary phases may precipitate from the solution at the expense of the passivating film. Among these three stages of alteration, residual regime is the most important and the less understood [Frankel et al., 2021, Gin et al., 2013]. CEA develops a model called GRAAL to investigate the durability of glass under disposal conditions over geological timescale [Rieke et al., 2018, Fournier et al., 2018, Frugier et al., 2018]. To date, GRAAL model is not supported by a deep understanding of mechanisms at atomistic level. Therefore, understanding the fundamental glass alteration mechanisms at the atomistic level becomes very important to support this model.

A specific difficulty with nuclear glass is the effect of composition, as major oxides can vary significantly within a given domain of interest. One key aspect concerns the role of Al and its synergy with other elements. Indeed, recent studies observed that addition of Al_2O_3 into the silicate glass modifies its properties significantly [Hamilton et al., 2001, Vienna and Crum, 2018, Gin et al., 2020b]. Vienna et al., [Vienna and Crum,

2018] observed the non-linear behavior of Al during the initial dissolution regime. Gin et al., [Gin et al., 2020b] observed that the addition of Al_2O_3 into the sodium borosilicate glass modifies the fundamental gel formation mechanism. Therefore, it becomes important to understand the synergy between Si and Al towards the origin of gel formation, and the consequences towards the release of other elements.

To understand the correlation between the chemical composition and the forward dissolution rate, we used classical molecular dynamics simulation and the results have been compared to experiments. Then, the objective is to introduce the glass compositional effect towards the alteration in a Monte-Carlo code to reproduce the dynamics of alteration along with the formation and aging of the protective gel layer. The fit of the Monte-Carlo method can be supported by experimental data. Current versions of Monte-Carlo models are not able to simulate the gel appropriately (details are given in the Section 1.4.3). This is why we developed a new Monte-Carlo model to simulate the glass alteration. The development of this Monte-Carlo model is a long-term work, aiming to simulate the gel formation and its aging mechanism. This will provide information to update other models at macroscopic level (GRAAL) and also complete other approaches at the mesoscopic level (under development). In this thesis, we investigated the glass alteration process in two directions as shown in the Figure 1.

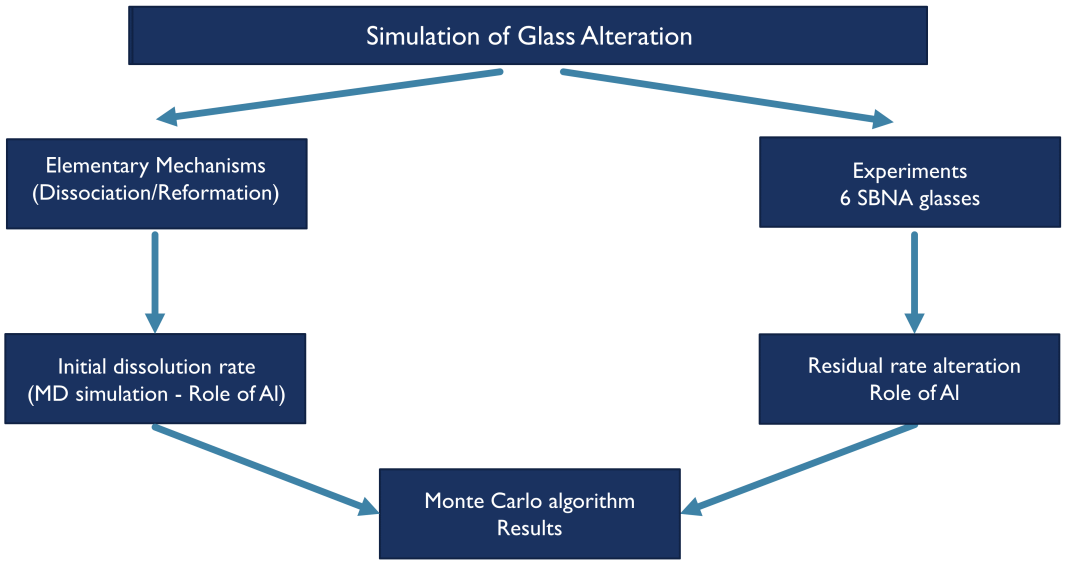

Figure 1: Schematic representation of global work flow of thesis.

1. The first part (left) focuses on elementary mechanisms accounting for the formation of the gel, along with their characteristic energies (like bond dissociation and reformation energies). These are investigated by molecular dynamics simulations.
2. The second part (right) aims at providing experimental data on residual rate for glasses with various Al content.

These two parts have provided us the data to develop a Monte-Carlo model able to better reproduce the role of the glass chemical composition on initial and residual rate. So

the development of the thesis is organized as follows. Firstly, information about elementary mechanisms have been gathered using both molecular modelling and experiments. Then, a Monte-Carlo method has been developed to reproduce the experimental leaching data (6 months duration), i.e., the dynamics of Si and B release in solution and the progression of the protective layer depth versus time. The Monte-Carlo parameters fitted to reproduce the experimental data have been validated, thanks to the atomistic simulation results.

It must be kept in mind that this work corresponds to the beginning of a long-term work. At the end of this thesis, the Monte-Carlo code is written and first fits on experimental data have been obtained. But a second thesis will follow, more dedicated to the Monte-Carlo approach to incorporate more mechanisms including those observed in this thesis.

Objectives

The global objective of our thesis is to understand the elementary mechanisms at atomic scale, involved in the long-term glass alteration process. This will help the researchers to develop the predictive models of glass alteration in geological timescale. The objectives are:

1. Recent study by Vienna et al., [Vienna and Crum, 2018] observed the non-linear effect of Al towards the durability of silicate glass. Increasing Al concentration increases the durability of glass up to a certain limit, then a decrease of the glass durability is observed beyond this limit. However, the atomistic mechanism behind this effect remained unclear. To understand this phenomenon, we will apply Potential Mean Force method to calculate the bond dissociation energy of Si and Al in silicate and aluminosilicate glasses. These activation energies will be correlated with the glass' structural features.

2. An important struggle in correlating the glass' structural features towards the durability is that, disordered nature of glass makes a broad distribution of bond dissociation energy for Si and Al. As a result, it remained mystery to understand the glass' structure towards the durability. To overcome this problem, we constructed an automated pipeline to investigate the bond dissociation energy of Si and Al from these glasses in large statistics. Such large statistical investigation will allow us to decipher the structural property of glass towards the durability.

3. To investigate the role of Al towards residual alteration rate of Na-borosilicate glass. First we will perform long term leaching experiments to monitor the release of glass elements during the alteration layer formation. Then a new Monte Carlo model will be developed to simulate the gel formation and aging mechanism by reproducing these leaching experiments. This will help us to understand the structural characteristics of the alteration layer when the Al_2O_3 concentration is modified.

4. Chapter 5.1 and a previous study by Gin et al., [Gin et al., 2020a] observed the retention of soluble elements (especially B) in the gel. Therefore, it becomes important to understand the behavior of B in the gel and its role towards the durability of glass alteration during residual regime. This will help us to understand the possible rate limiting steps during the residual regime.

Structure of the manuscript

This manuscript is organized into seven chapters.

Chapter 1 presents the review of literature. It starts by presenting the problem of the high level nuclear wastes and the current solution for the immobilization of these wastes, considering the importance of the engineered and natural barriers for the nuclear waste management. Then a general discussion about the structure of glass and its alteration behavior is proposed, with a description of the different stages of alteration. It starts with a summary of the initial dissolution rate investigations by atomistic simulations. (i) Ab initio calculations, (ii) ReaxFF, (iii) Development of classical dissociative potentials to investigate larger systems, and (iv) PMF studies with dissociative potentials to estimate the bond dissociation energy. It continues with discussing the current understanding of the residual alteration regime through both experiments and Monte Carlo models.

Chapter 2 presents the complete methodology of all the experiments and simulations conducted in this thesis. (i) Development of glass models and preparation of the glass/water interfaces. (ii) Procedure followed to perform the potential mean force (PMF) calculations along with statistical tests to estimate if a result is significant or not. (iii) Methodology of experiments and ReaxFF calculations to validate these PMF results. (iv) Preparation of 6 SBNA glasses and presentation of the long-term alteration experiments. (v) Monte-Carlo simulations to reproduce the experimental results.

Chapter 3 presents the PMF method to estimate the dissociation energy of the bonds around Si in pure silicate and aluminosilicate glasses. It begins with optimization of the time step to perform the PMF calculations. Then the measurements of the activation barriers for dissociating the bonds around Si in pure silicate and aluminosilicate glasses are detailed. These PMF results have been validated by comparison with experimental analysis. The number of bridged oxygen and the number of Al as second neighbours around Si have been correlated to the activation energies. Finally, we try to correlate the glass structural features to the distribution of activation energies.

Chapter 4 involves in validating the above PMF results through ReaxFF calculations to confirm qualitatively the conclusions. After validation, PMF protocol is extended to investigate more complex glasses by adding Na and Ca. Finally the energies required to reform the bonds around Si in pure silicate and aluminosilicate glasses have been measured.

Chapter 5 begins with the long-term alteration experiments of the 6 glass powders in distilled water with monitoring the release of Si, B, Na, and Al into the solution. Then we performed pilot study to understand the correlation between the Monte-Carlo parameters and the release of Si and Al into the solution before applying the Monte-Carlo method to reproduce the experimental release of Si and B into the solution. It allows to better understand the properties of the gel for different glasses.

Chapter 6 begins with investigating the impact of adding B and Ca in the solution of alteration (individually and together). This work has been completed by investigating the role of pH on the behavior of B retained in the gel.

Chapter 7: Finally, the manuscript ends with a global discussion on our results. Conclusions and perspectives of this study are then proposed.

Chapter 1

Literature Review

Contents

1.1 Nuclear waste Immobilization

Electricity production through nuclear power reactors involves the fission reaction of ^{235}U, which produces a broad spectrum of fission products and minor actinides. France is reprocessing these spent nuclear fuels (96 wt% reusable) to reduce the final wastes' radiotoxicity [Caurant and Majérus, 2021]. Nonetheless, fuel reprocessing generates High-Level Wastes (HLW), which must be isolated from the environment over several thousand years, to limit their impact [Pegg, 2015, Vernaz et al., 2012]. Therefore, many countries including France, the UK, Germany, and Japan, etc., are immobilizing these wastes by vitrifying them in the form of borosilicate glass and envision storing them in the deep underground [Frankel et al., 2021, Ojovan and Lee, 2011, Caurant and Majérus, 2021, Jantzen and Ojovan, 2019]. This has been recognized as the most promising solution to store them over the long term.

1.1.1 Criteria for selecting the immobilization of nuclear wastes

Material to immobilize the nuclear wastes is selected based on the balance between the long-term durability and the maximum loading capacity for nuclear wastes [Gin et al., 2017b]. Commercially available immobilization techniques are cementation, bituminization, and vitrification. Among them, vitrification is particularly interesting due to its high versatility (the possibility to incorporate various types of chemical elements) and the chemical durability of borosilicate glass [Ojovan and Lee, 2011]. Due to these reasons, France, the UK, Germany, and Japan, etc., are considering to immobilize HLW in the glassy forms.

1.1.2 Development of nuclear waste glass and its storage

Nuclear waste glasses are industrially produced at high temperature between 1000°C to 1200°C by using glass frits along with the fission products and actinides (feed) as shown in the Figure 1.1A. Feed-to-glass conversion takes place in the cold cap, where the reacting feed floats on the molten glass [Xu et al., 2016]. The final homogenous liquid is poured into metallic containers to obtain the final glass package. These nuclear waste glasses will be isolated from the biosphere by disposing them in a deep geological repository constructed at the appropriate depth. The waste glasses will be covered by the engineered barriers and further protected by the natural geological barrier [Norris, 2019]. This hierarchy of isolating the nuclear wastes from the biosphere is called multi-barrier system, as shown in Figure 1.1B [Ojovan and Lee, 2014].

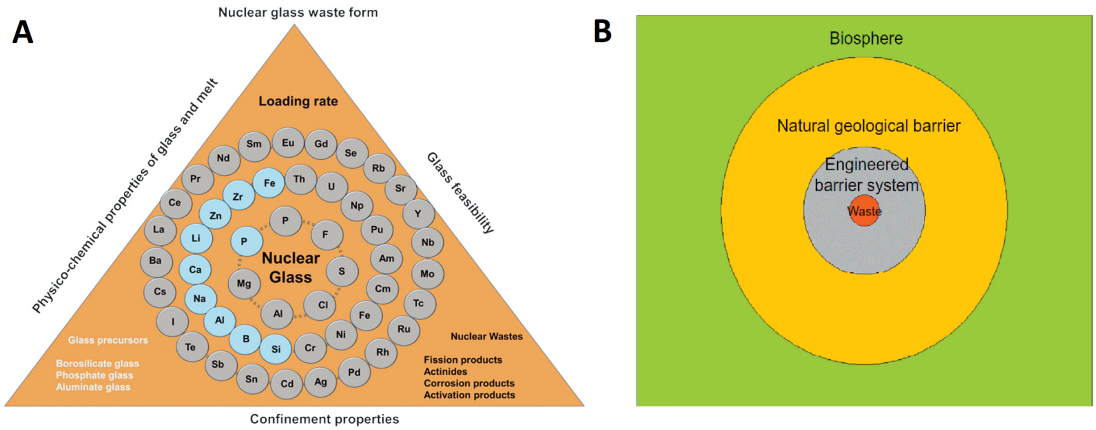

Figure 1.1: Schematic representation of multi barrier system for isolating the nuclear waste glass

1.1.3 Engineered Barrier System (EBS)

The Engineered Barrier System (EBS) encompasses the nuclear waste matrix, a metal container, an overpack, a buffer, repository walls, and wall lining. These multiple barriers initially act together to contain these radioactive wastes and prevent their release into the environment. The primary function of a geological repository is to isolate these wastes from human activities and protect the biosphere.

1.1.4 Natural Barrier System (NBS)

Long-lived radionuclides rely more on NBS than EBS to contain the wastes over a geological timescale [Ojovan and Lee, 2014]. France uses clay as a geological barrier due to its important properties that favor the safe geological disposal of nuclear wastes [Norris, 2019, Ewing et al., 2016]. Some of the important properties are (i) Very low water movement, (ii) Diffusive transport mechanism, (iii) Strong retention capacity, (iv) Buffer effect, (v) Self-sealing capacity, and (vi) Stability over the geological timescale. Due to these reasons, France has selected claystone as the reference host rock for storing high level, and intermediate-level radioactive wastes. Figure 1.2 shows the overview of the CIGEO project, which is a deep geological disposal facility built in France with long-term vision to store the HLW produced over 100 years.

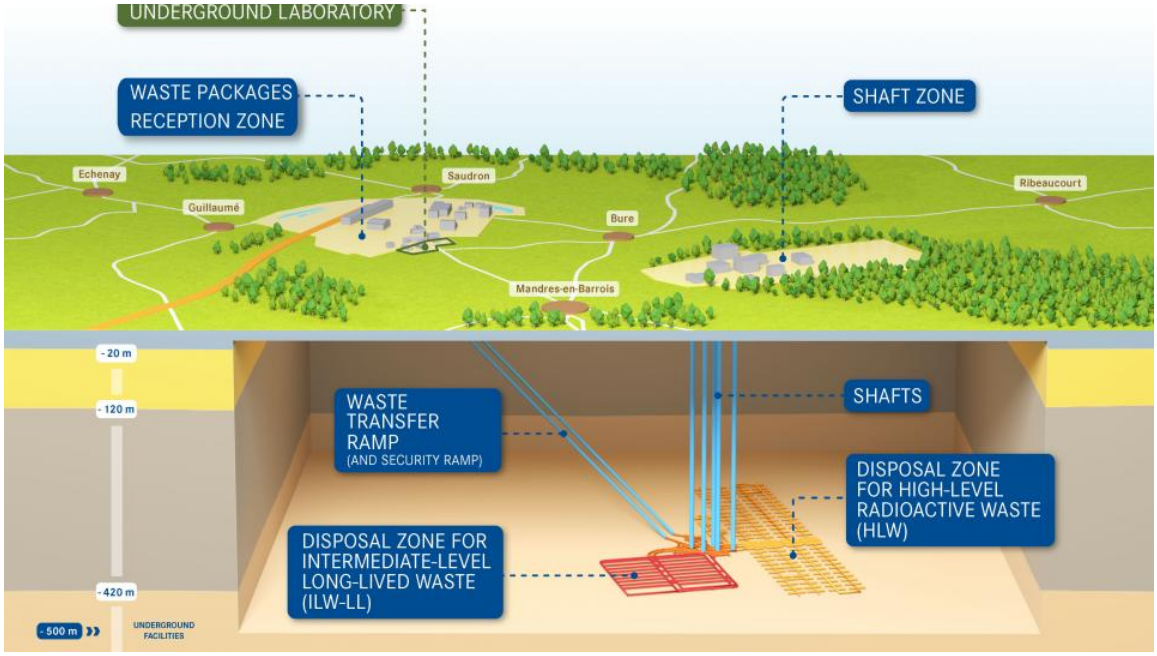

Figure 1.2: High-level radioactive wastes disposal through CIGEO project (French concept).

1.2 Glasses

Glasses are disordered materials without periodic arrangements of atoms [Shelby, 2020]. Glasses are prepared by melting chemicals and cooling them quickly to bypass nucleation and crystallization processes [Greer, 1999]. Finally, a super-cooled liquid, then glass, is obtained [Shelby, 2020]. During the cooling process, initially, the atomic structure of the liquid will continue to rearrange; eventually, the viscosity will rise significantly so that atoms can no longer rearrange completely. This is why the rapidly quenched glasses retain most of their structural characteristics from the high-temperature melt. In consequence, slow quenched glasses will be more ordered due to the larger relaxation time experienced by the system [Onodera et al., 2020].

1.2.1 Structure of glass

Glasses are formed by the network formers like Si, P, B, etc. When an oxygen atom is connected with two network formers, it is called bridging oxygen (BO). For Al, Loewenstein et al., proposed that the distribution of Al in aluminosilicate glass will avoid the formation of Al-O-Al bonds [Loewenstein, 1954]. Adding Alkali or Alkaline earth metals like K, Mg, Na, and Ca will further modify the material's physical properties in terms of density, refractive index, molar volume, and thermal expansion [Baral et al., 2019]. These elements are called network modifiers because they will break the bridging oxygen bond between the network formers leading to the formation of non-bridged oxygens (NBO). The structure of the glass can be characterized in general based on: (i) Coordination numbers of the network formers, (ii) bond angle distributions, (iii) connectivity of the network formers, (iv) field strength, bond strength, etc., The other types of elements (Al,

Fe, Zr, Zn, ...) are called intermediate elements as they can act as glass former or glass modifier elements depending on the whole glass composition and redox potential.

Borosilicate glasses are developed with SiO_2-B_2O_3-Na_2O and are most widely used for immobilizing nuclear wastes [Grandjean et al., 2007]. Boron present in this glass will mainly adopt the planar trigonal (BO_3) or tetrahedral (BO_4) form. In general, the non-bridged oxygen is located around the tri-coordinated B atoms and not around the tetra-coordinated B atoms. Therefore, the annealing temperature (T_g) and concentration of modifiers in the glass will determine the ratio BO_4/BO_3. Therefore, several studies attempted to develop mathematical models that can predict the coordination of the B along with the structural connectivity (NBO's) based on their composition, as shown below.

1.2.1.1 Model to predict the borosilicate glass structure

Dell, Yun, and Bray model

To describe the structure of borosilicate glass (SiO_2-B_2O_3-Na_2O), Yun et al., [Yun and Bray, 1978] and Dell et al., [Dell et al., 1983] proposed a model based on ^{11}B NMR results. They defined R and K to represent the glass composition, where R = Na_2O/B_2O_3 and K = SiO_2/B_2O_3. For K $\leq$ 8, Dell et al., [Dell et al., 1983] proposed four regimes to describe the glass structure based on R.

1. For R $<$ 0.5, all the added sodium atoms are involved in forming four co-ordinated boron irrespective of the presence of SiO_2.
2. For $0.5 \leq R \leq R_{MAX}$, (where $R_{MAX} = \frac{1}{2} + \frac{1}{16}K$), the added sodium atoms will involve in the formation of reedmergnerite group. (reedmergnerite - boron coordinated as tetrahedra with each oxygen bridged to silica tetrahedra).
3. For $R_{MAX} \leq R \leq R_{D1}$, *where* $R_{D1} = \frac{1}{2} + \frac{1}{4}K$, the reedmergnerite group adsorbed additional sodium atoms to form non-bridged oxygen.
4. For $R_{D1} \leq R \leq R_{D3}$, *where* $R_{D3} = 2 + K$, additional sodium atoms combine with diborate groups to form two non-bridged oxygen.

Manara et al., [Manara et al., 2009] revised the calculation of R_{MAX} based on more recent complementary experimental NMR results. They propose to consider the role of sodium oxide in the formation of the reedmergnerite and danburite groups by rewriting this equation to be more general as follows.

$$R_{MAX} = \frac{1}{2} + \frac{K}{2N} \tag{1.1}$$

They propose this equation to calculate the speciation of B [Krough-Moe, 1965]. The value of N is either 5 or 6 to represent the structure adopted by B. At N=5, it forms isolated

reedmergnerite units $\frac{1}{2}(Na_2O.B_2O_3.8SiO_2)$ and danburite rings $Na_2O.B_2O_3.2SiO_2$. For N = 6, the reedmergnerite rings of formula $Na_2O.B_2O_3.6SiO_2$ is formed.

1.2.1.2 Structure of hydrated glasses

Water has a vital role in the physical-chemical properties of the glass, which can largely reduce the viscosity and glass transition temperature (T_g) [Tomozawa, 1985]. Water is expected to react with glass, as shown in the following equation 1.2. It dissociates the bridged oxygen, resulting in two non-bridging oxygen and increases the glass disorder. Therefore it becomes very important to understand the role of water towards the glass structure. In many studies, the structure of glasses with different proportions of water, < 12 wt% have been investigated [Bartholomew et al., 1980, Acocella et al., 1984, Stolper, 1982]. They observed that increasing water content up to 5 wt% increases the Si-O-H formation, whereas further addition of water leads to the accumulation of molecular water within the glassy structure, as shown in Figure 1.3 [Acocella et al., 1984]. This suggests that some of the weak Si-O-Si bonds present in the glasses are dissociated initially by the water molecules to form silanol groups, beyond which the water molecules remain non-dissociated.

$$Si - O - Si \; + \; H_2O \rightleftharpoons \; Si - O - H \; + \; Si - O - H \tag{1.2}$$

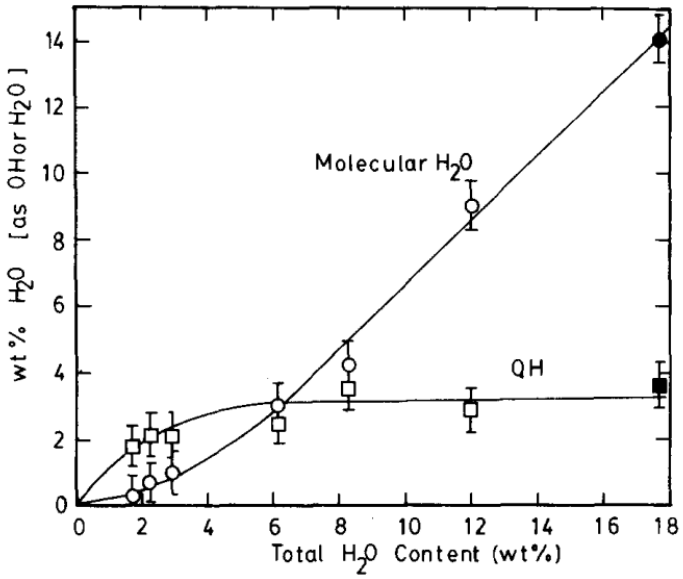

Figure 1.3: Concentrations of molecular water and water in the form of OH as a function of total water present in the specimens (from soluble silicate soln. of $Na_2O/3.3.3SiO_2$ - XH_2O) [Acocella et al., 1984].

1.2.2 Glass alteration

In France, High-Level Wastes (HLW) will be disposed of underground at a depth of about 500m by mining and engineering the repository. However, water re-saturation is expected to happen after the wastes are stored. The duration is difficult to estimate because the corrosion by the underground water will be preceded by the corrosion by water vapor, whose duration is not precisely known. Over 30 years, researchers have studied the mechanisms and kinetics of glass alteration [Gin et al., 2018, Gin et al., 2020b, Fournier et al., 2019, Cailleteau et al., 2008, Gin et al., 2004] with the idea to predict the long-term behavior of HLW glasses in geological disposal conditions [Rieke et al., 2018, Fournier et al., 2018, Frugier et al., 2018].

The glass corrosion process is complex, with an evolving set of reactions and transport mechanisms at various rates, depending on the corrosion stage. The kinetics of these stages are influenced by the composition and structure of the glass, and the effect of environmental parameters such as pH, temperature, ratio of surface area to the volume of solution etc., [Fournier et al., 2019]. Self-irradiation can also modify the alteration rate.

1.2.3 Stages of glass corrosion

Alteration of aluminoborosilicate glasses takes place in four stages, as shown in Figure 1.4. Among these regimes, the residual rate is important because it regulates the long-term behavior of glasses. The residual rate involves many complex reactions and transport mechanisms at variable rates. The mechanisms responsible for the formation of the alteration layer is still largely debated [Gin et al., 2018, Cailleteau et al., 2008, Neeway et al., 2011, Strachan et al., 2022, Hellmann et al., 2015a].

1.2.3.1 Initial dissolution rate

Glass alteration in a dilute medium starts with the diffusion of water into the glass, which initiates ion exchange (interdiffusion) between H^+ and Na^+. These reactions compete with matrix dissolution (hydrolysis of Si-O-M (M = Si, Al, Zr...) bonds). This resulting process is called forward dissolution rate or initial dissolution rate (r_0), which takes place only when the glass is in contact with the solution under dilute conditions [Vienna et al., 2018]. The (r_0) magnitude is regulated mainly through the temperature and pH with little contribution from the concentration of cation and anion in the solution [Jollivet et al., 2012]. Initial dissolution rate can be calculated by the following equation [Grambow, 1984]:

$$r_0 = k_0 \cdot 10^{\eta \cdot pH} \cdot exp\left[\frac{-E_a}{RT}\right] \tag{1.3}$$

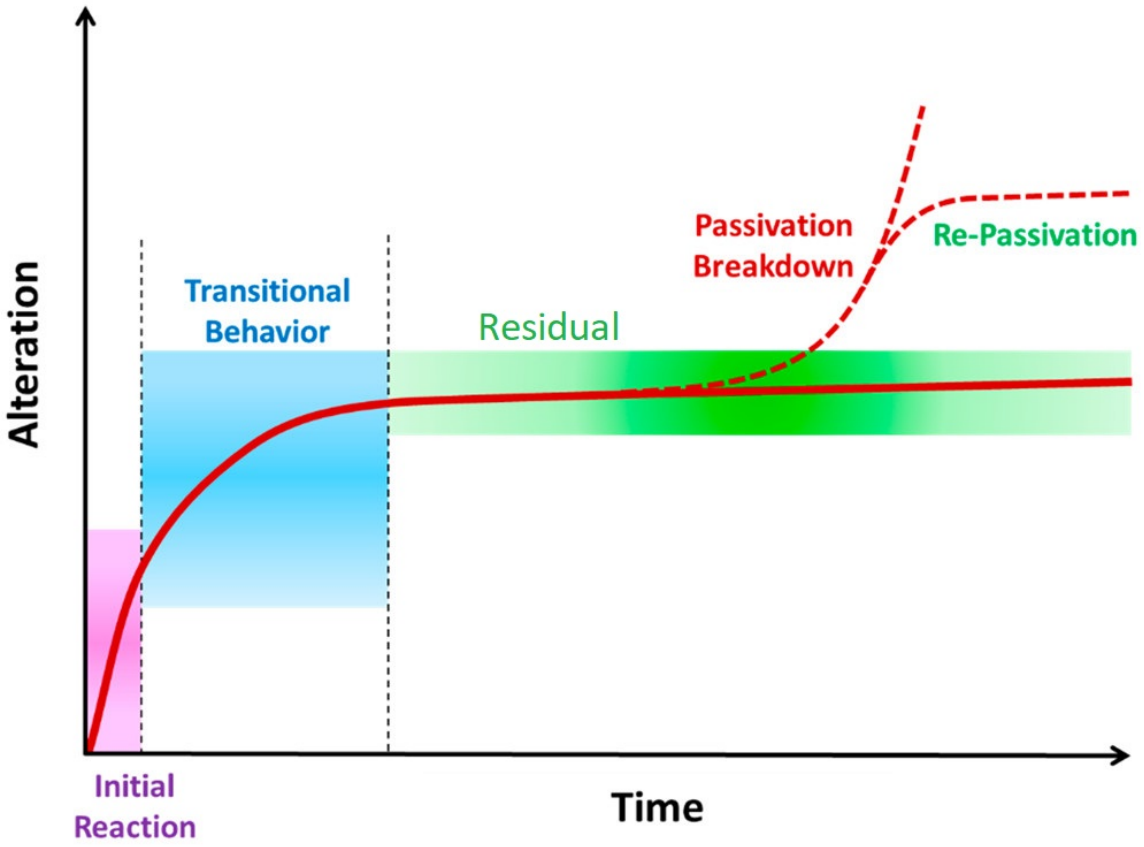

Figure 1.4: Schematic representation of general processes of glass corrosion [Frankel et al., 2021]

where k_0 is the rate constant in $g.m^{-2}.day^{-1}$, η is the coefficient of pH, E_a is the activation energy in $J.mol^{-1}$.

Strachan [Strachan, 2017] mentioned that equation 1.3 is followed only in a narrow pH domain, and so he updated the pH term $10^{\eta \cdot pH}$ with three individual components terms as $a\frac{\eta_{H+}}{H+} + a\frac{\eta_{H_2O}}{H_2O} + a\frac{\eta_{OH-}}{OH-}$. Alternatively, the temperature term can be modified based on hydrogenous species as follows:

$$\left(exp\left[\frac{-E_{aH^+}}{RT}\right] + exp\left[\frac{-E_{aH_2O}}{RT}\right] + exp\left[\frac{-E_{aOH^-}}{RT}\right]\right) \tag{1.4}$$

When the solution is under dilute conditions with no feedback, initial dissolution rate r_0 is dependent on properties of glasses (structure and composition), and also the solution's pH [Fournier et al., 2019] and temperature [Neeway et al., 2012] as shown in Figure 1.5. Understanding this relationship becomes very important to develop a predictive model to quickly design the durable glass composition.

1.2.3.2 Residual alteration rate

When the composition of the solution changes from dilute conditions to moderate (concentration in glass formers has increased), it slows down the glass corrosion process. This

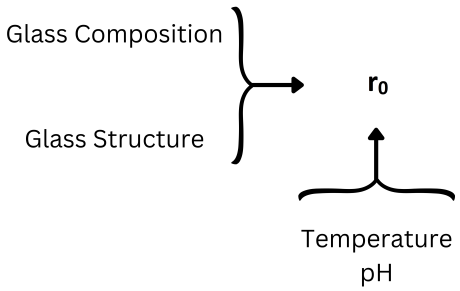

Figure 1.5: Schematic representation of Glass structure - Property relationship

feedback process will be favored while the solution is in static condition with a high glass-surface-area-to-solution-volume ratio. Constituents from the glass will build up quickly in the solution [Ebert, 1993]. As a result, the glass dissolution slows down following a square root of time dependency when the solution is saturated with silica [Gin et al., 2012]. The corresponding rate is called the residual rate, as shown in Figure 1.4. During this stage, an alteration layer is formed, which is generally made of a gel (amorphous, hydrated, and microporous silica-rich material) and secondary crystalline phases. For some glasses, only the gel develops. As the corrosion continues, the thickness of alteration layer increases by the release of B, Na, Ca from the glass. Furthermore, the structure of the gel layer keeps evolving.

It is evident that alteration layer acts as a barrier between the solution and glass to reduce its alteration rate through various mechanisms. It is reasonable to consider that the passivation layer might delay the transport of water or glass elements. However, the corrosion rate during this regime is not dependent on its thickness [Fournier et al., 2019]. Several studies have postulated various roles of gel towards the decreased dissolution rate [Gin et al., 2018, Gin et al., 2020a, Cailleteau et al., 2008], which are discussed with more details in Section 1.4.2.

Understanding how alteration layers form and their role in glass dissolution rate becomes crucial. In the literature, two main models account for the formation of the gel:

1. Dissolution/Precipitation model [Geisler et al., 2010, Hellmann et al., 2015b, Geisler et al., 2015]: It proposes the congruent dissolution of all the glass' elements into the solution, then supersaturating the solution in an interfacial film of water. As a result, the least soluble elements present in this film will re-precipitate to create the gel.

2. In-situ reorganization model [Gin et al., 2015, Gin et al., 2016, Gin et al., 2017a]: It proposes that the incongruent dissolution of the mobile species like boron, sodium and calcium occurs, followed by the reorganization of the remaining network glass formers. In this model, glass formers are not totally hydrolyzed and not transported before redeposition in the gel.

A recent corrosion study performed on two glasses, CJ1 (Na-borosilicate glass) and

CJ2 (Same glass as CJ1, but additionally doped with Al_2O_3), revealed that the glass composition regulates the gel-layer formation mechanism. This study conducted leaching experiments for both glasses in silica-saturated solution (tagged with ^{29}Si and ^{18}O) at pH9 90°C. Solution analysis after 33 days showed that glass CJ1 continued to release Si even after pre-saturating the solution (280 $mg.L^{-1}$) by increasing 99 $mg.L^{-1}$ of Si. This indicates that saturation with amorphous silica is not sufficient for CJ1 to directly build the passivating layer, and the Si saturation limit in solution is dependent on the glass composition. In contrast, CJ2 released only 0.7 $mg.L^{-1}$ of additional Si, corresponding to exchange with gel in the top 2 nm as shown in Figure 1.6C. These results suggest that the gel formation mechanism for CJ1 is by dissolution of Si from the glass into the solution and the silica precipitation from the solution back to the glass' surface. In contrast, CJ2 forms gel by the preferential release of the mobile elements and reorganization of the remaining network. The mechanisms of these glasses are schematically represented in the Figure 1.7. This suggests that none of the above-mentioned models is correct. Instead, the two models represent two extreme cases between which glass can explore all the possible configurations.

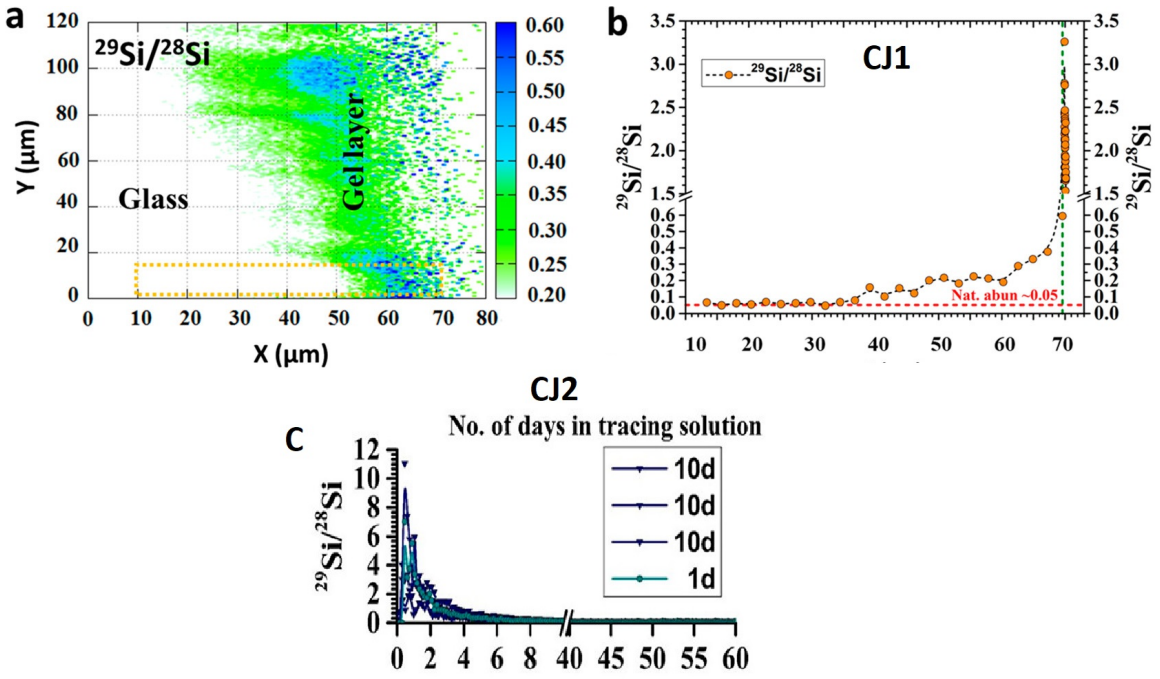

Figure 1.6: ToF-SIMS characterization of altered CJ1 and CJ2 glass resulting from the short-term stage II rate experiment. (a) $^{29}Si/^{28}Si$ distribution map. (b) $^{29}Si/^{28}Si$ profile combining data from the map by averaging values within the delimited area (results displayed on the left side of the green dashed line) and data obtained by depth profiling (on the right side of the green dashed line). This combination was made because it was not possible to analyze the whole layer by depth profiling. (c) $^{29}Si/^{28}Si$ profile showing an enrichment in isotope 29 only in the first 2 nm of the gel layer. [Gin et al., 2020b]

They further validated these results by performing TEM analysis on powder experiments of CJ1 and CJ2 glasses launched 21.4 years ago [Jégou et al., 2000]. TEM analysis confirmed the precipitation of Si sols on the surface of CJ1, which ranged in size from 90 to 180 nm as shown in the Figure 1.7B. This range is very close to those observed during its

early stage [Jégou et al., 2000], indicates that precipitated Si sols are stable. Investigating the CJ2 confirmed no precipitation of Si sols on its surface. These results suggest that CJ1 is more soluble than amorphous silica whereas CJ2 is less soluble than amorphous silica [Gin et al., 2020b] and also validates the gel formation mechanisms discussed above.

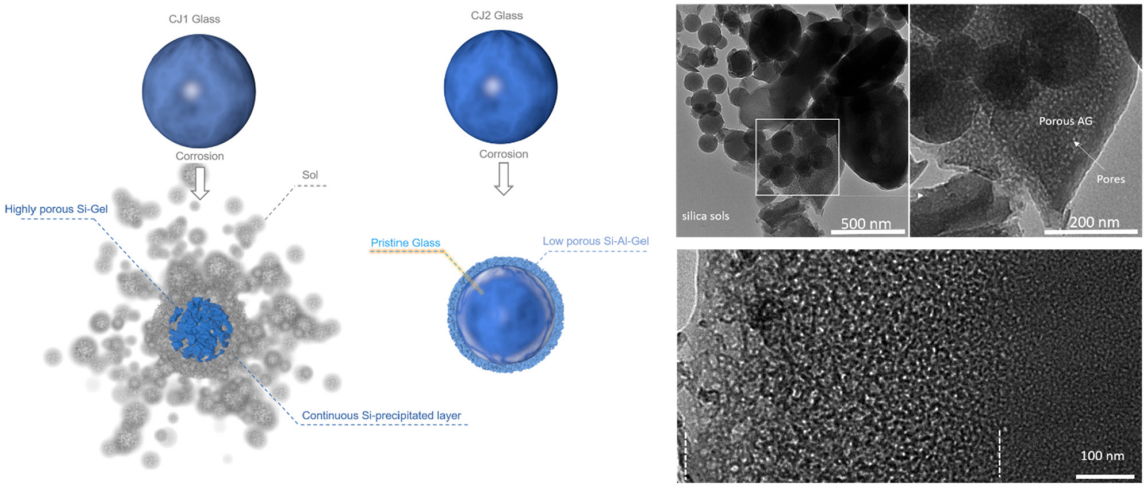

Figure 1.7: Gel layer formation mechanism in two borosilicate glasses, CJ1 (no Al_2O_3) and CJ2 (4 mol% Al_2O_3). Right figure displays TEM images of gel layers formed in two glasses. [Gin et al., 2020b]

1.2.3.3 Gel Breakdown and Rate Acceleration

After a long period of slow corrosion rate as discussed in Stage II, the gel may be destabilized with an acceleration of the glass corrosion rate. This acceleration stage of glass corrosion is commonly seen under extreme conditions like high temperature, high S/V ratio [Ebert et al., 1992], high pH, or when the unsaturated solution pass through it [Pierce and Bacon, 2009]. However, zeolites precipitation at high pH is most commonly observed during the resumption of alteration [Fournier et al., 2014]. The mechanism is, when large amounts of Al and Si are released into the solution, zeolites precipitate at the gel/solution interface, then disrupt the passivating gel that dissolves to supply zeolites in Si and Al. This phenomenon is favored at high pH [Fournier et al., 2014]. It is important to note that these acceleration rates of the glass corrosion are not permanent. In some systems, it alternates between acceleration and a slower alteration rate [Barkatt et al., 1993].

1.3 Initial dissolution rate: Insights from atomistic simulations

Hydrolysis around Si and Al in the glass by water has been extensively studied over the last several decades through computational and experimental approaches [Hiemstra and Van Riemsdijk, 1990, Nangia and Garrison, 2010, Nangia and Garrison, 2008, Pelmenschikov et al., 2001, Criscenti et al., 2006a, Du and de Leeuw, 2006, Gratz et al., 1991].

The dissolution reactions taking place between the glass and water are as follows:

$$Si - O - Si + H_2O \rightarrow Si - O - H + Si - O - H \tag{1.5}$$

$$Si - O - Al + H_2O \rightarrow Si - O - H + Al - O - H \tag{1.6}$$

1.3.1 Estimation with MD simulation approaches

In previous studies, the molecular dynamics (MD) simulation method has been widely used to model the glass structure depending on its composition [Xiang et al., 2013, Collin et al., 2018a, Charpentier et al., 2018, Zirl and Garofalini, 1990]. In addition, several approaches have been used to investigate the activation barriers for dissociating the bonds around Si by water [Kagan et al., 2014, Criscenti et al., 2006a, Del Bene et al., 2003, Xiao and Lasaga, 1994]. However, no correlations of the activation barriers with the structural features of the glass are yet available in the literature. At the same time, this is the key to understand the link between glass structure and alteration behavior.

1.3.1.1 Ab initio approach to estimate the activation energy

Ab initio calculations for small silicate clusters indicate the activation energy to be in the range of 0.78 – 1.69 eV [Criscenti et al., 2006a, Del Bene et al., 2003, Xiao and Lasaga, 1994], whose compilation is given in the Table 1.1. Throughout this thesis, the local coordination environment of the Si atom will be represented with the SiPi notation, where i is the number of bridging oxygen and P indicates dissociating the Si in pure silicate glass. Similarly, SiAi or AlAi is used, where A is to indicate dissociating the Si or Al from aluminosilicate glass and i is the number of bridging oxygen. The silicate cluster used in Criscenti et al., is of S type surrounded by three SiP1, one H_3O^+, and four H_2O molecules, as shown in Figure 1.8 [Criscenti et al., 2006a]. Here, H_3O^+ is intended to break the SiP3-O-SiP1, where the whole cluster is positively charged to represent the SiP3 in the acidic solution. They estimated the activation energy for dissociating Si under the acidic condition to be 0.466 eV. They mainly focused on tracing the reaction path by which the H_3O^+ dissociates the Si-O-Si bond. They observed three important steps taking place during this reaction pathway as follows:

1. The bridging oxygen gets protonated, as shown in Figure 1.9 B,C.
2. An intermediate entity corresponding to a 5 coordinated Si is formed as shown in Figure 1.9 D,E.
3. Cleavage of Si-Obr bond, as shown in Figure 1.9 F-H.

A similar study by Xiao [Xiao and Lasaga, 1994] estimated the activation energy of Si-O-Si and Si-O-Al by H_2O to be 1.25 eV and 1.13 eV, respectively. The same study

S. No	Literature	Simulation	Activation Energy	Target Bridge
1	[Criscenti et al., 2006a]	Ab initio	0.466 eV	Si-O-Si
2	[Xiao and Lasaga, 1994]	Ab initio	1.25 eV	Si-O-Si
3	[Xiao and Lasaga, 1994]	Ab initio	1.13 eV	Si-O-Al
4	[Dupuis et al., 2018]	Ab initio	0.10 eV	Si-O-Si
5	[Dupuis et al., 2018]	Ab initio	0.14 eV	Al-O-Si
6	[Xu and Van Deventer, 2000]	Ab initio	-2.53 eV (enthalpy)	Al-O-Si
7	[Xu and Van Deventer, 2000]	Ab initio	-0.35 eV (enthalpy)	Si-O-Si
8	[Yeon and Van Duin, 2016]	ReaxFF-2015	0.867 eV	Strained silica dimer
9	[Yeon and Van Duin, 2016]	ReaxFF-2015	1.3 eV	Unstrained silica dimer
10	[Rimsza et al., 2016]	ReaxFF-Fogarty	0.35 eV	Strained silica dimer
11	[Rimsza et al., 2016]	ReaxFF-Fogarty	0.72 eV	Strained silica dimer
12	[Rimsza et al., 2016]	Ab initio	1.09 eV	Strained silica dimer
13	[Kagan et al., 2014]	Mahadevan classical dissociative potential	0.46 ± 0.17 eV	SiQ4
14	[Kagan et al., 2014]	Mahadevan classical dissociative potential	0.61 ± 0.12 eV	SiQ3
15	[Kagan et al., 2014]	Mahadevan classical dissociative potential	0.61 ± 0.11 eV	SiQ2
16	[Kagan et al., 2014]	Mahadevan classical dissociative potential	0.54 ± 0.03 eV	SiQ1

Table 1.1: Compilation of all the literatures, simulation method, type of target atom with its corresponding activation energy.

also evaluated the dissociation energy for Si-O-Si and Si-O-Al by H_3O^+ to be 1.03 eV and 0.684 eV, respectively. However, Xiao's study [Xiao and Lasaga, 1994] differs from Criscenti's study [Criscenti et al., 2006a] by the target Si atom's local environment. In Criscenti et al., [Criscenti et al., 2006a], the Si atom is bridged with three other Si atoms through oxygen and terminated by one OH group. Whereas, Xiao connected the Si atom to 3 Hydrogen atoms and focused on the reaction between H_3O^+ and H_6Si_2O [Xiao and Lasaga, 1994]. In the first step, as shown in Figure 1.10, H is transferred to the bridging oxygen of the silicate cluster to create stable adsorption species. Then, the water molecule slowly approaches the Si of the target entity. Finally, it results in the dissociation of the

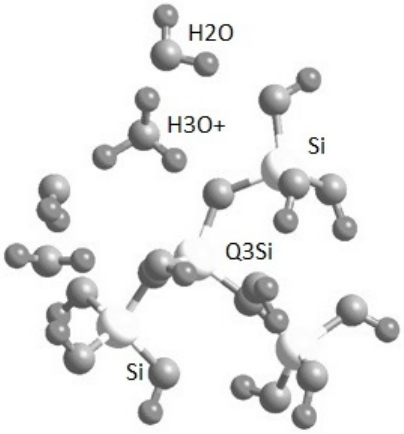

Figure 1.8: Cluster used in Criscenti et al., to estimate the activation energy for Si [Criscenti et al., 2006a]. The cluster has a SiP3 surrounded by three SiP1, one H_3O^+ and four H_2O molecules.

bridging oxygen between the two Si.

According to Xiao's study [Xiao and Lasaga, 1994], the activation energy to dissociate the Si-O-Al is easier than Si-O-Si, which contrasts with a recent ab initio calculation [Dupuis et al., 2018] performed using the metadynamics approach. In general, the free energy surface (FES) in the configuration space might have several local minima, and the initial configuration is stabilized in one of these minima [Laio and Parrinello, 2002]. The metadynamics approach allows the exploration of new minimal around the initial configuration by adding bias Gaussians at regular intervals. With this technique, the system can evolve through different chemical reactions. Dupuis et al., applied bias Gaussian of 0.1 Å width and 0.0005 eV depth for every 5 to 20 time steps [Dupuis et al., 2018] to investigate the role of Al doping in cementitious materials. It is observed that the activation energy of an alumino-silicate dimer is different from that of a silicate dimer. The pentacoordinate state formed with the presence of Al is the most stable state, which increases the stability of the Al-O-Si bond. The activation energy increases from 0.10 eV to 0.14 eV in the presence of Al in silicate chain.

In an ab initio study from Del Bene et al., [Del Bene et al., 2003], they also observed that the reaction path involves the formation of a five-coordinated Si atom as an intermediate stage before dissociating an $H_3Si–O–SiH_3$ cluster. Furthermore, they worked with different amounts of water molecules and observed that the binding energy (the energy necessary to dissociate the cluster) is in the order of one < three < two water molecules. This suggests that the dissociation of Si-O-Si bridge by two water molecules is the most challenging configuration.

This observation contrasts with the Michalske–Freiman model [Michalske and Freiman, 1983], which considers a Si-O-Si bridge interacting with only one water molecule. Michalske and Freiman worked with a single water molecule to mimic a crack tip in the glass. They demonstrated that the reaction between the water molecule and the Si-O-Si bridge occurs

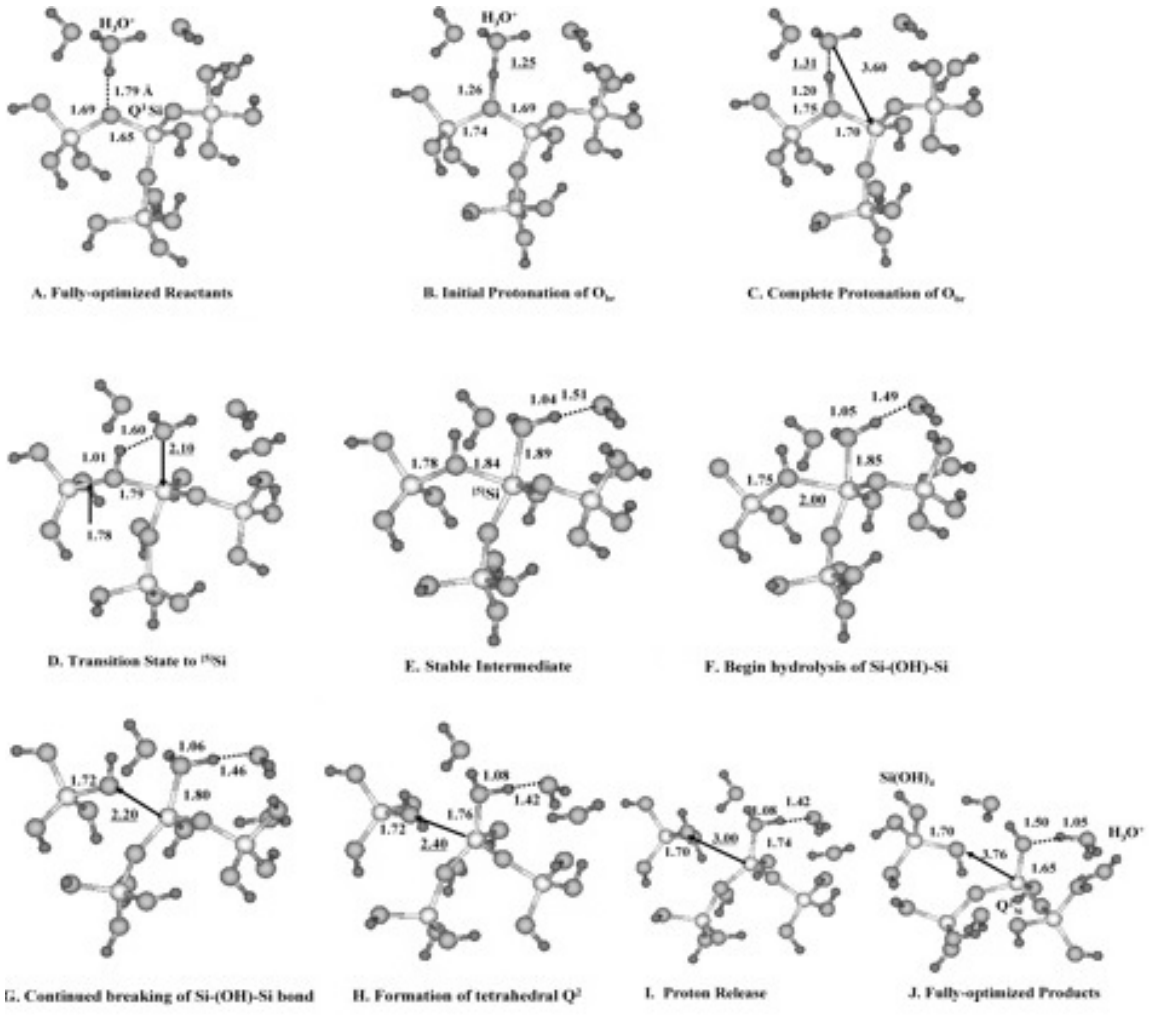

Figure 1.9: Geometries of the reaction path of H_3O^+ to dissociate the Si-O-Si bond. (A) Initial optimized reactants, (B) Initial protonation of the bridging oxygen, (C) complete protonation of bridging oxygen, (D) transition state to 5-fold silicon, (E) stable 5-fold intermediate, (F) hydrolysis of the Si-ObrH-Si begins, (G) Si-ObrH constrained to 2.2 Å, (H) Si-ObrH constrained to 2.4 Å, (I) Si-ObrH constrained to 3.0 Å, and (J) fully optimized products. The underscored distances in panels B-D and E-I indicate the constraint used in the optimization presented. The B3LYP/6-31G(d) configurations in panels B-C are taken from the backward reaction path in which the bridging oxygen is deprotonated to form the hydronium ion. Figure H illustrates the configuration for the highest energy point calculated along the reaction path using B3LYP/6-31G(d) [Criscenti et al., 2006a].

by proton transfer from H of water to O of the Si-O-Si bridge and simultaneously electron transfer from the O of water to the Si atom. As a result, two new bonds are formed to yield two Si-O-H groups. All these reactions are schematically represented in Figure 1.11. In a study of the same kind, Del Bene et al., observed the breakage of one Si-O bond (in a Si-O-Si cluster), then the formation of a new Si-O bond (with another individual Si of the cluster), and simultaneously, two protons moved to form silanol groups [Del Bene et al., 2003].

Another ab initio study conducted in alumino-silicate geopolymers [Xu and Van De-

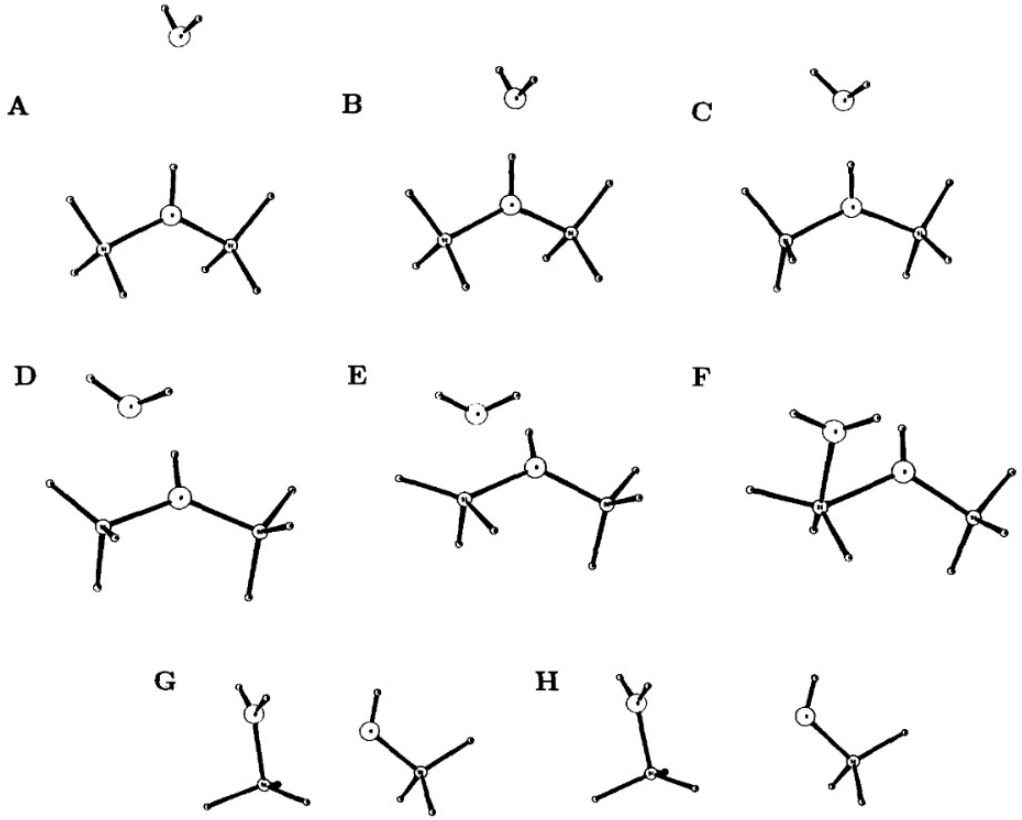

Figure 1.10: The reaction pathway of water molecule approacing towards the surface of Si-O-Si to dissociate under the presence of H^+ catalysis [Xiao and Lasaga, 1994].

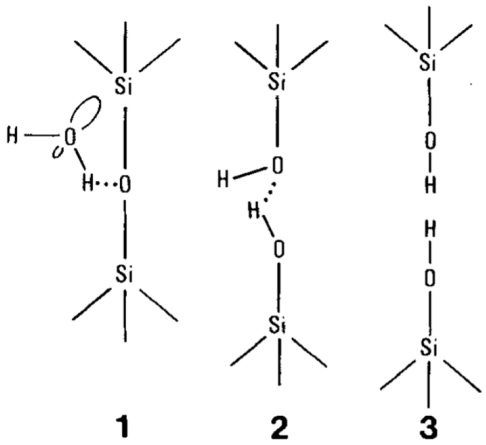

Figure 1.11: Representation of proposed reaction between water and strained Si-O-Si bond at crack tip. Reaction steps involve (1) adsorption of water to Si-O bond, (2) concerted reaction involving simultaneous proton and electron transfer, and (3) formation of surface hydroxyl groups.

venter, 2000], measured an exothermal reaction (enthalpy equal to -2.53eV) for a AlA3 entity, which can be dissociated more easily than a SiA3 entity (enthalpy equal to -0.35 eV). The study concluded that Al is dissolved more easily than Si in this material.

An ab initio study by Bouyer et al., [Bouyer et al., 2010a] working with small models of lime aluminosilicate glass (sample of 100 atoms), investigated its reactivity with water. Besides the peculiar chemical reactions between the glass and water, they observed Al could react with water to form -AlO_3-H_2O, as shown in Figure 1.12A. This entity is observed to be thermochemically stable. This indicates the significant reactivity of Al with water. They also attempted to correlate the standard deviation of Si-O-Si local angle to the nature (endothermic or exothermic) of the chemical reaction with water. The average bond angle is centered around 109° for a SiO_4 entity. The reaction is exothermic when the standard deviation is small around this value.

On the other hand, when the standard deviation is larger, the reaction becomes endothermic, as shown in Figure 1.12B. These results indicate the influence of glass disorder on the nature of the chemical reaction. As a result, it is more difficult to break an ordered local environment. Therefore, we can see from all these studies that the results are not always coherent, and it raises the question about the impact of Al addition into a silicate glass regarding the durability against water [Gin et al., 2020b].

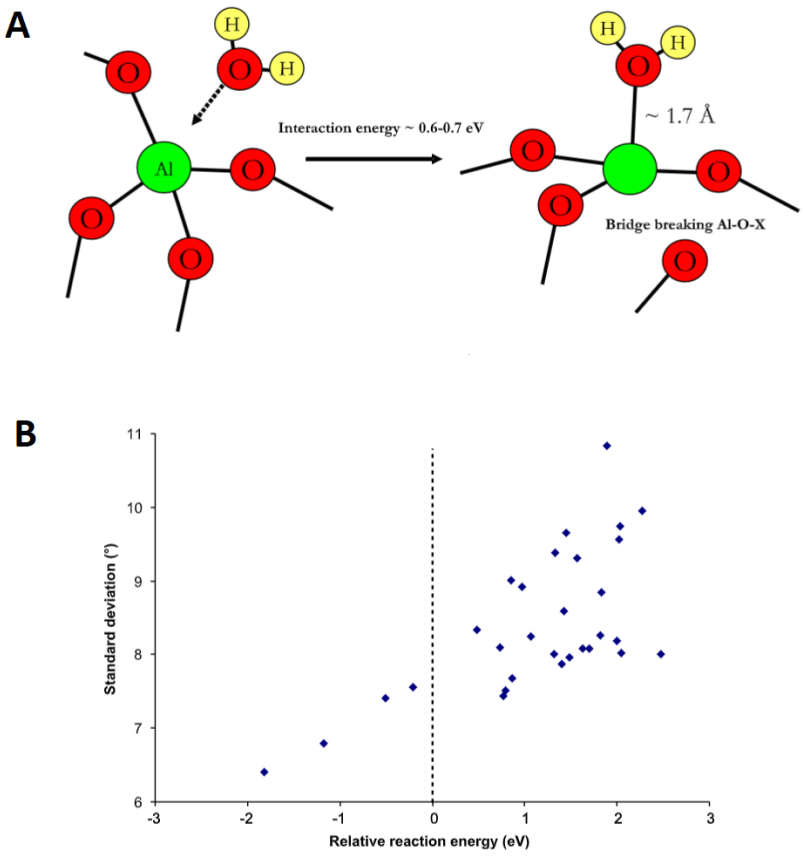

Figure 1.12: (A) AlO3–H2O species structure. (B) Standard deviation of the distribution of final O–Si–O angles after structural optimizations as a function of their energy configurations.

1.3.1.2 Reaxff to calculate the activation energy

In 2010, Fogarty [Fogarty et al., 2010] developed the reactive force field method (ReaxFF-Fogarty), capable of simulating the chemical reactions at a SiO_2-Water interface. For this, parameters were optimized to respect the interactions between the Si/O/H atoms [Van Duin et al., 2003]. This ReaxFF potential developed by Fogarty has been further improved by Yeon et al., (ReaxFF-2015) [Yeon and Van Duin, 2016] to better reproduce the reaction between Silica and Water. They estimated the activation energies required to dissociate bonds around strained and unstrained silica dimers to be 0.867 eV and 1.3 eV, respectively [Yeon and Van Duin, 2016].

Later, Rimsza et al., validated these two versions of Reactive Force Field (ReaxFF) with ab initio molecular dynamics (AIMD) simulations to investigate the interaction between the water and nanoporous silica [Rimsza et al., 2016]. Firstly, the study estimated the activation energy of strained silica dimers to be 0.35 eV from the ReaxFF-Fogarty forcefield. Similarly, the activation energy calculated with the ReaxFF-2015 potential for strained silica dimer equals 0.72 eV. Secondly, ab initio molecular dynamics simulation performed in the same study [Rimsza et al., 2016] estimated the activation energy to dissociate the Si dimer to be 1.09 eV, which validates the ReaxFF-2015 potential. Overall, these ReaxFF potentials show the activation energy for dissociating the silica dimers between 0.35 eV and 1.3 eV.

1.3.1.3 Development of dissociative classical potential for the silicate-water reaction

In ab initio calculation, it was possible to access the reaction pathway and the reaction products formed during the chemical reaction between the Si-O-Si or Si-O-Al bonds with water molecules. However, understanding the role of the glass structure on the activation energy is not accessible due to the computational cost associated with the ab initio calculations. This also limited the researchers to investigate only small clusters. Some studies also used classical potentials to study the structure and energy of SiO_2-H_2O interactions by either artificially inducing the formation of silanol or using non-dissociative water potentials [Puibasset and Pellenq, 2004, Du and Cormack, 2005]. Subsequently, researchers developed dissociative water potentials to simulate the water adsorption on the vitreous silica surface [Feuston and Garofalini, 1990b] and the sol-gel polymerization [Feuston and Garofalini, 1990a, Garofalini and Martin, 1994]. However, only a few bulk water properties have been reproduced with these water potentials. The most common reaction pathway for water dissociating a siloxane bond is shown in Figure 1.13.

In 2007, Mahadevan et al., [Mahadevan and Garofalini, 2007] developed a dissociative water potential matching the bulk water properties including diffusion constant, bulk water structure, vibrational density of states, dipole moment, enthalpy of formation, and equation of state from 273 to 373 K [Mahadevan and Garofalini, 2007]. They also

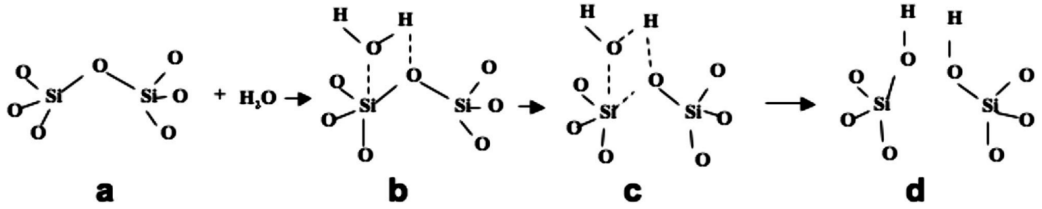

Figure 1.13: The schematic representation of reaction mechanism for breaking the siloxane bonds to form silanol groups [Mahadevan and Garofalini, 2008].

developed this potential by considering interactions between pure silica glass and water. Further, they improved this potential to handle glass with more complex oxides, SiO_2-Al_2O_3-CaO-Na_2O+H_2O [Mahadevan et al., 2019, Mahadevan and Du, 2021]. More details about the potentials and their performance are given in Chapter 2.1.3.1.

We have used the refined potentials to perform the calculations presented here using classical molecular dynamics simulation to investigate the chemical reaction at the glass / water interface.

1.3.1.4 Potential Mean Force (PMF) Method

In 2014, Michael Kagan [Kagan et al., 2014] investigated the activation energy for the dissociation of Si-O-Si in water with the classical reactive potential developed by Mahadevan [Mahadevan and Garofalini, 2008, Mahadevan et al., 2019]. The power of classical potential allowed them to investigate the chemical reactions through the PMF method, and they tried to understand the correlation between the structural features of glass against the activation energy. The PMF method will be described in detail in section 2.2.3. Most of the chemical reactions followed similar mechanisms, with H_2O forming a pentacoordinated trigonal bipyramidal complex with Qi site of the glass. Subsequently, the siloxane bridge opposite the attacking water is dissociated from the Qi site to create non-bridging oxygen attached to the Si, as shown in Figure 1.14.

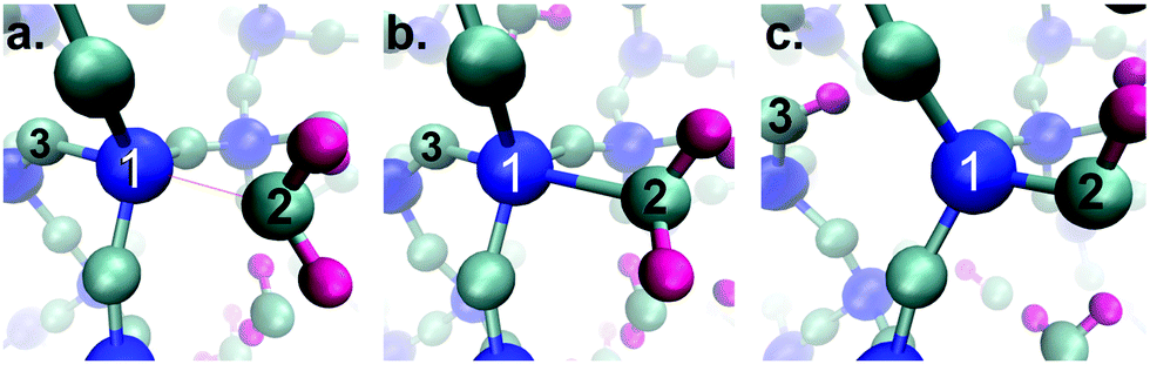

Figure 1.14: The C43 reaction, showing the Si Q4 site (1) in (a) and formation of a pentacoordinated complex in response to an attacking H2O (2) in (b). Dissociation of the back siloxane bridge (3) in (c) to form a Q3 site. [Kagan et al., 2014]

When a water molecule approaches a tetra-coordinated Si, a pentacoordinated Si structure is formed, as shown in Figure 1.15b. During this stage, they observed that the bond angle distribution around the target Si significantly differs from the initial distribution. In Figure 1.15, the average O-Si-O angle of the initial tetra-coordinated Si is represented with a dotted line, and the O-Si-O angles of pentacoordinated intermediates are represented as a distribution. Subsequently, they estimated the chemical reaction's activation energy between silicate glass and water. As mentioned before, Si in pure silicate glass with 'N' number of bridged oxygen is represented as SiPN. They investigated 15 targets to estimate the activation energies for the dissociation of Si-O-Si. In each case, the dissociation of initial Si in SiP4 state will go to SiP1 through the states of SiP3 and SiP2. They obtained the final activation barrier for these reactions by integrating the mean force against the water molecule's distance between Si and O. The average activation energies are categorized with respect to the number of bridged oxygen, as shown in Figure 1.16. It is observed that the reaction around the SiP4 has lower activation energy than for three other states (SiP3, SiP2, and SiP1). The position of the saddle point for the energy changes with the polymerization level of the target Si. So the average activation barriers around the local environments SiP4, SiP3, SiP2, and SiP1 reactions are equal to 0.46 ± 0.17, 0.61 ± 0.12, 0.61 ± 0.11, and 0.54 ± 0.03 eV respectively. Activation energies for the SiP3 and SiP2 local environments are the largest. They can be considered as the limiting step for the dissolution of Si in silicate glass.

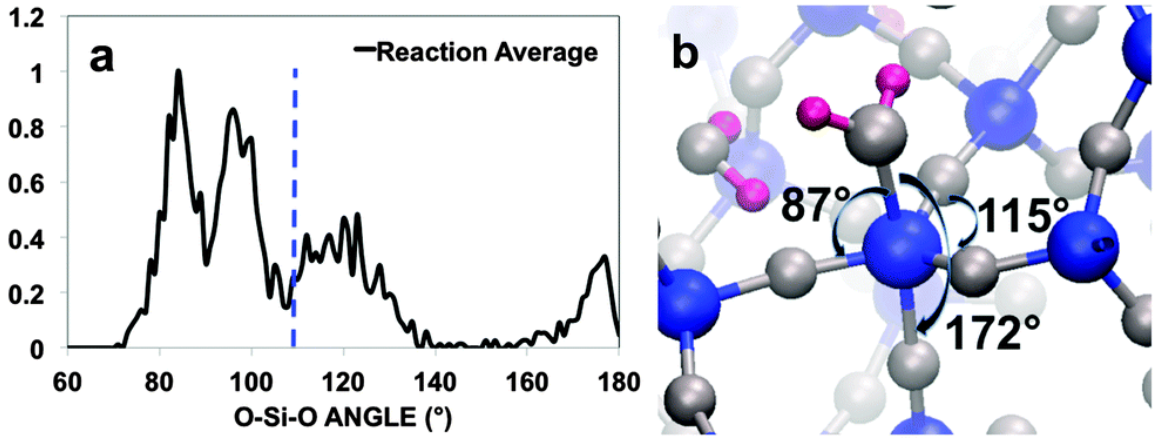

Figure 1.15: (a) O–Si–O bond angle distribution during the hydrolysis reaction averaged over the Q43 samples starting from the water oxygen – Si Q4 site distance of 2.3 Å. Dashed line at the tetrahedral angle at 109.51. (b) Example of an instantaneous structure showing three of the triplets that contribute to the bond angles in (a). [Kagan et al., 2014]

1.3.2 Models to predict the initial dissolution rate

Developing a model to understand the initial dissolution rate with glass composition has been interesting for researchers across various domains [Bisbrouck et al., 2022, Liu et al., 2019, Krishnan et al., 2018, Lillington et al., 2020, Du et al., 2021, Han et al., 2020]. Bisbrouck et al., [Bisbrouck et al., 2022] attempted to investigate this paradigm experimentally by employing the topological constraint theory (TCT) to correlate the number

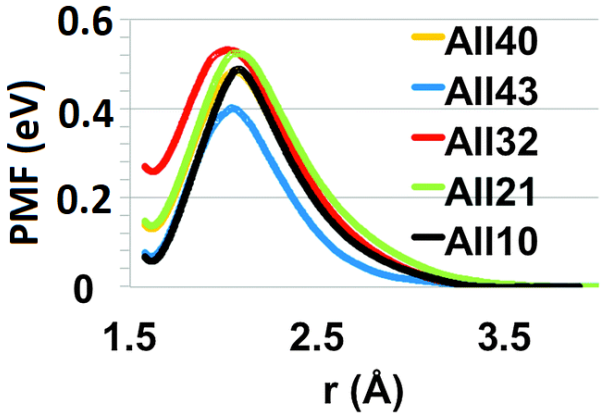

Figure 1.16: The average activation barrier curves in each of the four reactions for each sample. The overall average for the four reactions over the 15 samples is labeled as Q40. [Kagan et al., 2014]

of constraints per atom with r_0. However, no clear correlation was obtained, underlying the need to refine the TCT approach [Bisbrouck et al., 2022]. Machine learning models are more robust in deciphering this paradigm. But the hurdle is that such models require more data to train them. Hamilton et al., developed a database of 299 initial dissolution rates by investigating 9 sodium alumino silicate glasses under different pH conditions [Hamilton, 1999, Hamilton et al., 2001, Hamilton et al., 2000]. Many researchers have utilized this dataset to develop a better machine learning model, demonstrating that AI is a promising tool for this objective [Krishnan et al., 2018, Liu et al., 2019, Lillington et al., 2020].

Krishnan et al., tested various models to find that artificial neural network performs well [Krishnan et al., 2018]. Additionally, they pointed out that all tested models performed better when they completed the training with physics-informed inputs [Krishnan et al., 2018]. Similarly, Liu et al., [Liu et al., 2019] observed that the topology-informed machine learning model improves the prediction accuracy of the initial dissolution rate. Du et al., experimentally measured the initial dissolution rate r_0, and simulated the glass structures for the same compositions [Du et al., 2021]. Then they successfully developed a model to correlate the structural descriptors, F_{net} obtained from the simulated structures against the experimental initial dissolution rate.

Although all the above studies demonstrate the possibility of AI models to predict the dissolution rate, the models need the dissolution rate of relevant reference glasses to predict r_0 for the unknown compositions [Gin et al., 2021b]. Indeed, all these approaches depend on experimental datasets whose accessibility is limited when the researchers are scaling up the method with more complex glasses or different combinations of oxides. To overcome this barrier, in Chapter 4.1, we will present an automated pipeline prepared to rapidly perform the potential mean force calculations to estimate the distribution of activation energies by dissociating the bonds around the Si and Al atoms. Then we will try to correlate the glass' structural features to these activation energies. Through this process, we intend to decipher the rate limiting mechanisms explaining the initial dissolution rate. These data could also be used as input to train other machine learning

models to predict glass durability.

1.3.3 Summary

Researchers across different domains observed the non-linear role of Al_2O_3 towards the durability of silicate glass, but the underlying atomistic mechanism remains unclear. To decipher this phenomenon, the correlation of glass structural features against the activation energy is required. However, existing studies reported a broad range of activation energies for dissociating Si-O-Si by water. This is because energy values depend on the simulation method, size of the system, number of water molecules involved in the reaction, broad distribution of bond angles, local environment of the atoms, disorder of the glass, and so on. In consequence, it becomes impossible to correlate the glass' structural features with activation energy. To overcome this problem, we performed a large number of PMF simulations to estimate the activation energies, and statistically investigated their correlation with the glass structural features. By then, we will understand the role of Al_2O_3 towards the durability of silicate glass, and then fit a Monte-Carlo model to simulate the formation and aging of the alteration layer when a glass is put in contact with water. These large data of activation energy along with the structural features of glass might help researchers to develop machine learning models that can predict glass durability.

1.4 Residual alteration rate

During the residual rate, the glass alteration slows down roughly to the square root of time [Gin et al., 2012]. Eventually, the rate drops further, making the alteration process extremely slow. Mechanisms controlling such phenomenon are highly investigated and debated in many review articles [Vienna et al., 2013, Gin et al., 2004, Vernaz et al., 2001, Gin et al., 2020a, Gin et al., 2021a]. This residual regime must involve the following four processes:

1. Transport of the solution from the external through the gel to reach the reaction front of glass.
2. Dissolution of glass elements in the reaction front.
3. Formation or reorganization of alteration layers.
4. Transport of ions from the reaction front to the external solution through the gel.

One of these processes or their combination must be responsible for the rate limiting mechanism of residual alteration.

1.4.1 Morphology of gel towards the residual rate

Cailleteau et al., combined both experiments and Monte-Carlo simulations to investigate the structure of gel corresponding to very slow alteration during the residual regime [Cailleteau et al., 2008]. They worked with 6 glasses by varying the concentration of ZrO_2 from 0 to 8 mol%. They observed an enriched layer formed on the surface of the gel without any pores in it. They concluded that the thick Si enriched layer with closed pores is an important reason to account for the sharp drop in the alteration rate. They also explained that the presence of insoluble elements like ZrO_2 prevented the formation of a such enriched layer on the gel's surface, which resulted in continuous alteration of glass. They concluded such enriched layer limits the accessibility of water passing through the gel to reach the reaction front of the glass. However, the study was not able to precisely understand why the glass with ZrO_2 also has a drop in the residual alteration rate without formation of such a dense layer.

1.4.2 Transport properties of gel towards the residual rate

Gin et al., designed a novel experimental setup with isotopically tagged solutions to investigate if such pore closure is permanent or temporary by investigating the young and mature gel [Gin et al., 2018]. Addressing this question is important to understand the transport mechanism of elements across the gel. They worked with International Simple Glass (ISG), which is a benchmark glass designed by researchers, to share the results with others [Gin et al., 2013]. The ISG glass contains SiO_2-B_2O_3-Na_2O-CaO-ZrO_2 in proportions relative to the French nuclear glass.

1. **For young gel:** They altered 3 ISG coupons in a solution enriched with isotopic ^{29}Si, at pH7 and recovered 1 coupon for analysis. The other two coupons were transferred to another solution spiked with $H_2{}^{18}O$, and recovered the coupons after 7 days and 10 days. The study observed no exchange of ^{29}Si in none of the three coupons. However, they observed an exchange of ^{18}O from the solution into the gel. This indicates that not all Si-O bonds are broken simultaneously, and even the young gel undergoes hydrolysis and local recondensation reactions. As a result, water transportation across the gel occurs, whereas no isotopic ^{29}Si is allowed to enter [Gin et al., 2018].

2. **For mature gel:** They altered the ISG coupons in Si saturated solution for three different durations. (i) Several days, (ii) 1 year, and (iii) 4.5 years [Gin et al., 2018]. Upon gel formation, the coupon is placed in isotopically tagged O and Si solutions for different durations. They observed the transport of tracing solution across the gel in both a fast (at the beginning) and slow diffusion process (at the end). The study concluded that gel developed after a long duration contains both connected channels (minor) and disconnected pores (majority of pores), which is the reason

for observing both fast and slow diffusion of the elements of isotopic solution across the gel (Figure 1.17) [Gin et al., 2018].

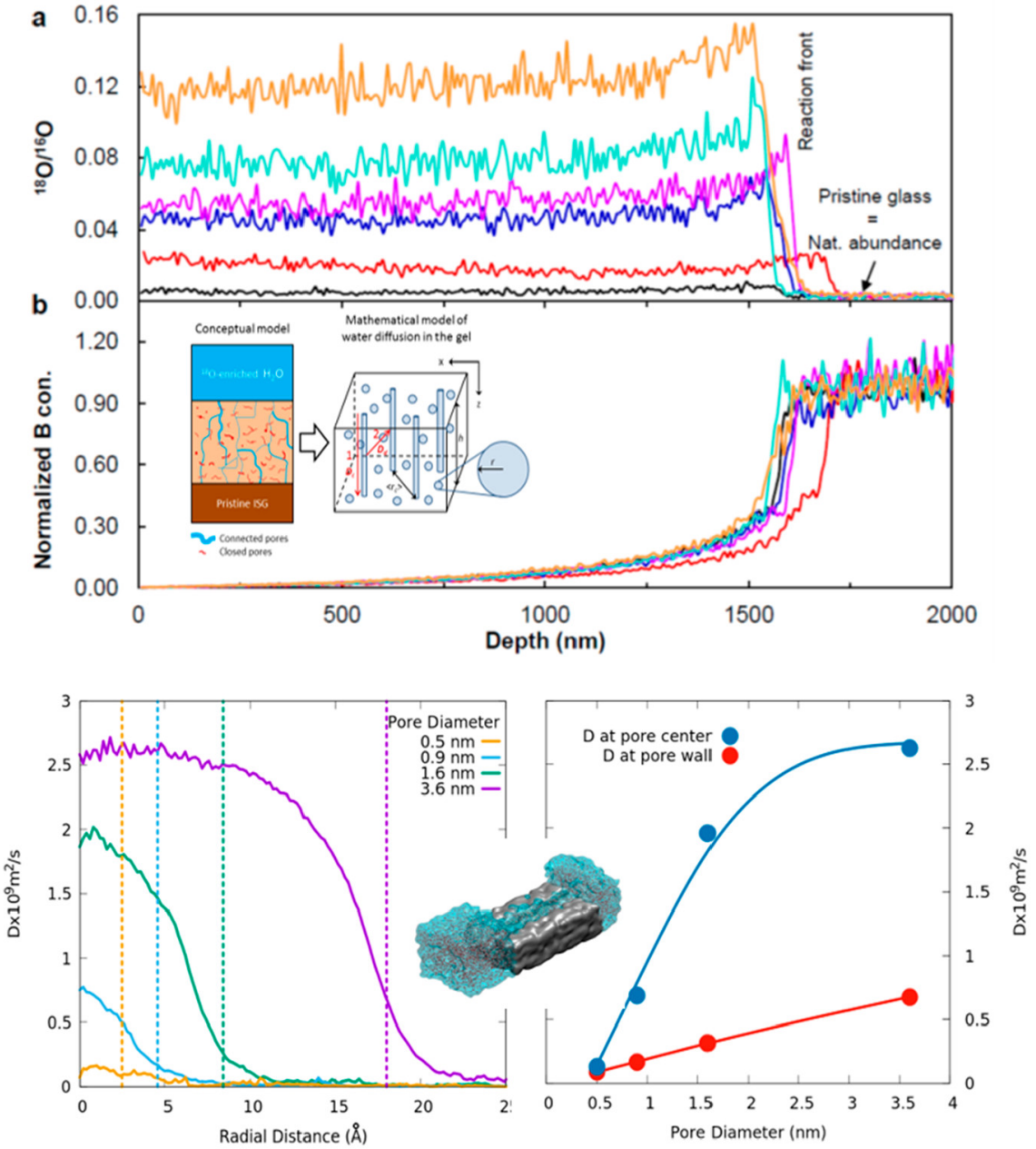

Figure 1.17: (Top) ToF-SIMS analysis result displaying the $^{18}O/^{16}O$ isotope and boron concentration as a function of depth from the water/gel layer interface after exposing the alteration layer to $H_2{}^{18}O$-enriched solution for varying periods of time. From bottom to top: 3 min (black), 3 h (red), 24 h (blue), 96 h (pink), 504 h (cyan), and 2184 h (orange). The inset shows a schematic illustration of porous microstructure inside the gel layer including open channels accounting for rapid transport of water molecules and closed pores accounting for solid-state diffusion of the other water molecules. (Bottom) Water diffusivity (D), obtained from MD simulations, as a function of distance from the pore wall in silica cylindrical pores with diameters varying from 0.5 to 3.6 nm. The average D values at the pore center and wall are also plotted for different pore diameters [Gin et al., 2018].

These results indicate that both young and mature gels can undergo hydrolysis and

local recondensation reaction, suggesting that gel reorganization is a continuous process. However, the role of such hydrolysis and condensation mechanisms in the gel during the residual alteration regime remains unclear. But this interpretation can be discussed in light of more recent results, and Chapter 6.1 will present some of them.

1.4.2.1 Exchange with tracing solution (^{18}O) depending on the gel's age

While comparing the young and matured gels, [Gin et al., 2018] observed that the intensity of ^{18}O exchanged by the young gel was at least three times higher than the exchange occurring in the old gel, as shown in Figure 1.18. It is important to notice that the inner part of the mature gel (close to the pristine glass) is a newly formed gel, meaning that it corresponds to a young gel. This region of mature gel was able to exchange almost twice ^{18}O than the other region, as highlighted in Figure 1.18B (highlighted region). A molecular dynamics simulation study performed by Taron et al., [Taron, 2022] indicates that water molecules initially introduced in pores prepared inside a model gel can diffuse quite easily in the reticulated network of the gel. It seems that, such diffusion of water in the reticulated network of the young gel might be easier than in the mature gel. As a result, we observed a significant difference in the intensity of ^{18}O based on their age. Contrary to the previous experiments, it seems that the water molecules can diffuse anywhere in the gel, but the exchanges occur only with the weakest sites. Therefore, as the quantity of weakest sites is larger in the young gel, the concentration of ^{18}O measured in the gel is larger than in the mature gel.

1.4.2.2 Retention of soluble elements in the mature gel

In another study, Gin et al., altered ISG coupons in a solution saturated with Si for 6 years in pH9 90°C [Gin et al., 2020a]. ToF-SIMS performed on this mature gel revealed that glass altered only around 250 nm thickness. Two silanol groups are formed when the B atom is dissolved from the glass, which can later undergo bond reformation to form a siloxane bond. This process results in the closure of pores or channels that lead to the retention of both B and Ca within the gel. In turn, it might reduce the inward diffusion of water. To test these closed pores' efficiency in terms of B and Ca retention, they transferred the coupons into the solution at pH3 and pH5, saturated with Si for 35 days at 90°C. ToF-SIMS performed after alteration under such conditions revealed that gel thickness increased only by 400 nm and 250 nm for pH3 and pH5 solution respectively, as shown in Figure 1.19. Indeed, the composition of the gel revealed significant retention of B and Ca, while we expect a quick dissolution under acidic conditions. This clearly suggests the efficiency of mature gel with closed pores to strongly trap more B and Ca.

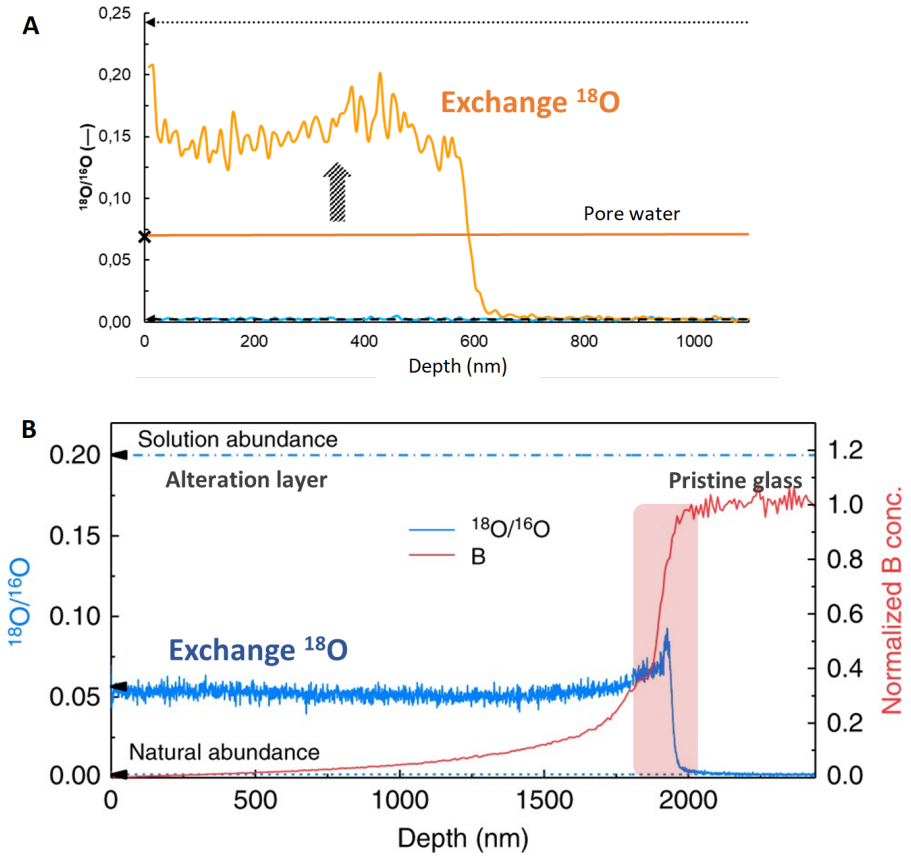

Figure 1.18: Comparison of $^{18}O/^{16}O$ intensity estimated by ToF-SIMS for young and mature gels. (A) ISG coupon altered in pH7, 90°C for 3 days in $H_2{}^{16}O$ (Si saturated solution). Then coupon is transferred to another Si saturated solution with isotopic water $H_2{}^{18}O$ for 4 days. (B) Oxygen isotopic ratio and B profiles recorded by ToF-SIMS depth profiling on a piece altered 1625 days (experiment 3) in the initial experiment and then placed 1 month in similar conditions (90 °C, pH90 °C 7, silica-saturated solution) with water spiked with 18O (18O/16O = 0.24). During this 1-month experiment, the oxygen isotopic signature of the gel raised from natural abundance to 0.125 on average, leading to a fraction of exchanged O of 21.1% [Gin et al., 2018].

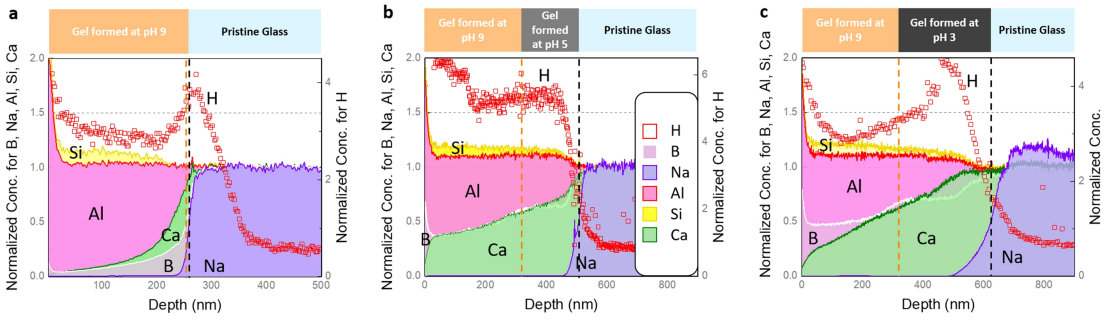

Figure 1.19: Effect of a decrease in pH on ISG samples altered for 6 yr at pH 9. Elemental ToF-SIMS profiles of glass cations and H. (a) Before the pH swap. (b) After a 35-day immersion at pH 3. (c) Same as (b) but for the re-corrosion stage at pH 5. For (b) and (c) plots the orange dotted line indicates the position of the pristine glass surface before the pH swap. Therefore the gel located in between the orange and the black lines was formed during the stage of acid corrosion [Gin et al., 2020a].

1.4.3 Monte Carlo method

Leaching experiments might investigate the alteration of glasses, development of gel, and some of its ripening mechanisms. However, understanding the elementary mechanisms at the origin of glass alteration is difficult with till-date experimental techniques or even through potential based simulations. This fuels the need for mathematical models to understand the gel properties at a longer duration by reproducing the leaching experiments. Researchers employed the Monte Carlo simulation method based on the stochastic technique to reproduce the glass alteration process for more than two decades [Aertsens and Ghaleb, 2001, Cailleteau et al., 2008, Kerisit and Pierce, 2011, Kerisit and Pierce, 2012, Gin et al., 2020b, Ledieu et al., 2004, Jan et al., 2019b, Devreux et al., 2004]. In these Monte Carlo models, the glass structure is represented as an ordered network (cubic one) to simulate the alteration by water. Basic principle behind this simulation is to incorporate the fundamental glass alteration mechanisms like hydrolysis, redeposition, diffusion through gel layer, etc., in MC models. And these mechanisms are controlled by a set of probabilities optimized to reproduce the experimental glass alteration. While reproducing the experimental results, it becomes possible to understand the glass alteration at atomic resolution through the MC model, which is difficult through currently available analytical techniques (both experimental and MD simulations).

Aerstens and Van Iseghem [Aertsens and Van Iseghem, 1995] first developed a simple MC model for three particles with 6 possible bonds among them: (i) Water (H_2O), (ii) Network former (Si), and (iii) Network modifier (Na). Diffusion of water molecules across the glass is introduced through the ion-exchange mechanism. i.e., when water comes in contact with sodium, a quick exchange is possible between them, so water diffusion occurs [Aertsens and Van Iseghem, 1995]. Whereas, if water comes in contact with Si, the energy state of the Si is assigned based on its coordination number. And the exchange is allowed depending on a probability that depends on the Si local enrichment. This study's main drawback is that considering Si's diffusion in water explicitly restricted them to work with small systems. Later Devreux and Barboux neglected the diffusion process in water and treated only the dissolution/redeposition processes at the surface of the glass [Devreux and Barboux, 2001]. It allowed them to work with larger systems. Ledieu et al., used the same algorithm to work with glasses of 3 elements (B, Na, and Si) [Ledieu et al., 2004]. According to this corrosion scheme, B and Na are quickly released into the solution when they are in contact with water, and Si dissolution is based on the number of siloxane bonds around them. They introduced the redeposition mechanism to investigate the gel's morphology after a prolonged alteration. An additional refinement has been introduced by considering the Si concentration profile in solution and its redeposition at the surface. It was a way to reproduce the impact of diffusion in the porous gel network [Ledieu et al., 2004]. However, this model is limited by the absence of water diffusion in the solid. When an external layer enriched in Si is formed, as no diffusion of water in the glass is considered, the alteration becomes rigorously equal to zero, which is not physical. Later, Devreux et al., tried to introduce gel aging by allowing the Si atoms dissolved in closed pores to diffuse at the surface of the pores. This technique simulates gel maturation

even after the alteration is stopped but not the residual alteration regime [Devreux et al., 2004]. Both studies observed a thick enriched Si layer formed on the surface of the gel close in contact with water, as shown in Figure 1.20. They proposed that such a layer would limit water transportation across the gel. As a result, the release of B and Na into the solution is limited. Ledieu et al., and Cailleteau et al., observed that incorporation of Zr or Al (insoluble elements) into the glass delays the formation of this enriched and blocking zone [Ledieu et al., 2005, Cailleteau et al., 2008]. This is because the insoluble element's presence delays the bonds' reorganization around Si. This prevents formation of blocking layer, as a result, glass alteration continues.

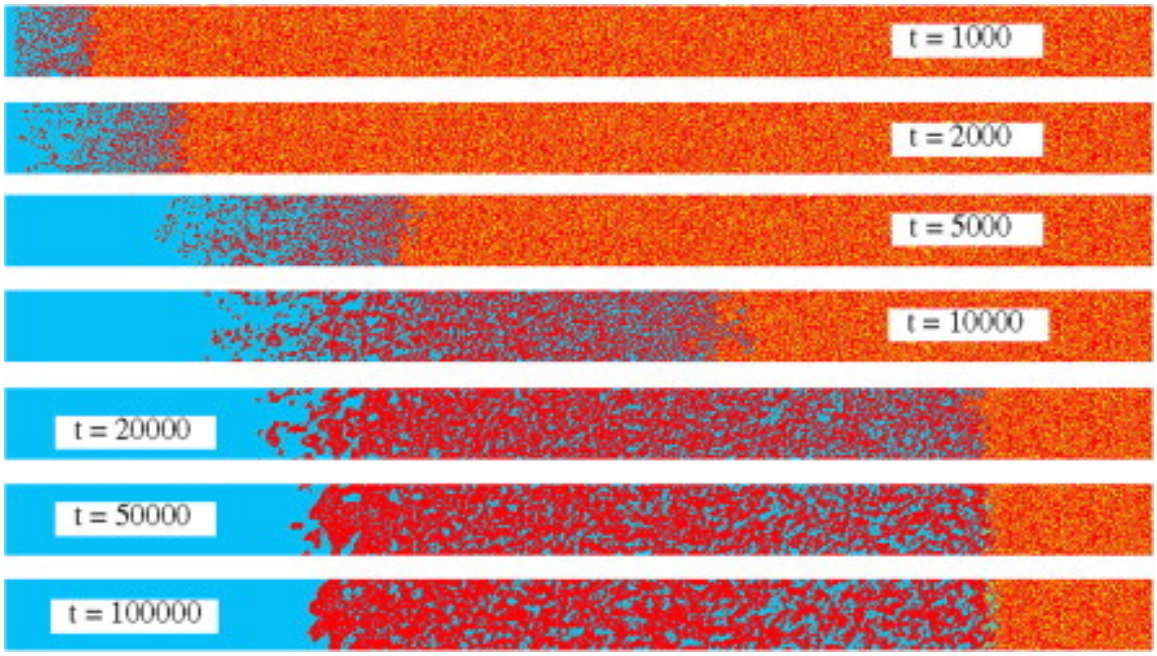

Figure 1.20: Evolution of the morphology of the altered layer. The picture shows two-dimensional cross-sections of the altered glass at different times. Silicon and boron are represented by red and yellow pixels, respectively. Sodium is not shown. The final shrinkage and gel thicknesses are 80 and 185 nm, respectively (assuming 1 pixel = 0.3 nm) [Devreux et al., 2004].

Kerisit et al., [Kerisit and Pierce, 2011] independently developed a Monte-Carlo model by following the same principle as Devreux et al., [Devreux et al., 2004], and investigated the impact of glass structural features on the dissolution. They worked with glasses by varying the B_2O_3 content to have the Si/B ratio ranging from 8 to 0.7. With these glasses, they observed that the dissolution rate of glass increased with the number of NBO's at all Si/B ratios, as shown in Figure 1.21. Indeed, this increase was dependent on the number of Si sites with more NBO. It is not surprising because this study incorporated three different probabilities (w1, w2, and w3) for dissociating the Si based on the number of coordination. As the dissolution of B from the glass is always considered to be immediate, they observed that the presence of boroxol rings or clusters of B resulted in an increase of glass dissolution rate at all Si/B ratios. Apart from these structural characteristics, it is important to notice that the implementation of the aluminum avoidance rule increased the glass dissolution rate [Kerisit and Pierce, 2011] compared to random distribution. In these studies, 10 times stronger dissolution probabilities are used for Al than Si since

adding Al into the glass increased the durability against water. In 2022, [Damodaran et al., 2022] observed that Al is an element easier to dissociate from the glass than Si. And the increase of glass durability when the Al_2O_3 concentration increases is due to a strengthening effect on the bonds around the Si. So the choice of the probabilities for the Si and Al dissolution in S. Kerisit's work can be discussed.

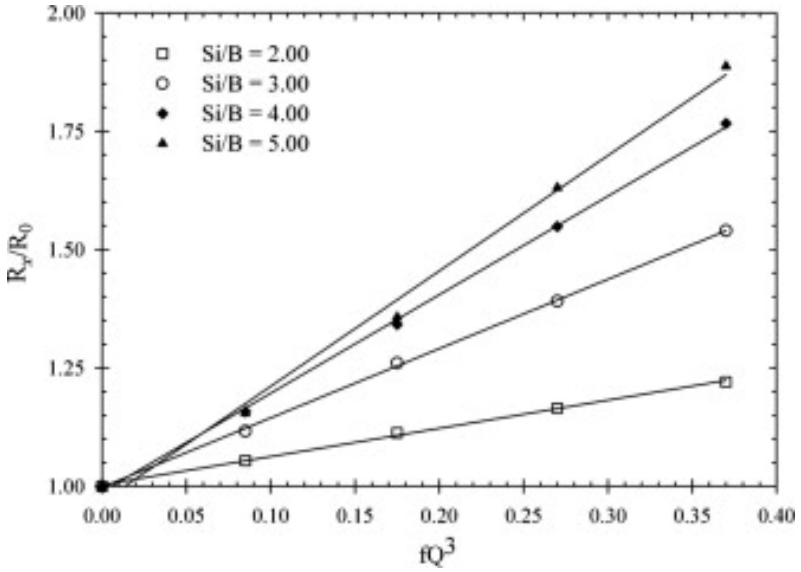

Figure 1.21: Glass dissolution rate (R_x) relative to that with no NBOs (R_0) as a function of the fraction of silicon sites with a NBO (fQ_3) for a range of Si/B ratios [Kerisit and Pierce, 2011].

Jan et al., [Jan et al., 2019b] compared the efficiency of the MC model developed by Kerisit et al., [Kerisit and Pierce, 2011] and Devreux et al., [Devreux et al., 2004]. It was found that both models are in agreement after investigation concerning the varying surface area to volume ratio, Si/B content, coordination of B, number of NBO's. Gin et al., investigated the residual alteration rate for two types of borosilicate glasses named CJ1 (without Al_2O_3) and CJ2 (with Al_2O_3) [Gin et al., 2020b]. They observed experimentally that CJ1 glass undergoes dissolution and reprecipitation mechanisms to form the alteration layer. Whereas Al present in CJ2 glass leads to local reorganization of Si to develop the alteration layer. Jan et al., reproduced the dissolution behavior of these two types of glasses with the MC model (she used the model of Kerisit version) [Kerisit and Pierce, 2011]. It is important to notice that this model can perform only complete dissolution/reprecipitation of Si based on the number of bridged oxygen. After releasing Si from the glass and saturating the solution, an equilibrium between the solution and altered glass is attained. Then Si starts to deposit on the surface to form a dense blocking layer after 10,000 and 20,000 steps for CJ1 and CJ2, respectively. As a result, the total reactive surface area decreases sharply because only the sites of glass connected to the main solution can react. This confirms that the development of passivation layer for CJ1 is quicker than CJ2. The morphology of the gel indicated that it is more rugged in CJ2 than CJ1 due to hard spots of Al that are difficult to dissolve. As a result, water bypass these hard spots leading to the heterogeneity in the gel formation for CJ2, as shown in Figure 1.22A. Consequently, the fraction of gel sites exposed to the water connected to the main solution is higher for CJ2 than CJ1 (Figure 1.22B). This study proposed

that the more rugged structure of the gel formed on the CJ2 glass compared to the CJ1 glass can lead to a larger quantity of local dissolution–reprecipitation. This explanation was proposed to explain the difference in alteration mechanisms between the CJ1 and CJ2 glasses. But this explanation is probably incomplete, as we will see from the results presented in this manuscript. Finally, Jan et al., [Jan et al., 2019b] tried to reproduce the large increase in width of the alteration layer observed experimentally in a glass pre-irradiated by heavy ions. To do this, she introduced a larger depolymerization level and disorder on the glassy network (i.e. on the ordered network representing the glass). But she was not able to reproduce this large increase. This underlines again the limits of these Monte Carlo approaches. As the water molecule can't diffuse inside the glass network, it is impossible to represent the residual alteration rate on the one hand, but also the large increase of the width of the alteration layer after irradiation on the other hand. It is why a new Monte Carlo method has been developed, and this new algorithm will be presented in Chapter 2.4.3 and Chapter 5.1. This method will consider the possibility of the water molecules diffusing on the glass network. Indeed, gel ripening mechanisms will be introduced to regulate the formation of pores. Implementing these new mechanisms will be key for simulating the alteration of the CJ2 type of glasses with MC model.

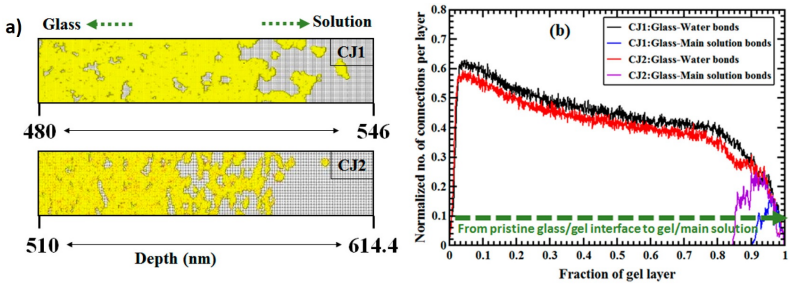

Figure 1.22: Cross sections of the gel layers after formation of the blocking layer for CJ1 (taken at 17000 steps) and CJ2 (taken at 50000 steps). (a) Snapshot of the CJ1 and CJ2 gel layers (Si sites are shown in yellow, Al sites in red, and water sites in gray) (b) Fraction of glass sites exposed to water sites inside closed pores (black and red lines) and water sites in the main solution (purple and blue lines) as a function of depth inside the gel layer. [Gin et al., 2020b].

1.4.4 Summary

Long-term alteration of glasses without sparingly soluble elements such as ZrO_2 or Al_2O_3 quickly released Si and developed a protective layer. As a consequence, the alteration rate for such glasses quickly drops. Investigation through experiments and Monte Carlo simulations revealed a thick enriched layer formed on the gel's surface, which was initially proposed to block the diffusion of water. However, further studies proved that diffusion of water was not limited by such gels. This reopens the question, why the glass alteration is dropped sharply? Monte Carlo simulations combined with long-term leaching experiments have the potential to investigate the properties of gel. However, previous version of Monte Carlo method was not able to simulate the gel appropriately. Therefore, we need to develop a new Monte Carlo model that can simulate the formation and ripening of the gel. Moreover, in this thesis we have investigated 6 glasses with varying concentrations of Al_2O_3 and performed long-term alteration experiments. The newly developed Monte Carlo model will be applied to reproduce these experimental results and gained insights on rate limiting steps of residual regime.

Chapter 2

Methods and models

Contents

2.1 Basics of Molecular Dynamics Simulation

Before we start the experimental procedure followed during this thesis, this section will detail the basic concepts of classical Molecular Dynamics simulation.

2.1.1 Principles of Molecular Dynamics

Molecular Dynamics (MD) is very similar to the real experiments in various aspects. In experiments, we prepare a sample and measure the interesting properties through an instrument during a certain time. If the measurements have statistical noise, we measure on a longer time and take average to increase the accuracy of the measurements. Similarly in classical MD, a small volume of materials, containing few hundreds or thousands of atoms, is simulated and from the trajectories of the atoms, it is possible to measure different properties. Each atom is represented as a point in a three dimensional space with its mass and its charge (partial). The electrons are not considered assuming they are included in the point charge. The forces exerted between the atoms are calculated from the derivatives of the interatomic potentials, already described in Chapter 1 (paragraph 1.3.1.3). Hence for a system of N atoms, the Newton's equations of motion are applied by discretizing the time, to displace the atoms step by step depending on the forces acting on them. A stationnary state is reached that corresponds to the state of equilibrium (properties of the system no longer change with time). The actual property measurements are performed after this equilibration. The Newton's equation of motion is represented as follows:

$$F_i = m_i.a_i \tag{2.1}$$

Where i indicates each atom of the system containing N atoms, m_i is the mass of the atom i, a_i is the acceleration of the atom i given by $\frac{d^2r_i}{dt^2}$, and F_i is the force acting on atom i due to the interactions with the other atoms. Various algorithms are available to discretize this equation in time (with a time interval dt), which will allow to calculate the successive positions and velocities of each atom. Velocity Verlet algorithm will be used to obtain the consecutive position r(t+dt) and velocity v(t+dt) for each atom at the time (t+dt) from the current position r(t) and velocity v(t). Following equations are solved for computing the new position and velocity of each atom:

$$r(t+dt) = r(t) + v(t).dt + \frac{F(t)}{2m}dt^2 \tag{2.2}$$

$$v(t+dt) = v(t) + \frac{F(t+dt) + F(t)}{2m}dt \tag{2.3}$$

Force acting on each atom i, due to the interactions with the other atoms j in the

system, can be represented by the following equation:

$$\vec{F_i} = \sum_{j \neq i} \vec{F_{ij}} \tag{2.4}$$

More details about the interactions between the atoms will be described in the upcoming sections.

2.1.2 Statistical Mechanics

Statistical mechanics employs the law of quantum and classical mechanics to bridge between the behavior of molecules at microscopic level to predict the property at macroscopic scale. For a system comprising N atoms, at the molecular level, each atom is represented by 6 variables: 3 for its position ($\overrightarrow{p}$) and 3 for its momentum ($\overrightarrow{q}$), resulting in 6N variables for such system (with N atoms). The ensemble of all these possible states are called "phase space". Let us abbreviate one particular point in phase space to be Γ (state of the system), and let us assume that an instantaneous function A(Γ) corresponds to some macroscopic property 'A' of the system. When the system evolves, Γ changes, and the A(Γ) will also change. Thus, any experimentally observable A (macroscopic property) can be obtained through time average of A(Γ) taken over a long time interval:

$$A_{obs} = \langle A \rangle_{time} = \langle A(\Gamma(t)) \rangle_{time} = \lim_{t_{obs} \to \propto} \frac{1}{t_{obs}} \int_0^{t_{obs}} A(\Gamma(t)) dt \tag{2.5}$$

Newton's equation of motion governing the time evolution of atomic positions and velocities can be solved through computers only for practical proposition, for instance for systems containing several 10^5 particles. However, investigating systems with one mole of atoms will demand solving the $6N_A$ differential equations, which is practically not possible (where N_A is Avogadro number in order of 10^{23}). And we cannot extend the integration of equation 2.5 up to infinite time, but might be satisfied over a long finite time Γ_{obs}. Therefore we may rewrite equation 2.5 as follows:

$$A_{obs} = \langle A \rangle_{time} = \frac{1}{\Gamma_{obs}} \sum_{\Gamma=1}^{\Gamma_{obs}} A(\Gamma(t)) \tag{2.6}$$

By this equation, it becomes possible to rely on the microstates of the system to obtain the macroscopic properties. Here, the microstates are the collection of N-atom configurations, each represented by 3N coordinates and 3N momenta (totally 6N), and each corresponding to one single point in the phase space (Γ). Using them in equation 2.6 will provide possibility to obtain the thermodynamic state of that particular system. A statistical *Ensemble* corresponds to a collection of points in the phase space satisfying specific conditions about the energy, the volume, the temperature or the pressure. Hence, several statistical ensembles can be defined as explained below:

1. Micro-canonical ensemble: also called NVE *ensemble*, where the number of particles (N), Volume (V) and energy (E) are fixed. This is because the system is considered to be isolated, without exchange of mass and energy. Therefore, total energy of the system will be conserved.

2. Canonical ensemble (NVT): It is a closed system that is in contact with a heat bath. As a result, the number of particles (N), Volume (V) and Temperature (T) are fixed. Energy of the system is not constant. Indeed, it is allowed to fluctuate in such a way that conditions of the ensembles are maintained. Collection of these microstates are called NVT *ensemble*.

3. Isothermal-Isobaric ensemble (NPT): It corresponds to conducting the experiments at a particular temperature and pressure. Therefore, total number of particles (N), Pressure (P), and Temperature (T) are kept constant. It is similar to the Canonical *ensemble*, with the difference that the volume is allowed to fluctuate with time.

In this thesis, we worked with all three above ensembles to prepare the glass models. As output of MD simulations performed in one specific ensemble, we will obtain a collection of trajectories in phase space (Γ) from which it is possible to extract different macroscopic properties.

2.1.3 Force Field or Potentials

MD simulation requires the description of terms (set of rules) by which the atoms of the system will interact with each other. These terms are referred to as Force field, which comprise information about all the possible interactions allowed and disallowed between the atoms present in the system. They are composed of many components called potentials that will be used to calculate the system's energy (pair terms, Van der Waals, multipolar terms, repulsion terms, angular terms, torsion terms, electrostatic contributions etc.,). Comprising all these, typical expression of the force field may look like following:

$$U = \sum_{bonds} \frac{1}{2} k_b (r - r_0)^2 + \sum_{angles} \frac{1}{2} k_a (\Theta - \Theta_0)^2 + \sum_{torsions} \frac{V_n}{2} [1 + cos(n\Phi - \delta)] + \sum_{improper} V_{imp} + \sum_{LJ} 4E_{ij} [\frac{\sigma_{ij}^{12}}{r_{ij}^{12}} - \frac{\sigma_{ij}^{6}}{r_{ij}^{6}}] + \sum_{elec} \frac{q_i q_j}{r_{ij}} \tag{2.7}$$

In this thesis, to calculate the glass structures, we used only two body terms and three body terms in addition to the Coulombic terms as it is done classically. Torsional angles and improper torsion angles are not defined for glass systems. The last two terms in the above equation correspond to the short and long-range interactions based on Lennard-Jones potential also called pair potentials (repulsive and van der waals interaction) and the Coulombic interactions. In our case, we will use an exponential repulsive term at short distance, a dipolar term in $1/r^6$ and the Coulombic interactions.

2.1.3.1 Classical dissociative potential for glass-water

In 2007, Mahadevan developed a classical dissociative potential to perform the chemical reaction between the silicate glass and water [Mahadevan and Garofalini, 2007]. The different terms of this potential are as follows. It contains two and three-body terms.

$$U_{2-body} = U_{qq} + U_{qdqd} + U_{qqd} + U_{qdqd} + U_{rep} + U_{disp} \tag{2.8}$$

$$U_{qq}(r_{ij}) = \frac{q_i.q_j}{r_{ij}} \times erfc(\frac{r_{ij}}{\beta}) \tag{2.9}$$

$$U_{qdqd}(r_{ij}) = \frac{q_i^d.q_j^d}{r_{ij}} \cdot erf(\frac{r_{ij}}{2\varepsilon_{ij}}) \times erfc(\frac{r_{ij}}{\beta}) \tag{2.10}$$

$$U_{qqd}(r_{ij}) = \frac{q_i.q_j^d}{r_{ij}} \cdot erf(\frac{r_{ij}}{\sqrt{2}\varepsilon_{ij}}) \times erfc(\frac{r_{ij}}{\beta}) \tag{2.11}$$

$$U_{qdq}(r_{ij}) = \frac{q_i^d.q_j}{r_{ij}} \cdot erf(\frac{r_{ij}}{\sqrt{2}\varepsilon_{ij}}) \times erfc(\frac{r_{ij}}{\beta}) \tag{2.12}$$

$$U_{rep}(r_{ij}) = A_{rep}^{ij} \times \frac{erfc(z_{ij})}{z_{ij}},\ where\ z_{ij} = \frac{r_{ij}}{2\varepsilon_{ij}^r} \tag{2.13}$$

$$U_{disp}(r_{ij}) = \frac{-C_6^{ij}}{r_{ij}^6} \tag{2.14}$$

Symbols used in the above equations refer to: i and j are any two atoms of the glass and water. q is the point charge of any particular atom, q_d is the diffuse charge calculated based on the distance for any particular atom. r_{ij} is the distance between two atoms. erf function will involve modifying the point charge based on distance, i.e., diffuse charge for the atom. Therefore, the charge of an atom i will be reduced as a function of distance between ij pair and the value of parameter ε. erfc function will involve modifying the charge based on long-range interactions computed through the Wolf-Summation method. In this case, parameter β will involve in modifying the charge based on long-range interaction with erfc function [Mahadevan and Garofalini, 2008].

In a nutshell, for a simple system like SiO_2 reaction with water, the charge of silicon is four times hydrogen, and the charge of oxygen is twice the opposite charge of hydrogen. The long-range terms are handled through the Wolf summation methods, and the final equation's summary looks like the following.

$$E_{tot}^{Mad}(R_C) \approx \frac{1}{2}\sum_{i=1}^{N}\sum_{j\neq 1}\frac{1}{4\pi\varepsilon_0}\left(\frac{q_i q_j erfc(\alpha r_{ij})}{r_{ij}}\right.$$
$$\left.-\frac{q_i q_j erfc(\alpha R_C)}{R_C}\right) - \left(\frac{erfc(\alpha R_C)}{2R_C} + \frac{\alpha}{\pi^{1/2}}\right)\sum_{i=1}^{N}\frac{q_i^2}{4\pi\varepsilon_0} \tag{2.15}$$

where E_{tot}^{Mad} is the Madelung energy, R_C is the cut off radius, erfc is the complementary error function and α is the damping parameter [Wolf et al., 1999]. This reduces the computational cost for calculating the coulombic interactions. The computational cost for the Wolf summation increases at the order N (linearly) [Wolf et al., 1999, Sadeghifar et al., 2012, Gdoutos et al., 2010] while the computational cost of the Ewald summation increases at the order N^2.

Similarly, three body terms were also used whose equation is below:

$$U_3(r_{ij}, r_{jk}, \Theta_{jik}) = \lambda_{jik} exp\left[\frac{\gamma_{ij}}{(r_{ij} - r_{ij}^0)} + \frac{\gamma_{ij}}{r_{ik} - r_{ik}^0}\right][cos(\Theta_{jik}) - cos(\Theta_{jik^0})]^2 \tag{2.16}$$

Three-body terms favor some particular angles (reference angles) for the H_2O molecules and around the Si environments. Three body potentials are used only for the H-O-H, Si-O-H, Si-O-Si, and the O-Si-O triplets when considering the reaction between SiO_2 + H_2O. Penalty energy is considered when the instantaneous angle differs from the reference angle.

These potentials for the simple system were further improved by incorporating Al_2O_3 and modifier elements like sodium and calcium to have the possibility to simulate hydrated SiO_2-Al_2O_3-$_3Na_2O$-CaO systems [Mahadevan et al., 2019] [Mahadevan et al., 2022]. Two-body and three-body parameter terms for such complex systems are given in Table 2.1 and Table 2.2 respectively. For sodium silicate glass, it has been shown that these potentials can reproduce the structure and density appropriately [Mahadevan et al., 2019]. Indeed, the reactivity of modifiers with water has also been validated by investigating the dissociation of NaOH in water [Mahadevan et al., 2019]. They observed that the results were in good agreement with the ReaxFF forcefield. In parallel, the parameters for hydrated calcium aluminosilicate glass were developed through the force matching technique, based on DFT calculations. Doing this has obtained a first starting set of parameters [Mahadevan et al., 2022]. These parameters have been further refined by targeting bond length and bond angle distribution to reproduce the pair distribution functions, average coordinations, and densities of the glass structure. The structure factors obtained by Neutron Diffraction experiments were also well reproduced, as shown in Figure 2.1. It is observed that the starting potentials were able to reproduce the experimental curves only at large Q values, whereas the structure factor at small Q values was mismatched in terms of intensities and positions of the peaks. After the refinement process, the reproduction of the structure factor is clearly improved and were able to reproduce the experimental data

as shown in Figure 2.1. It is concluded from this study that fitting a classical potential purely on ab initio data by Force Matching is not sufficient, and a refinement step is necessary to correct some discrepancies.

Atomic pair	A_{ij}^{rep}	ε_{ij}^{r}	C_{ij}^{6}	ξ_{ij}
O-O	265.29	0.61	26.38	24
O-H	1425.09	0.20	0.00	24
O-Si	1666.67	0.373	43.70	24
O-Ca	1530.21	0.467	9.36	9.798
O-Al	4305.12	0.347	24.97	24
H-H	0.0	1.0	0.0	24
H-Si	3121.10	0.43	23.72	24
H-Ca	0.0	1.0	0.0	9.798
H-Al	0.0	1.0	0.0	24
Si-Si	436.95	0.64	0.0	24
Si-Ca	885.27	0.57	0.0	9.798
Si-Al	0.0	1.0	0.0	24
Ca-Ca	720.10	0.71	0.0	4
Ca-Al	599.19	0.611	0.0	9.798
Al-Al	137.33	0.60	0.0	24

Table 2.1: Pair term parameters of the FMrefined potential. A_{ij}^{rep} in eV, ε_{ij}^{r} in Å, C_{ij}^{6} in eV/Å^6, ξ_{ij} in Å. The parameter β=4.46Å

Triplet	λ_{ijk}	$r_{xy}^{0}(xy = ij,\ ik\ when\ j \neq k)$	$\gamma_{xy}(xy = ij,\ ik\ when\ j \neq k)$	θ_{ijk}^{0}
Si-O-Si	6.180	2.6	2.0	109.47
Si-O-Al	637.64	2.28 / 1.98	2.06 / 1.50	139.5
O-Si-O	93.01	3.0	2.8	109.47
O-Al-O	7.99	2.08	1.68	109.20
Al-O-Al	210.80	2.00	3.47	145.0
H-O-H	187.27	1.60	1.30	100.0
Si-O-H	132.33	2.60 / 1.60	2.00 / 1.30	109.47
Al-O-H	511.23	2.24 / 1.40	2.02 / 1.50	99.9

Table 2.2: Three body term parameters of the FMrefined potential. The triplets are represented as j-i-k. λ_{ijk} in eV, $r_{xy}{}^{0}$ in Å, γ_{xy} in Å, $\theta_{ijk}{}^{0}$ in °

To further validate the refined potential, the energy between Ca-O and Al-O with respect to the distance was measured and compared to ab initio calculations. The curves (Figure 2.2) were shifted over the vertical direction to have coincidence at the minimum region. The ab initio results are well reproduced. They also measured the diffusion coefficient for Ca^{2+} and obtained a value equal to 8.81 x 10^{-10} m^2/s as shown in Table 2.3. This value is very close to the experimental diffusion coefficient of 7.9 x 10^{-10} m^2/s. In a nutshell, the refined potentials could reproduce both the dry and hydrated glass structures correctly [Mahadevan et al., 2022].

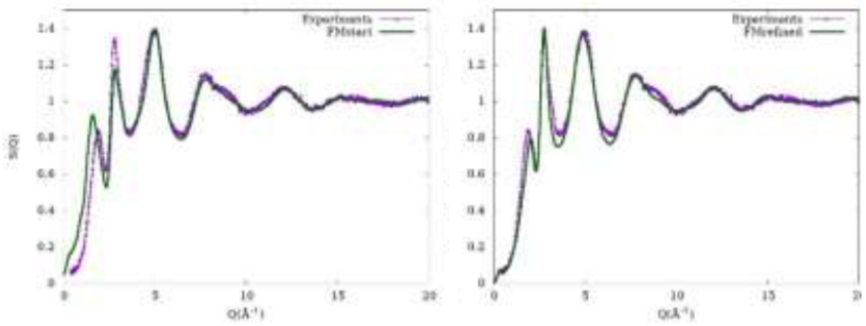

Figure 2.1: Structure factors for trajectories calculated with the two parameter sets compared separately with the experimentally measured structure factor (neutron diffraction) [Mahadevan et al., 2022].

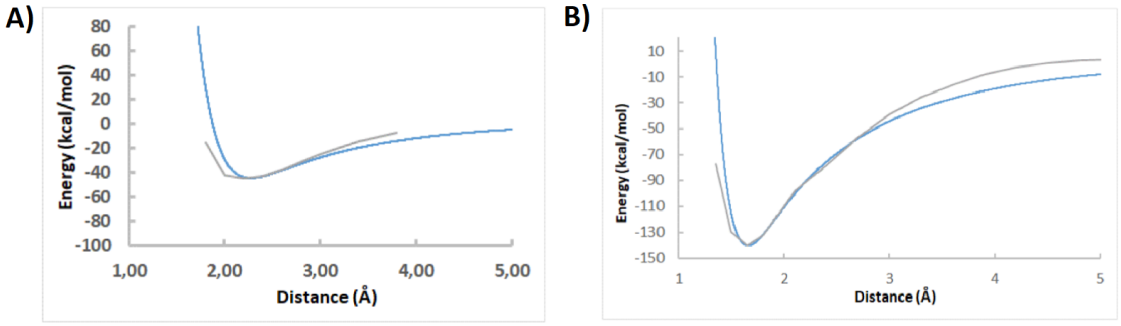

Figure 2.2: (A) Energy of the Ca-O pair calculated with the FMrefined potential (blue line) compared to the Ca-O pair energy measured by ab initio (grey line). The curves were shifted vertically to have a coincidence at the minimum. (B) Energy of the Al-O pair calculated with the FMrefined potential (blue line) compared to the Al-O pair energy measured by ab initio (grey line). The curves have been shifted vertically to coincide at the minimum. The three body potential O-Al-O is not considered. [Mahadevan et al., 2022]

Ca	O	H
8.81×10^{-10}	8.81×10^{-9}	8.81×10^{-9}

Table 2.3: Ca, O, and H diffusion coefficients in m^2/s. The Ca diffusion coefficient integrates the correction due to the finite size effect

2.1.4 Importance of force field

All the two body, three body terms, and long-range interactions used in this thesis are from Mahadevan et al [Mahadevan and Garofalini, 2008], detailed in the section 1.3.1.3. So in regard to glass simulation, we will start the system with randomly placing all the atoms. The number of atoms are calculated based on the desired glass compositions. Then, the system, submitted to the Newton's equations of motion, will reach an equilibrium state corresponding to a minimum of the energy. This process will result in developing a glass structure, which is achieved through the combination of different statistical ensembles, which are detailed in Section 2.2.1.

Due to these reasons, force fields are very important for the classical MD simulation

to develop a good model at the atomic scale. These force fields with all the body-terms and long-range interactions are developed by fitting the experimental data like X-ray diffraction, NMR etc or from ab initio calculations or semi-empirical quantum mechanical calculations. This procedure to fit the interatomic potentials used in this thesis has been detailed in section 1.3.1.3.

2.1.5 Challenges in force calculation

It is important to consider that, force computation for short range non-electrostatic interactions are not calculated for the target atom against all other atoms present in the system as that will be too computationally expensive. To solve this, a 8 Å cut-off radius will be chosen and only the atoms within the cut-off radius will be considered for the force calculations. Similarly, for long-range coulombic interactions, the Wolf et al., [Wolf et al., 1999] method will be used. This method is applied with a 10 Å radius. For each pair of atoms i-j within this radius, the Coulombic interaction is calculated normally, and the Coulombic interaction between the atom i and an image of the atom j (with an opposite charge) projected on the sphere of radius 10 Å centred on the atom i is added. It allows to calculate precisely and rapidly the Coulombic interactions by preserving the global neutrality of the system. Equation of the Wolf method with explanation is given under the section 2.2.1.

2.2 Estimating the activation energy through Potential Mean Force method and Experiments

2.2.1 Glass models preparation

Silicate and alumino-silicate glasses were modeled using the MD simulation approach with the DL_POLY software package [Todorov et al., 2006]. For preparing the silicate glass model structure, 130 Si atoms and 260 O atoms were randomly placed into a cubic simulation box initially with an edge of 18.06 Å. For preparing the aluminosilicate glass model, the simulation box contained 38 atoms of Al, 25 atoms of Ca, 252 atoms of O, and 85 atoms of Si. The positions of all atoms in the simulation box were initially relaxed for 10,000 MD steps (1 time step = 1 femtosecond) at a temperature of 1000 K. The atomic interactions in the system were described by the Mahadevan and Du [Mahadevan and Du, 2021] potential with a 8 Å cut-off radius for short-range non-electrostatic interactions while the long-range Coulombic interactions were treated by the Wolf method [Wolf et al., 1999], which is given in equation 2.15. Best choice of cut-off radius for the wolf method can be any value between 10 - 12 Å[Demontis et al., 2001, Rahbari et al., 2019], and we chose 10 Å in this study. The reason why we preferred to use this force field instead of another one, for example ReaxFF, is developed in the discussion (Section 3.3).

The glass model preparation for each system then continued in several stages. The system was equilibrated at a temperature of 4000K for 100,000 time steps in the NVT statistical ensemble (constant number of particles, constant volume, and constant temperature). Subsequently, a thermal quench was applied by decreasing the temperature of the systems 100 K by 100 K until the target 300 K temperature was reached. At each intermediate temperature, the system was equilibrated in the NVT ensemble for 20,000 steps. The equilibrium volume of the system at 300 K was then determined in a further calculation in the NPT ensemble (constant number of particles, constant pressure, and constant temperature) for 20,000 steps at a pressure of 1 bar. Finally, the systems were further relaxed for 5000 time steps in the NVE ensemble (constant number of particles, constant volume, and constant energy) using the equilibrium volume determined previously to obtain the equilibrated glass structure. The glass preparation procedure followed in this study is discussed in more details in a previous work [Jan et al., 2019a].

2.2.2 Addition of water on the glass surface

The size of the simulation box containing the equilibrated glass structures were then doubled along the z-axis to create an empty space for the addition of water molecules to form a water–glass interface. The simulation BoxA (containing the glass and the empty space) was then relaxed through a NVT-ensemble MD run for 10,000 steps at 10 K to control the mobility of atoms and allow the stabilisation of the surface. Subsequently, an additional relaxation in the NVT ensemble for 10^6 steps at 300 K was applied over BoxA

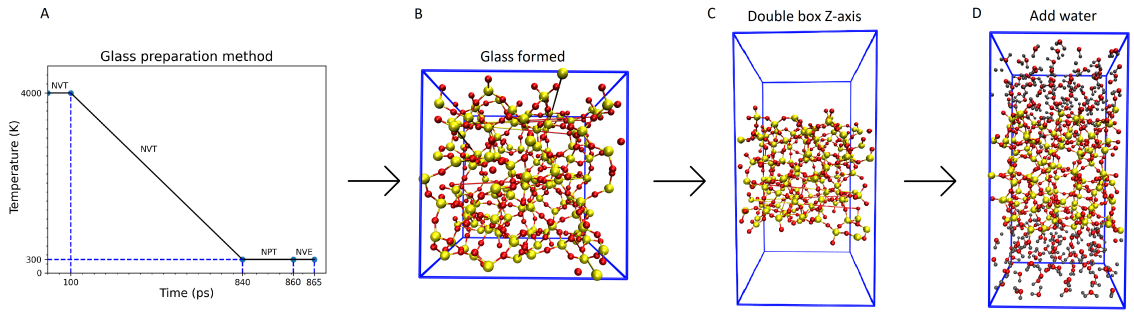

Figure 2.3: : Graphical flowchart of the glass model preparation for further PMF calculations. (A) Glass preparation procedure through classical MD simulation method. (B) Snapshot of the prepared glass as per protocol in (A). (C) Snapshot of the box size doubled along the z-axis. (D) Addition of water into the empty space of the simulation box. Color scheme: Yellow–Si glass forming element; red–oxygen atoms; gray–hydrogen atoms [Damodaran et al., 2022].

to ensure that the structure of glass remains well equilibrated. Then a final relaxation was performed in the NVE ensemble at 300 K for 5000 steps to validate that fluctuation of temperature is not far from the target.

In parallel, an empty simulation box of exactly the same size was prepared into which H_2O molecules were added randomly to equilibrate a bulk water system with a density of 1 g/cm^3 (BoxB). The water box was equilibrated under the NVT (100,000 steps) and NVE (100,000 steps) ensemble at 300 K using the SPC/E water potential to stabilize the temperature and energy of the system respectively [Berendsen et al., 1987]. To create the glass-water interface, we superimposed the two boxes BoxA and BoxB. A 0.6 Å cut-off distance was applied so that the H_2O molecules whose one atom is less than 0.6 Å from one atom of the glass are eliminated. This will ensure the water molecules close to the glass structure are removed. After this operation, we observe that a few water molecules are still present inside the rings of the glass structure. Those water molecules have been removed with the help of python scripts based on known glass region.

Dissociative potentials [Mahadevan and Du, 2021, Mahadevan and Garofalini, 2008] were used to relax the (glass + water) system in the NVT ensemble at 10 K for 100,000 steps, then at 300 K for 10^6 steps, and finally in the NVE ensemble at 300 K for 50,000 steps. These large MD steps will be sufficient to dissociate the weak Si-O-Si bonds of the glass, to form the silanol groups and equilibrates the interface between glass surface and bulk water. The timestep for these calculations are set to be 0.1 fs. In general, the timestep will be chosen sufficiently smaller than the fastest vibrating atom of the system to avoid overlapping between the atoms. Since H is present in our system, we chose 0.1 fs as the timestep to avoid the explosion of the system's energy. A pipeline in python was developed to automate the process of glass model preparation until the glass-water interface creation, and was used to prepare 17 independent glass models for pure silicate glasses and 25 independent models of aluminosilicate glasses to improve the statistics of the PMF calculations. This pipeline is presented graphically in Figure 2.3.

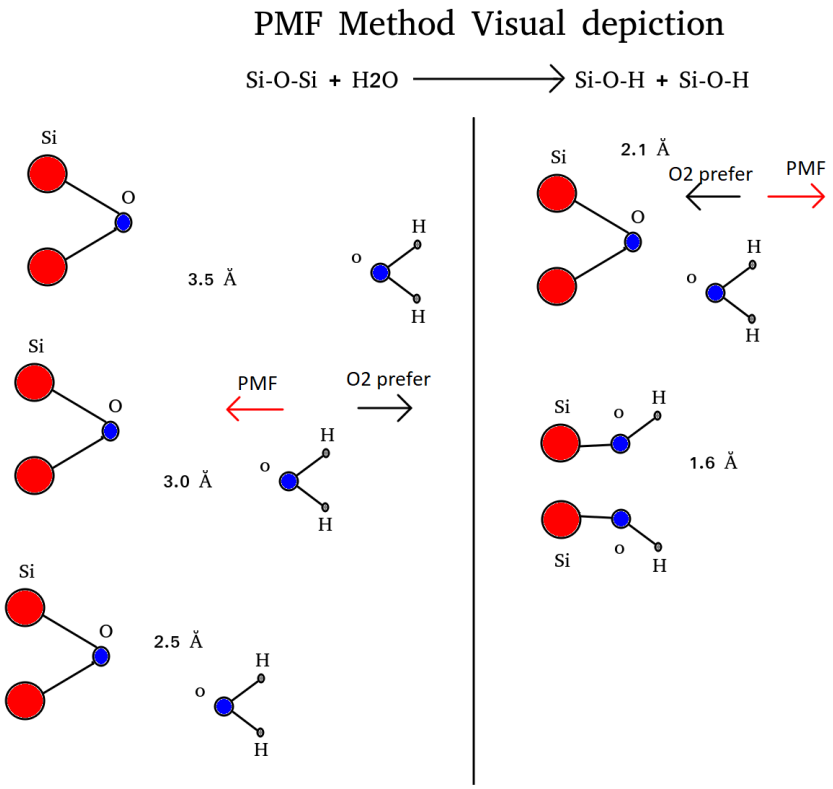

Figure 2.4: Graphical representation to explain the mechanism of PMF method for dissociating the Si-O-Si bond of glass by water.

2.2.3 Potential Mean Force (PMF)

Potential mean force (PMF) calculations were used to quantitatively estimate the activation barrier required for the hydrolysis of the Si-O-Si bonds in pure silicate glass and Si-O-X or Al-O-X bonds in aluminosilicate glass. (The second neighboring atoms of the aluminosilicate glasses are represented as X throughout the study because they can be either Al or Si). To apply the PMF method, one water molecule was progressively moved closer to one atom of the glass surface (the target atom) by gradually imposing a lower and lower distance between the two as shown in Figure 2.4. A complete PMF calculation requires a number of separate MD simulations to sample all the possible distance between water molecule and the glass atom (the reaction coordinate). In each of these "sampling windows" the distance between the reacting species is restrained at a particular position using a harmonic force to allow the system to sample all possible configurations around that particular value of the reaction coordinate. The additional force required for maintaining each intermediate distance is registered and the integration of this force along the reaction coordinate followed by the water molecule corresponds to the free energy required to approach the water molecule near the target atom of glass [Kagan et al., 2014].

To have large statistics, the PMF is performed using all the water molecules close to the glass' Si or Al atoms within a cut-off radius of 3.5 Å. When several water molecules are within the cut-off radius around one target atom, the closest water molecule to this target atom was selected. The distance constraints were applied between the O atom of

the water molecule and Si or Al atoms of the glass by gradually decreasing the distance between them by steps of 0.05 Å until the constraint distance reached 1.5 Å. For each intermediate distance, the system was relaxed with the NVT ensemble for 10,000 timesteps. The average additional force applied to maintain the separation distance was calculated during the last 9000 timesteps at each distance. Integrating the complete profile of the additional force plotted against the constraint distance between the two atoms yield the activation barrier. The method was applied to estimate the activation energies necessary to dissociate the Si-O-Si, Si-O-Al, Al-O-Si, and Al-O-Al bonds in pure silicate and in the aluminosilicate glasses. (The atom before the oxygen in this notation represents the target atom, the atom after the oxygen represents the second neighbor, and the bond is broken between the target atom and the oxygen). In some PMF calculations, water molecules did not dissociate any of the above-mentioned bridges; those activation energies were discarded to construct a clean dataset. To correlate these activation energies with structural features, we also calculated the target atoms' bond angle, local hydrostatic pressure, and shear stress. The stress tensor on one atom was calculated with the following equation:

$$\sigma_{ij}^{m} = \frac{-1}{V_m}\left[\frac{1}{2}\sum_{n=1,n\neq m}^{N} X_i^{mn} f_j^{mn} + m^m V_i^m V_j^m\right] \tag{2.17}$$

where X_i^{mn} and V_i^m are the position and velocity of the atom along the i direction, f_j^{mn} is the force exerted by the atom n on the atom m in the j direction. The summation is done over all the neighboring atoms around one particular atom using the same cutoff radii as for the classical force fields. V_m corresponds to the local volume around the atom m. Here the average volume per atom (V_{total}/N) is used. And m^m corresponds to the mass of atom m.

Hydrostatic pressure and shear stress were derived from the atomic stress tensor as follows:

$$p(i) = \frac{(\sigma_{11}^i + \sigma_{22}^i + \sigma_{33}^i)}{3} \tag{2.18}$$

$$\tau(i) = \sqrt{3p(i)^2 - \sum(i)} \tag{2.19}$$

where $\sum(i) = (\sigma_{11}^i\sigma_{22}^i - \sigma_{12}^i\sigma_{21}^i) + (\sigma_{22}^i\sigma_{33}^i - \sigma_{23}^i\sigma_{32}^i) + (\sigma_{11}^i\sigma_{33}^i - \sigma_{13}^i\sigma_{31}^i)$. These local hydrostatic pressure and shear stress exerted on the target atom are calculated [Zimmerman et al., 2004, Zhou, 2003] to correlate with the local activation energies.

2.2.4 Statistical tests to investigate the hypothesis

The quantitative data generated during these simulations were subjected to different statistical tests to investigate if the mean of two groups under comparison were significantly different or not. To investigate whether the distribution of data is normal, the Kolmogorov-Smirnov test was used when the sample size was more than 50 and the Shapiro-Wilk test was used when the sample size was less than 50 [Mishra et al., 2019, Mohd Razali and Yap, 2011]. Kolmogorov-Smirnov test assesses the normality of distribution by investigating the goodness of fit between the theoretical distribution against the sample distribution, whose formula is given in the following Equation 2.20.

$$T = sup\,|F*(X) - F_nX| \tag{2.20}$$

where, F*(X) - Hypothesized theoretical distribution, F_nX - Empirical distribution function of sample, sup - Supremum, which chooses the greatest value of the set of numbers.

Shapiro Wilk's test involves arraying the sample values based on their size (n) and measures their fit against the expected means, variance, and covariance.

$$W = \frac{(\sum_{i=1}^{n} a_i y_i)^2}{(\sum_{i=1}^{n} y_i - \bar{y})^2} \tag{2.21}$$

where, y_i is the i^{th} order statistic from the sample, $\bar{y}$ is the sample mean, a_i is coefficients, obtained from the relevant tables.

For both statistical tests, the data distribution is considered normal if the P-value is greater than 0.05, whereas it is not normal if the P-value is less than 0.05 [Mishra et al., 2019]. Non-parametric tests were selected if the distribution of at least one of the two groups under comparison is not normal, whereas parametric tests were used for the normally distributed data [Parab and Bhalerao, 2010]. For comparing the two groups of data with unequal sample sizes, we applied Welch's t-test for the parametric tests and the Mann-Whitney U-test for the non-parametric tests. For both tests, the null hypothesis states that the distribution of two samples under the comparison is very similar and the alternate hypothesis states that the distribution of two samples under the comparison is significantly different. In Mann-Whitney U-test, sample X and sample Y distribution are arranged in increasing order. Each sample of X is compared against each sample of Y, and the bigger number will be labeled. Then, the number of times a value from X or Y is bigger than the other will be calculated with n(X) and n(Y) respectively.

$$U = min(nX, nY) \tag{2.22}$$

From the 'U value' of equation 2.22, the statistical table will be used to obtain the p-value. For Welch's T-test, the equation is as follows:

$$t = \frac{m_A - m_B}{\sqrt{\frac{S_A^2}{n_A} + \frac{S_B^2}{n_B}}} \tag{2.23}$$

where m_A is the Mean of Sample A, S_A is the standard deviation of sample A, nA is the size of sample A, and the same for sample B with respect to m_B, S_B and n_B. With the T value from the equation 2.23 and calculating the degrees of freedom, P-value can be obtained from the statistical table. In both statistical tests, when a P-value is less than 0.05, it means that the two sets of data under comparison are significantly different, whereas a P-value larger than 0.05 indicates that the difference between the means of the two data sets is not statistically significant.

2.2.5 Leaching experiments of ISG-AL-05 and ISG-AL-06 in distilled water

Leaching experiments were performed with the ISG-AL-05 (40.6 SiO_2, 16.8 Al_2O_3, 16.5 B_2O_3, 4.8 CaO, 18.3 Na_2O, 3.1 ZrO_2 in mass %) and ISG-AL-06 (26.4 SiO_2, 26.5 Al_2O_3, 15.7 B_2O_3, 4.5 CaO, 23.8 Na_2O, 3 ZrO_2 in mass %) glass powders with particle size range of 75–150 μm. These two glasses belong to a series of glasses already studied numerically and experimentally, whose preparation can be find in [Lu et al., 2021, Reiser et al., 2021]. The specific surface area, measured by the Brunauer, Emmett and Teller (BET) method, was equal to 220 cm^2/g and 210 cm^2/g, respectively, and the leaching solution was 18 MΩ.cm deionized water initially adjusted and maintained during the experiment at $pH^{90°C}$ 7. Small quantity of lithium chloride was added to help the probe sense and optimize the pH of the distilled water.

Then 0.1072 g of ISG-AL-05 and 0.0430 g of ISG-AL-06 was added to the 250 ml and 400 ml of the solution, respectively, to investigate the initial dissolution rate of these two glasses. Samples were taken from the solution containing the ISG-AL-06 powder every 45 min during the 4 h of the experiment and from the solution containing the ISG-AL-05 powder at every hour during the 7 h of the experiment. Then the samples were analyzed by inductively coupled plasma-optical emission spectrometry (ICP-OES at FiLAB – Laboratoire d'analyses en chimie organique, minéraux et matériaux in France) with ± 5 % uncertainties to estimate the concentration of Si, B, Al and Na released from the glass powders. From the concentration data, the normalised mass loss was calculated as follows:

$$NL(i)(g \cdot m^{-2}) = \frac{C(i) \cdot V}{S.X_i} + \sum NL(i)_{samplings} \tag{2.24}$$

where C(i) is the concentration of an element i in the solution, V is the solution volume, S is the glass surface area, X_i is the mass fraction of i in the glass, and $\sum NL(i)_{samplings}$ represents the contribution of the various samples taken in the leachate.

The initial dissolution rates of the two glasses, r_0, were calculated from linear regression of the normalized mass loss of Si. To capture the dissolution of the first few nanometers of polished glass, coupons of ISG-AL-05 and ISG-AL-06 were prepared, and both were leached in distilled water at neutral pH, 90 °C for 1 h and 5 min, respectively. The altered glass surfaces were analyzed by X-ray photoelectron spectroscopy (XPS) and by time-of-flight secondary ion mass spectrometry (ToF-SIMS). XPS (NOVA – KRATOS, TESCAN ANALYTICS, France) was used to quantitatively estimate the elemental composition of the glass surface before and after leaching for both the coupons. The analysis was conducted with a 75 W Al Kα beam, with charge compensation and a 0° detection angle. The analyzed surface was 300 × 700 μm^2 and the depth of analysis was < 10 nm. The uncertainty on the Al/Si ratio was estimated to be around 10%. ToF-SIMS (IONTOF GmbH TOF 5 spectrometer, TESCAN ANALYTICS, France) was used to perform a semi-quantitative depth-profiling analysis of the altered ISG-AL-05 sample. The analysis was performed under the following conditions: primary beam of Bi_1^+ 25 KeV-1.7 pA and O_2^+ 1 KeV, 306 nA to record positive ions in the analysis area of 60 × 60 μm^2 and 190 × 190 μm^2, respectively. More detailed information about the application of ToF-SIMS to glass analysis can be found elsewhere [Collin et al., 2019].

2.3 Activation energy for Dissociation, Reformation, and validating PMF results with ReaxFF

2.3.1 PMF method to calculate activation energy for dissociation and reformation

An automated pipeline was constructed to perform all the above sections from the glass model preparations, preparation of the interface with water, estimation of the activation energy by the Potential Mean Force method until the final statistical analysis. Using this pipeline, we investigated 6 different glass compositions as shown in Table 2.4. For each composition, we developed multiple glass models to estimate the activation energy for the dissociation of bonds around Si and Al as shown in Table 2.5. We have also categorized the activation energy of Si based on number of Al as second neighbors for each type of glass. The activation energy for the chemical reaction between water and glass is estimated through integrating the positive region of the PMF curve as shown in Figure 2.5. The principle is, we will compute the force required to push the water molecule from its initial position towards the glass target atom. When the force is positive, the water molecule will prefer to go back to its initial position as shown in the Figure 2.4. Whereas, when the distance between the oxygen of water molecule and Si of the glass decreases less than around 2.1 Å, the oxygen is attracted by the target atom. As a result the PMF constraints will act against this pulling force as shown in Figure 2.4. This is why the PMF curve becomes negative, while decreasing the distance below 2.1 Å. When the distance decreases less than 1.6 Å, there is a strong repulsion between the two atoms due to unfavourable contact. So by integrating the negative part, roughly between 2.1 and 1.6 Å (PMF curve shown in Figure 2.5), we obtained an over estimation of the bond reformation energy around the target atom.

Glass types	**SiO2**	**Al2O3**	**CaO**	**Na2O**
Pure silicate glass	100	-	-	-
CASN1 glass	65.89	14.72	19.3	-
CASN2 glass	65.6	14.8	14.6	5
CASN3 glass	65.6	14.8	9.6	10
CASN4 glass	65.6	14.8	4.6	15.0
CASN5 glass	65.28	15.28	-	19.42

Table 2.4: Composition of the pure silicate, calcium aluminosilicate, sodium aluminosilicate, sodium lime aluminosilicate glasses used for estimating the activation energy of Si and Al. Glass compositions are given in molar percentages.

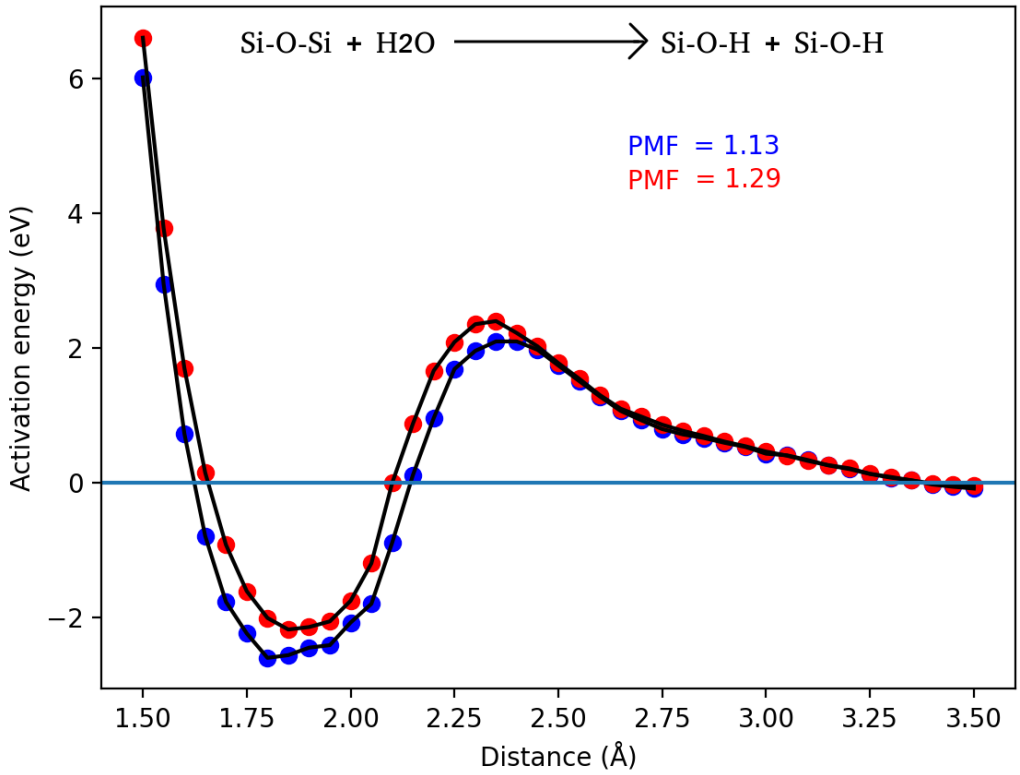

Figure 2.5: Example of a PMF curve for two chemical reactions for water dissociating silicate glass.

Glass types	Number of glasses	Number of chemical reactions	Target element for the reaction
Pure silicate glass	17	302	Si
CASN1 glass	25	227	Si
CASN1 glass	25	68	Al
CASN2 glass	14	177	Si
CASN2 glass	14	to cal	Al
CASN3 glass	25	267	Si
CASN3 glass	25	98	Al
CASN4 glass	14	150	Si
CASN4 glass	14	to cal	Al
CASN5 glass	18	210	Si
CASN5 glass	18	78	Al

Table 2.5: Details about the number of chemical reactions performed for each glass targeting the Si and Al

2.3.2 ReaxFF method to investigate the chemical reaction between water and silicate/aluminosilicate glass

Lammps package [Plimpton, 1995] were used to perform some Steered Molecular Dynamics (SMD) [Izrailev et al., 1999] simulations to estimate the activation energy of Si and

Al in silicate and sodium aluminosilicate glass using the ReaxFF force field [Deng et al., 2020, Hahn et al., 2018, Yu et al., 2017]. In SMD, a time-dependent external spring force is applied between the water and Si or Al of the glass. During this chemical reaction, potential mean force along the reaction coordinates can be computed through Lammps package. We prepared the pure silicate and sodium aluminosilicate glasses with the composition as shown in the Table 2.4 through the classical dissociative potential developed by Mahadevan et al., [Mahadevan and Du, 2021]. Among the 6 glasses listed in Table 2.4, we selected only pure silicate and CASN5 glass for the ReaxFF calculations. The structures corresponding to the glass-water interfaces are further optimized using the ReaxFF force field by relaxations in the NPT and NVT ensembles (Nose-Hoover barostat and thermostat). The glass structures are optimized in the NPT and NVT ensembles for 1000000 timesteps. Long-range coulombic interactions were performed with the Ewald summation and the short-range cutoff was defined as 8.0 Å. We selected the water molecules that are 3.5 Å away from the Si belonging to the surface of the glass. Then applied a pulling velocity of 0.00005 Å/timestep to the water with a spring constant of 1000 $\frac{Kcal}{mol.Å}$, will apply the force of 0.05 $\frac{Kcal}{mol}$ for every timestep, to push the water molecule towards the target atom of glass. During this process, the water molecule is free to rotate or even explore different paths to reach the target Si or Al, meaning that there is no rigid constraints applied on the distance between the water molecule and the target atom unlike in potential mean force method. All these above calculations were performed with the timestep of 0.1 fs.

2.4 Long-term glass dissolution experiments and Monte Carlo simulations

2.4.1 Development of the glasses and analyzing the composition

To prepare 6 SBNA glasses with compositions given in the Table 2.6, corresponding mass of the oxides were weighed to finally obtain a 200 gram bar for each glass. The measured oxides were mixed well to pour on platinum/rhodium crucible. Then crucible containing oxides was heated in furnace with increasing temperature of 300°C/h for 3 hours to reach 850°C, and maintained the same temperature for 1 hour. Then we continued to increase the temperature at the same rate to reach the target of 1450°C. After 3 hours and 20 minutes, the furnace was opened at 1450°C to directly take the crucible containing the glass melt and pour it on the steel slab at room temperature. After overnight cooling at room temperature, the glass was broken and remelted in the furnace, to reach a final temperature of 1450°C. Details are provided in Figure 2.6. Simultaneously, a graphite mold was pre-heated in another furnace at 550°C (Tg - Glass transition temperature) to prepare the glass slab from the melt. Then the glass molten at 1450°C was directly transferred onto the graphite mold at 550°C. Then T is decreased at the rate of 50°C per hour to the room temperature. We prepared 12 small coupons for each glass slab with dimensions of 20 x 20 x 1 mm^3. All the faces of the coupons were polished upto

grade 4000. The compositions of these glasses were measured from the coupon (SEM) and from the powder (ICP-OES). SEM results are shown in Table 2.7. It can be noted that the actual glass compositions are very close to the nominal ones. ICP-OES results are shown in Table 2.8. They confirm that actual glass are in close agreement with nominal compositions.

Wt%	**SiO_2**	**B_2O_3**	**Na_2O**	**Al_2O_3**
SBNA1	65.6	20.2	14.2	0
SBNA2	61.2	18.9	13.3	6.6
SBNA3	57	21.9	15.5	5.6
SBNA4	60.5	20.8	17.1	1.6
SBNA5	57.9	22.3	18.2	1.6
SBNA6	62.4	17.2	10.9	9.5

Table 2.6: Theoretical glass compositions of all the six glasses designed to investigate the influence of Al on aluminoborosilicate glass

SEM ANALYSIS %	SiO_2		Na_2O		Al_2O_3	
Sample name	SEM	Theoretical	SEM	Theoretical	SEM	Theoretical
SBNA1	65.7	65.6	11.9	14.2	0	0
SBNA2	60.4	61.2	11.7	13.3	7	6.6
SBNA3	57.9	57	13.2	15.5	6.2	5.6
SBNA4	60.5	60.5	14.9	17.1	1.7	1.6
SBNA5	58.8	57.9	15.3	18.2	1.7	1.6
SBNA6	60.6	62.4	10	10.9	9.6	9.5

Table 2.7: Comparison of SEM analyzed compositions with theoretical compositions of the six glasses

ICP-OES %	**SiO_2**	**Na_2O**	**Al_2O_3**	**B_2O_3**
SBNA1	69.6	12.7	0	17.7
SBNA2	63.4	12.7	6.6	17.2
SBNA3	59.4	15	5.7	19.9
SBNA4	63.6	16.2	1.6	18.6
SBNA5	62.1	16.8	1.7	19.4
SBNA6	62.9	10.6	9.6	16.9

Table 2.8: Compositions of the six glasses analyzed with ICP-OES

2.4.2 Long-term glass alteration experiments

Long-term leaching experiments were performed with the 6 SBNA glass powders (particle size ranging between 40 - 100 μm). Experiments were conducted in 60 ml perfluoroalkoxy alkane (PFA, Savillex) vessels without magnetic stirrer. Then powder of mass between 3.2092 to 3.8791 g were added to 50 ml of distilled water with pH9 (adjusted with LiCl) at 90°C to maintain the surface area of glass on volume of distilled water (SA/V ratio) to be around 50 cm^{-1}. High SA/V ratio is chosen to quickly allow the solution to saturate

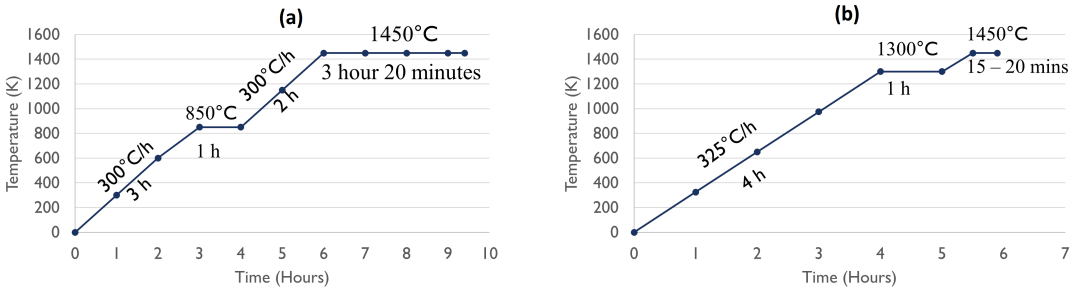

Figure 2.6: Temperature of the furnace with respect to time in hours during the glass preparation process: (a) Phase I, (b) Phase II

with silica and to investigate the residual alteration rate. The specific surface area of these glasses were measured with Brunauer, Emmett and Teller (BET) method and it is in range between 645 - 780 cm^2/g for the 6 glasses. More details for each glass are given in the Table 2.9. Then approximately 0.5 ml of samples were taken with a syringe, filtered with a 0.2 μm pore size filter and diluted with 2 ml of 0.5 N HNO_3. These samples were collected at regular intervals every 7 days during first month and then every 15 days for the next 5 months. Collected samples were analyzed with inductively coupled plasma-optical emission spectrometry (ICP-OES from FiLAB – Laboratoire d'analyses en chimie organique, minéraux et matériaux in France). Concentrations of Si, B, Na, and Al are given with an uncertainty of ± 5%. Once the solution gets saturated with Si, we calculated its speciation in the solution through Jchess geochemical code [Van Der Lee et al., 2003] using the thermodynamics database named CTDP [CTD,]. Silica species considered mainly for the calculations are H_4SiO_4, H_3SiO_4 and $NaHSiO_3$. $H_2SiO_4^{2-}$ can also be calculated but expected to be low in the basic pH.

Glass name	**Volume of solution (ml)**	**Mass of powder (g)**	**Specific surface area of powder (cm^2/g)**	**Total surface area (cm^2)**	**SA/V (cm^{-1})**
SBNA1	50	3.6	690	2502.5	50
SBNA2	50	3.5	720	2500.8	50
SBNA3	50	3.5	715	2590.6	51.8
SBNA4	50	3.9	645	2336.9	46.7
SBNA4_R	50	3.9	645	2336.9	46.7
SBNA5	50	3.5	720	2608.7	52.2
SBNA6	50	3.2	780	2826.1	56.5

Table 2.9: Details of long-term glass alteration of 6 glass powders along with the solution

To investigate the gel formation mechanism, we prepared ^{29}Si rich solutions at 280 ppm concentration with pH9 at 90°C. The 6 SBNA glass coupons were added into the solution in different containers and incubated at 90°C for 1 month. Then 0.5 ml of sampling were taken once in every 7 days and diluted with 2 ml of HNO_3. These samples were analyzed with inductively coupled plasma-optical emission spectrometry (ICP-OES from FiLAB – Laboratoire d'analyses en chimie organique, minéraux et matériaux in France) to measure the concentrations of Si, B, Na and Al in the solutions. The SBNA glass coupons were

recovered after 1 month, and incubated in tracing solution containing 99% of $H_2{}^{18}O$ for 24 hours. We performed ToF-SIMS in both positive and negative mode to investigate the depth wise ratio of $^{29}Si/^{28}Si$ and $^{18}O/^{16}O$ in the alteration layer. ToF-SIMS analysis carried out in Tescan Analytics, Fuveau, France using ToF-SIMS 5 spectrometer (Iontof – Münster, Germany), with following conditions for positive mode: primary beam of Bi_1+, 25 keV, I 0.2 pA with analyzed area of 50 x 50 μm^2 and sputter beam of 1 keV, I 300 nA Cs+ with abrasion area of 200 x 200 μm^2. Similarly, ToF-SIMS conditions of negative mode were: Primary beam of $Bi_3{}^{++}$, 25 keV, I 0.1 pA with analyzed area of 50 x 50 μm^2 and sputter beam of 2 keV, I 94 nA Cs+ with abrasion area of 200 x 200 μm^2.

2.4.3 Monte Carlo method

As in the previous Monte Carlo methods described in the literature, this new Monte Carlo approach is based on an ordered network to represent the glass structure, the solution and the interface between them. The network corresponds to a cubic one. Which means a set of nodes connected to six other nodes at the summits of a cubic network. In order to introduce four coordinated elements like Si, Al and B, some bonds are suppressed.

Once the glass composition (SiO_2-Al_2O_3-B_2O_3-Na_2O type) is chosen, the required quantity of Si, Al and B atoms are located randomly on the network. Depending on the Na_2O concentration, the B atoms can be tri or tetra coordinated if we consider that one Na atom is able to compensate one B atom. The non-compensated B atoms are considered tri coordinated. To introduce the tri coordinated B atoms, the procedure used is as follows. Two B atoms are located conjointly on two neighboring sites connected with each other, and the bond between the two nodes are removed. This procedure is not modified in comparison with the previous Monte Carlo algorithm.

Eventually, the network contains tetra-coordinated species (Si, Al, B) and tri-coordinated species (B). An example of an ordered network representing the solid part of the system is represented on Figure 2.7. In the remaining of the manuscript, this ordered network will be called "the solid network".

A major difference compared to the previous Monte Carlo algorithm is the definition of a second sub network, called the "liquid network" to simulate the glass – water interactions. This liquid network is used here to host the solution. The nodes of this liquid network are located at the center of the bonds connected two nodes on the solid network. It means that the liquid network is intricated with the solid network. The red points on Figure 2.7 represent some nodes able to host water molecules. They are located between two nodes containing atoms from the glass.

Initially, the glass is incorporated on one part of the solid network, and a second part is left empty. The water molecules are introduced on the nodes of the liquid network corresponding to the empty part of the solid network. By this method, an interface between the liquid and solid networks are created.

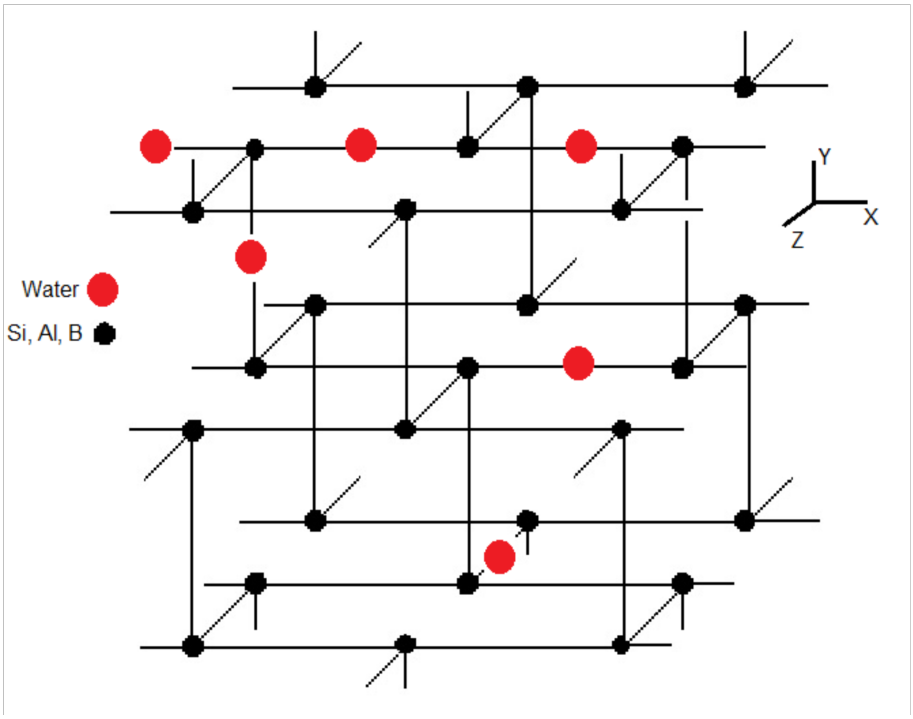

Figure 2.7: Ordered network to represent the solid glass. It contains tetra-coordinated species (Si, Al, B) and tri-coordinated species (B).

Two intricated networks for the solid and liquid phases are used to allow diffusion of water molecules inside the solid network without hydrolysis in addition to the classical hydrolysis mechanisms used previously. At the beginning of a Monte Carlo calculation, a part of the solid network is filled with the glassy species leaving empty the nodes of the upper part of the solid network. Then, the liquid network is filled with water molecules in the upper part, leaving the nodes representing the glass to be empty. Figure 2.8 shows an example of such initial network.

Once the initial network is prepared, a Monte Carlo calculation consists of simulating the different mechanisms to represent the glass alteration and the gel layer formation. Several mechanisms are considered, and for each mechanism a probability is associated to regulate its occurrence. We will now list these different mechanisms.

The first mechanism corresponds to the diffusion of water on the liquid network. A probability is defined to regulate the jump frequency of the water molecule from one site to another. This probability is called Wjump. One water molecule can jump only on neighboring sites of the liquid network which are empty. At the beginning, the solution and the glass are separated, but rapidly because of the diffusive jumps, the water molecules can occupy interstitial sites inside the solid network. In consequence, when one water molecule has jumped inside the glass, it can be located at the center of a bond joining two atoms of the glass and hydrolysis of the bond becomes possible. When one water molecule belonging to the main solution jumps on the solid network, a new water molecule is introduced on the initial site. We consider here that the main solution is an infinite reservoir.

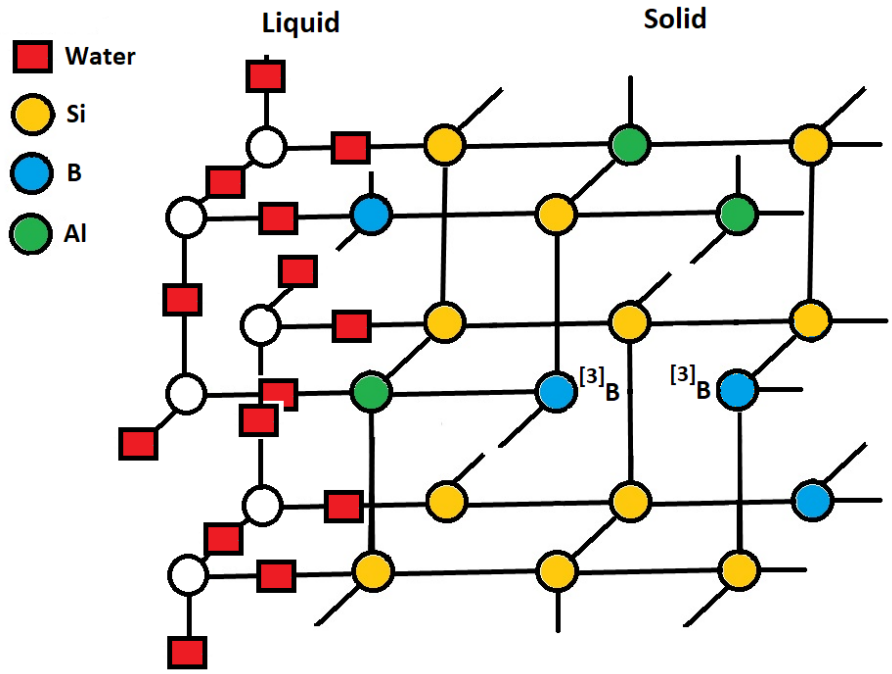

Figure 2.8: Example of an initial network used to start a Monte Carlo calculation. The water molecules (red) are located at the center between the two nodes on the empty part of the solid network (on the left). The atoms (Si in yellow, Al in green, B in blue) are located on the full part of the solid network (on the right). An example of two B3 introduced as a pair is also represented. In this case, the bond between the two B atoms is removed.

The second mechanism corresponds to the breakage of a bond on the solid network. The breakage probability is called wbreak. Several probabilities can be used depending on the chemical nature of the X-O-Y bonds (X, Y = Si, Al). When one water molecule is located at the center of a X-O-Y bond containing a boron atom, the hydrolysis is immediate i.e. the probability of hydrolysis is equal to 1.0. We consider that the B atoms are much more soluble than the Si or Al atoms. The breakage of a X-O-Y bond corresponds to the following chemical reaction:

$$X - O - Y + H_2O \rightarrow X - O - H + Y - O - H \tag{2.25}$$

Due to the hydrolysis mechanisms, the glassy structure is progressively depolymerized with the formation of non-bridging oxygen atoms.

The third mechanism corresponds to the possibility for chemical bonds to reform. This mechanism is controlled by a probability called wrefor. This mechanism is not applied for the bonds removed initially on the cubic network to introduce tri or tetra coordinated nodes. Also a bond can't be reformed around a B atom. When a X-O-Y bond (X, Y = Si, Al) is reformed, it corresponds to the following chemical reaction:

$$X - O - H + Y - O - H \rightarrow X - O - Y + H_2O \tag{2.26}$$

After the application of a reformation mechanism, one water molecule is reintroduced on the liquid network and can again diffuse on the liquid network inside the solid network.

As the glassy network is progressively depolymerized, it can happen for an atom (Si, Al or B) to be completely surrounded by broken bonds. Then these atoms can be released in solution. It corresponds to the fourth mechanism.

For the Si and Al atoms, two cases are considered. If these atoms completely surrounded by broken bonds, and in contact with the main solution, then they are hydrolyzed i.e. they are released in the main solution. If they are not in contact with the main solution, they remain on their sites. The main solution (or ocean) is defined here as the collection of water molecules connected to the initial solution.

For the B atoms completely surrounded by broken bonds, they are immediately dissolved into the main solution irrespective of their locations. In future, it will become possible to make them diffuse on the liquid network before reaching the main solution, but this option is not considered for the simulations described here.

Following the glass dissolution process, the concentrations of Si and Al increase in the solution. The fifth mechanism consists in considering the possibility for a Si and Al atom dissolved in the solution to be redeposited at the glass – water interface. The glass – water interface is defined as the ensemble of sites of the solid network in contact with a water molecule belonging to the ocean. The probability regulating this redeposition is called wred. Lets consider the case of the Si atoms. If CSi is the concentration of Si in solution, the quantity of Si atoms redeposited during one Monte Carlo step is given by wred * CSi. The redeposited Si atoms are located randomly on the available sites at the glass – water interface. The same procedure is applied for the Al atoms. This step allows forming progressively the alteration layer enriched in Si and Al between the pristine glass and the main solution.

The sixth mechanism concerns the possibility for a vacancy to jump on the solid network. When the B, Si and Al atoms completely surrounded by the broken bonds are released in solution, they leave an empty site, i.e. a vacancy, on the solid network. We considered the possibility for these vacancies to diffuse on the solid network with a probability called wvacan. Different probabilities can be considered depending on the change of the number of neighboring vacancy pairs after the jump. In particular, a larger probability could be applied to favor the clustering of vacancies i.e. when the number of neighboring vacancy pairs increases after a jump. It allows forming progressively larger and larger pores. It is to be noted that when a vacancy jumps, the broken bonds are reorganized around the exchange sites in order to keep the same number of broken bonds. A vacancy jump is neither associated to a hydrolysis or a reformation mechanism.

The seventh mechanism corresponds to the possibility for a water molecule located on the liquid network to jump into a neighboring vacancy on the solid network. When a water molecule is located on a site which is a neighbor of an empty vacancy, the water molecule is displaced into the vacancy systematically and is removed from the liquid network.

The eighth mechanism consists in removing the clusters formed by atoms of the solid network that are isolated in the ocean. When such clusters are detected, they are suppressed and the Si and Al atoms of the clusters are released into the solution. The Si and Al concentrations in the main solution are increased accordingly.

In summary, the different steps corresponding to the application of this new Monte Carlo algorithm are the following. First, the initial network representing the interface between the solid and liquid networks is built. Then several steps are applied to simulate the glass alteration and each step is separated into multiple elementary mechanisms:

1. Determination of the water molecules belonging to the "ocean" and the isolated water molecules.
2. Determination of the possible jump events for one water molecule on the liquid network. The events are carried out depending on the probability wsaut.
3. Determination of the possible breakage events for the chemical bonds on the solid network. The breakages are carried out depending on the probability wbreak.
4. Determination of the possible events for the bond reformation. The reformation is applied depending on the probability wrefor.
5. Determination of the water molecules belonging to the ocean and of the isolated water molecules.
6. Determination of the possible events for the release of Si, Al and B atoms into the solution. The Si and Al atoms completely hydrolyzed are released if they are in contact with the ocean. The B atoms completely hydrolyzed are released in any case.
7. Determination of the water molecules belonging to the ocean and of the isolated water molecules.
8. Elimination of the solid clusters isolated in the ocean.
9. Determination of the possible events for the Si and Al redeposition at the glass – water interface. The events are carried out depending on the probability wred.
10. Determination of the water molecules belonging to the ocean and of the isolated water molecules.
11. When a vacancy on the solid network has one or more neighboring water molecules located on the liquid network, this vacancy is filled with one water molecule chosen randomly among the neighbors. This selected water molecule is then removed from the liquid network.
12. Determination of the possible events for a vacancy (filled or empty) to jump on the solid network. The events are carried out depending on the probability Wvacan. The clustering of vacancies can be favored using different probabilities.

2.4.3.1 Details about calculating the probabilities from Monte Carlo parameters

To reproduce the long-term experimental release of Si and B into the solution, we controlled three important parameters of Monte Carlo as given in the Table 2.10.

Parameters	**Role**
Wsaut	Jump of the water molecules on the liquid network
Wbreak	Opening of the chemical bonds
Wrefor	Reformation of the chemical bonds
Wred	Redeposition of the Si and Al atoms at the glass – water interface

Table 2.10: The different probabilities used in the Monte Carlo code and their roles

1. Wbreak - Probability to break the bond around one Si/Al in the glass is derived from this parameter. For every bond superimposed with a water molecule, a random number (RandN) is generated between 1 to 100000. If RandN is lower than Wbreak, then bond is broken. This explains why the probability Wbreak presented in Chapter 5.1 could be larger than 1.

2. Wred - Probability for a Si/Al atom to redeposit on the surface of the glass is derived from this parameter. Prob(Si+Al) = Wred * Conc of Si+Al in the solution. Ref_num = Generate random number between 1 to Prob(Si+Al). For each atom that can be redeposited, a random number between 1 to Prob(Si+Al) is generated. If this number for that particular site is the same as Ref_num, then the Si/Al atom is redeposited. Here again, it explains why the probability Wred could be larger than 1.0. But it has to be noted that the probability of redeposition increases when this parameter increases.

3. Wsaut - It is the probability for a water molecule to jump from one site to another. For example: If Wsaut is equal to 1/5, it means there is 1 chance over 5 for the water molecule to jump.

One complementary point has to be specified to complete the previous scheme. It concerns the introduction of an additional parameter called srempt. This parameter defines the maximum percentage of sites on the liquid network that can be occupied by water molecules. Only the water molecules not belonging to the ocean are considered. In fact, the probability for a water molecule to jump on the liquid network is multiplied by the term (srempt – srempli)/srempt. The quantity srempli corresponds to the current percentage of sites occupied by the water molecules. It means that the jump probability is equal to zero when the maximum quantity of sites that can be occupied by water molecules is reached. In this case, no additionnal water molecules coming from the ocean can penetrate on the liquid network. When water molecules continue to diffuse deeper on the liquid network, the quantity srempli decreases, and the penetration of water molecules

coming from the ocean can restart. In practice, a stationnary state is reached after several thousand steps. If no limit is applied to the quantity of water molecules on the liquid network, the liquid network will be rapidly completely filled with water which is non-physical. A value of 10% is chosen for the parameter srempt.

When a Monte Carlo calculation is performed, the water molecules initially in the ocean progressively penetrate on the liquid network. The atoms of the glass can be hydrolyzed and released in solution and it is possible to follow the quantity of elements (Si, Al or B) released in solution versus time. An alteration layer, hydrated and porous, forms between the pristine glass and the main solution and the ripening of this alteration layer is simulated thanks to the migration of vacancies on the solid network.

Outputs from Monte Carlo:
Monte Carlo calculation will be stopped once all the B from the glass are released into the solution or when the defined number of Monte Carlo steps is reached. At this stage, Monte Carlo code will produce a three dimensional structure of the altered glass, that can be visualized slice by slice with VMD visualizing tool. Another file contains different information concerning the gel, the number of Si, B, Al, water belonging to the ocean, isolated water, number of voids. For every 100 Monte Carlo steps, we will get the number of elements (B, Si, Al) in the solution, water belonging to the ocean, isolated water, etc. Based on the number of Monte Carlo steps it takes to saturate the solution with Si, we will equate this to the experimental duration to determine the equivalence in second of one Monte Carlo step. In consequence, the absolute duration of one Monte Carlo step depends on the experiment we try to reproduce. The objective is to reproduce the experimental data using the Monte Carlo code (Chapter 5.1).

2.5 Behavior of B

2.5.1 Assessing the role of pore water elements in gel against glass alteration

International simple glass (ISG) composition of SiO_2 – 60.2, B_2O_3 – 16.0, Na_2O – 12.6, CaO – 5.7, Al_2O_3 – 3.8, and ZrO_2 – 1.7 in mol% was used throughout this study. To investigate the role of B and Ca retained in the 7-year-old altered sample, the concentration of each element was calculated from the ToF-SIMS profiles [Gin et al., 2020a] and displayed in Supplementary Table 1. The estimated concentration of elements present in the gel is higher than the saturation with respect to secondary phases such as Na, or Ca bearing borate minerals. Since this study proposes to mimic the gel pore water, a clear solution was prepared with maximum concentrations of all the required elements but avoiding precipitation. Following chemicals were used to saturate the solutions: SiO_2 (99.5% purity – Alfa Aesar), NaCl (>99% purity, VWR International), $B(OH)_3$ (>99.9% - VWR chemicals), and $CaCl_2$ (98.0% purity - Merck KGaA). The concentration of three solutions are Sol. 1 : B – 7000 ppm, Ca – 6000 ppm, Na – 24000 ppm, Si – 180 ppm, Sol. 2 : B – 7000 ppm, Na – 24000 ppm, Si – 180 ppm, Sol. 3 : Ca – 6000 ppm, Na – 24000 ppm, Si – 180 ppm. Concentrations are given with 5% uncertainty. For all three solutions, Si was dissolved at first, and we verified the concentration with UV spectrophotometer before adding the other elements. According to previous studies, the concentration of Si in the onset solutions insures that an aluminosilicate gel, occupying the same volume as that previously occupied by the glass (isovolumetric alteration), will form with almost no Si atom of the solid exchanged with that of the solution [Gin et al., 2015, Gin et al., 2017a]. The pH of these solutions were maintained at neutral conditions between 6 to 7 at 90°C by using diluted LiOH and HNO_3 solution. An ISG coupon (8 x 8 x 1 mm^3, polished up to 1µm grade (< 5 nm roughness)) was added to each solution of 25 ml volume (SA/V ratio was 1.6 cm^2/25 cm^3 = 0.064 cm^{-1}). The coupon was taken out after 21 days, and put in the $H_2{}^{18}O$ tracing solution ($^{18}O/^{16}O$ ratio of 12, for 24 hours at 25°C and neutral pH). Then the coupon was analyzed with ToF-SIMS in negative mode to quantify the amount of ^{16}O in the gel exchanged with ^{18}O from the tracing solution. ToF-SIMS analysis carried out in Tescan Analytics, Fuveau, France using ToF-SIMS 5 spectrometer (Iontof – Münster, Germany), with the following conditions: primary beam of Bi^{3++}, 25 keV, I 0.1 pA with analyzed area of 50 x 50 m^2 and sputter beam of 2 KeV, I 150 nA Cs^+ with abrasion area of 200 x 200 m^2. To investigate the behavior of Ca, all three above coupons were analyzed with ToF-SIMS in positive mode under following conditions: primary beam of Bi^{3++}, 25 keV, I 0.5 pA with analyzed area of 50 x 50 m^2 and sputter beam of 1 KeV, I 240 nA Cs^+ with abrasion area of 200 x 200 m^2. Detailed calculations on processing these ToF-SIMS data are given in the supplementary methods.

2.5.2 Tracing the ^{10}B in gels formed in basic and acid pH conditions

Two Si-saturated solutions were prepared at pH 3 and 9 at 90°C with a concentration of 160 ppm and 280 ppm, respectively (close to saturation with respect to amorphous silica). A fresh ISG coupon (8 x 8 x 1 mm^3, polished up to 1µm grade (< 5 nm roughness)) was placed into each solution of 10 ml volume (SA/V ratio is 1.6 cm^2/10 cm^3 = 0.16 cm^{-1}). The coupon was taken out after 1 hour and 48 hours from pH 3 and pH 9 solution, respectively. It was then rinsed with deionized water, and dried at room temperature in a dry atmosphere. During this process, it was noticed that a small amount of Si from the solution deposited on the surface of the gel. To differentiate the precipitate of SiO_2 from the gel, Zr was used as a marker of the gel, as Zr does not dissolve during the alteration process. This first stage of the experiment was dedicated to the preparation of gels with thickness close to (70-90 nm). These young gels are supposed to be more reactive – they undergo more hydrolysis-condensation reactions and less protective than mature gels formed after years [Gin et al., 2018].

In a second stage, the coupons altered at pH 3 or pH 9 were immersed in a tracing solution containing 1000 ppm of ^{10}B at the room temperature in the corresponding pH. After 1 minute contact time, the coupons were taken out and frozen with liquid nitrogen to analyze the sample under the cryogenic mode in ToF-SIMS. This mode is used to prevent pore water evaporation during the analysis [Collin et al., 2019]. Tracing with ^{10}B were extended to 5 minutes, 1 hour, 1 day, 2 days, and 10 days contacting time for both pHs and analyzed through ToF-SIMS under the same cryogenic mode. The condition of the ToF-SIMS were as follows: Primary beam of Bi^{1+}, 25 KeV, I 1.4 pA with analyzed area of 60 x 60 m^2 and sputter beam of 1KeV, O^{2+}, I 300 nA with abrasion area of 190 x 190 m^2. Then the quantity of 10Bs (s stands for solution) entered into the gel from the solution at the different contact times was estimated by using ToF-SIMS profile with 1-minute contacting time as a reference, assuming that no B diffusion from the solution into the gel took place. More details about these calculations are given in the supplementary method section. To validate the ToF-SIMS results, a XPS analysis was performed within the gel on the sample altered at pH 9 and immersed for 10 days in the tracing solution, as XPS is more accurate in quantifying the elemental composition. For that, a first analysis was performed with a 20 keV Ar cluster beam to determine the abrasion speed of the material. Then, a quantitative analysis was performed after 300s of abrasion with the same Ar cluster beam, which corresponds to a depth of 25-30 nm below the surface (approximately the middle of the gel). The XPS analysis was performed at 225 W monochromatized Al K beam at 0° detection angle with charge compensation, analyzed the surface area of 110 x 110 m^2. The uncertainty of the elemental composition estimated by the ToF-SIMS and XPS are 10%. More detailed explanations about the comparison of ToF-SIMS with XPS are given in the supplementary method section.

In order to understand B retention in the gel, B adsorption experiments were performed on amorphous silica and mesostructured aluminosilicates. In this study, amorphous sil-

ica (99.8%, 90-110 m^2/g, Alfa Aesar) and mesostructured MCM-41 aluminosilicate (3% aluminium, 900-1100 m^2/g, 2-4 nm pore size, Sigma-Aldrich) were used. A series of adsorption experiments were conducted using an aqueous solution of $B(OH)_3$ (5.5 $mg.L^{-1}$ of B) and $CaCl_2$ (4 $g.L^{-1}$ of Ca), at room temperature in perfluoroalkoxy reactors. Volume of 15 mL solution was left in contact with either 1 g of amorphous silica or 0.3 g of aluminosilicate, and the pH was adjusted using the small amount of LiOH or HNO_3. Homogenization of the solution was achieved with sequences in an ultrasonic bath during the experiment. After 48h, the solutions were centrifuged for 20 min at 4500 rpm and filtered using 0.20 µm PTFE filters. Boron concentration in these solutions was then determined with UV-vis spectroscopy (5% uncertainty).

Chapter 3

Deciphering the non-linear impact of Al on chemical durability of silicate glass

Published in *Acta Materialia, 2022*

Contents

3.1 Introduction

Addition of Al_2O_3 into the silicate glass improves its mechanical properties, chemical durability and optical properties [Zheng et al., 2012, Smedskjaer et al., 2012, Mauro and Smedskjaer, 2014, Wondraczek et al., 2011]. Similarly, the addition of Al into the borosilicate glass significantly decreases the dissolution rate of glass elements in water [Gin et al., 2020b] . Hamilton et al, have investigated the effect of the Al/Si ratio on the plagioclase glass dissolution from pH 1 to pH 12 [Hamilton et al., 2001]. They observed that the dissolution rate of three glasses is increasing with increasing the Al/Si ratio independent of the pH, which is contradictory to the case of nuclear waste glass where the addition of Al significantly lowers the dissolution rate [Hamilton et al., 2001]. It is observed experimentally that the addition of Al in small quantities to a silicate glass leads to a strong decrease in the dissolution rate whereas the addition of Al in glass at very high concentrations significantly increases the dissolution rate [Vienna and Crum, 2018]. However, the fundamental mechanisms regulating this controversial role of Al are hardly accessible through experimental approaches and poorly understood in the glass community even through atomistic computer simulations.

In previous studies, molecular dynamics (MD) simulation method has been widely used to model the glass structure depending on its composition and several approaches have been used to investigate the activation barrier for dissociating the bonds around Si by water [Kagan et al., 2014, Criscenti et al., 2006a, Del Bene et al., 2003, Xiao and Lasaga, 1994]. However, the reported activation barriers are in broad range, which makes it difficult to correlate with the structural properties of glass. Reasons for such broad distribution of activation energy are given in the Section 1.3.3. To overcome these problems, we are performing a comparative study between the pure silicate and an aluminosilicate glass. Where we will estimate the activation barrier for dissociating the bonds around Si and Al by statistically averaging over a large number of local structural situations to address the following four open questions:

1. What is the rate-limiting step for dissociating the bonds around the Si and Al atoms in silicate and aluminosilicate glasses?
2. What are the structural features of the glass contributing towards the durability in both pure silicate and aluminosilicate glass?
3. Does the addition of alumina to pure silicate glass yield a significant rise in durability due to a synergistic effect of Si and Al or due to the individual contribution of Al?
4. What mechanism can explain the higher durability of aluminosilicate glass over pure silicate glass?

Two mechanisms were proposed previously to explain this phenomenon. Firstly, the addition of alumina reduces the sodium ions bonded to non-bridging oxygen atoms (easy

to leach) by consuming them as a charge compensator for the tetrahedral co-ordination $[AlO_4]^-$ (comparatively harder to leach). Secondly, the addition of Al_2O_3 would increase the network connectivity of the glass that resists the diffusion of water [Smets and Tholen, 1984]. We address the four questions above by developing an automated pipeline of MD simulations which takes the glass composition as an input, then creates a glass model, adds water molecules onto its surface, relaxes the system, performs PMF calculations between an H2O molecule and a target glass forming atom, finally stores all the structural information of the target atom (like the coordination environment, bond angles, local hydrostatic pressure and shear stress force) together with their corresponding activation energy. This method of analysis allows us to statistically decipher the role of Al towards the increased durability of aluminosilicate glass. Agreement of these simulation results with available experimental data strengthens the reliability of our answers and the method used. As a whole, we demonstrate the mechanism by which Al atoms play two different roles based on their concentration in aluminosilicate glass.

3.2 Results

3.2.1 Time step optimization to perform PMF calculations and to estimate the activation barrier

To determine the activation barriers corresponding to the dissociation of the bonds in the silicate and aluminosilicate glasses using PMF calculations, we first performed a small pilot study to estimate the number of steps required to obtain stabilized values. The numbers of steps selected to test the PMF method were 1000, 3000, 5000, 8000, 10,000 and 15,000. The PMF calculations were performed using one glass containing 23 Si atoms that are in close contact with H_2O. The distribution of the activation energies are shown in Figure 3.1.

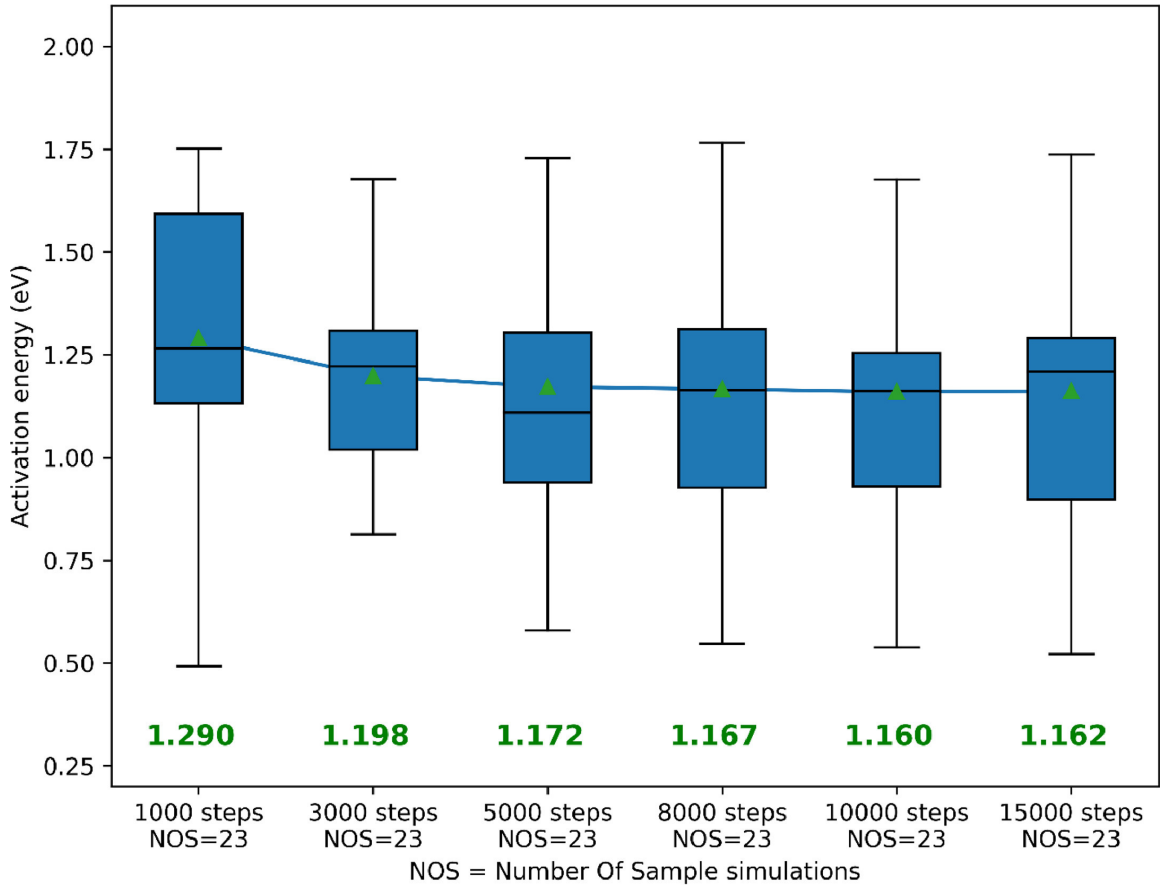

Figure 3.1: Activation energy distribution for the activation energy of Si in pure silicate glass with different number of optimization steps. The △ triangles represent the mean values; the blue line connects the mean; the exact mean value is displayed in green color below each boxplot, respectively; the boxplot represent the standard Q1–25th percentile, Q3–75th percentile and median–50th percentile. The two whiskers extending the boxplot represent standard boxplot minimum and maximum [Damodaran et al., 2022].

For 1000 steps duration, relaxation of the glass structure is not yet sufficient, leading to a significant overestimation of the activation energy. With increasing the number of steps, the average activation barrier decreases and starts to stabilize beyond 5000 steps.

The mean activation energies for the last three durations are converged within the range of 1.16 to 1.167 eV, as shown in Figure 3.1. Thus, we chose to apply the PMF calculations with a duration equal to 10,000 time steps for the relaxation at each intermediate distance.

With the PMF method, we estimated the activation barriers of chemical reactions corresponding to the water molecule dissociating the bonds around the glass network formers [Bouyer et al., 2010b] as shown in Figure 3.2. Quantitatively investigating this chemical reaction is crucial for assessing the durability of the glass because bond dissociation offers a way for water molecules to diffuse through the glass [Gin et al., 2020b, Frankel, 2018, Frugier et al., 2005]. In both pure silicate and aluminosilicate glasses, water molecule approaching the target glass network former atom, establishes an additional bond between the oxygen of H_2O and Si or Al atom of the glass around 2.35 Å during the intermediate stage of the calculation. Subsequently, moving H_2O more towards the Si-O-Si, Si-O-Al, Al-O-Si or Al-O-Al surface bridge, it undergoes dissociation [Kagan et al., 2014].

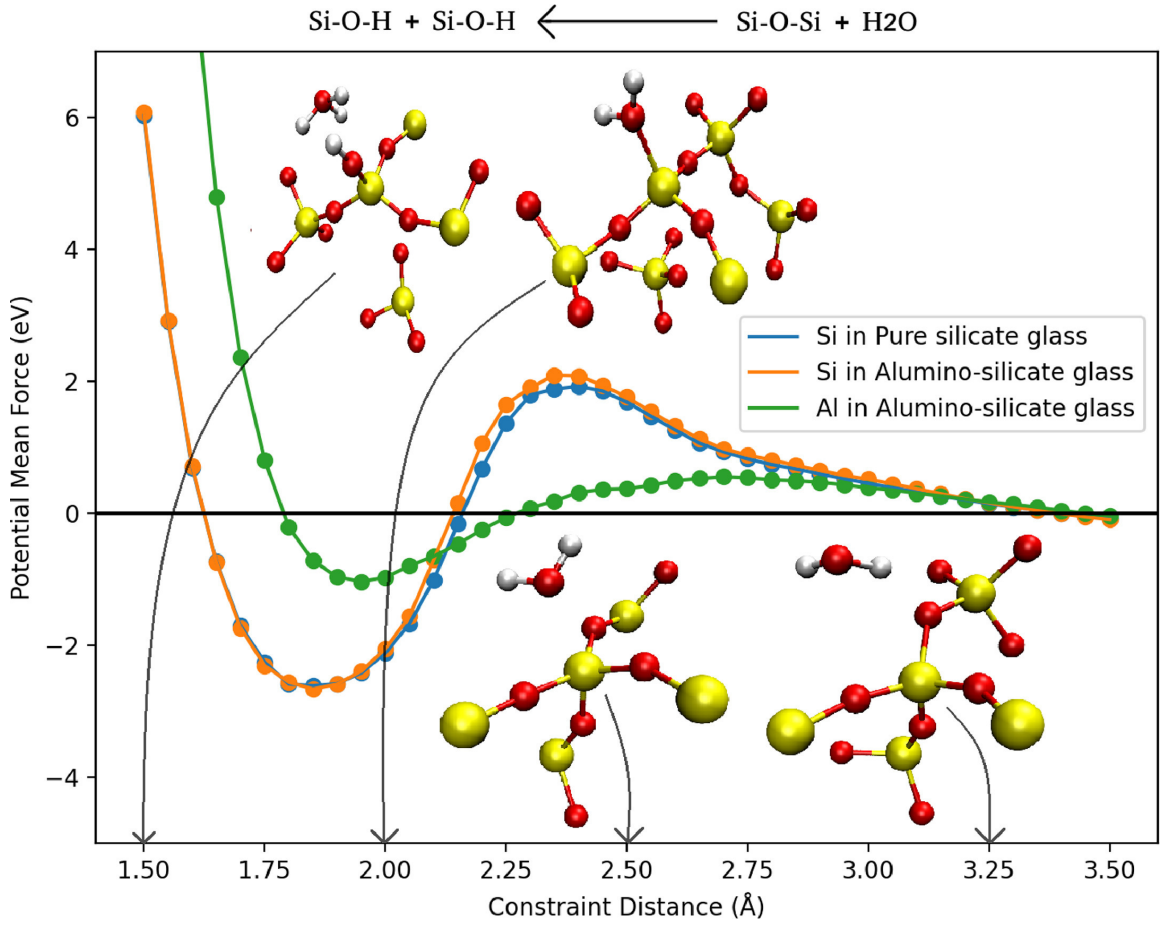

Figure 3.2: Average activation barrier for dissociating Si in pure silicate, Si and Al in aluminosilicate glass. Blue–Activation energy of bond dissociation around Si in pure silicate glass; orange – Activation energy of bond dissociation around Si in aluminosilicate glass; green–Activation energy of bond dissociation around Al in aluminosilicate glass. The H_2O molecules approaching towards the Si–O–Si bridge is visualized at each step and the constraint distance of the snapshots are pointed by the arrows [Damodaran et al., 2022].

3.2.2 Estimating activation energy for the chemical reaction between glass and water

For the statistical analysis of the activation energies for water dissociating the Si–O–Si bridges in pure silicate, and the Si–O–X and Al–O–X bridges in aluminosilicate glass, we performed PMF calculations for all the 17 models of pure silicate and 25 models of aluminosilicate glasses. Using 3.5 Å as the cut-off radius for the pure silicate glass models, 282 calculations have been performed approaching water molecules close to the Si–O–Si bridges. Similarly, for the aluminosilicate glass models, 227 and 68 calculations have been performed approaching the water molecules close to the Si–O–X bridges and Al–O–X bridges, respectively. The distance between the water molecule and the target atom has been restrained and progressively decreased to estimate the activation energy of the three bridges by water.

As shown in Figure 3.3, the mean activation energy of 1.34 eV for dissociating bonds around the Si in aluminosilicate is comparatively higher than for Si in pure silicate with the mean of 1.22 eV. The mean activation energy required to dissociate Al atom in aluminosilicate glass is equal to 0.49 eV, which is not even half of the activation energy for dissociating Si. Such a low activation energy is quite surprising, because the addition of Al atom into a silicate glass is expected to improve the mechanical properties and chemical durability of the glass [Xiang et al., 2013, Weigel et al., 2008].

To investigate if these differences in the activation energies are significant or not, we have first analyzed the distribution of data using the Kolmogorov-Smirnov test whose P-value is given in the Table A.1 (see the Appendices). Based on the P-values, the activation energies of dissociating bonds around Si in pure silicate and Si, Al in aluminosilicate are not normally distributed. Since the sample sizes are not equal and their distributions are not normal, we chose the non-parametric Mann-Whitney U-test (MWU) to investigate if the means are significantly different or not. The P-values < 0.05 indicate that the means of the two compared sets of data are significantly different. In Figure 3.3, by keeping Si in pure silicate as a reference, we performed the MWU test for other two sets of data and found that the mean dissociation energies of both Si and Al in the aluminosilicate glass are significantly different.

3.2.3 Experimental validation of the activation energies estimated through PMF calculations

XPS analysis was performed for the ISG-Al-05 (Si/Al=2.04) and ISG-Al-06 (Si/Al=0.5) glasses to record all the elemental compositions before and after leaching in distilled water with neutral pH in the range from 6.5 to 7.5 as shown in Table 3.1. A comparison between the Al/Si ratios recorded before and after the alteration directly indicates which element is preferentially dissolved from the glass and released into the solution. In pristine glass, Al/Si ratio of ISG-Al-05 and ISG-Al-06 are 0.51 and 1.08, respectively. After altering the

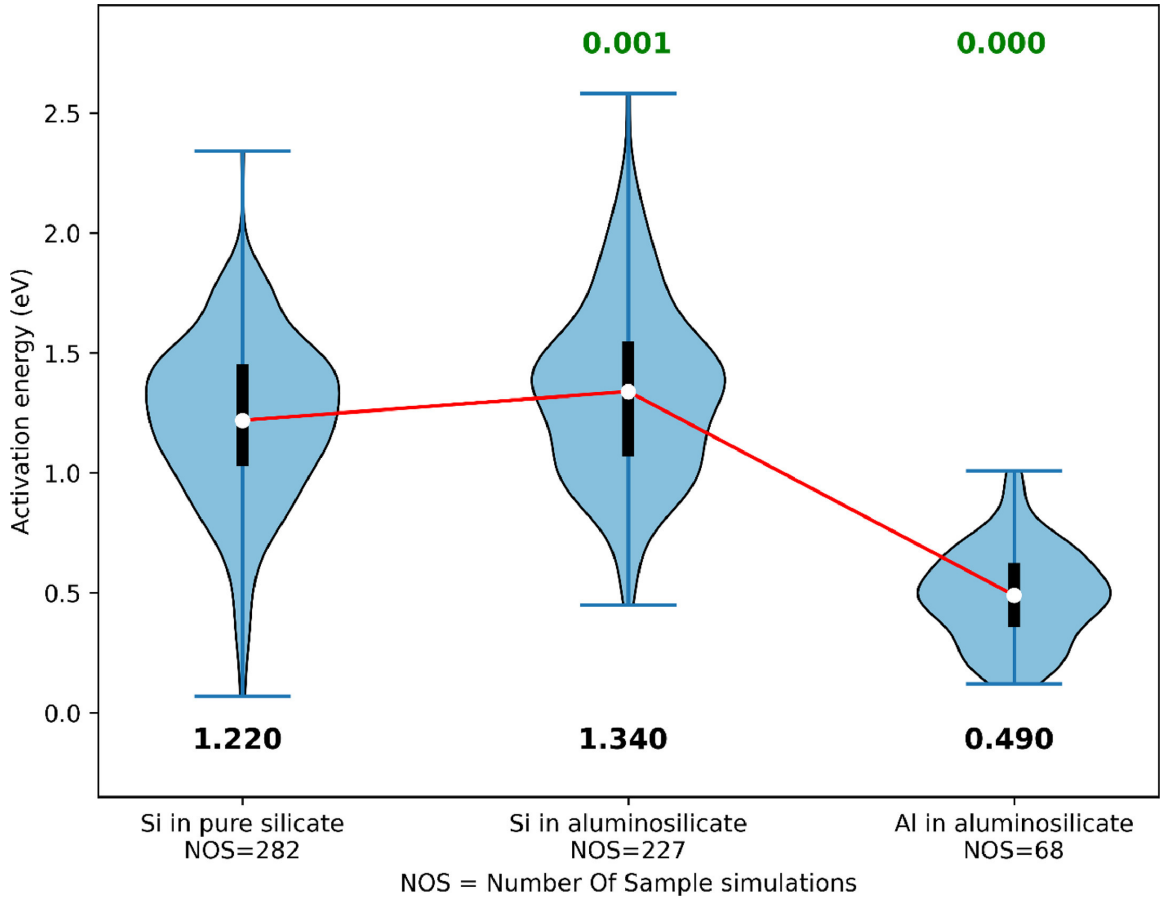

Figure 3.3: Distribution of activation energies for bond dissociation of Si in pure silicate, Si and Al in aluminosilicate glass. The blue violin shaped curve represents the distribution of data. Solid white circles represent the mean of the distribution, the red line connects the mean values and the black line represents the standard boxplot of Q_1–25th percentile, Q_3–75th percentile. The two whiskers extending the boxplot represent the standard boxplot minimum and maximum. Green colored numbers on top of each violin plot represents the P-value with respect to the comparison of the first violin plot. Black colored numbers below each violin plot represent the mean score in eV. [Damodaran et al., 2022].

top 20 nm of glass, we observed that the Al/Si ratio drops by 27% in ISG-Al-05, whereas it drops by 41% in ISG-Al-06. This indicates that the addition of more Al into the glass leads to a faster dissolution of Al, which correlates with the activation energy of Al computed through PMF calculation being lower. The elemental composition depth profile of the altered layer formed on the ISG-Al-05 sample was obtained through the ToF-SIMS profiling. The intensities were mean normalized with respect to the glass composition as shown in Figure 3.4. ToF-SIMS is comparatively less quantitative than XPS, but the first 5 nm data of the Al/Si ratio being consistent with XPS seems to increase the ToF-SIMS data reliability. The B profile indicates that the leaching of glass took place only within the first 20 nm, and retention of Na in the altered layer could possibly be due to charge compensation.

The initial dissolution rate, r_0 measurements were performed through shorter leaching tests with the ICP-OES analyses on the samples taken from the leachate at regular intervals. This parameter refers to the matrix dissolution, it is thus derived from the release

Name	Analysis	Na	O	Ca	K	B	Zr	Si	Al	Al/Si
ISG-AL-05	Theoretical composition	11.4	57.8	1.6	-	9.2	0.5	13.1	6.4	0.48
	XPS before leaching	10.1	59.3	1.3	0.7	6.1	0.5	14.6	7.4	0
	XPS after leaching	8.7	63.2	0.5	0.8	-	1.2	18.7	6.9	0.37
	XPS variation before and after leaching (%)	-14%	7%	-62%	14%	-100%	140%	28%	-7%	-27%
ISG-AL-06	Theoretical composition	15.0	55.5	1.6	-	8.8	0.5	8.5	10.1	1.18
	XPS before leaching	11	58.3	1.3	1.2	5.8	0.5	10.6	11.4	1.08
	XPS after leaching	2.1	66.1	4.1	0.1	1.2	1.4	15.2	9.8	0.64
	XPS variation before and after leaching (%)	-81%	13%	215%	-92%	-79%	180%	43%	-14%	-41%

Table 3.1: XPS composition analysis of the ISG-Al-05 and ISG-Al-06 glasses before and after the alteration in distilled water [Damodaran et al., 2022].

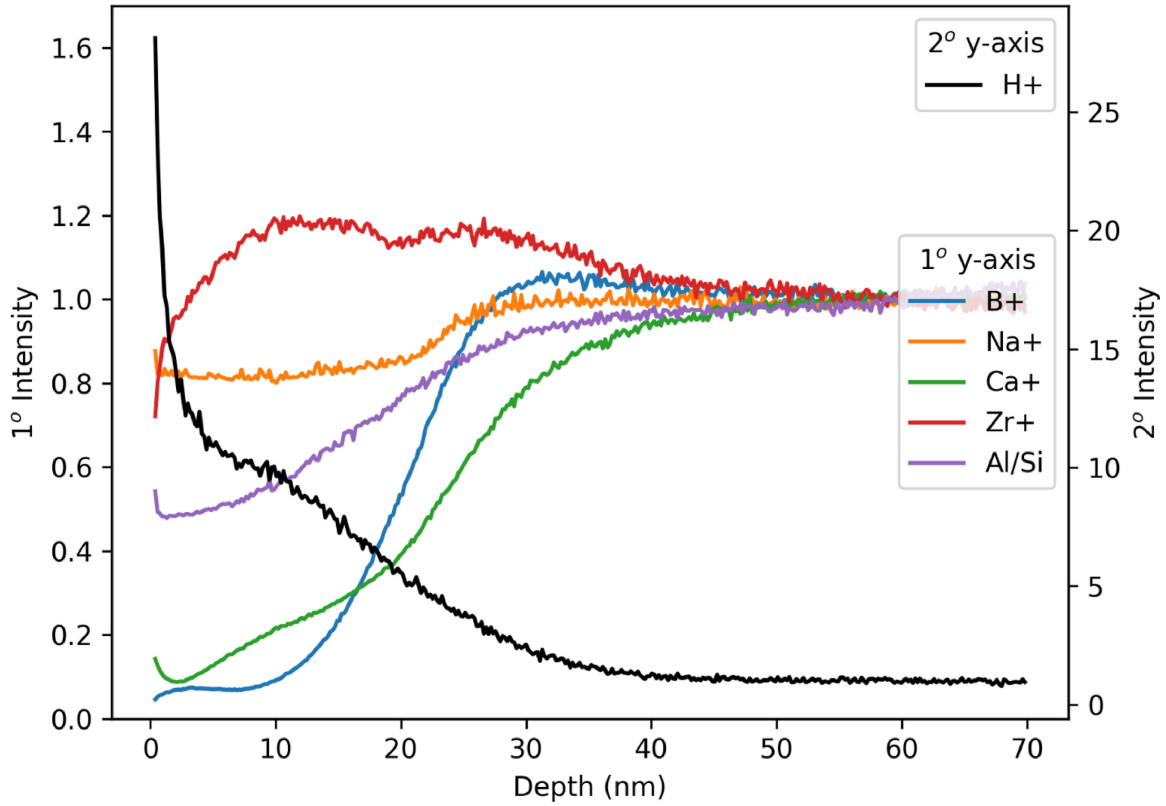

Figure 3.4: ToF-SIMS depth profiling of a coupon of ISG-AL-05 glass altered for 1 h in deionized water at 90 °C normalized to the mean of the pristine glass. The 1° y-axis in legend represents the primary y-axis, whose values correlated with the 1 intensity and the 2° y-axis represents the secondary y-axis, the H^+ data are to be correlated with the 2° intensity. The intensities are normalized to the mean of pristine glass [Damodaran et al., 2022].

of Si into the solution, taking care that the solution remains sufficiently diluted to avoid feedback effects [Fournier et al., 2016, Gin et al., 2020a]. The results shown in Figure 3.5

indicate that r_0 is 64 times faster for the ISG-AL-06 glass than for the ISG-AL-05 glass. These results are in agreement with Hamilton's jadeite and nepheline glasses dissolution behavior [Hamilton et al., 2001], where the glass with the lowest Si/Al ratio displays the fastest initial dissolution rate.

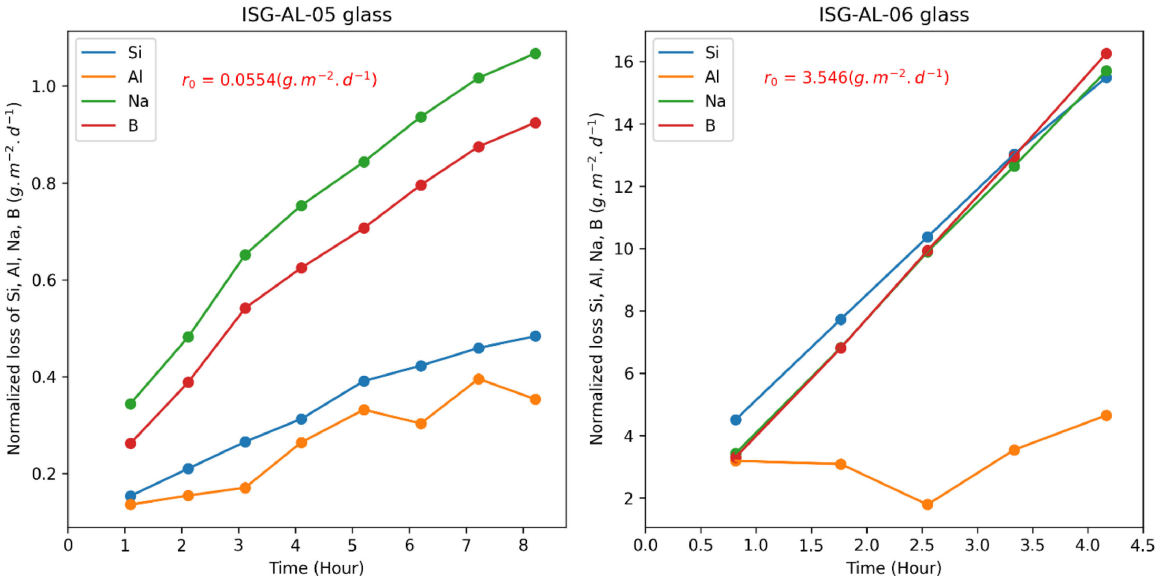

Figure 3.5: Initial dissolution rate of ISG-AL-05 and ISG-AL-06 glasses at 90 °C and neutral pH. Blue–Si, orange–Al, green–Na, and red–Boron. Initial dissolution rate of Si is displayed in red color text for both glasses [Damodaran et al., 2022].

Note that the preferential release of Al evidenced by the ToF-SIMS and XPS measurements cannot be seen here for several reasons: the uncertainties of the ICP-OES data are quite large (5% for Si and 10% for Al), the elemental concentrations in the onset solutions have not been measured, the alteration proceeds much deeper than for the solid-state characterization (300 nm in the case of ISG-AL-06) which could disturb Al release due to the re-organization of the Si-rich altered layer, and the leachate readily reaches saturation with respect to a low soluble Al-hydroxide mineral such as gibbsite, which explains the incongruency of the dissolution. For these reasons, monitoring the release rate of the various glass cations into the solution cannot be used to understand the processes taking place at the atomistic scale. In conclusion, the experimental data provided here confirm that Al dissolves faster from the glass than Si, and that the glass with the highest Si/Al ratio has the lowest value of r_0, in agreement with Hamilton's results [Hamilton et al., 2001]. It remains to understand how Al, when added at low concentration into the glass, increases the glass chemical durability.

3.2.4 Effects of the number of bridging oxygen atoms in pure silicate glass and of the local chemical environment of aluminosilicate glass on the activation barrier

Recent study has shown that the activation energy required to dissociate the bonds around the Si atoms changes with the number of bridging oxygens to the target atom [Kagan et al., 2014]. Therefore, we have statistically investigated the possible correlation between the number of bridging oxygens to the target atom with their corresponding dissociation energies of the bonds. The distribution of activation energies required to dissociate the bonds around Si atoms in pure silicate glass based on the number of bridging oxygens in Si coordination is shown in Figure 3.6a. Analysing the activation energies for more than 100 data points indicates that the mean energy required to dissociate a bond to change a SiP3 into a SiP2 species is higher than the one necessary to dissociate a bond to change a SiP4 into a SiP3 speices. (Here SiP4 means Si in Pure silicate with 4 bridging oxygens. Similarly, SiA4 and AlA4 will be used to represent Si and Al in Aluminosilicate glass, respectively, with 4 bridging oxygens). With the Kolmogorov-Smirnov test, both of these data sets are not normally distributed. (Their p-values are given in the Table A.2 of the Appendices). Therefore, we proceed to conduct the non-parametric MWU test to investigate if the two means are significantly different or not. Interestingly, we found the p-value to be 0.034, indicating that a dissociation of a SiP3 species requires significantly more energy than a dissociation of a SiP4 species.

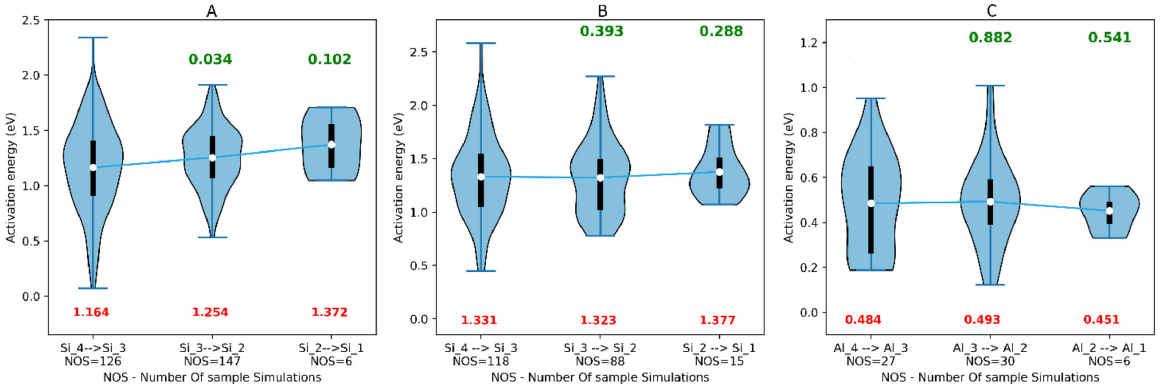

Figure 3.6: Distributions of the activation energies for bond dissociation of Si in pure silicate (A), Si in aluminosilicate glass (B), and Al in aluminosilicate glass (C), each categorized based on the number of bridging oxygens. The violin shaped curves represent the distribution of the data points. Solid white circles represent the mean of the distribution, blue line connects the mean values, and black line represents the standard boxplot of Q1–25th percentile, Q3–75th percentile. The two whiskers extending the boxplot represent the standard boxplot minimum and maximum. Green numbers on top of each violin plot represent the p-values with respect to a comparison with the first violin plot. Red numbers below each violin plot represent the mean score. On the x-axis, for instance, Si_4 → Si_3 means that the target atom Si with initially 4 bridging oxygens, becomes coordinated with three bridging oxygens after dissociation by water. [Damodaran et al., 2022].

Similarly, we can classify the activation energies for the bonds around the Si and Al atoms in the aluminosilicate glass based on the number of bridging oxygens in their

coordination (Figure 3.6). We note that the mean activation energy required to dissociate a bond around the SiA4 species is as strong as that for the SiA3 species for dissociating a bond around a Si atom in aluminosilicate glass. Additionally, both of these activation energies are above 1.3 eV, which is higher than what is observable for the SiP3 and SiP4 species in pure silicate glass. Therefore, the rate limiting step for the dissolution of aluminosilicate glass starts from SiA4 species and continues with SiA3 species, whereas pure silicate is rate limiting only starting from the SiP3 species.

To understand the reason for a higher strength of the SiA4 species, we investigated the effects of the local environment on the dissociation energies around Si atoms in the aluminosilicate glass. We categorized them using the activation energy based on their coordination with the number of Al atoms as their second neighbors. Interestingly, when the second neighbors of the target Si atom do not contain Al, its average activation energy was 1.23 eV, which is less than for the SiP3 species, but the presence of single Al as a second neighbor increased the activation energy to 1.35 eV and further to 1.42 eV for two Al as second neighbors, as shown in Figure 3.7A.

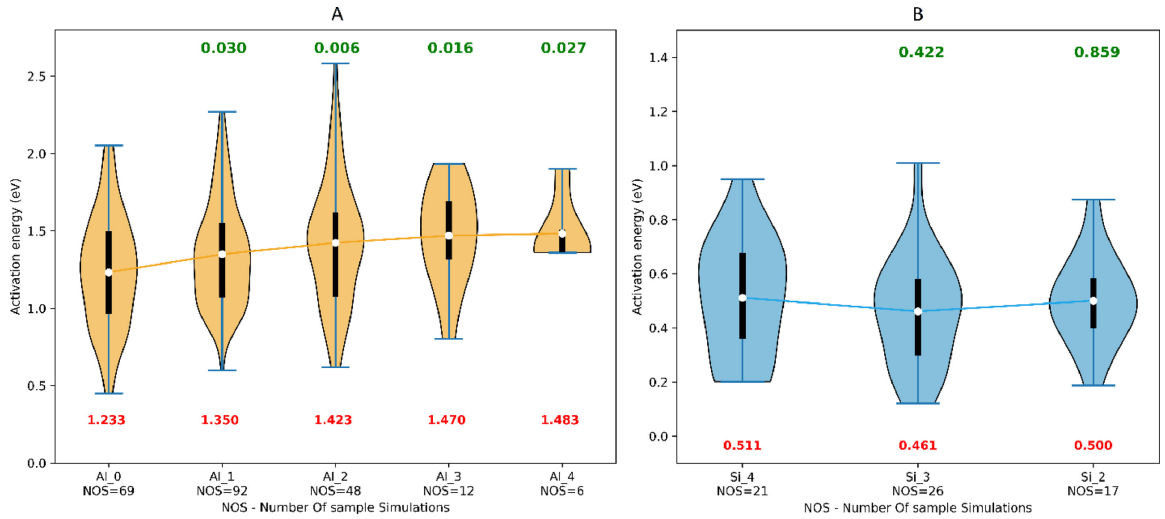

Figure 3.7: Distribution of the activation energies for bond dissociation: (A) Si in aluminosilicate glass based on the presence of Al as second neighbors; (B) Al in aluminosilicate glass based on the presence of Si as second neighbors. The violin shaped curves represent the distribution of data points. Solid white circles represent the mean of the distribution, red line (A) and blue line (B) connect the mean values. The black boxplots represent Q1–25th percentile and Q3–75th percentile. The two whiskers extending the boxplots represent standard boxplot minimum and maximum. Green numbers on top of the each violin shape represents the p-values with respect to a comparison with the first violin plot. Red numbers below each violin plot represent the mean score. For figure (A), on the x-axis, Al_0 represents no Al as a second neighbor for the target Si atom, and extends through Al_1, Al_2, Al_3 up to Al_4 indicating four Al as second neighbours. For figure (B), on the x-axis, Si_4 represents 4 Si as second neighbours for the target Al atom, up to Si_2 having two Si as second neighbours. [Damodaran et al., 2022].

The species Al_0, Al_1 and Al_2 have more data to rely upon their significance, but beyond them the number of data points is less. Nevertheless, it is very clear that a Si species in aluminosilicate glass with no Al as a second neighbor is easier to dissociate than a Si species with Al as a second neighbor. This indicates that Al has a significant

local effect on the Si to strengthen the glass, which is responsible for rise in activation energy. In oxide glasses, Al atom has always been of great interest for its ability to increase the polymerization of the glass structure due to its network forming role [Weigel et al., 2008] and the reduction of the non-bridging oxygen content with the formation of negatively charged $\left[AlO_{\frac{4}{2}}\right]^{-1}$ tetrahedral units, charge balanced by modifiers [Greaves and Sen, 2007]. Therefore, despite Al being such a weak element with low activation energy, Al atom increases the network connectivity of glass by making more SiA4 species (which is stronger than SiP4 or SiP3), and so these indirect benefits outweigh the easier dissolution of the Al atom. Finally, the mystery appears to be solved that the Al itself is not the strong element in aluminosilicate glass, but it plays a vital role in strengthening the major element Si to increase the durability of the glass, which is in agreement with the XPS results and ToF-SIMS data.

3.2.5 Correlating the structural features of the glass with the activation energies

Chemical composition determines the structure and mechanical properties [Hand and Tadjiev, 2010], both of which, in turn, control the durability of the glass [Frankel, 2018, Charpentier et al., 2018]. Therefore, we investigated if there is any correlation between the structural properties like bond angles or the mechanical properties like the local stress tensors (hydrostatic pressure and shear) with the activation energies for the dissociation of Si–O–Si bridges in pure silicate, and Si–O–X or Al–O–X bridges in the aluminosilicate glass. The calculated bond angles of the three-atom bridge dissociated by water are in the range of 115°–180° for pure silicate, whereas in the aluminosilicate glass, the average bond angles are a little lower: Si–O–Si (150°), Si–O–Al (135°), Al–O–Si (139°), and Al–O–Al (135°). Regression analysis performed to correlate these structural features against activation energies are shown in Figure 3.8, and indicates that the activation energy required for dissociating the bond increases with increasing the bond angle. The hypothesis with 95% confidence interval has been tested statistically and it is found that the activation energy depends on the bond angle for Si in pure silicate and Si, Al in aluminosilicate glass with the p-values less than 0.05 (Table A.7 Appendices).

Then linear regression for the local shear stress vs activation energy revealed that increasing the shear stress decreases the activation energy. By statistically testing this hypothesis, the existence of this correlation is confirmed in pure silicate and in the aluminosilicate glasses (bonds around Si), but not for the bonds around the Al in the aluminosilicate glass. On the other hand, the linear regression of hydrostatic pressure with hypothesis testing shows that there is no significant correlation between the local hydrostatic pressure and the activation energy for the bonds around the Si, Al atoms in the aluminosilicate glass and around Si in pure silicate glass. However, the distribution of local hydrostatic pressures for Si in the aluminosilicate glass is more skewed towards negative than for Si in pure silicate, probably because of the lower number of non-bridging oxygens around the tetra-coordinated Si. As we can see in Figure 3.8, not all the points

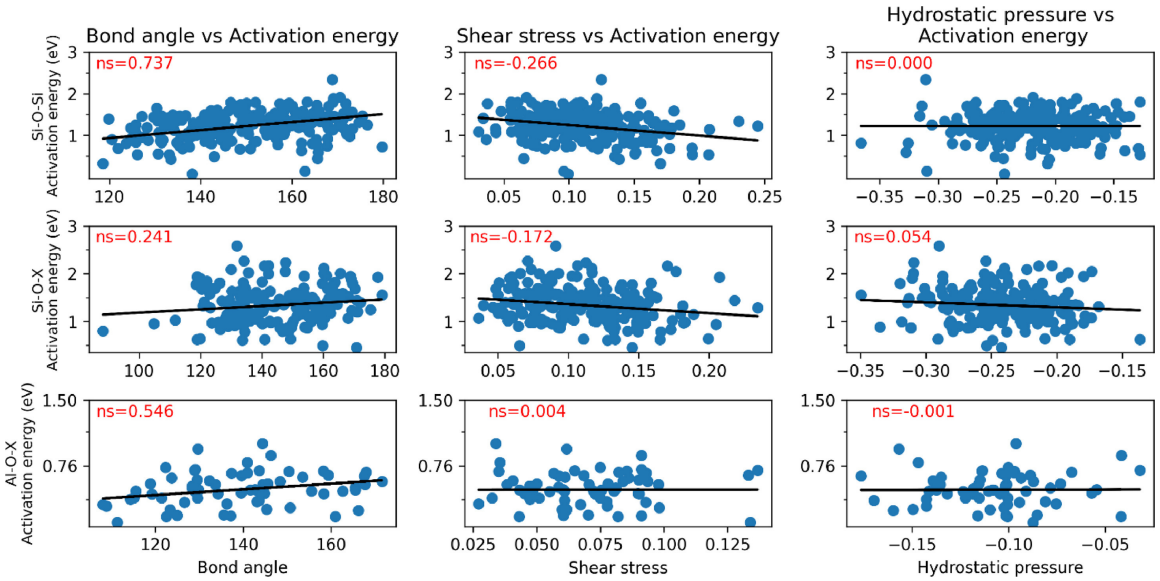

Figure 3.8: Correlation of the bond angle, shear stress and hydrostatic pressure with the activation energy for Si in pure silicate, Si and Al in aluminosilicate glass. Data points are represented by blue dots, and the regression black lines are fits to the data. The scale of bond length is 100 times of its activation energy, so both the x-axis values and the y-axis values for all plots are divided by their respective maximum values to normalize both x and y-axes and then slope is calculated to represent as NS – Normalized slope. Three plots in the first column are the correlations of the bond angle vs activation energy, the second column shows the correlations of the Shear stress vs activation energy, and the third column shows the Hydrostatic pressure vs activation energy correlation [Damodaran et al., 2022].

are closely fitted by a straight line; rather we are just able to observe a certain trend for all three parameters. This is because several structural features simultaneously control the activation energy required by the water molecule to dissociate the bridges, and not only one. Nevertheless, these results indicate that the bond angle and the local shear stress have a larger effect on the activation energy, while the local hydrostatic pressure is not affecting the dissociation of bonds in silicate and aluminosilicate glass.

3.3 Discussion

The durability of the silicate glass against water is increased by the addition of a small amount of Al in the CJ2 type of glass [Gin et al., 2020b]. However, in our study, surprisingly, the average activation energy necessary to break a bond around one Al atom in an aluminosilicate glass is estimated to be just 0.49 eV. This is not even half of the energy required to dissociate a bond around one Si atom in pure silicate glass. These results are in agreement with experimental data obtained from solid state characterization at a nanometer scale with XPS and ToF-SIMS on two model aluminosilicate glasses. Statistically, it is found that the energy required to dissociate a bond around Si atom in the aluminosilicate glass is significantly higher than in pure silicate glass. This indicates that the addition of Al strengthens the bonds around Si atoms in the glass. Interestingly, a Si atom surrounded by four bridging oxygens (SiP4) in pure silicate glass is weaker than a Si atom surrounded by three bridging oxygens and one non-bridging oxygen (SiP3) in the same glass and the difference is statistically significant. This is in agreement with previous studies on water dissociating the silicate glass by PMF method for a small number of samples [Kagan et al., 2014]. It is important to notice the activation energy estimated in Ref. [Kagan et al., 2014] is in range between 0.17 eV and 0.95 eV which is different from the range in our study. It seems that a water molecule approaching the reaction site with a specific orientation modifies the energy barriers. In Ref. [Kagan et al., 2014], the authors have chosen one particular orientation for the water molecule to target the silicate bond. And this orientation corresponds to the easiest way to break the Si-O-Si bond. It is interesting to notice that we measured some activation energies in the regime from 0.1 ev to 0.95 eV. Additionally, we also observed the same mechanism as theirs. i.e.

1. In our study, it seems that the water molecule dissociates the back siloxane bridge is same as in Figure 1 of the Ref. [Kagan et al., 2014].
2. The mechanism of higher activation barrier for SiP3 than SiP4.

However, we observed much broader regime for activation energy as we did not change the orientation of every water molecules against the Si-O-Si bond. Therefore, the scale of activation energy is slightly different between the two studies yet the mechanisms understood remains the same. We also found that, the bonds around the Si surrounded by four bridging oxygens (SiA4) in the aluminosilicate glass are as strong as the ones around the Si surrounded by three bridging oxygens and one non-bridging oxygen (SiA3), and additionally both activation energies are higher than for the SiP3 and SiP4 species. Investigating the reason for such rise in the activation barrier revealed that when there is no Al as a second neighbor around a Si atom in aluminosilicate glass, its activation energy is very close to SiP. However, in the presence of one or two Al atoms connected as second neighbors, the activation barrier for Si becomes significantly higher which indicates that it is exactly the presence of Al in the local environment that is actually responsible for this rise. Recent abinitio study associated with metadynamics has also found that

activation energy required to break the Si-O-Al bridge is higher than dissociating Si-O-Si [Dupuis et al., 2018], which supports our results. The scale of activation barriers in Dupuis et al.'s study [Dupuis et al., 2018] is very different from our study because they worked with short silicate chains and that could modify the activation barrier. In fact Pelmenschikov et al. [Pelmenschikov et al., 2000] have observed that activation barrier increases when Si-O-Si has more constraints nearby, and vice versa. It is also important to note that the content of SiA4 species in the aluminosilicate glass is larger than SiP4 in pure silicate glass because Al increases the polymerization of the network. Therefore, addition of Al is strengthening the bonds around the major glass-forming element, i.e. Si, and these features differing from the pure silicate glass is what increases the durability of the aluminosilicate glass.

This type of chemical reactions between water and silicate systems can also be studied through the ReaxFF force field [Yu et al., 2016]. Some recent studies used the advantage of the ReaxFF potential associated with parallel tempering method [Dupuis et al., 2020] or high temperature MD method [Dupuis et al., 2019] to accelerate the mechanisms of bond formation or dissociation to better understand the silicate gel formation or evolution of these gels by chemical attacks. However, in our study, we were particularly interested in estimating the activation barrier for silicate dissolution reaction at 300 K with very large statistics to understand the relation between the glass structure and the durability against water. So we chose here the classical reactive potential developed by Mahadevan and Garofalini (MG) [Mahadevan and Du, 2021, Mahadevan et al., 2019, Mahadevan and Garofalini, 2008]. It is estimated that MG forcefield is at least ten times faster than a similar ReaxFF calculation [Mahadevan et al., 2019]. The development of MG potential is inspired by the concept of varying the ion charge as function of the distance [Guillot and Guissani, 2001], fitted through quantum mechanical calculations. They added intramolecular interactions along with two and three-body terms, to allow the water for dissociation of the silicate molecule [Mahadevan and Garofalini, 2008]. It is very important to notice, this reactive potential was evaluated [Mahadevan and Du, 2018], and found very well comparable with the ReaxFF potentials. Later the authors improved this potential for sodium silicate glasses [Mahadevan et al., 2019], which is also found to be very well in agreement with the available experimental structural information. More recently, a reactive potential for more complex systems was developed and validated with the inclusion of SiO_2-Al_2O_3-CaO + H_2O set of parameters [Mahadevan and Du, 2021]. It is why we chose the MG potential for generating the large statistical dataset to investigate the glass structural parameters and the activation barriers.

Recent study has found that the glass dissolution rate drops significantly with the addition of a small quantity of Al to silicate glass ($< 3.5\%$), and the decline rate of glass dissolution becomes gradual at intermediate concentration of Al (3.5%19%) [Vienna and Crum, 2018]. However, the addition of more than 19% of alumina triggers a significant rise of the dissolution rate of the glass [Vienna and Crum, 2018]. The statistical PMF simulation results in our study are explaining quite well the possible atomistic mechanism behind the role of Al towards dissolution rate of the glass. The incorporation of a small

quantity of Al in the glass increases its durability. See, for instance the CJ1 glass (with no Al) with an initial dissolution rate 4 times larger than for the CJ2 glass (containing 4% Al) [Gin et al., 2020b]. Despite Al has less activation energy and being weak element to easily dissociate from the glass, it increases the polymerization of the network resulting in the introduction of more Si with 4 bridging oxygens. Additionally, Al being a second neighbor strengthens the bond around Si in the glass. Both mechanisms together outweigh the low activation energy of Al and make the CJ2 type of glasses to be more durable.

Al at intermediate concentration (3.5% to 19%), this regime from the mid towards 3.5% converts three co-ordinated Si to become four co-ordinated Si surrounded by Al as second neighbor. The concentration regime from the mid towards the 19% involves in preferential dissolution of Al, which weakens the silicate network due to the percolation of the bonds containing the Al, so the decline rate of dissolution becomes gradual when the Al percentage exceeds a critical value. The addition of Al at high concentrations makes the dissolution of Al too much preferential, which completely weakens the silicate network. Under these circumstances, the low activation energy of Al becomes dominant over the two strengthening mechanisms of Al, which totally collapse the durability of the glass. This effect has been observed for our two model glasses and in the literature data on plagioclase glasses [Hamilton et al., 2001].

It has been reported previously that the addition of Al to pure silicate glass increases the durability by two mechanisms. The first mechanism is by reducing the Na coordination with non-bridging oxygen (weak) and increasing the coordination of Na with Al (strong). The second mechanism is by increasing the connectivity of the glass network, which appropriately reduces the diffusion of water [Smets and Tholen, 1984]. Between these two mechanisms, our simulation results, along with the previous experimental results [Vienna and Crum, 2018], propose that the second mechanism plays a dominant role in improving the durability of glass over the first mechanism. With respect to the first mechanism, increasing the Al content in glass will decrease the Na coordinated to non-bridging oxygens (Na is easier to dissociate when coordinated with non-bridging oxygen). However, with respect to the second mechanism, Al increases the network connectivity, increases the strength of Si through local effects, and so reduces the diffusion rate through hydrolysis processes of water molecule inside the glass. For these reasons, following this study, Al strengthening a major glass-forming element like Si is considered as the main contributing factor towards the durability of glass and so the second mechanism plays dominant role over the first mechanism.

In recent years, traditional "trial-and-error" methods to design the glasses are replaced with artificial intelligence to accelerate the discovery of advanced materials [Liu et al., 2021, Kraus and Drass, 2020, Vasudevan et al., 2019]. Current machine learning models for predicting the dissolution kinetics of the glass are trained with input data such as the composition of the glass, pH of the solution, and their corresponding dissolution rates observed experimentally [Anoop Krishnan et al., 2018, Liu et al., 2019]. However, there is a lack of data to understand in detail the relationships between the composition, structure, and durability. The automated pipeline designed in our study takes the composition as an

input and provides structural information of the atom (the number of bridging oxygens, bond angles, local hydrostatic pressure and shear stress, etc.) with their corresponding activation energies as an output. The statistical analysis revealed the role of Al towards the increased durability of aluminosilicate glass. The correlation of our simulation data with experimental results provides more confidence to the simulations reliability, and the use of classical potentials to perform such simulations makes it computationally affordable to generate large amounts of data. This method cannot be limited to pure silicate and aluminosilicate glasses, but can also be extended to include Na, Mg or B into the glass composition to investigate more complex and more realistic glass compositions. Therefore, we believe that this method of automated pipeline to create the wide set of data on composition-structure-durability interdependencies along with experimental dissolution analysis of extreme compositions would be a promising fast method to develop a strong machine learning model in glass science.

3.4 Conclusion

Al causes opposing effects on glass durability against water when added at low and high concentrations. To reveal the structural mechanism behind this behavior, it is very important to understand the correlation between local structural features of the glass and the activation energies of individual bonds. However, finding the correlation between these two parameters is very complicated because the range of activation energies for bond dissociation is very narrow with large standard deviations. In this study, we overcome this difficulty by estimating the activation energy barrier for a statistically large set of configurations to understand their relation with local structural features. The calculated PMF results along with experimental data revealed that it is very easy to dissociate Al from the glass and found with statistical significance that dissociating Si from aluminosilicate glass is much more difficult than dissociating Si from pure silicate glass. Further investigation of the local environment of Si in aluminosilicate glass has shown that the activation barrier for Si dissolution is significantly increases by the presence of Al as a second neighbor. As a result, the addition of Al in small concentration increases the durability by reinforcing the strength of Si and increasing the polymerization of the glass network. Whereas at high Al concentration, the preferential release of Al results in the weakening of the silicate network and so the durability of plagioclase-type mineral glasses decreases with increasing Al concentration. The developed methodology has helped us in understanding the role of Al in silicate glasses, but can also be extended to include Na, Mg, or B for the investigation of more complex glass compositions. Generating huge data sets of structural features with their corresponding activation energies for all the glass elements will serve as an input for developing a strong machine-learning tool, which will help us to design the glass compositions to obtain the desired quality glass quickly.

Chapter 4

Classical MD to estimate Bond reformation energies, and ReaxFF calculations

Contents

4.1 ReaxFF calculations to validate the PMF activation energy for silicate and aluminosilicate glasses

4.1.1 Introduction

ReaxFF is a reactive force field developed initially for hydrocarbon materials. Then the method has been extended to many other different materials including oxide crystals and glasses. As the ReaxFF potentials can deal with silicate systems in contact with water, it can help to improve our understanding towards the interface between these two dissimilar systems [Van Duin et al., 2003, Senftle et al., 2016]. An important property of ReaxFF making it differs from other force fields is the continuous calculation of bond order for the elements, based on the instantaneous interatomic distances. Such correlation between the bond distance against the bond order was first proposed by Tersoff [Tersoff, 1988]. As a result, the bonds are dynamically allowed to create or break, which allows to investigate many chemical reactions.

In previous chapter, we estimated the activation energy for bond dissociation of Si in pure silica and aluminosilicate glasses with classical MD simulation using the Potential Mean Force (PMF) method. Classical dissociative potential from Mahadevan [Mahadevan and Du, 2021, Mahadevan and Garofalini, 2008] helped us to estimate the activation energy for the bond dissociation around Si with a large number of statistics, and we observed that dissociating Si in pure silica is easier than dissociating Si in aluminosilicate glass. The dissociative classical potential remains a classical force field with two-body and three body terms. On the other hand, ReaxFF is even better framework to investigate the interface of heterogeneous materials because this potential based on the bond orders has been fitted with a large number of parameters to represent very precisely the structures and the bond strengths around each element. However, one drawback with ReaxFF is that it is 10 times slower than the calculations with the classical dissociative potential [Mahadevan et al., 2019]. Therefore, in this study we tried to validate the results obtained with the PMF method by different ReaxFF calculations but using a smaller statistics because of the computational time. The composition of glasses, relaxation method, timestep and the mechanism for water molecule dissociating the glass are detailed in Section 2.3.2.

4.1.2 Results

Using PMF calculations performed with classical potential, it is observed that activation energy required to dissociate the Si or Al from the glass had a quite wide distribution ranging from 0.35eV to 2.1eV [Damodaran et al., 2022]. Attempts to correlate these activation energies with the structural features in the glass displayed the existence of some correlations, but the trends are not very strong. Using ReaxFF, the different mechanisms by which the water molecule is dissociating the glass elements are investigated more deeply. The ReaxFF force field is used in conjunction with the SMD method to perform the

chemical reaction and calculate the corresponding activation energy. One typical example of a SMD curve is shown on Figure 4.1. It represents the energy of the system versus distance between the water molecule and the target atom. Interestingly, we observed three mechanisms when the water molecule is approaching the glass which also explains the noise in the correlation between structure of the glass with their activation energy. The first stage is visually represented in the Figure 4.2. Initially, the water molecule is inverted against the target Si of the glass. In Figure 4.2 at timestep 79000 and 230000, the water molecule starts tilting towards the Si of the glass. Eventually, the water molecule approaches closely towards the Si and establishes a bond with it around timestep 305000. Subsequently it dissociates the Si-O-Si bond of the glass, which results in the formation of two silanol groups. So when the water molecule is inverted from the target Si of the glass, an energy is needed to rotate the water molecule before dissociating the bond. In the second mechanism, the water molecule is initially exploring multiple channels before approaching the target Si atom. Eventually it finds one suitable channel and takes that path to dissociate the target Si atom as shown in the Figure 4.3, where all the snapshots are captured without changing the orientation to display the motion of Si. As we can see in the first row of Figure 4.3, the position of the water is largely deviating with respect to the Si at different timesteps. From the timestep 231000, the water molecule has found the best channel and takes that path continuously to dissociate the bond around the target atom.

We plot the accumulated energy required to push the water molecule from its initial site with respect to the distance between the water molecule and the Si belonging to the glass as shown in Figure 4.1. We observed that the energy required to move the water molecule has two different slopes, where the first slope corresponds to the water molecule exploring multiple channels to dissociate the target Si atom. Simultaneously, the water molecule decreases its distance progressively towards the target Si atom. During this process, the water molecule will choose one channel to dissociate the bond which corresponds to the second slope. Additionally, when the water molecule approaches less than 2.3 Å towards the target atom of the glass, additional repulsion of the water molecule by the Si is increasing the slope leading to the second hill. As the first hill corresponds to the exploration of multiple channels or rotation of the water molecule etc., we considered to estimate the activation energy necessary to dissociate the bond only from the second hill to be coherent with the PMF calculations.

Apart from these two mechanisms, we also observed a third mechanism, where the target Si is tetra-coordinated with three bridged-oxygen and one OH. This OH attached to the Si is exposed perpendicular to the position of water in such a way that it prevents the water molecule to find a path to dissociate the bond. In such cases, when the water molecule starts approaching towards the target Si, first it is getting closer to the OH group. The water molecule waits for the OH group to change its position in such a way that a path is created for the dissociation. Different stages of this mechanism is depicted in the Figure 4.4, where initially the OH attached to the Si is oriented perpendicular to the water molecule. The water molecule is stammering to approach the target Si upto the

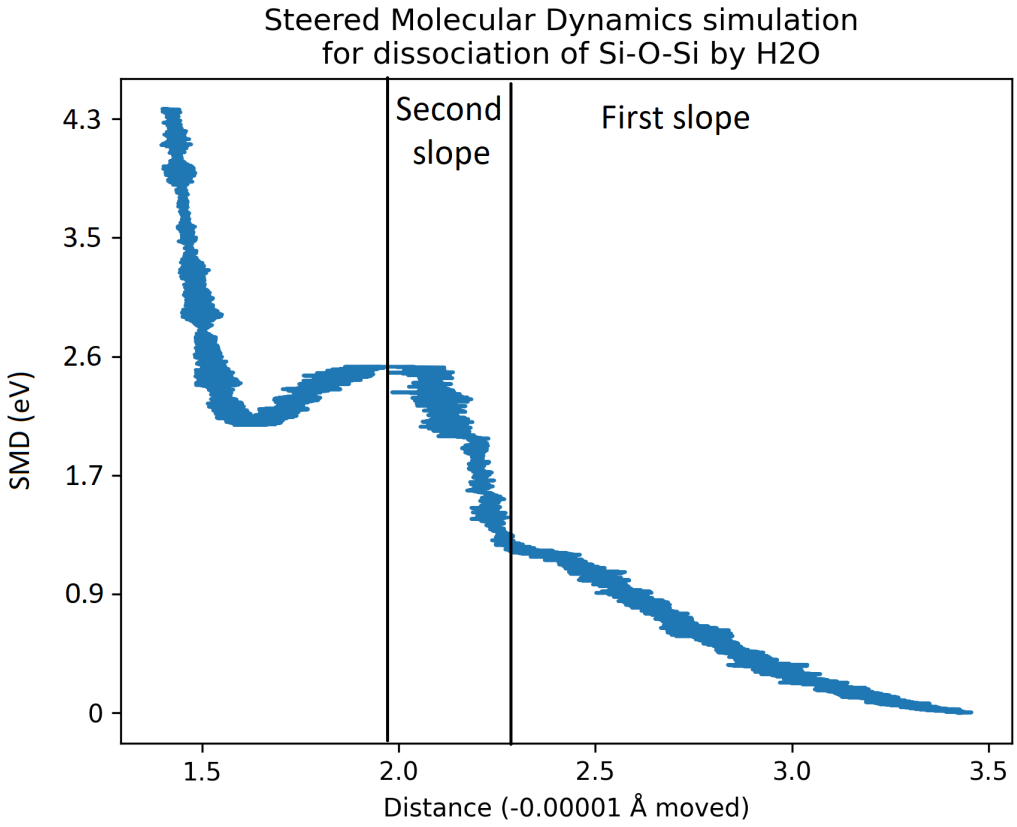

Figure 4.1: An example of SMD calculation with ReaxFF for estimating the activation energy of bond dissociation energy for Si in pure silica or aluminosilicate glass. X-axis represents the distance between the oxygen of water and Si of the glass. Y-axis represents the accumulated energy through SMD in kcal/Mol to reach that particular distance.

timestep of 145000 and the OH group moves to open the way for the water molecule at the timestep of 233000 and 293000. At timestep 327000, we can clearly see the complete change in position of the OH group, with no more obstacle for the water molecule, and subsequently it establishes one bond with the target Si atom for the dissociation.

To compare the activation energy for bond dissociation around Si in pure silica and sodium aluminosilicate glasses, we estimated 12 and 4 cases respectively. We ignored the case where Si in pure silica glass is surrounded by one OH group blocking the water molecule (Third mechanism), because we do not have similar case in sodium aluminosilicate glass for the comparison. The distribution of the activation energies for the two glasses are plotted in Figure 4.5. Then we have estimated the mean of dissociating the bond around Si in pure silica glass to be 21.625 kcal/mol, on the other hand in sodium aluminosilicate glass, this mean is equal to 24.95 kcal/mol. Using the PMF calculations, the dissociation energy for Si in pure silica and calcium aluminosilicate glasses based on larger statistics are 28.13 Kcal/mol and 30.90 Kcal/mol respectively. ReaxFF results are quite close to the PMF results. Indeed the differences between the two glasses observed with the PMF calculations is reproduced with ReaxFF quite well. This supports the concept of Al strengthening Si for dissociation by the water molecule. However, it is also important to consider that the number of calculations performed with ReaxFF remains

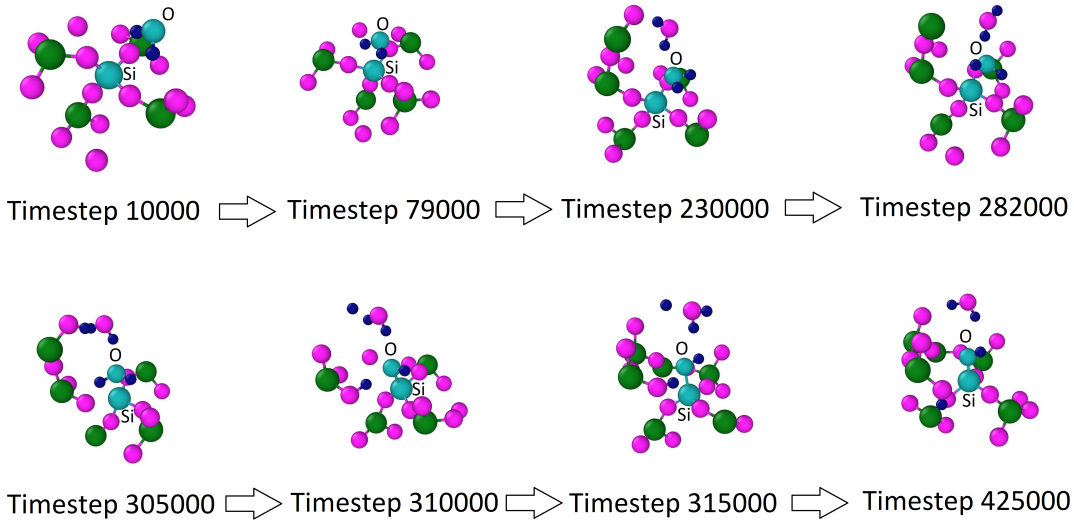

Figure 4.2: Reaction pathway between the inverted water molecule and Si-O-Si of glass through ReaxFF: Multiple snapshots of water molecule dissociating the Si-O-Si of glass through ReaxFF calculation. Timesteps of each snapshots are indicated respectively. Reaction between the Oxygen belonging to the water molecule and Si belonging to the glass for each snapshots are highlighted in cyan color and labelled to trace their trajectory across the snapshots.

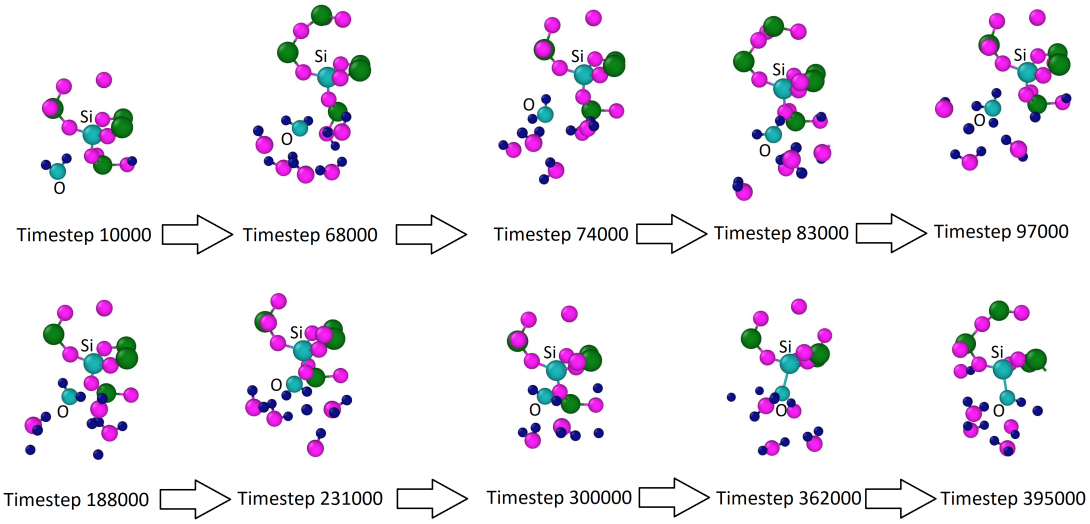

Figure 4.3: Reaction pathway of water molecule exploring multiple channels to dissociate Si-O-Si of glass through ReaxFF: Multiple snapshots of water molecule dissociating the Si-O-Si through ReaxFF calculation. Timesteps of each snapshot are indicated respectively. Reaction between the Oxygen belonging to the water molecule and Si belonging to the glass for each snapshot are highlighted in cyan color and labelled to trace their trajectory across the snapshots.

small.

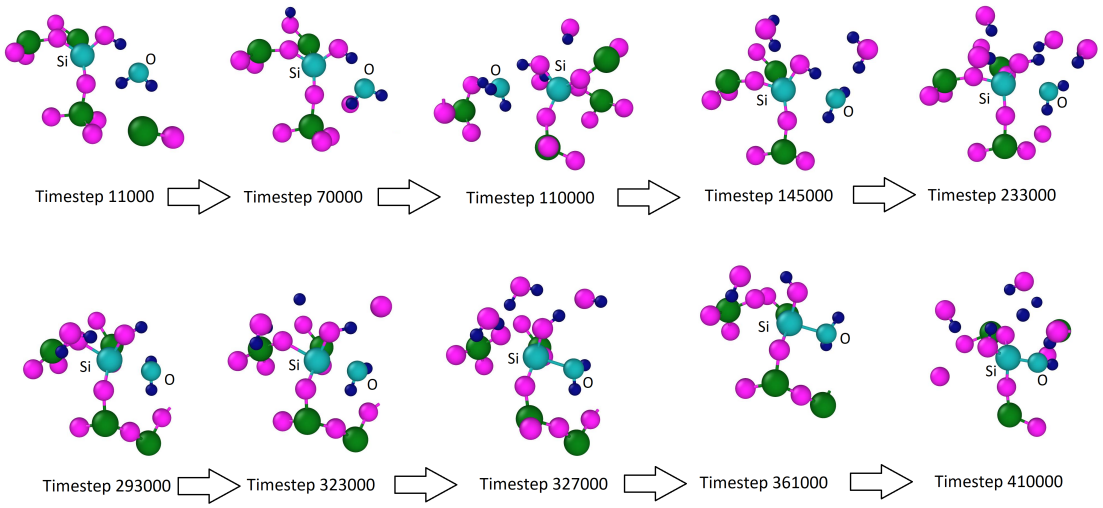

Figure 4.4: Reaction pathway between the water molecule and Si-O-Si of glass through ReaxFF in presence of Silanol: Multiple snapshots of water molecule dissociating the Si-O-Si of glass through ReaxFF calculation. Timesteps of each snapshot are indicated respectively. Reaction between the Oxygen belonging to the water molecule and Si belonging to the glass for each snapshot are highlighted in cyan color and labelled to trace their trajectory across the snapshots.

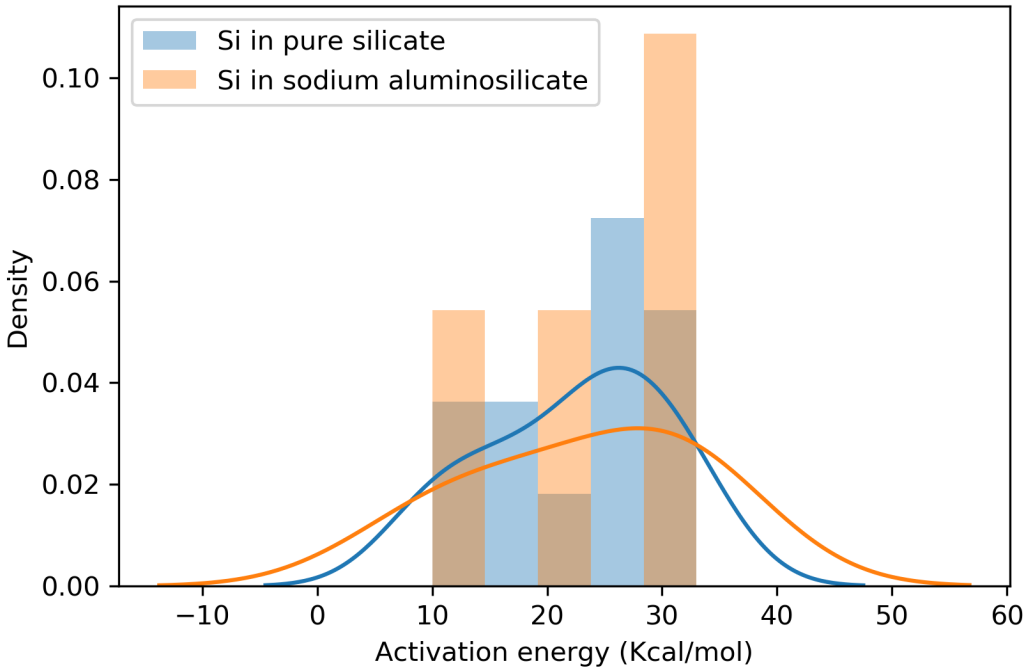

Figure 4.5: Distribution of activation energies for Si in pure silica vs sodium aluminosilicate glass: Histogram plot represents the real value distribution of activation energies for dissociating the Si. Approximate Kernal Density Estimation of the data are displayed as line plot. Color scheme: Blue - Si in pure silica; Orange - Si in sodium aluminosilicate glass.

4.2 Bond dissociation in pure silica and aluminosilicate glasses with different compositions

4.2.1 Difference between divalent and monovalent cations

Recent study has observed that the incorporation of alumina into the silicate glass significantly improves the durability of the glass against water [Gin et al., 2020b]. However, modifiers like potassium, magnesium, sodium or calcium are needed to compensate the charge of aluminum atoms in the glass. Addition of these modifiers at different compositions can largely change the physical properties like density, refractive index, molar volume and thermal expansion [Baral et al., 2019]. At atomic scale, sodium and calcium used as modifiers in the aluminosilicate glass, play different roles due to their size and charge difference. Because for a given Al_2O_3 content in glass, fewer divalent cations like Ca^{2+} will be sufficient to balance the overall charge of the glass compared to monovalent cations like Na^+ [Thompson and Stebbins, 2012]. In general, the number of Non-Bridging Oxygen (NBO - Oxygen atom bonded to only one glass network former and to one modifier to balance the charge) is estimated based on several assumptions. If the system is formed of perfect tetrahedra containing only two coordinated oxygen atoms, then the number of NBO will be $N_{NBO} = 2N_{Ca} - N_{Al}$ [Ganster et al., 2004]. In MD simulation of the sodium aluminosilicate glass [Xiang et al., 2013], it is observed that most of the Si exist in Q4 species (Q4 - Si with 4 bridged oxygen, Q3 - Si with 3 bridged oxygen and so on), with a small number of Q3 in peralkaline regime and very little Q2 species. Increasing the Al_2O_3/Na_2O ratio in the glass favors the formation of bridging oxygen by increasing Q4 of Si from 73% to 98% and reducing Q3 from 22% to 2%. These results are in agreement with the experimental Raman spectroscopy [McKeown et al., 1984]. On the other hand, MD simulation analysis of Calcium aluminosilicate glass leads to a large number of NBO than predicted by the above formula [Ganster et al., 2004]. The excess quantity of NBO is increasing with the size of the glass system, and the proportion of NBO's in glass is between 10.7% to 11.8%. Another NMR study has investigated if the increasing excess number of NBO's in calcium aluminosilicate glasses are due to the size or charge of the calcium ions. They observed that the Ba-aluminosilicate glass contains the same number of NBO's as in the Ca-aluminosilicate glass, whereas in K-aluminosilicate glass the quantity of NBO is lower. This indicates that the difference in charge of the cation plays an important role in the creation of NBO's [Thompson and Stebbins, 2012]. A divalent cation has difficulties to compensate two Al entities and it is why the formation of NBO is favored. On the other hand, monovalent cations balance the charge of only one Al entity and so the quantity of NBO is expected to be low [Thompson and Stebbins, 2012]. It is very important to note that, in each type of aluminosilicate glasses, majority of the NBO's are located on the Si tetrahedra, and very few NBO's are located on the Al tetrahedra [Ganster et al., 2004, Xiang et al., 2013]. So changing the modifiers in an aluminosilicate glass leads to differences in the glass structure at the atomic scale. It motivates us to investigate the impact of these structural differences on the distribution

of activation energies for bond dissociation using the potential mean force method in the same way as in Chapter 3.1.

4.2.2 Results

In chapter 3.1, we compared the activation energy between pure silica and lime alumino silicate glasses. It was observed that Al is strengthening the neighboring Si by increasing its activation energy. In this chapter, we have investigated the compositional effects of Na or Ca or both in aluminosilicate glasses to better understand the role of these modifiers. We used 3.5Å as cut-off for selecting the water molecules close to the Si atoms at the interface, for performing the chemical reactions using the PMF method. By this approach, we investigated several chemical reactions for six different compositions with multiple glasses for each composition. The details are given in the Table 2.5. We prepared 15 glasses for each composition and investigated the basic structural features like average bond angles and coordination chemistry. It is observed that all the 6 compositions of glasses share almost similar structural properties as shown in Table 4.1. Then we calculated the activation energy through Potential Mean Force (PMF) method as described in Section 2.2.3. Concerning the dissociation of Si in the CASN1 glass containing only Ca as modifier, we observed that the activation energy is significantly increased in comparison with the pure silica glass as shown in the Chapter 3.1. We wanted to test if the strengthening effect of Si by Al remains valid after replacing the Ca by Na. It corresponds to the CASN5 glass. We observed that the average activation energy is 1.307 eV and the statistical test comparison with pure silica indicates that the two distributions are significantly different with P-value of 0.009 as shown in Figure 4.6. However, mixing both the modifiers Ca and Na equally in the CASN3 glass indicates that the strengthening effect of Al on the dissociation of Si is less or not present. We observed that the average dissociation energy decreases to 1.27 eV and the distribution of data is not statistically different from the distribution in pure silica glass. As shown in the Figure 4.6, we observed that for CASN5, most of the data are populated between 1 eV to 1.5 eV. On the other hand, the distribution for the CASN1 glass indicates that the data are more distributed between 0.8 eV to 1.6 eV, and the distribution has two maxima.

When we investigated the effect of mixing equal amount of Ca and Na in the aluminosilicate glass, we observe a decrease in the mean activation energy around Si at 1.277 eV (glass CASN3). Statistical test indicates that the distribution is not significantly different from that in pure silica glass with P-value of 0.139. To investigate if this decrease in activation energy is due to a compositional effect or is linked to disorder, we designed two more glasses containing both the modifiers. One glass contained more Ca and less Na, another glass contained more Na and less Ca. They are named CASN2 and CASN4 respectively. The distribution of dissociation energies in the CASN4 is more disordered than in the CASN5 glass with a single maximum as for the CASN5 glass. The CASN4 distribution is wider than in CASN5 and narrower than in CASN3. This can be clearly seen in Figure 4.7, where we calculate the standard deviation for distribution of dissoci-

Structural features	Pure silica	CASN1	CASN2	CASN3	CASN4	CASN5
Si-O-Si	151.15	148.59	150.43	148.02	149.987	151.23
O-Si-O	109.4	109.38	109.40	109.39	109.40	109.41
O-Al-O	-	108.95	109.19	109.14	109.20	109.21
Si-O-Al	-	134.52	139.61	136.44	137.855	134.92
H-O-H	104.25	104.23	104.21	104.47	104.26	104.28
NBO O	213	209.72	207	217.90	213	207
O2	242	205.90	213.9	198.8	197.0	193.9
O3	1	13.36	8.09	12.27	10.0	12.09
Ca5	-	9.09%	16.26%	15.9%	12.72%	-
Ca6	-	27%	44.01%	41.6%	52.7%	-
Ca7	-	23.26%	28.2%	34.09%	34.5%	-
Si4	99.23%	100%	100%	100%	100%	100%
Al4	-	98.3%	94.4%	99.0%	100%	97%
Na6	-	-	3.7%	10.5%	10.76%	11.02%
Na7	-	-	18.93%	19.6%	27.75%	23.98%
Na8	-	-	34.09%	27.6%	28.9%	35.78%
Na9	-	-	28.78%	27.27%	20.5%	17.21%

Table 4.1: Comparison of structural features for pure silica, calcium aluminosilicate, sodium aluminosilicate, sodium lime aluminosilicate glasses

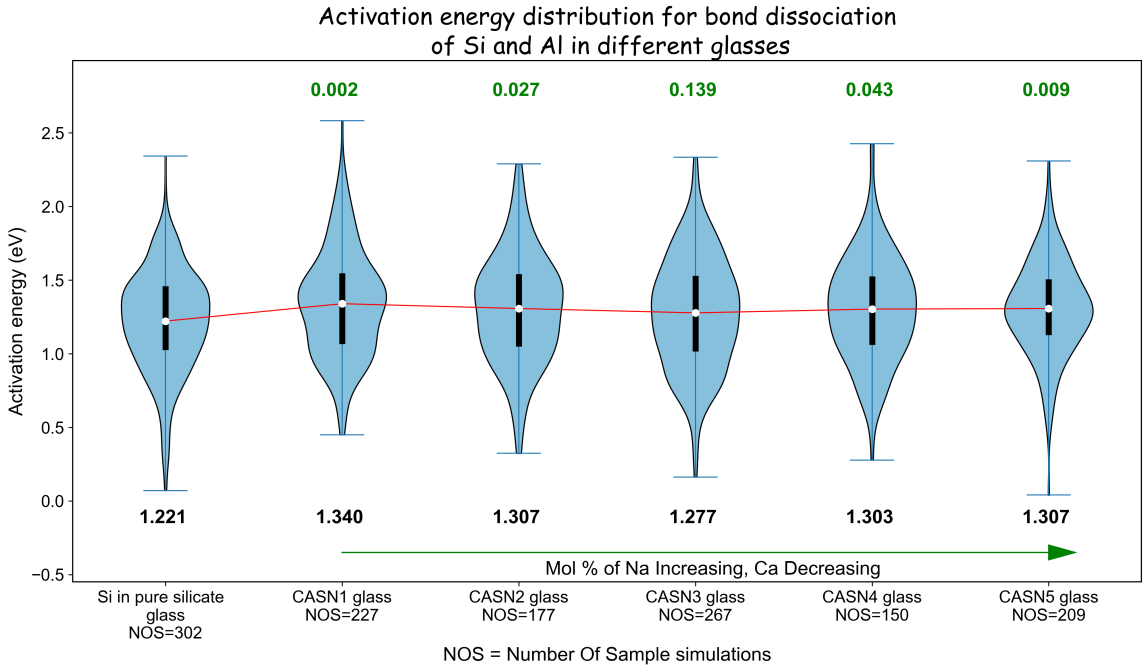

Figure 4.6: Distribution of activation energy for Si in pure silica and 5 CASN series of glasses. The blue violin shaped curve represents the distribution of data. Solid white circles represent the mean of the distribution, the red line connects the mean values and the black line represents the standard boxplot of Q_1–25th percentile, Q_3–75th percentile. The two whiskers extending the boxplot represent the standard boxplot minimum and maximum. Green colored numbers on top of each violin plot represents the P-value with respect to the comparison of the first violin plot (Si in pure silica glass). Black colored numbers below each violin plot represent the mean energy in eV.

ation energies for each glass. Similarly, in the CASN2 glass with more Ca and less Na, the standard deviation is larger than in CASN1 but lower than in CASN3. These results indicate that the effect of mixing Na and Ca in the aluminosilicate glasses on the mean dissociation energy is not linear and both the chemistry and the topological order have an impact.

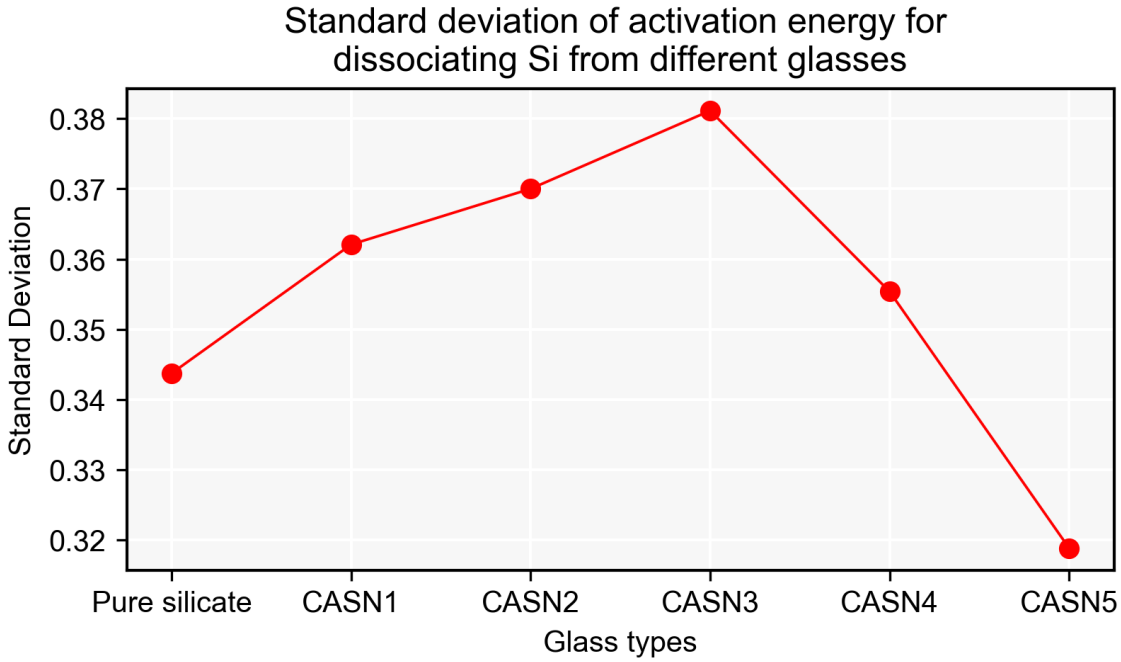

Figure 4.7: Standard deviation of the distribution of activation energy for dissociating Si in pure silica and all 5 CASN series of glasses.

4.3 Bond reformation energies in silica and aluminosilicate glasses

4.3.1 Introduction

Monte-Carlo models fitted on experiments are promising approaches to investigate the origin of gel formation and its aging mechanism as discussed in the Section 1.4.3. To develop such models, it becomes very important to understand the elementary mechanisms especially the bond dissociation and reformation, as they play vital role in the gel formation mechanisms. Most of the research, based on classical Molecular dynamics [Kagan et al., 2014], ReaxFF [Rimsza et al., 2016], Ab initio [Pelmenschikov et al., 2001, Criscenti et al., 2006b] and experimental methods [Icenhower and Dove, 2000] are focused on estimating the activation energy to dissociate the Si-O-Si bonds. However, the energy required for the Si-O-Si bond reformation remains poorly understood. So in this study, we try to estimate these reformation energies in pure silica and in different compositions of aluminosilicate glasses.

4.3.2 Results

Activation energy for bond dissociation can be estimated by progressively approaching one water molecule towards the Si or Al of the glass using the PMF method until the water molecule dissociates one bond around the Si or Al atom. However, there is no straight-forward approach to estimate the bond reformation energy because once the water molecule has dissociated the Si-O-Si bond, two silanol groups are formed. Approaching the oxygen of one silanol group towards the Si of the other silanol group is complicated because the silanol groups formed after the dissociation are not always close to each other. To overcome these issues and to estimate the bond reformation energies of bonds around the Si and Al atoms, we used a different approach. In Figure 3.1, we have applied the potential mean force method to approach the oxygen belonging to one water molecule close towards the Si or Al of the glass (target atoms) for the dissociation. During this process, from the distance of 3.5 Å to an average 2.1 Å distance, a positive force is applied to compensate the repulsion between the water molecule and the target atom. On the contrary, below 2.1 Å the water molecule tends to be attracted by the target atom and in this case a negative force has to be applied to compensate this attraction. This is the reason why we observe that the potential mean force becomes negative between 2.1 Å and 1.6 Å (See Figure 3.1 and the Figure 2.4). Due to these reasons, we propose to integrate the potential mean force curve from 3.5 Å to 2.1 Å to have an estimation of the activation energy for the bond dissociation and to integrate the negative part of the force to have an estimation of the activation energy required for the bond reformation. This represents an over estimation of the reformation energy because in this case, we suppose that the reverse way of the bond dissociation is also the way for the bond reformation. Likewise,

the estimation of the activation energies for bond reformation in pure silica, and in lime aluminosilicate glasses are shown in Figure 4.8.

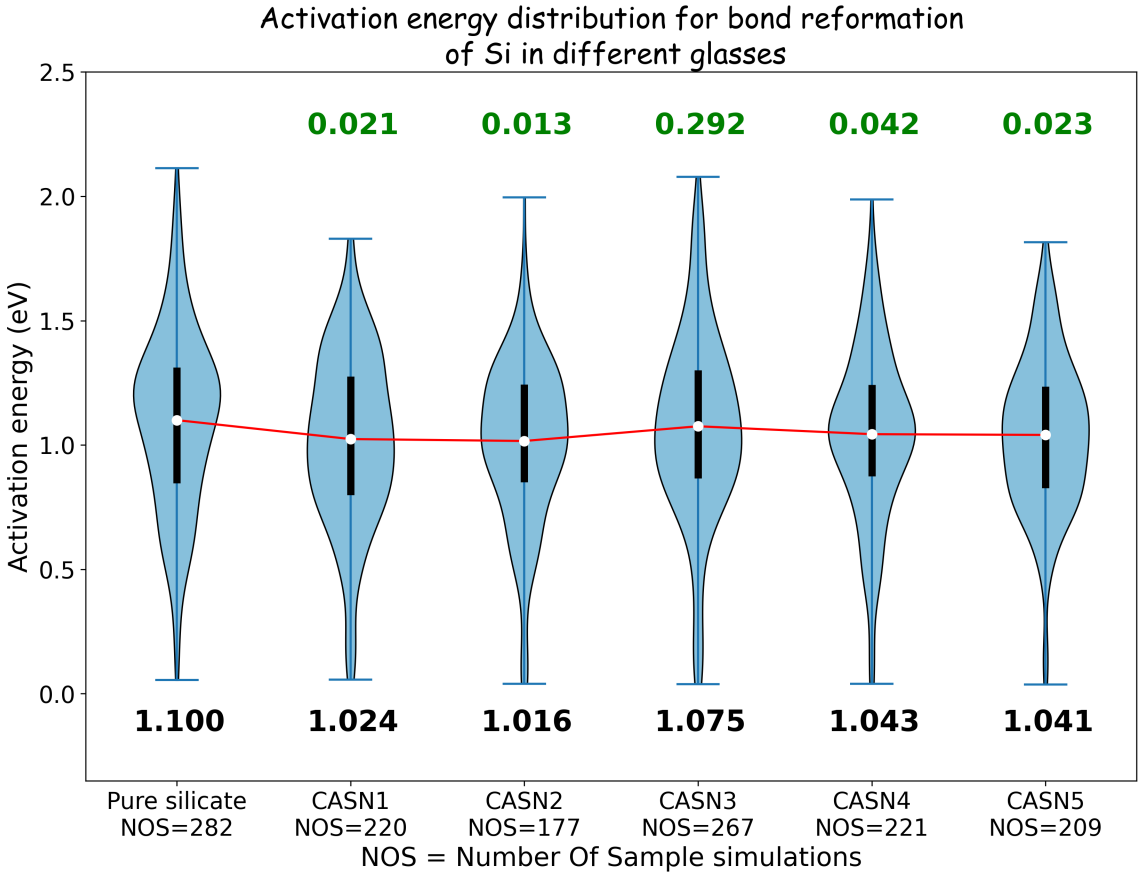

Figure 4.8: Distribution of bond reformation energies of Si in pure silica and in the CASN series of glasses. The blue violin shaped curve represents the distribution of data. Solid white circles represent the mean of the distribution, the red line connects the mean values and the black line represents the standard boxplot of Q_1–25th percentile, Q_3–75th percentile. The two whiskers extending the boxplot represent the standard boxplot minimum and maximum. Green colored numbers on top of each violin plot represents the P-value with respect to the comparison of the first violin plot (Si in pure silica glass). Black colored numbers below each violin plot represent the mean score in eV.

This study finds that, in general, the energy required to reform the bonds is lower than to dissociate the bonds, which is in agreement with what is observed experimentally. Otherwise, the glass will be rapidly and completely dissolved. We have observed that the average activation energy required to reform the bonds is 1.1 eV for Si in pure silica glass. On the other hand, reforming a bond around Si in all other CASN glasses is easier than in pure silica glass with exception of CASN3 whose reformation energy is close to the energy in pure silica. Statistical test to compare the distribution of these reformation energies to pure silica glass indicates that all distributions in the CASN series are significantly different with P-value less than 0.05 except for the CASN3 glass. This is in agreement with what we observed for the activation energy of bond dissociation, where CASN3 displayed an energy value close to that of the pure silica glass. So in general, addition of Al into the silicate glass increases the durability by increasing the activation energy required to break the bonds around Si and by decreasing the activation energy required

to reform the bonds around Si. Similar to the activation energy for bond dissociation, energy required for reformation around Al in lime aluminosilicate glass is low comparing to the reformation energy around Si. This suggests a possible correlation between the reformation energy and dissociation energy. i.e., Si bonding with Al as second neighbor could be more robust, but reformation of a bond around Si is also more difficult.

4.4 Discussion

Calculations performed with ReaxFF to investigate the different mechanisms for the bond dissociation around Si in silicate glasses shed some light on the understanding of the PMF calculations performed with larger statistics. In ReaxFF, we observed initially that the water molecule is exploring multiple channels and selects one channel to progressively approach the target Si atom. In some other cases, initial orientation of the water molecule has been inverted with respect to the target atom and so the water molecule has to rotate first before it approaches and dissociates the bond around the target Si atom. In PMF calculations, we observed that activation energy for dissociating the bond around Si is in range from 0.1 - 2.35 eV. On the other hand, in another recent study using the same reactive classical potential with the PMF approach, they estimated the activation energy in the range between 0.17 eV - 0.95 eV [Kagan et al., 2014]. In Ref [Kagan et al., 2014], the authors have chosen one particular orientation for the water molecule to target the siloxane bond, which corresponds to the easiest way to dissociate the Si-O-Si bond. However in our PMF calculations, the orientation to attack the target siloxane bond is constrained through the PMF method with respect to its initial orientation. The orientation of the water molecule is not optimized to follow the easiest way to dissociate the bonds. It can be concluded that the initial orientation of the water molecule has a significant impact on the dissociation energy.

In PMF results, we also observed that dissociating a bond around Si coordinated with three bridged oxygen is more difficult than around a Si with four bridged oxygen. But we were not able to trace any reason for this increase in activation energy. In ReaxFF, when the target Si is surrounded by three bridged oxygen, we observed that the non-bridged oxygen attached to the Si is oriented very perpendicular to the initial position of the water molecule, which blocks the approach of the water molecule. In such case, the water molecule first "waits" until the hydroxyl group moves in such a way that the path is created for the water molecule to approach near the target Si. Therefore, we observed the activation energy to be higher than in the other cases where the Si is surrounded by the four bridged oxygen. The rise in activation energy could vary and depend on the orientation of the OH group (Sometimes, the OH can potentially block the water molecule, leading to a high increase of the activation energy). As a result, the fact that in PMF calculations, it is more difficult to dissociate the bond around a Si with three bridged oxygen than four bridged oxygen can be associated to the presence of the dangling bond that blocks the water molecule.

After comparing our PMF results with ReaxFF results, we proceed to investigate more complex glasses by replacing Ca with Na or by mixing both Ca and Na in varying compositions. We observed that Ca as modifier made the aluminosilicate glass to be more disordered which can be seen through the wider distribution in Figure 4.6. Then replacing Ca by Na leads to a decrease of the standard deviation of the distribution of dissociation energies. Also, the mean activation energy slightly decreases. Yet the distribution remained significantly different from the pure silica glass, and the strengthening effect of

Al on Si remains valid. On the other hand, when both Ca and Na are mixed equally, the overall activation energy decreased even less compared to the glass containing only Na, and the distribution remained very wide indicating an increase of the disorder (CASN3 shown in Figure 4.6). To better understand this compositional effect, we designed two more glasses, one containing more Ca and less Na (CASN2) and another containing more Na and less Ca (CASN4). The standard deviation of the distribution for these glasses are shown in Figure 4.7. We observed that standard deviation of CASN2 lies between those of CASN1 and CASN3, on the other hand, standard deviation for CASN4 lies between those of CASN3 and CASN5. These results suggest two important correlations between the distribution of the dissociation energies and the structure of the glass:

1. Both Ca and Na lead to an increase of the dissociation energy for the bonds around Si. However, Ca seems to be more efficient than Na.

2. Glass structure becomes more disordered when Ca and Na are mixed together. This increase of the disorder leads to a decrease of the activation energy for dissociation.

3. In consequence, the dissociation energy changes in a non-linear fashion with the Ca/Na ratio.

4.5 Conclusion

ReaxFF calculations revealed three important mechanisms by which the water molecule dissociates the Si-O-Si bonds of the silicate glass. (i) The initial water molecule might be inverted against the target Si, and water needs energy to rotate before it dissociates the bond around the target Si. (ii) The water molecule explores multiple channels, before "choosing" one channel to progressively approach near the Si and finally dissociates the bond. (iii) In some cases, when the target Si is connected to three bridged oxygens, the OH group attached to the Si might be oriented perpendicular to the water molecule. As a result, the water is approaching near the Si in a more constrained environment, and the dissociation is possible only when the OH group reorients itself in such a way that the channel for the water to approach the Si is opened. These results can explain why the activation energy for the bonds around a Si with three bridged oxygen is higher than around the Si with four bridged oxygen in PMF calculations. We observed that, adding Ca in aluminosilicate glass increases the disorder of the glass; On the other hand, replacing the Ca by Na leads to a slight decrease of the activation energy for bond dissociation around Si. In both the glasses, the strengthening effect of Al on Si is observed. However, when we mixed an equal quantity of Ca and Na in aluminosilicate glass, it becomes more disordered and it can explain a decrease of the activation energy compensating the strengthening role of Al. Finally, the estimated activation energy for bond reformation was lower than the bond dissociation. It is why the formation of the gel is possible. Also, the bond reformation energy around Si in aluminosilicate glass is lower than around Si in pure silica glass.

Chapter 5

Long-term glass dissolution experiment and fitting with Monte-Carlo simulation method

Contents

5.1 Introduction

Role of Al on silicate glass has been of great interest, as it regulates the glass durability in a non-linear fashion [Damodaran et al., 2022, Vienna and Crum, 2018, Gin et al., 2020b, Hamilton et al., 2001]. A recent study showed that adding Al_2O_3 into sodium borosilicate glass changes the gel formation mechanism [Gin et al., 2020b]. In the glass with no Al_2O_3 (CJ1) [Gin et al., 2020b], Si is released into the solution and once the solution achieves saturation with respect to amorphous silica, Si precipitates on the surface of glass to form a gel layer enriched in silica. On the other hand, for the glass with Al_2O_3 (CJ2) the gel layer is formed by partial hydrolysis (local reorganization around Si) without releasing much Si into the solution. To understand the impact of Al_2O_3 on the long term dissolution of these glasses, we designed 6 glasses with varying wt% of Al_2O_3 (from 0 wt% to 9.6 wt%) and these glasses were altered at 90°C, in deionized water, high SA/V for 180 days. To start understanding the gel formation mechanism, and what are the contributions from hydrolysis, redeposition and diffusion, we used the Monte-Carlo method presented in Section 2.4.3. The objective is to reproduce the experimental results. By fitting the MC parameters on the experimental release of B and Si into the solution, a new understanding of the actual mechanism at the origin of the residual regime is proposed.

5.2 Results

5.2.1 Results of the 180-day alteration experiments

6 SBNA glasses with varying concentration of Al_2O_3 were designed to study the role of Al on mechanisms of gel formation and resulting residual alteration. These glass powders were put in distilled water (pH9 in 90°C) at high SA/V ratio for long-term alteration. During the first few samplings, the pH of the solutions for all the glasses were monitored and the pH was 9 ± 0.25. More experimental details are given in the section 2.4.2. Figure 5.1 shows the Si equivalent thickness, Eth(Si) plotted against square root of time. In all cases, Eth(Si) readily increases and eventually achieves a plateau, which can be considered as the saturation of the solution with respect to the gel. The value of the plateau broadly varies depending on the glass. The three glasses with the lowest Al content (SBNA1, SBNA4 and SBNA5) have the highest Eth(Si), whereas the glasses with increasing concentration of Al display a decreasing Eth(Si) at saturation.

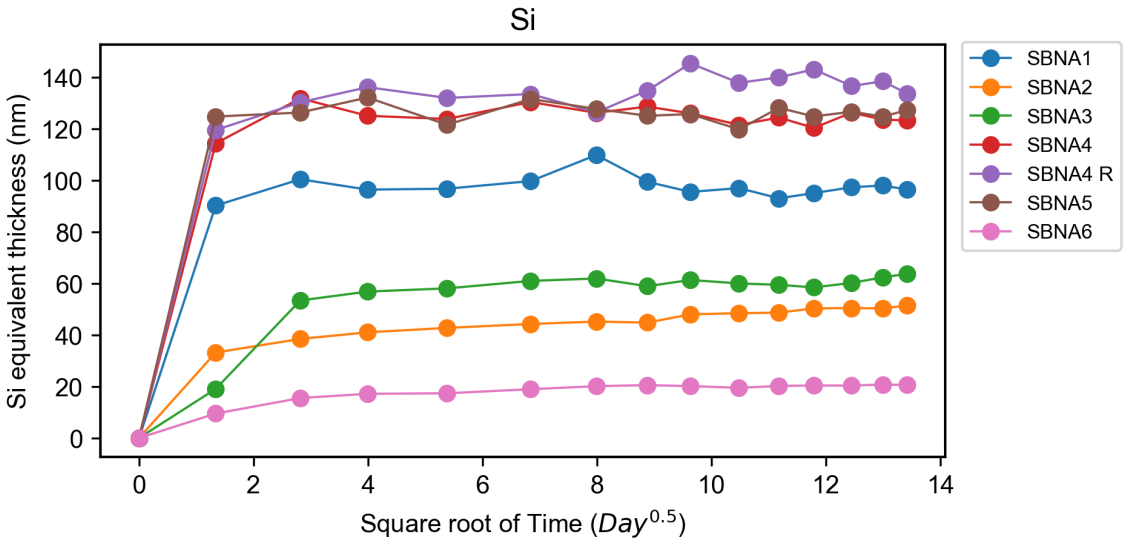

Figure 5.1: Long term dissolution of Si from SBNA series of glasses recorded with respect to the square root of time. Color scheme for each glasses are indicated appropriately. SBNA4 R is repeat of SBNA4 to verify the consistency of the dissolution experiments.

If one consider that the residual rate regime begins when solution is saturated, it can be noted that all 6 SBNA glasses reach residual rate almost at the same duration, the difference arise depending on the quantity of Si needed to reach the residual regime. Based on pH (remained constant with 9 ± 0.25 during the experiments) and temperature ($90°C$) in which the experiment was conducted, the concentrations of H_4SiO_4 species during the saturated condition were calculated using the Jchess geochemical code [Van Der Lee et al., 2003], whose details are given in the Section 2.4.2. It is verified that solutions are undersaturated with respect to most of aluminosilicate minerals, so that in our tested conditions, the only alteration product is the gel. Furthermore, a decreasing trend between the activity of H_4SiO_4 and the Al_2O_3 content of glass is observed (Figure

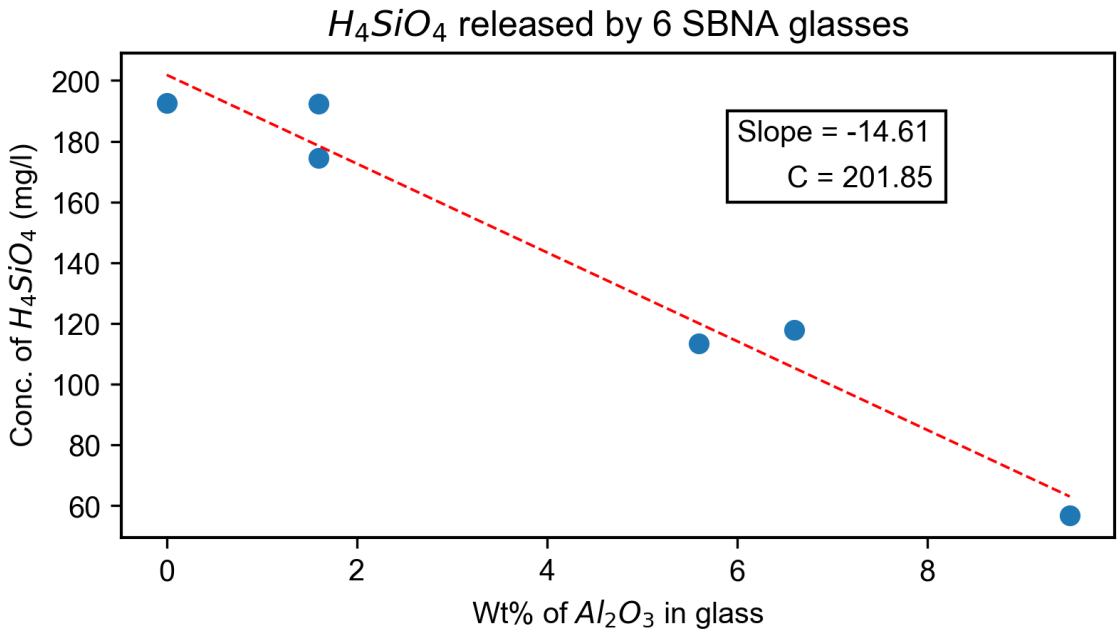

Figure 5.2: Correlation between the concentration of H_4SiO_4 present in the solution upon saturation vs concentration of Al_2O_3 in SBNA series of glasses. Linear regression of the correlation are displayed with red dotted line.

5.2). This suggests the presence of Al is efficiently controlling the release of Si into the solution. This is because the concentration at saturation of the solution with Si is at equilibrium between the bond dissociation and bond reformation. Our PMF result shows that Al as second neighbour strengthens the Si for bond dissociation and lowers the activation barrier for bond reformation as discussed in Chapter 4.1. As a result, gel formation gets more dependent on the concentration of Si added to the glass.

On the other hand, the dissolution pattern of B and Na into the solution followed an identical trend as shown in Figure 5.3 and 5.5. After the glass reaches residual rate ($3\frac{1}{2}$ days), it is important to note that glasses with 0 to 1.6 wt% of Al_2O_3 offered a strong protection against the release of B and Na into the solution. In contrast, the glasses which had between 5.5 to 9.6 wt% of Al_2O_3 continued to release B and Na at a much higher rate than the other glasses. For these glasses, the release rate of B and Na into the solution starts to be limited beyond 81 days of alteration. Hence, two opposite patterns of B and Na release into the solution with respect to the quantity of Al_2O_3 are observed. To mathematically evaluate this behavior, for each sampling t, we calculated the slope of the B released for sample t-1 and t+1, to monitor the velocity of B released into the solution as shown in Figure 5.4. It is observed that, glasses with more Al_2O_3 limits the release of B at least 10 times slower than the glasses with less Al_2O_3. It is important to note that release of Na into the solution was less than B for glasses with more Al content. Whereas, glasses with less Al content had similar equivalent thickness of B and Na. This could be possible because some of the Na might be retained in the gel to compensate the charge of Al.

This work confirms what has been observed previously for the CJ1 and CJ2 glasses

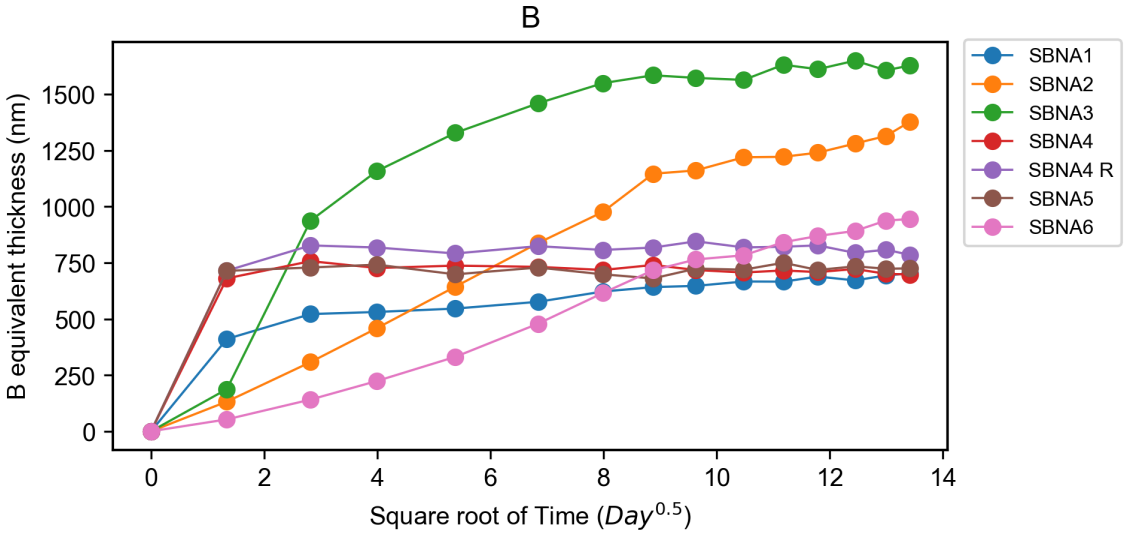

Figure 5.3: Long term dissolution of B from SBNA series of glasses recorded with respect to the square root of time. Color scheme for each glass are indicated appropriately. SBNA4 R is repeat of SBNA4 to verify the consistency of dissolution experiments.

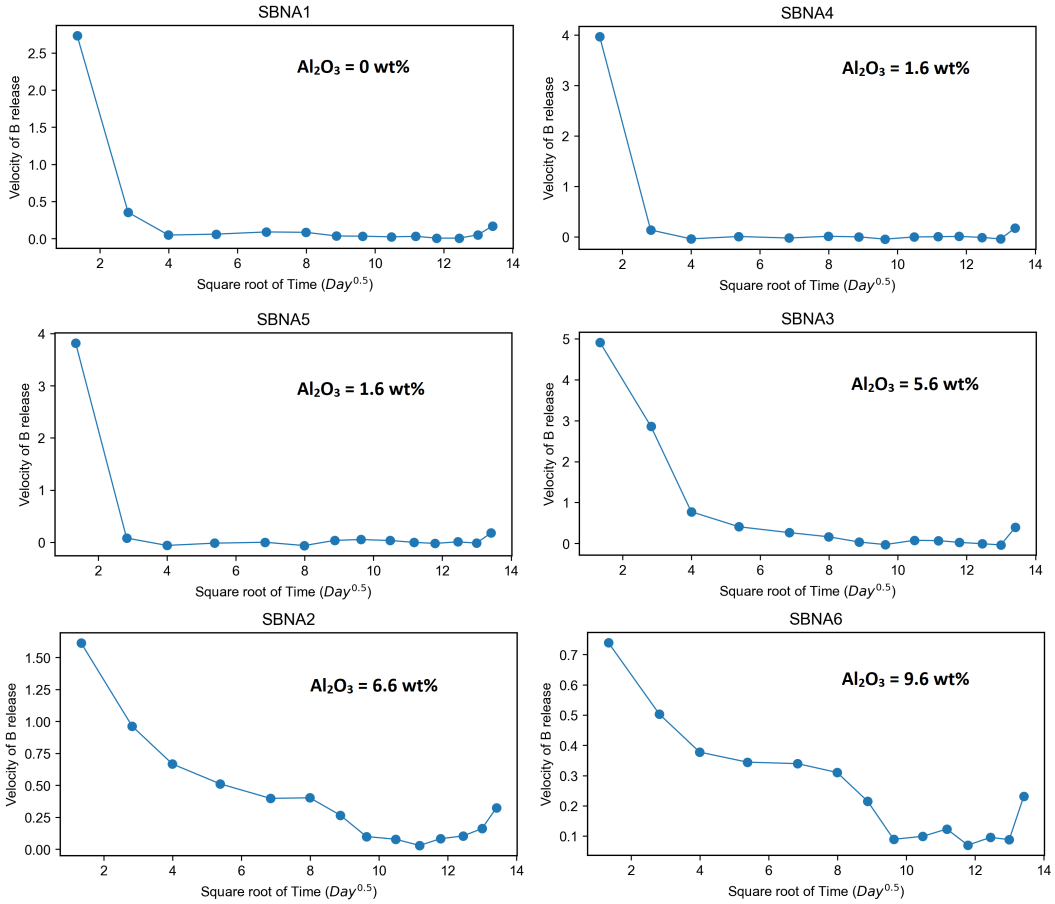

Figure 5.4: Velocity of B release rate for each glass is plotted individually. The rate drop of glasses with low concentration of Al_2O_3 (SBNA1, SBNA4, SBNA5) is very sharp. The rate drop of glasses with high concentration of Al_2O_3 (SBNA2, SBNA3, SBNA6) is gradually decreasing.

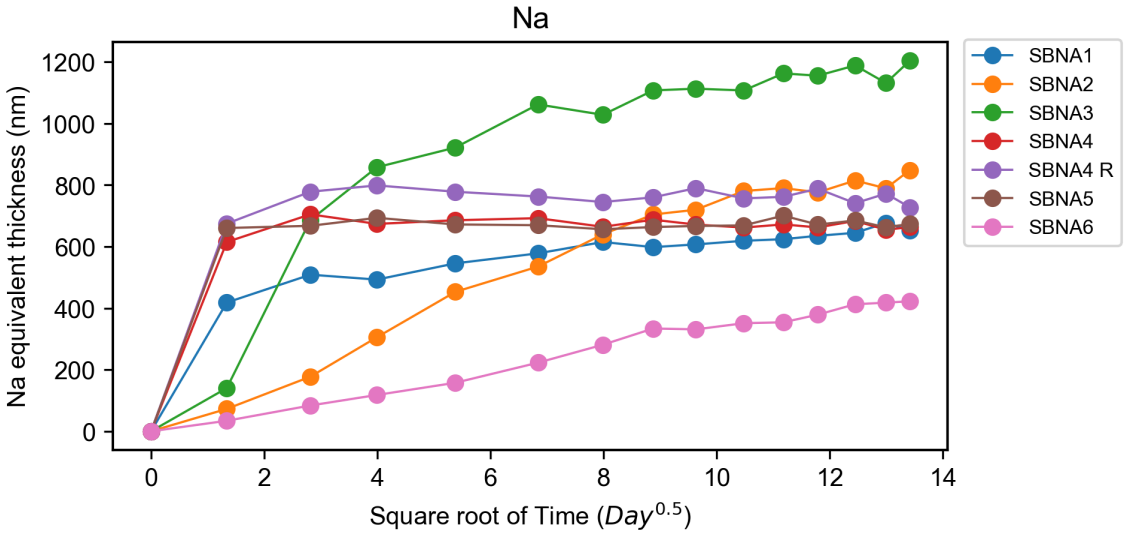

Figure 5.5: Long term dissolution of Na from the SBNA series of glasses recorded with respect to the square root of time. Color scheme for each glass are indicated appropriately. SBNA4 R is repeat of SBNA4 to verify the consistency of dissolution experiments.

i.e., a glass without Al_2O_3 and another glass containing 6 wt% of Al_2O_3 [Gin et al., 2020b]. Gin et al., [Gin et al., 2020b] observed two different gel formation mechanisms for the sodium borosilicate and sodium aluminoborosilicate glass: Former glass develops the gel through dissolution and reprecipitation mechanism, whereas in the later glass, local reorganizations are at the origin of the gel formation. We investigated if the addition of a small quantity of Al_2O_3 into the glass as in the case of SBNA4 and SBNA5 is sufficient to modify the dissolution/reprecipitation mechanism of gel formation. Indeed the release pattern of B and Na for these two glasses were similar to the SBNA1 = CJ1 of [Gin et al., 2020b]. To investigate its gel formation mechanism, we altered the SBNA4 glass coupon in ^{29}Si saturated solution for 1 month at pH9, 90°C. Then we investigated the exchange mechanisms in the SBNA4 glass with ToF-SIMS in positive mode to estimate the ratio of $^{29}Si/^{28}Si$, and results are shown in Figure 5.6. The ratio of $^{29}Si/^{28}Si$ in the alteration layer is 0.005 which is equal to the natural abundance, indicating that gel was formed in local reorganization mechanism similar to the CJ2 type of glass. This suggests that, adding a small quantity of Al_2O_3 into the glass is sufficient to change the gel formation mechanism from dissolution/reprecipitation to local reorganization. Surprisingly, we observed the retention of B in the gel, and the concentration profile is a decreasing gradient from the reaction front of the glass to the surface of the gel in contact with water. This signifies that there is a strong limitation of B release into the solution during the residual regime.

5.2.2 Pilot study about Wbreak, Wred, and Wsaut, the Monte-Carlo parameters

In this paragraph, we will present the pilot studies performed to better understand the impact of each Monte-Carlo parameter on the results. The next section will present

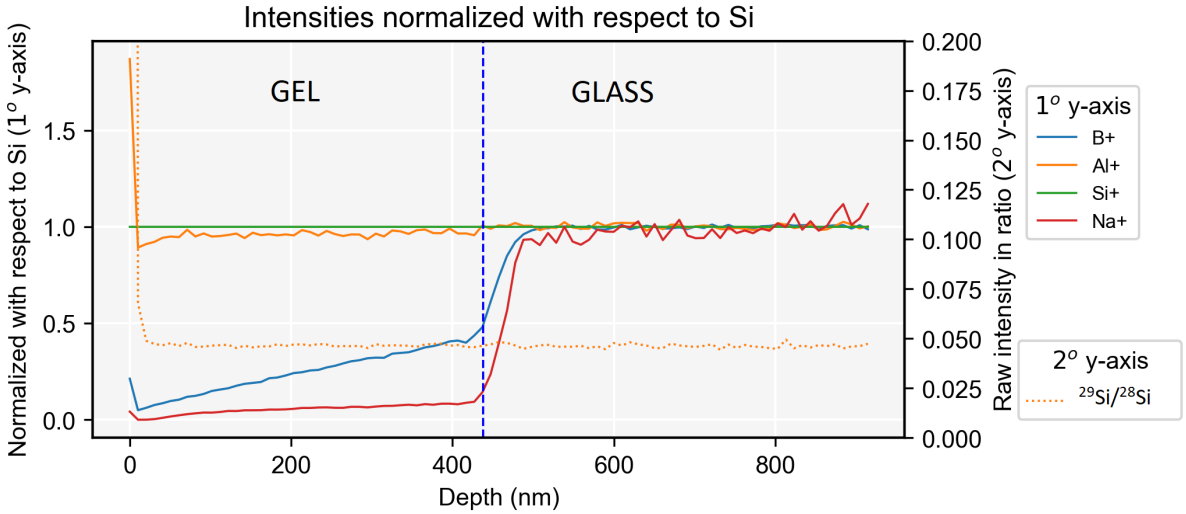

Figure 5.6: SBNA4 coupon after 1 month of alteration in Si saturated solution, analyzed with Tof-SIMS in positive mode. Solid lines are plotted for primary y-axis, whose values are normalized with respect to the intensity of Si. Details about the element normalization are given in Section D.1.3; Dotted lines are plotted for secondary y-axis; A blue straight dotted line separates the altered gel and pristine glass.

the fitting of the Monte-Carlo approach to the experimental results. This Monte-Carlo approach considered 8 mechanisms to simulate the glass alteration, which are listed below:

1. Water diffusion into the solid network (Wsaut),
2. Bond breakage in the solid network (Wbreak),
3. Reformation of the chemical bonds in the solid network,
4. Si/Al can be conditionally released into the solution,
5. Si/Al can be conditionally redeposited on the glass surface (Wred),
6. Migration of vacancy on the solid network (Wvacan),
7. Jump of the water molecule from the liquid network into the neighboring vacancy,
8. Removing the isolated clusters of solid into the solution,

All these mechanisms are described in detail in section 2.4.3. To reproduce the experimental data of Si and B released from the glass into the solution over a long term, we concentrate on three preponderant parameters. The three probability terms are Wbreak, Wred, and Wsaut, which regulate the bond dissociation on the solid network, the redeposition of Si/Al on the glass surface, and the diffusion of water on the liquid network inside the solid network, respectively. To better understand their impacts, a pilot study was performed with 5 different values for each probability term for the same glass. So a total of 5 x 5 x 5 = 125 simulations are performed, and the total number of Si and B released into the solution are measured for each simulation. The results are shown in Figure 5.7.

It is observed that the increasing value of Wbreak has a direct influence on the number of Si released into the solution, as seen in Figure 5.7A. When the value of Wbreak increases, it favors the dissociation of bonds around Si in the solid network. It is also important to note that increasing Wbreak not only increases the average number of Si released into the solution, but also increases the standard deviation of the points. This indicates the control from the other parameters are growing, and Wbreak is less preponderant. It can be noted that Wbreak does not have any influence on the number of B released into the solution because, in MC-calculations, a B-O-X bond is opened immediately when one water molecule arrives on it. The rate of the B-O-X bond breakage is independent of Wbreak. Correlation with Wred revealed that the release of Si has an inverse relation with increasing this parameter, and Wred has no control over the release of B into the solution since B is not considered for the redeposition. Finally, the investigation of Wsaut revealed it has strong correlation with the number of B released into the solution. This is because increasing Wsaut increases the jump probability of water from the liquid into the solid network. Since B dissolves instantly when all the bonds around it are hydrolyzed, Wsaut strongly correlates with B dissolution. On the other hand, Wsaut controls the release of Si only to a certain extent, beyond which it does not influence, as shown in Figure 5.7E. It is worth noting that increasing the value of Wred decreases the standard deviation of the total number of Si released into the solution, which is opposite to the trend observed with Wbreak. This suggests a correlation between the Wbreak and Wred parameters to control the release of Si in solution. Nevertheless, we can see that with the three parameters, Wbreak, Wred, and Wsaut, we have several degrees of freedom to fit the quantities of Si and B released in the solution.

5.2.3 Monte-Carlo simulations to reproduce the experimental release of Si and B into the solution

To better understand the dynamics of the gel formation for SBNA glasses, Monte-Carlo simulations were performed to reproduce the experimental long-term glass dissolution. However, the glasses with 0 to 1.6 wt% of Al_2O_3 quickly released the Si, B, and Na into the solution initially, and during the residual regime, the release of B and Na are highly controlled. Since the mechanism behind the limitation of B and Na released into the solution is not understood correctly, these glasses were not included in this study using the MC simulation. Therefore we performed multiple MC calculations to search for the best parameters to reproduce the experimental dissolution data of the three SBNA glasses, which have more than 5.6 wt% of Al_2O_3. More details about the simulation box size and numbers of Si, B, and Al atoms for each glass network are listed in Table 5.1. The simulation box size is given as the number of edges along the particular axis, where the size of each edge considered during the MC simulation is 3.5 Å. Therefore, when we have N atoms of Si, B, Na, O, and Al on the MC network, the system's density will be close to the experimental glass density ≈ 2.5 g/cm^3. Therefore, even if Na and O atoms are not explicitly introduced on the solid network, they must be considered to estimate

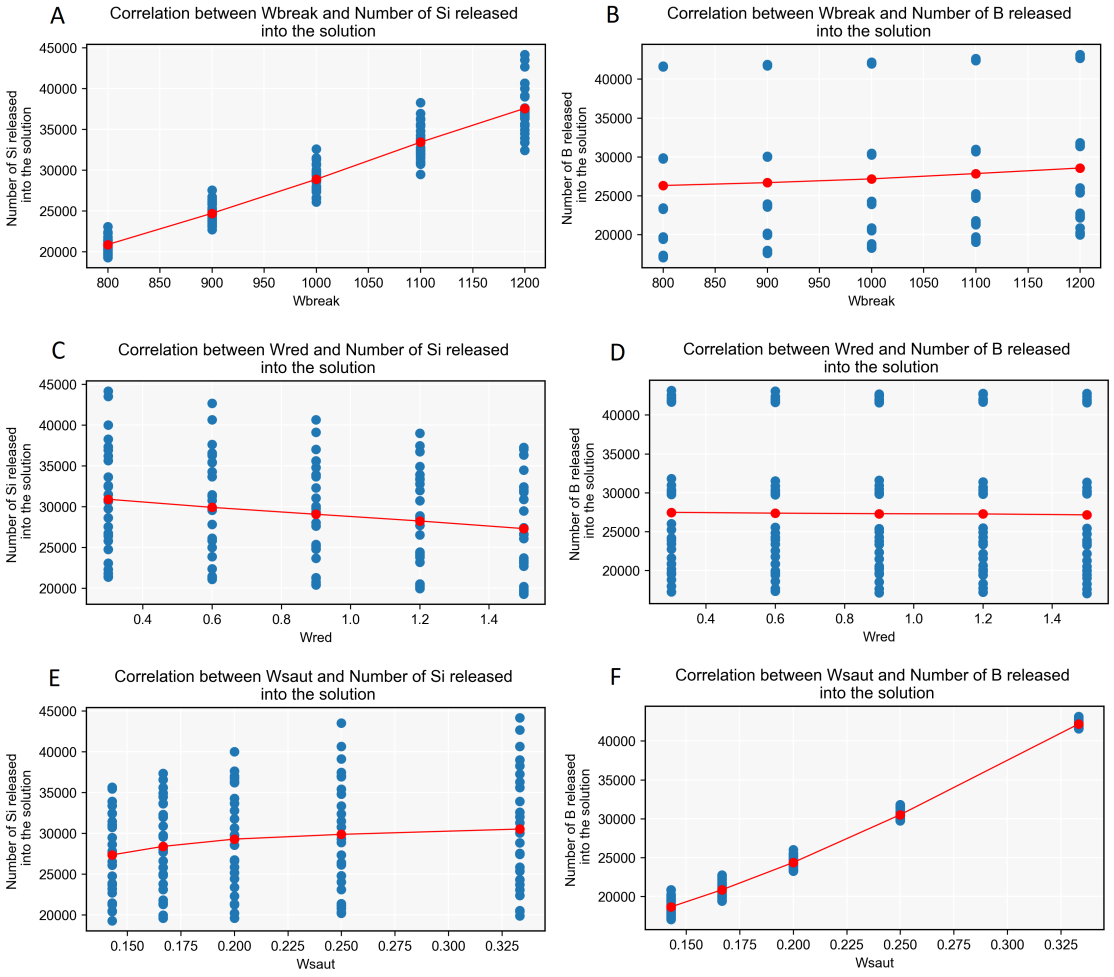

Figure 5.7: Pilot study to understand the correlation between release of Si and B with Wbreak, Wred and Wsaut parameters of Monte-Carlo.

the system density. Also, assigning the size of an edge in the MC network will help us to compare with the experimental equivalent alteration thickness of glass.

With this, we reproduced the release of B and Si with respect to the square root of time (hour) for the three glasses in Figure 5.8, and the fitted parameters are listed in Table 5.1. However, these MC calculations cannot reproduce the slow drop of B release rate into the solution. This is because when one B atom is completely hydrolyzed, it is released directly into the solution, irrespective of its location. Consequently, it is impossible to reproduce the progressive slowing down of the B release in the solution as long as the alteration gel forms between the pristine glass and the solution. The current version of the Monte-Carlo code does not account for the diffusion of B atoms across the gel. Therefore, we reproduced the release of B and Si until the gel controlled the B release (i.e., before the slope modification). It is also important to consider that it takes more than 20 days to complete 1 calculation for the selected MC parameters, as the code is not yet parallelized (the code is running on 1 core processor). Therefore, we performed multiple calculations with different MC parameters simultaneously to find the best parameters.

To estimate the equivalence between the actual time and one Monte-Carlo step, we first calculate the number of MC steps necessary to reach the Si saturation in the solution. Then we associate this number of MC steps with the time (in seconds) required to experimentally reach the saturation point for Si in the solution. So the number of MC steps it takes to saturate the solution in MC (T_{sat}-MC) will be equated with time in hours to reach the Si saturation in experiments (T_{sat}-exp). By this, we estimated the duration of one MC step in seconds or minutes, as given in Table 5.1, allowing a direct comparison between MC calculations with the long-term experimental dissolution. To compare the MC parameters among the glasses, we normalized each parameter by dividing them with the duration of one MC step in minutes. The normalized values of the parameters are given in Table 5.1. By doing this, we can estimate the number of elementary events, bond breakage, redeposition, or jump of a water molecule per unit of time. It becomes possible to compare the MC calculations with each other.

MC characteristics	**SBNA2**	**SBNA3**	**SBNA6**
Wbreak	800	900	1000
Wred	0.3	0.4	0.95
Wsaut	1/10	1/3	1/5
Wbreak normalized	17440	8802	3550
Wred normalized	6.54	3.912	3.3725
Wsaut normalized	2.18	3.26	0.71
Tsat MC/Tsat exp	21.8	9.78	3.55
1 MC step (in seconds)	2.7	6.1	16.8
1 MC step (in minutes)	0.045	0.101	0.28
Number of Si	2410398	2808726	1208175
Number of Al	304551	324979	217038
Number of B	1285051	1866295	574787
Size along X-axis	1600	2000	1600

Table 5.1: Composition of all the six glasses analyzed through ICP-OES

By this approach, we could reproduce the release of Si and B for all three glasses, as shown in Figure 5.8. However, it is important to notice for SBNA2, that the initial release of Si is more into the solution and then converges towards the experimental data after saturating the solution. This is because the current MC version does not form the gel by local reorganization but through dissolution/reprecipitation. Therefore, we try to reproduce only the asymptotic values but not the shape at the curve's origin. Then we calculated the total number of Si, Al, and water molecules present in the gel layer for the three glasses (Figure 5.9 - 5.11). For SBNA2, an enrichment of Si and Al is observed on the top 50 layers that are in contact with the ocean (the ocean is the main solution). We tried to determine the origin of this enrichment. There are two possibilities. It can be due to the presence of Si and Al in the solution or the parameter Wvacan, which regulates the migration of vacancies. We wonder if the migration of vacancies, inducing the removal of voids in the solution, could be at the origin of this dense external layer. Therefore, we investigated three different values for Wvacan to estimate this second possibility. The results are shown in Figure 5.12. It is observed that changing values of Wvacan involves only a slight modification in terms of the intensity of Si and Al enrichment. Therefore,

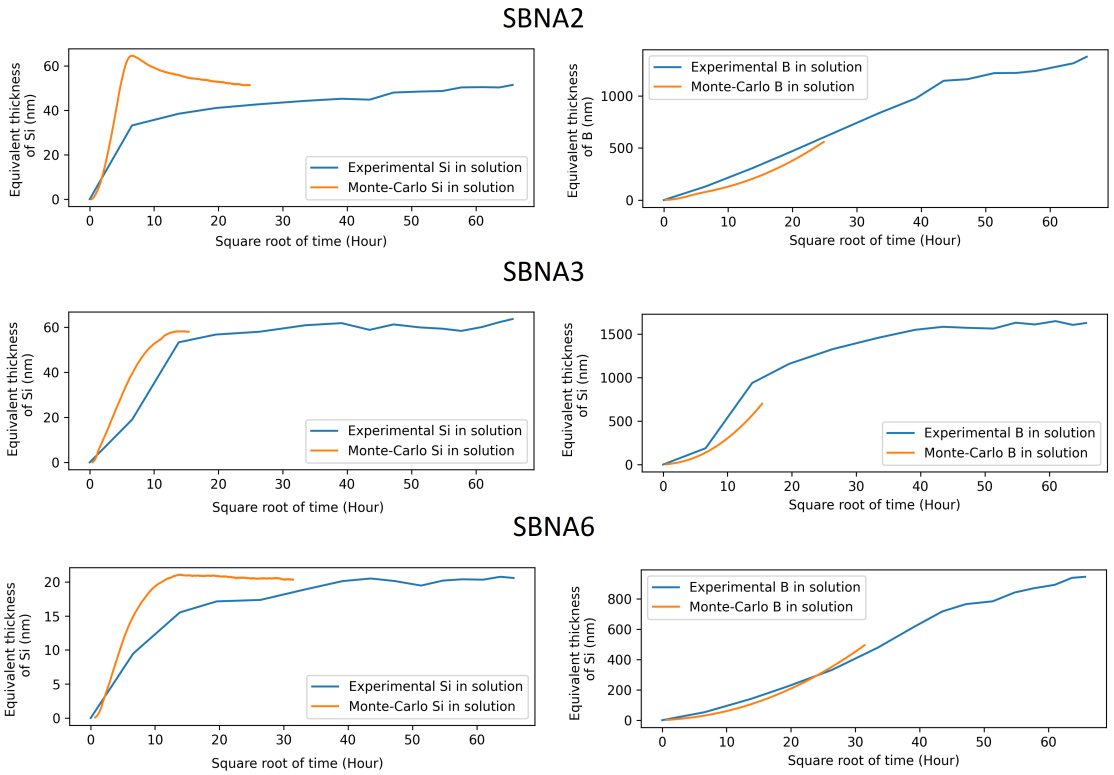

Figure 5.8: Long-term dissolution of Si and B from SBNA2, SBNA3 and SBNA6 glasses and reproduction with Monte-Carlo simulation. Color scheme: Blue - Experimental release of elements. Orange - Monte-Carlo simulation reproducing the experimental data.

it can be concluded that this parameter is not at the origin of the formation of the external dense layer. On the contrary, a large peak associated with the release of Si (MC calculation) shown in Figure 5.8 might explain the formation of the external layer. To investigate this, we modified the Wsaut by keeping two other parameters constant and indicated their results in Figure 5.13. It is evident that the decreasing value of Wsaut (decreasing the jump probability of water) is directly associated with the enrichment layer formation, as this will favor the redeposition process. In Figure 5.13, when Wsaut is 1/12, Wbreak releases more Si into the solution, and Wred redeposits more Si back into the gel's surface, which results in thick enriched layer formation. On the other hand, when Wsaut is 1/9, Wbreak releases less Si into the solution, and Wred redeposits less Si back into the gel's surface, which results in a relatively thin enriched layer formation. Si concentration in the solution is decreasing in all these calculations, which is an artifact of MC calculation since the such phenomenon is not physical.

Further investigations on SBNA3 and SBNA6 revealed that such a layer enriched with Si on the gel surface is less developed (Figure 5.10 and 5.11). This is because the formation of this layer needs a large quantity of Si released into the solution and a sufficiently long time for these Si to be redeposited. In case of the SBNA3 glass, the simulation is stopped soon after the saturation of Si in solution is reached, so the gel does not have sufficient time to develop, and only a narrow Si enriched layer is formed (Figure 5.8). The simulation cannot be extended beyond because all the B atoms were released in solution, and the

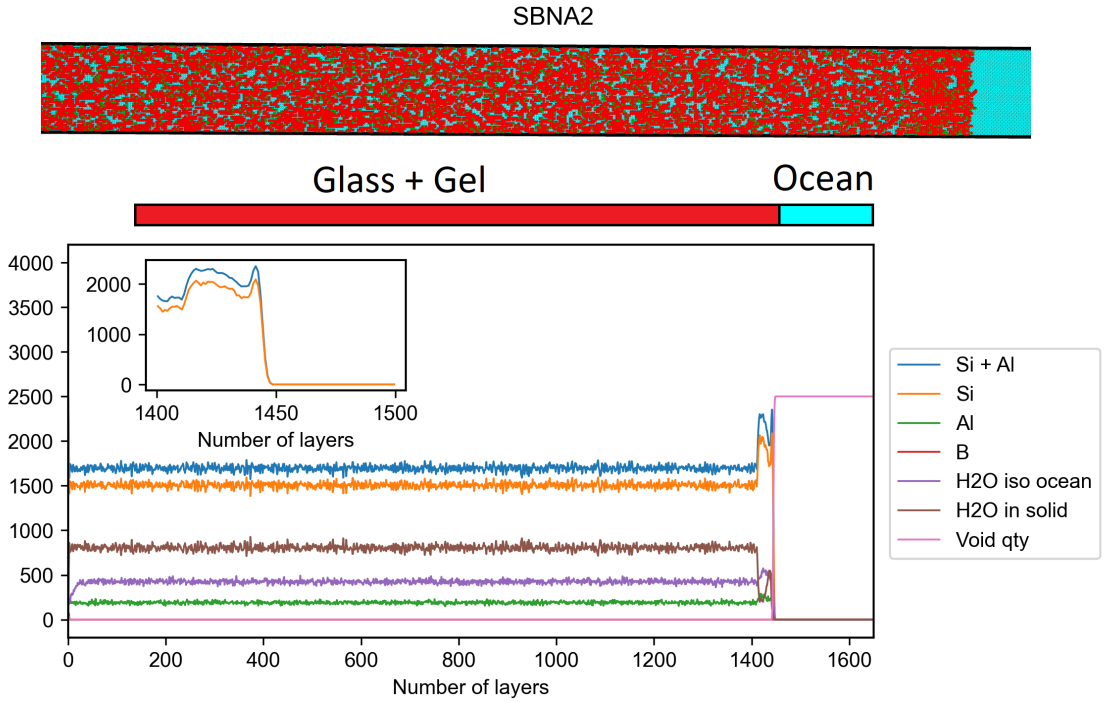

Figure 5.9: (Top) - Snapshot of the fragment of altered gel layer and its contact with water. Color scheme: Red - Si and Al; Cyan - Water; (Bottom) - Layer wise number of elements present in the gel of Monte-Carlo simulation reproducing the experimental SBNA2 long-term dissolution. The elements are calculated in gel region at the end of Monte-Carlo simulation after releasing all the B present in it. To clearly visualize the enrichment zone, layers between 1400 to 1500 is displayed as zoomed-in insert, only for the data of Si and Si + Al.

system is completely altered. Therefore, such enriched layer development is not observed for SBNA3. Again for the SBNA6 glass, only a narrow layer enriched with Si is observed. In this case, there is insufficient Si released in the solution at saturation, so we could not know if the width of this external layer would grow with time.

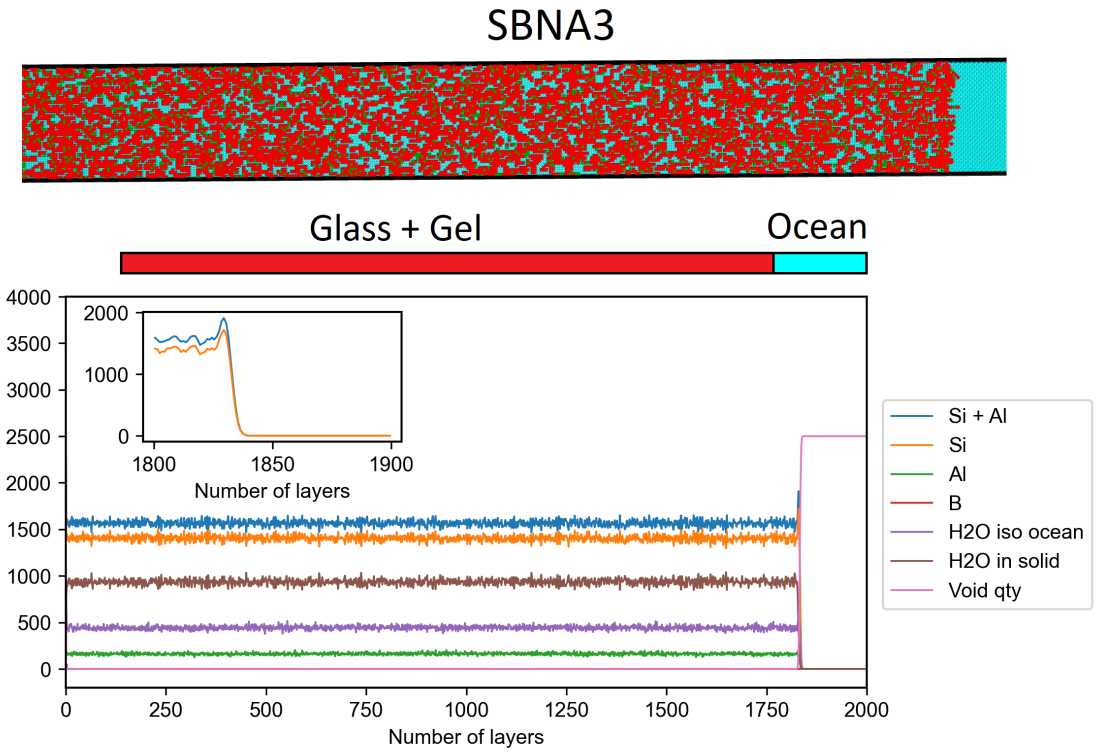

Figure 5.10: (Top) - Snapshot of the fragment of altered gel layer and its contact with water. Color scheme: Red - Si and Al; Cyan - Water; (Bottom) - Layer wise number of elements present in the gel of Monte-Carlo simulation reproducing the experimental SBNA3 long-term dissolution. The elements are calculated in gel region at the end of Monte-Carlo simulation after releasing all the B present in it. To clearly visualize the enrichment zone, layers between 1800 to 1900 is displayed as zoomed-in insert, only for the data of Si and Si + Al.

5.3 Discussion

In chapter 3.1 and chapter 4.1, we observed that adding Al_2O_3 in silicate glass increased the activation energy for bond dissociation of Si by water and favored the process of bond reformation. Accordingly, we observed that SBNA1, SBNA4, and SBNA5 glasses (with low wt% of Al_2O_3 <= 1.6) quickly released a large amount of Si into the solution initially, and developed a gel layer efficiently which controlled the release of B and Na into the solution during residual regime. On the other hand, SBNA2, SBNA3, and SBNA6 glasses (with wt% of Al_2O_3 >= 5.6) release comparatively less amount of Si into the solution but continue to release B and Na into the solution even after the protective gel layer is formed. Moreover, when we calculated the Si concentration in solution during the residual regime of 6 SBNA glasses, it decreased when the wt% of Al_2O_3 increased. This is because Al is strengthening the Si [Damodaran et al., 2022], so the glasses with a larger Al content like SBNA6 released less Si into the solution.

Among the two different gel formation mechanisms [Gin et al., 2020b], we suspected that low Al_2O_3 content in SBNA4 and SBNA5 glasses might make them undergo a dissolution/reprecipitation mechanism for the gel formation. However, investigating these glasses with isotopic ^{29}Si revealed that the gel is formed by local reorganization in the

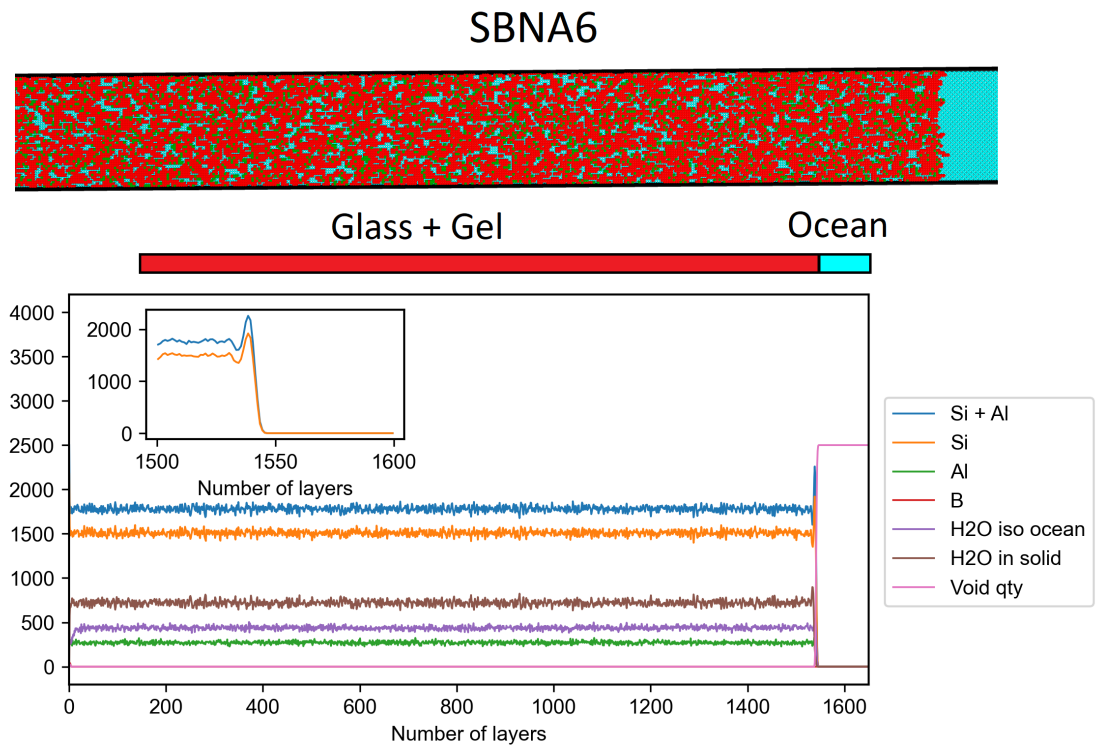

Figure 5.11: (Top) - Snapshot of the fragment of altered gel layer and its contact with water. Color scheme: Red - Si and Al; Cyan - Water; (Bottom) - Layer wise number of elements present in the gel of Monte-Carlo simulation reproducing the experimental SBNA6 long-term dissolution. The elements are calculated in gel region at the end of Monte-Carlo simulation after releasing all the B present in it. To clearly visualize the enrichment zone, layers between 1500 to 1600 is displayed as zoomed-in insert, only for the data of Si and Si + Al.

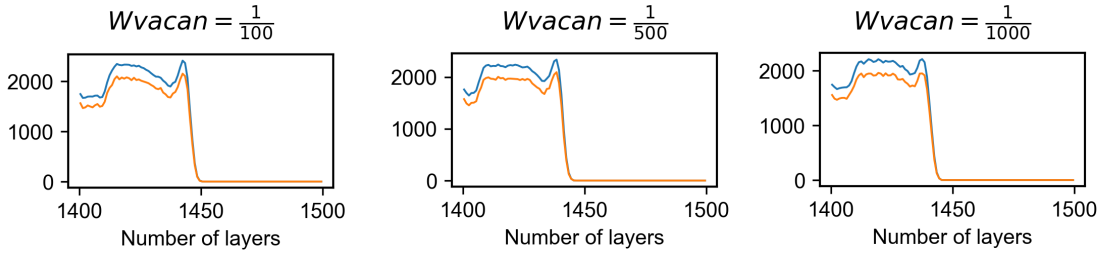

Figure 5.12: Investigating the role of MC parameter Wvacan towards the enriched layer formation. Color scheme: Blue - Total number of Si + Al. Orange - Total number of Si.

same way as glasses with a large amount of Al_2O_3. This suggests that the origin of gel formation mechanism is not associated with the sharp drop in release of B and Na into the solution since SBNA4 follows local reorganization to develop the gel.

To characterize the gel developed in these glasses, we performed Monte-Carlo (MC) simulations to reproduce the long-term experimental dissolution of Si and B into the solution. Since the release of B drops sharply for SBNA1, SBNA4, and SBNA5 soon after they enter the residual regime, reproducing these glasses with MC is difficult as the mechanism limiting the B release was not known precisely. Therefore, we worked with the three

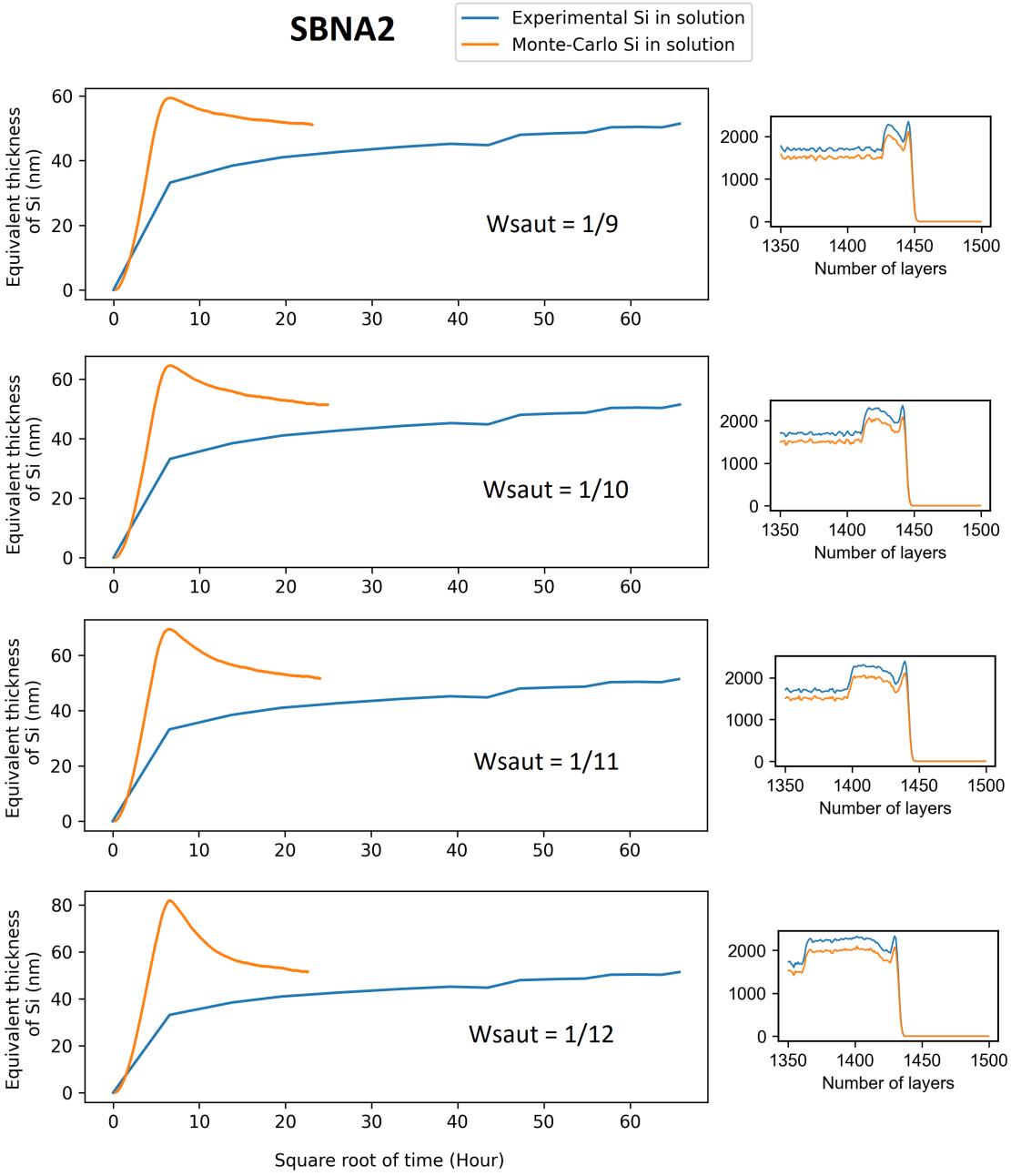

Figure 5.13: Investigating the role of MC parameter Wsaut towards the enriched layer formation. MC reproducing the experimental data are given in the left. Zoomed in investigation of enriched layer formation with respect to the number of layers are given correspondingly at right. Wbreak = 800, wred = 0.3 are kept constant for all the 4 simulations. Varying Wsaut parameters are indicated in each plot.

other glasses. Interestingly, we can connect the values of the different parameters to what was expected physically. In fact, we observed a good correlation between water diffusion (Wsaut), the bond dissociation probability (Wbreak), and the redeposition probability (Wred) towards the Al_2O_3 content of glass. In Table 5.1, normalized values of Wbreak indicate that the release rate of Si for SBNA2 is much higher than SBNA6, as expected, because the Al_2O_3 content is significantly lower in this glass.

The case of the SBNA3 glass is special because the second sampling during the long-term experimental alteration was significantly lower for this glass and outside the trend of the other SBNA3 samplings. Therefore, it could be an outlier. The MC calculation reproduced this point, which might be the reason why the value of Wbreak for SBNA3 is intermediate between the values for the SBNA2 and SBNA6 glasses. However, according to the Al_2O_3 quantity in SBNA3, we expect a Wbreak value even larger than in SBNA2. Accordingly, SBNA2 glass with a larger Wbreak needs a significant value of Wred to quickly allow the redeposition of Si from the solution back on the glass surface. On the other hand, smaller normalized Wred values are sufficient to develop the gel on the SBNA3 and SBNA6 surfaces.

Finally, correlations between water diffusion in the glasses and the chemical compositions can be proposed. The Wsaut parameter is directly related to the release of B into the solution. Experimentally we observed that the release rate of B increases with the decreasing Al content of glass (for glasses with > 5 wt% of Al_2O_3). The MC results show that the release rate of B in solution is intimately correlated to the water diffusion inside the glass. The normalized Wsaut values are in the order SBNA3 $>$ SBNA2 $>$ SBNA6. Water diffusion seems to accelerate when the quantity of Na_2O and/or B_2O_3 increases (and in parallel, the quantity of Al_2O_3 decreases). So the presence of weak bonds associated with B and/or the formation of empty spaces associated to Na could favor water diffusion.

Investigating these glasses' gel properties will help us understand the possible reason for the slowing down of the B release in SBNA glasses with low Al content. To characterize the alteration layers more precisely, we attempt to calculate the distribution of pore size for three glasses (Figure B.5). We calculated the pore size distribution by investigating each site of the MC network. The following method has been applied. In the beginning, a specific index is associated with each site. Then, we investigated its four neighbors, whenever a site is found empty or occupied by a water molecule. If one of these neighbors is an empty site or occupied by a water molecule, we assign the same index position to both these sites. We repeated this process until the final set of indexes remained constant. Then we calculated the distribution of pores across the gel by calculating the cluster of sites with similar indexes. In these glasses (SBNA2, SBNA3, and SBNA6), we observed one or two very large clusters of sites connected together (>100,000 sites). This is because there is quite a large quantity of Boron atoms on the initial glass network. After the release of the Boron atoms in solution, connected sets of empty sites (or sites occupied by water molecules) are formed. We don't specifically work on the aging of the alteration layer (by playing on the Wvacan parameter); consequently, we obtain percolating networks of sites empty or occupied by water molecules.

Surprisingly, investigating the gel properties of the SBNA2, SBNA3, and SBNA6 glasses leads us to propose a possible explanation for slowing down the B release in the SBNA glasses with lower Al content. By comparing the MC results with experiments, we propose the following conclusions by categorizing the glasses based on the Al content. A common phenomenon is observed for SBNA1, SBNA4, and SBNA5 glasses. These three

glasses contain small quantities of Al, so they quickly released more Si into the solution. Additionally, the less/no Al present in the gel allows it to reorganize easily, so a thick enriched layer is formed quickly. This enriched layer might limit the release of B into the solution. For the three other glasses with more Al content (SBNA2, SBNA3 and SBNA6), Al is strengthening the Si, so the release of Si into the solution is more limited. Simultaneously, Al present in the gel does not easily allow Si reorganization. As a consequence of these two phenomena, there is a delay in forming the Si enriched layer for such glasses. This is why the mechanism which limits the release of B into the solution is delayed with respect to the increasing Al content of glass. All three glasses simulated by MC calculations systematically observed the formation of an external Si enriched layer (only thickness varies). We suspect such a layer is also present experimentally, whose formation could depend on the Si concentration in solution and the easier local reorganization mechanisms.

In conclusion, it seems that during long-term alteration, an external layer enriched with Si is formed, sufficiently thick to block the B release when the quantity of Si in the solution is large. However, when the quantity of Si in the solution is low, the enriched layer is not sufficiently thick to block the B release. Therefore, these glasses require a longer time for the gel reorganization to form such thick enriched layer. Therefore, forming this Si enriched layer on the gel surface could be an important rate-limiting mechanism explaining the residual alteration rate. However, it doesn't mean that the aging of the alteration gel doesn't significantly impact the B release in the solution.

5.4 Conclusion

Long-term alteration of 6 SBNA glasses followed two different trends for releasing Si, B, and Na into the solution. Glasses with low Al content quickly released large amount of Si into the solution, which highly controlled the release of B and Na into the solution during the residual rate. On the other hand, glasses with more Al content released less Si into the solution due to the strengthening effect of Si by Al in the glass. And the release of B and Na into the solution continued during the residual regime, eventually it gets slowed down after a long time. MC simulations show that an external Si enriched layer is rapidly formed on the gel's surface. As a result, a thicker Si enriched layer on the surface of the gel could be formed at the gel's surface of glasses with low Al_2O_3 content, and it might impact the release of B into the solution. Investigating the SBNA4 glass with ToF-SIMS showed the gel's capacity to retain B in it. However, the role of B retained in the gel remains unknown, which need to be investigated. Therefore, we suspect that Si enrichment layer developed on the gel surface during the residual rate is expected to play an important role in controlling the residual glass alteration process.

Chapter 6

Behavior of B in passivating gels formed on International Simple Glass in acid and basic pH

Published under special issue in *Journal of Non-Crystalline Solids, 2022*

Contents

6.1 Introduction

Chapter 5.1 observed that SBNA4 retained B in the gel during the residual rate alteration. Similarly, recent study conducted on International Simple Glass (ISG) altered for 6 years long in Si saturated solution also observed the retention of B and Ca in the gel [Gin et al., 2020a]. Subsequently, that coupons were transferred into acidic solutions at pH 5 or pH 3 for 35 days. The resulting gel accumulated more B and Ca, with alteration rate being 50 to 100 times slower than that of a reference sample. These phenomena motivated us to study the role of ions present in pore water of the gels towards glass alteration. More precisely this work focused on the following questions:

1. Have the elements present in the pore water of the gel (B, Na, Ca, Si) a role towards the decrease in the residual rate?
2. What makes the residual rate in basic pH slower than neutral or acid pH?
3. What mechanism controls the retention of B in the gel?

To investigate these questions, this study discusses two sets of experiments conducted with ISG glass. (i) In a first part, glass coupons were altered at 90°C pH 7 in solutions containing the elements present in pore water (Si, Na, B and Ca). It was investigated the importance of different elements by conducting the experiments in a solution without that particular element of interest (Si, Na, B or Si, Na, Ca). Solid analyses were performed with ToF-SIMS depth profiling. (ii) In the second part, gels of similar thickness (70-90 nm) prepared at pH 3 or pH 9 at 90°C, were put in a solution spiked with 1000 ppm of ^{10}B for different durations. B retention in gel was monitored with ToF-SIMS. From the first set of experiments, deposition of B in the gel is observed, which is favored by the presence of Ca and that phenomenon significantly reduces the rate of glass alteration. From the second set of experiments, it is shown that B retention in the gel was highly favored in the basic pH over-acidic pH, which can explain why the gel formed in basic pH gives more protection than gel in acidic pH < 3 [Fournier et al., 2019].

6.2 Results

6.2.1 Importance of B and Ca together in pore water against the glass alteration

To understand the role of B and other elements in the gel pore water, fresh ISG coupons were altered in solution mimicking the pore water (Sol. 1) as discussed in the method section. After the 21 days of reaction, ToF-SIMS analysis revealed that a gel only 40 nm thick had formed, as shown in Figure 6.1(a). In a Si-saturated solution free of B, Na and Ca, a gel of 2185 nm thickness is expected after 21 days by interpolating solution data of pH7 90°C experiment between 13 days and 26 days [Gin et al., 2020a]. This result demonstrates that the presence of soluble elements in the leachate (here B, Ca, Na) could significantly impact (50x) glass alteration in silica saturation conditions. This phenomenon could partly explain why the 7 years long matured gel that trapped B and Ca in its inner region offers more protection against the glass alteration than the young gel. i.e., the deposition of B and Ca together in the gel plays a role in reducing the glass alteration rate, whereas the young gel cannot trap B and Ca. To check which element or combination of elements in pore water plays an important role, two other solutions were prepared, one containing B, Na, Si (Sol. 2) and another containing Ca, Na, Si (Sol. 3) at pH 7 – 90°C. After 21 days, the glass corrosion took even further to reach around 665 nm and 718 nm for both Sol 2 and Sol 3 as shown in Figure 6.1(b) and (c). Therefore, when the B and Ca reacted with the glass separately, the capacity of gel to reduce the glass alteration was approximately a factor of 3 (comparison with the B, Na, and Ca free solution). A former study with CJ7 (Ca-free ISG glass) glass coupon added in the solution containing Ca and Si found that the gel developed in such a solution reduced the glass alteration rate by 4 [Chave et al., 2011]. Furthermore, the addition of Ca to a glass composition has been shown to drastically reduce the residual rate, as exemplified by the residual rate 4 times lower between a Si-Al-Na-B glass with or without Ca added [Gin et al., 2012]. Authors argued that Ca favored the Si gel network's reformation and pore closure, which helped the gel to be more protective against the alteration [Chave et al., 2011, Jollivet et al., 2008, Cailleteau et al., 2008]. The efficiency of the gel created in the presence of only Ca and Si in the solution is very close to the Sol. 3 of this study that contained additional Na, which indicates Na did not have a significant impact. Moreover, this result is confirmed by depth-profiling analyses, which showed under all the conditions tested to date (acidic or basic pH, short or long-term experiment) that Na is never retained in the passivating gels formed on the ISG. From these experiments, it can be said that the presence of Ca and B together in the solution gives significantly more protection for the glass alteration than Sol. 2 and Sol. 3. Previous work on ISG showed that large alkali (K, Cs) ions in the pore water of passivating gels formed at pH 7 could also dramatically reduce both the water content in gels and the alteration rate although water diffusion was only slightly affected [Collin et al., 2018b].

To check if the elements trapped in the gel retroact on the diffusion of water molecules,

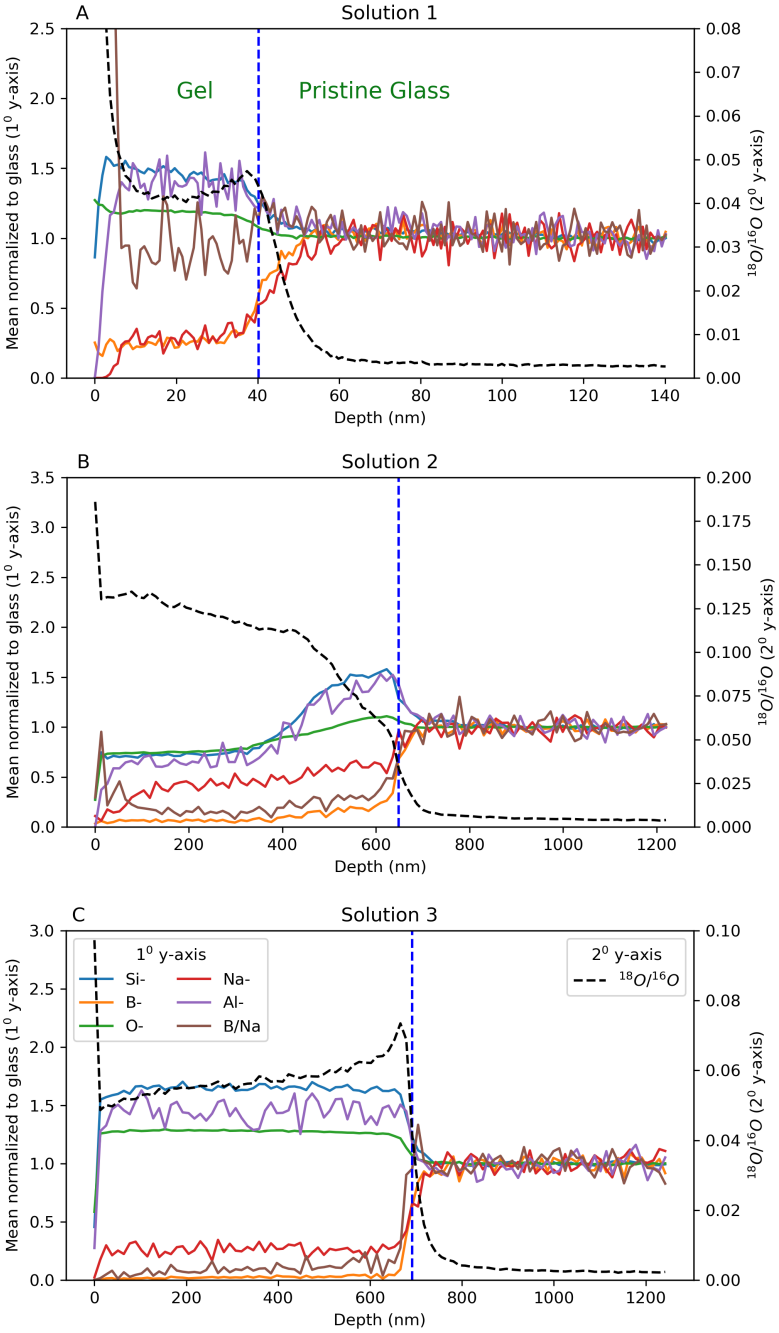

Figure 6.1: ToF-SIMS analysis of ISG coupon altered for 21 days in pH7 90°C in three solutions. (A) Sol. 1: Saturated with B, Ca, Na, Si; (B) Sol. 2: Saturated with B, Na, Si; (C) Sol. 3: Saturated with Ca, Na, and Si; Common for all three plots: Vertical dotted blue line – Indicates the alteration depth, which separates the interface between silica rich gel layer (left) and the pristine glass (Right) as shown in plot A. All the elements are mean normalized to the pristine glass, displayed along with primary y-axis as solid lines (left y-axis as 1^0 y-axis). Ratio of $^{18}O/^{16}O$ corresponds to secondary y-axis as dotted lines (right y-axis as 2^0 y-axis). O isotopic ratio was not normalized. Verification was made to obtain the value of the natural abundance (0.002) in the pristine glass. The $^{18}O/^{16}O$ in the solution was 12. Color scheme to represent each elements are consistently same on all three plots and the details are given in plot C (Sol. 3).

tracing experiments were performed at room temperature with ^{18}O labeled water for 24 hours with the glass coupons recovered from the three different solutions after 21 days (Sol 1-3). ToF-SIMS analysis was performed to investigate the quantity of ^{18}O exchanged with ^{16}O present in the gel for all three-glass coupons. However, this tracing experiment cannot tell us what type of O are exchanged: it could be O from free water molecules in pores, O from water molecules bonded to the surface, O from silanol or aluminol groups, or bonding O from the gel skeleton. This study showed that the ratio of $^{18}O/^{16}O$ for gel prepared in Sol. 2 is 0.127, which is twice that of the coupon obtained from Sol. 3, 0.057. For the glass coupon whose alteration significantly dropped in Sol. 1 (solution containing the four glass elements); $^{18}O/^{16}O$ ratio was 0.045, which is 2.8 times smaller than the ratio obtained from Sol. 2. This reduction of water exchange is measurable, but small compared to the reduction of glass alteration due to the presence of both B and Ca in the solution. This result strongly suggests that protection offered by the presence of B and Ca is not through limiting the transportation of water. Further investigation of the gel composition through ToF-SIMS was performed by estimating the average B/Na present in it. The mean B/Na value in the gel of the glass coupon altered in Sol. 3 (0.14) is relatively lower than the glass coupon altered in Sol. 2 (0.23). The mean B/Na for the glass coupon prepared in Sol. 1 is 1.01, which is significantly higher than the two other coupons, indicating the strong retention of B in the gel. It is also important to notice that the gel developed in Sol. 1 retained significantly more Ca than the gels developed in Sol. 2 and Sol. 3, as shown in Supplementary Figure D.1, where the ToF-SIMS data are normalized with respect to Si. These results indicate the presence of B and Ca together in the gel plays an important role in significantly reducing the alteration rate.

6.2.2 Role of pH on glass dissolution in silica saturated solution

Regarding the effect of pH on the residual rate, a hypothesis is that the activation barrier to release the B, which is used as a glass dissolution tracer, from the B-O-B and B-O-Si linkages is much lower in acidic conditions than in neutral or basic pH conditions [Zapol et al., 2013], another is that the condensation reactions allowing pore closure are slower in acidic pH than in basic pH [Fournier et al., 2019]. To understand the detailed mechanism behind the different glass alteration rates in two different pH, ISG coupons were corroded in Si saturated solution at 90°C pH 3 and 9 for 1 hour and 48 hours respectively. This protocol permits the formation of similar gel thickness at both pHs. The altered coupons were placed in a tracing solution containing 1000 ppm of ^{10}B rich solution at room temperature with the corresponding pH for 1 min, 5 min, 1 hour, 1 day, 2 days, and 10 days to understand the diffusion and retention of B across the two gels. Room temperature was selected to prevent further glass alteration and gel structure modifications. ToF-SIMS analysis was performed after each contact time in the tracing solution, and the total number of ^{10}B retained in the gel was quantified and shown in Figure 6.2 (see calculation details in the supplementary method section). As discussed in the method section, Zr profile was used to indicate the outer interface of the gel (the profile for each contact time is displayed in the Supplementary figure 2). To compare the

deposition of B in the gel across the different contact time, it was convenient to consider the outer surface of the gel to be same for all the contact time. In both ISG coupons altered in pH 3 and pH 9 solution, beyond 10 nm depth, all the Zr profile has reached at least half of their stable value in the bulk gel, as shown in Supplementary Figure 2. Therefore, it was considered that gel starts from 10 nm for all the contact time. Since in ToF-SIMS, the intensity for each element is matrix dependent, the ^{10}B signal was compared with other durations through computing the $^{10}B/^{11}B$ ratios (see calculation details in the method section). As shown in Figure 6.3(a), $^{10}B/^{11}B$ steadily increased over the incubation time in the tracing solution for the gel prepared at pH 9, unlike in pH 3. The average $^{10}B/^{11}B$ ratio for pH 9 1 min, 5 min, and 1 hour is 0.20, 0.23, 0.36, respectively, whereas for pH 3 1 min, 5 min and 1 hour it is 0.28, 0.31, 0.80, respectively. The average $^{10}B/^{11}B$ for gel from pH 9 1 min is close to the natural abundance (0.205), indicating that practically no ^{10}B from the solution has entered into the gel, but there was a slight rise in ratio for pH 9 5 min and 1 hour.

In contrast, the pH 3 1 min $^{10}B/^{11}B$ ratio is already close to the pH 9 1 hour, indicating that it is easier for the B to diffuse through the gel prepared in pH 3 than in pH 9. Correspondingly, pH 3 5 min and 1 hour ratio were even higher. Interestingly, the average ratio of $^{10}B/^{11}B$ for pH 9 1 day, 2 days, and 10 days constantly increases with time and becomes significantly higher than pH 3 1 day, 2 days, and 10 days, as shown in Figure 6.3(a). To verify if the increase in $^{10}B/^{11}B$ ratio is due to the constant increase of ^{10}B into the gel irrespective of ^{11}B quantity, the amount of ^{10}B that has entered into the gel from solution was estimated (see detailed calculations in Supplementary Method section D.1.1). Briefly, the total number of ^{10}B atoms per nm^3 in the gel were estimated by calculating the area under the curve for each duration with reference to the 1 min in tracing solution (assuming no ^{10}B entered into the gel in 1 min) from Figure 6.2. It is observed that the number of $^{10}B/nm^3$ consistently increases over the duration in the case of pH 9 altered glass coupon. On the other hand, diffusion of ^{10}B from the solution into the gel prepared in pH 3 is not increasing consistently with increasing duration in tracing solution. To validate the quantification of ^{10}B from ToF-SIMS, an XPS analysis was performed on the pH 9 10 days sample. Detailed calculations for the comparison are given in Supplementary method section D.1.2. Table 6.1 shows that ToF-SIMS data reasonably agrees with XPS, which increases the reliability of ToF-SIMS estimation of ^{10}B deposited in the gel for other incubation times.

Lastly, after validating the presence of large amount of ^{10}B within the gel prepared at pH 9, the ISG coupon incubated for 10 days was further placed in silica saturated and B free solution for another 10 days at room temperature. Then ToF-SIMS was performed to check whether B was mobile or was still trapped in the gel when the driving force for B dissolution was maximum (no B in solution). Results are displayed as solid line in Figure 6.2(a). It is observed that more than 50% of the ^{10}B are still retained in the gel, indicating that the gel properties developed in basic pH favors the strong retention for a large fraction of B.

In Figure 6.3(b), the total quantity of ^{10}B accumulated in the gel of the pH 3 10 days

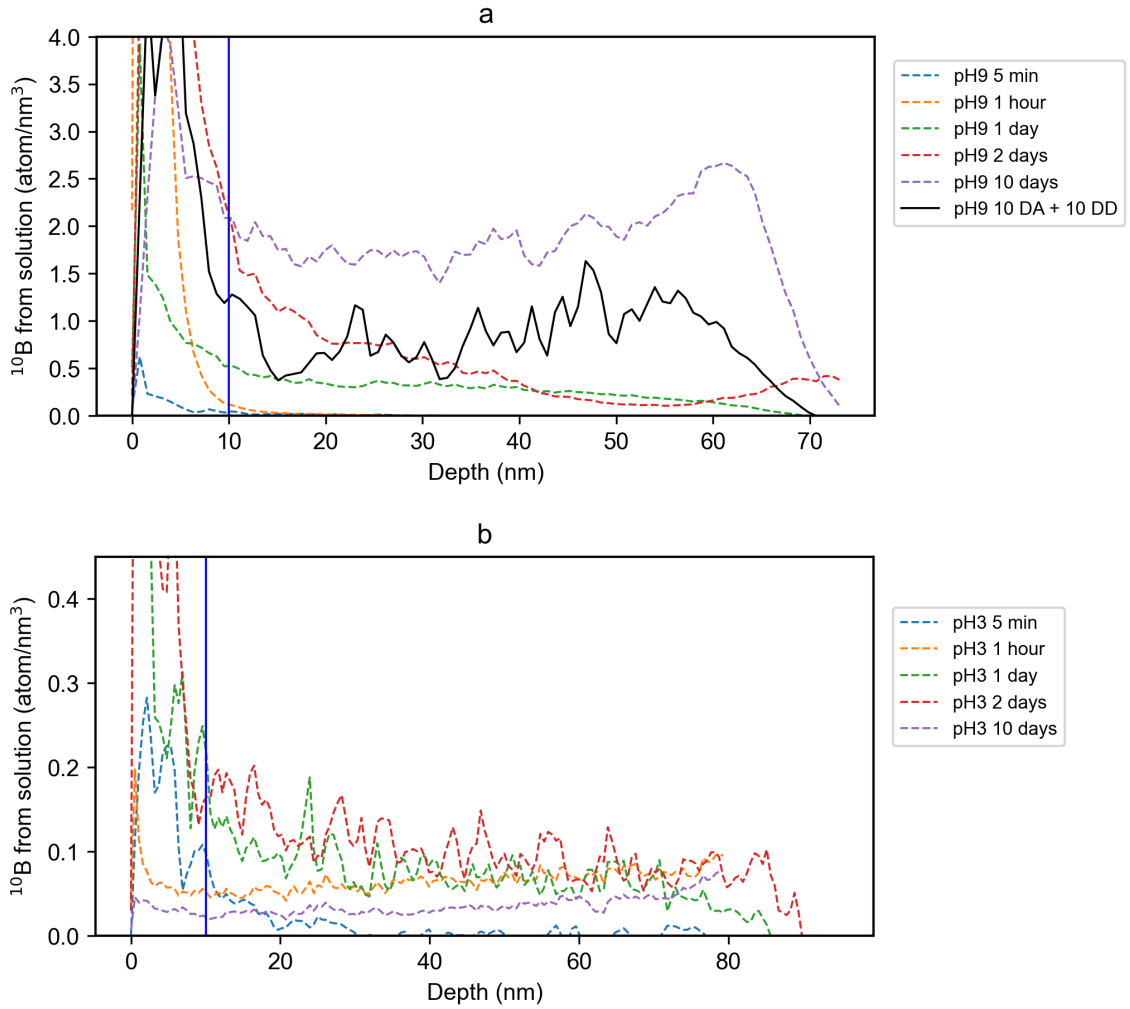

Figure 6.2: ToF-SIMS analysis of altered ISG coupon incubated in tracing solution for 5 min, 1 hour, 1 day, 2 days, and 10 days in isotopic ^{10}B tracing solution at pH 9 (a) and pH 3 (b). A vertical blue solid line defines the gel start region based on Zr^+ profile from ToF-SIMS. Incubation of altered coupon in isotopic ^{10}B tracing solution (B adsorption mechanism) are represented with dotted line. In plot (a), pH9 10 DA + 10 DD in solid line corresponds to the incubation of coupon for 10 days in isotopic ^{10}B tracing solution and 10 days in Si saturated solution at room temperature. In both plot (a) and (b), number of ^{10}B atom/nm^3 diffused into the gel for different duration of incubation is quantified by considering the ^{10}B signal of 1 min incubation as reference (Assuming no ^{10}B entered into the gel in 1 min). Color scheme for ^{10}B diffusion into the gel for different durations in pH 9 and pH 3 are shown in plot (a) and plot (b) respectively.

sample is slightly lower than for pH 3 1 hour, 1 day, and 2 days incubation time. It is important to consider that the range of ^{10}B/nm^3 on pH 3 altered coupon as shown on Figure 6.2(b) is very small while compared to the Figure 6.2(a), which could make it difficult for the ToF-SIMS to detect precisely the penetration of ^{10}B at the low range. Based on these data, we predicted the diffusion speed of ^{10}B through the gels prepared in two different pH by considering the time it took to saturate the whole gel with ^{10}B. As shown in Figure 6.2, this time is between 2 days to 10 days for the gel formed at pH 9 and between 5 minutes to 1 hour for the gel formed at pH 3. These data provide an

Elements	XPS (atomic %)	ToF-SIMS (atomic %)
O	68.5 ± 6.8	71.3 ± 7.1
Si	24.2 ± 2.4	21.3 ± 2.1
Al	3.1 ± 0.3	2.7 ± 0.3
B	1.7 ± 0.2	2.6 ± 0.3
Na	0.5 ± 0.1	0.5 ± 0.1
K	1.2 ± 0.1	n/a
Ca	0.6 ± 0.1	0.6 ± 0.1
Zr	0.5 ± 0.05	0.6 ± 0.06

Table 6.1: Gel composition determined by ToF-SIMS and XPS are given in atomic %. Sample formed at pH 9 and incubated in ^{10}B enriched solution for 10 days. XPS analysis was performed at a depth of 25-30 nm (center of the gel)

estimation of the diffusion coefficient that ranges from 2.8 x 10^{-20} m^2/s to 5.6 x 10^{-21} m^2/s for pH 9 and 2.7 x 10^{-17} m^2/s to 2.3 x10^{-18} m^2/s for pH 3. These diffusion coefficients can be compared to that obtained from the parametrization study of B release from ISG at the beginning of the alteration in Si saturated solution and controlled pH [Gin et al., 2020a]. This work provided a value of 10^{-17} $m^2.s^{-1}$ at pH 3 25°C and 10^{-20} $m^2.s^{-1}$ at pH 9 25°C, in fair agreement with that derived from ^{10}B diffusion experiments. All the above results thus indicate that ^{10}B can diffuse much faster through the gel prepared at pH 3, whereas diffusion of ^{10}B is very slow through the gel prepared at pH 9. However, ^{10}B did not settle in the gel prepared at pH 3, whereas gel prepared at pH 9 can store a large amount of ^{10}B with increasing time in the tracing solution.

The results of B adsorption on gel-like surface (amorphous silica and aluminisilicate MCM-41) as a function of pH and the presence of Ca^{2+} are presented in Figure 6.4. B adsorption is shown to be doubled at pH 9 compared to pH 3 when no Ca is present in the solution. While the addition of Ca leads to further increase in adsorption of B varying between 40% and 150%. This tendency is consistent with what is observed for the retention of B in ISG gel. Note that experiments with longer adsorption times only shows a minimal increase in the amount of adsorbed B, which can be attributed to the residual deagglomeration of the powder. The results from the adsorption experiment can be compared with the data from the B retention experiment, using the specific surface and density of ISG gel [Collin et al., 2018b]. These results would lead to around 0.2 – 14 x 10^{-3} atoms per nm^3, which is at least a hundred time lower than what was observed in the B retention experiment. Even if the material compositions are different, the composition of the ISG gel is close enough to the aluminosilicate which was used, that composition alone cannot account for such a difference. The major difference between the structures come from the morphology, where the mean pore diameter in MCM-41 aluminosilicate structure in around 3 nm while it is around 0.5 nm in the fresh gel. Moreover, the ISG gel is formed with a mix of open and poorly or non-connected pores. Hence, the nano-confinement in the gel porosity may be considered to be a major reason for the boron retention in the gel.

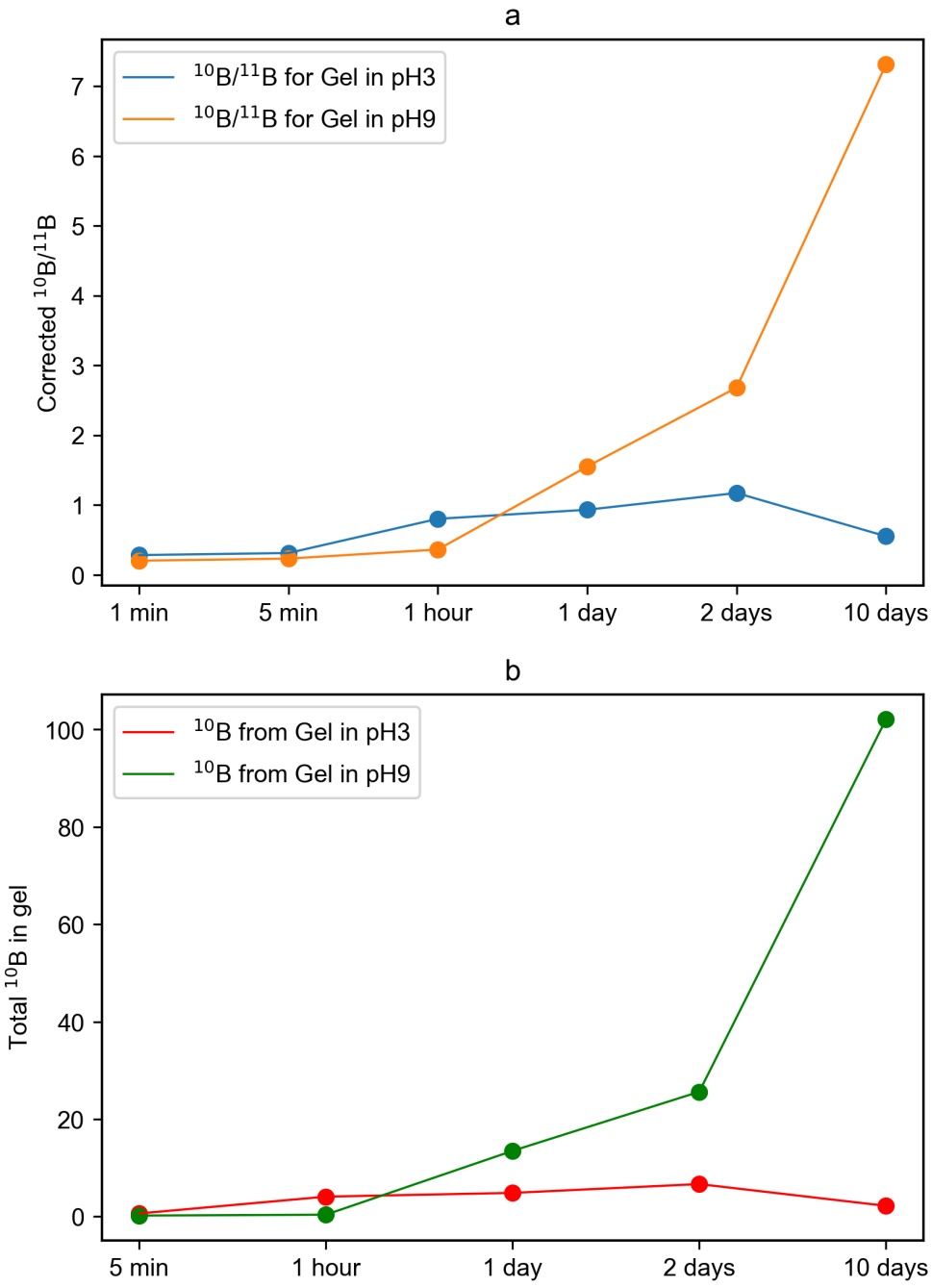

Figure 6.3: Diffusion of ^{10}B from the tracing solution into the gel prepared in pH 3 and 9 for different incubation times quantified in two ways: (a) average ratio of $^{10}B/^{11}B$ in the gel region (b) Integration of total ^{10}B atom per nm^2 of gel. Quantification is made using the 1 min in tracing solution as a reference.

6.3 Discussion

In many studies, B is used as a tracer to monitor the glass alteration process at any stage of the reaction. The residual rate is generally calculated from the release of B into the bulk solution [Gin et al., 2021a]. Moreover it was calculated that for ISG-type glass composition, B release accounts for 90% of porosity of the gel [Collin et al., 2018a].

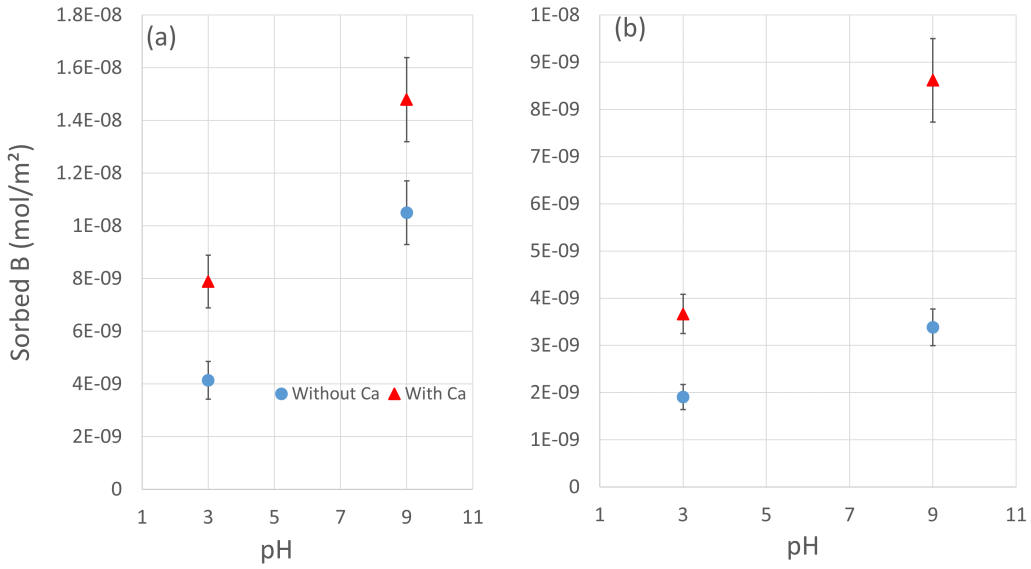

Figure 6.4: Amount of adsorbed B on amorphous silica (a) and aluminosilicate MCM-41 (b) after 48h in a $B(OH)_3$ solution. In both (a) and (b) adsorption of B in the absence of Ca is indicated with blue circle, in the presence of Ca is indicated with red triangle.

However, some recent studies observed that some B could be retained in the passivating gels formed on ISG [Gin et al., 2017a, Gin et al., 2020a]. After a long stage of alteration at pH 9, authors of these studies recovered the glass coupons and continued the alteration process for 43 days at pH 7, 35 days at pH 5, and 3. Solution analysis revealed that gel thickness increased only by 5 nm for pH 7, whereas gel thickness increased comparatively larger for pH 3 and pH 5 to be 400 nm and 250 nm, respectively [Gin et al., 2020a]. This observation is surprising because a fresh coupon in pH 3 can reach the alteration depth of 500 nm in just 1 to 2 hours. Another recent study conducted on SON68 glass altered at pH 9 for three years [Strachan et al., 2022], also have the B deposited in the gel while deciding the gel/pristine glass interface based on the penetration of H+ from ToF-SIMS signal as shown in the Figure 6 of that study [Strachan et al., 2022]. These motivated us to delve into the mechanisms involving B. Experiments with Sol. 1-3 suggested that removing either Ca or B from the solution does not yield the same effect triggered by Sol. 1. Water diffusion experiment across the gel formed in the 3 solutions suggested that B and Ca reduced the glass alteration not through transportation of water but by some other mechanism. B retention in gels was estimated through mean B/Na ratio from ToF-SIMS depth profiles (1.01, 0.23, and 0.14 for Sol. 1, Sol. 2, and Sol. 3, respectively). The results suggest that B deposition in the gel, favored by the presence of Ca contributes to the protection against the glass alteration. Notably, the mean B/Na ratio for Sol. 1 is close to its value in pristine glass, and then it significantly gave more protection to the gel. Since B is dissolved faster in acidic pH than in basic pH, this study also tested the efficiency of gels prepared in two different pH conditions to retain B.

In experiments performed with gels prepared at pH 3 and pH 9, then immersed in ^{10}B rich solution, it was observed that ^{10}B diffuses faster through the gel prepared at pH 3

but does not stay in the gel. On the contrary, diffusion of ^{10}B into the gel prepared in pH 9 solution is slow but it is strongly retained. Various possible mechanisms could explain these observations,

1. The gel prepared in basic pH had disconnected pores, whereas the gel prepared in acidic pH had more interconnected pores [Huseyin Kaya et al.,]. This is consistent with our results showing that ^{10}B species could diffuse faster through the gel prepared at pH 3 than 9.

2. The gel undergoes hydrolysis and condensation reactions that could contribute to the retention of aqueous species. In one of our previous study three ISG coupons were altered in a solution saturated with ^{29}Si and ^{16}O for 3 days at pH 7 90°C [Gin et al., 2018]. As expected, ToF-SIMS analysis on the gel prepared in this solution indicated that the gel contained O and Si in natural abundance. The coupon was then transferred to the solution saturated with isotopic ^{29}Si and ^{18}O at pH 7 90°C to continue the alteration for 7 and 13 more days [Gin et al., 2018]. Surprisingly, the gel was exchanged with ^{18}O from the new solution; however, no exchange of ^{29}Si took place. This indicates that gel has undergone constant hydrolysis and condensation reactions preventing the exchange of ^{28}Si with ^{29}Si while permitting O exchange with bonding O of the gel network. As condensation reaction are favored in basic pH, this could be an important possible reason why the large amount of ^{10}B being stored in the gel developed in basic conditions. Especially the retention of ^{10}B within the gel, even after incubating them in pure silica saturated solution (for same duration as adsorption of ^{10}B into the gel), strongly suggests that ^{10}B entered into the gel could be stored behind the several layers of complex condensation reaction.

3. The speciation of B in two different pHs is different [Schott et al., 2014], where most of the B in acidic pH contains only $B(OH)_3$. B in basic pH contains many different species, including $B(OH)_3, B(OH)_4^-, B_4O_5(OH)_4^{2-}$ *and* $B_3O_3(OH)_5^{2-}$[Mesmer et al., 1972]. The pKa of a borate/boric acid solution is around pH 9. B(OH)3 and $B(OH)_4^-$ can condense together to form a dimer, or larger oligomers [Nils Ingri, 1962]. A pH of 9 is thus the most favorable conditions to form large molecules. This might explain why B diffuse more slowly at pH 9 than pH 3.

4. Sorption of B at the surface of silica or aluminosilica-type structures tends to favor the negatively charged tetrahedral B compared to a neutral trigonal B, hence the greater accumulation at higher pH [Saldi et al., 2021, Kim and Kirkpatrick, 2006]. It was also noted that the presence of Ca in solution leads to an increase of adsorbed B_{IV}.

5. Water molecules form stronger hydrogen bonds with the nano-porous gel at pH 9 than at pH 7 [Ngo et al., 2020]; as a result, the mobility of water is slowed down at basic pH. However, it is important to remember that the same study was not investigated under acidic conditions. Therefore, these reasons could explain why B can diffuse faster through the gel prepared in acidic pH than basic pH.

6.4 Conclusion

In this study, silica saturated solutions enriched in Na, Ca, and B were used to mimic the conditions inside the porous gel during a long-term alteration, as well as ^{10}B-spiked solutions, in order to investigate the role of these species in the residual alteration of glass. ISG alteration under a Si, B, Ca, Na-saturated solution lead to an alteration depth 50 times thinner than what was expected in a Si-saturated solution free of the other elements. However, when removing either B or Ca, this reduction was only about 3 times lower. Comparisons with another study [Chave et al., 2011] with identical conditions, except for the absence of Na in solution, lead us to conclude that the presence of Na in the pore water did not impact the alteration rate. Tracing experiments using $H_2{}^{18}O$ did not show a correlation between the alteration rate and the diffusion rate of water in the gel, suggesting that water transportation is not the mechanism responsible for the reduced alteration. ToF-SIMS analyses revealed that the retention of B in the gel is heavily favored by the presence of Ca in the solution, which is correlated with the reduction in glass alteration. ToF-SIMS analyses of ISG coupons altered either at pH 3 or 9 then placed in a tracing ^{10}B solution revealed that B could diffuse faster in acidic conditions, but would accumulate more in the gel prepared in basic pH. These results are consistent with the difference in porosity at various pH, where the porosity in gels prepared at acidic pH tend to form interconnected networks while it forms disconnected pores in basic pH. Thus, the accumulation of B in the gel, allowed by the presence of Ca, tends to increase the protection provided by the gel towards further alteration. It remains to be understood how B and Ca react together and by which mechanism and under which chemical form B is retained in gels.

Chapter 7

Discussion and Conclusion

7.1 Possible origin of the Al role in glass alteration

Al_2O_3 in silicate glass plays some mysterious role in controlling the durability against water [Hamilton et al., 2001, Vienna and Crum, 2018, Gin et al., 2020b] during both forward and residual alteration regime. Vienna et al [Vienna and Crum, 2018] observed that addition of a small concentration of Al_2O_3 (< 3.5 %) into the glass significantly increases the durability against water. Al_2O_3 concentration between 3.5 to 19% increases the durability initially and decreases towards the end. Finally, a high concentration of Al_2O_3 in the glass significantly decreases the durability of glass, and the elementary mechanism behind this role remained elusive. To address this question, it was decided to investigate the problem through performing numerical MD simulations and long-term leaching experiments. Then we will develop a new Monte-Carlo model to fit the experimental results. These developments will eventually support the improvement of GRAAL model, developed in CEA to investigate the durability of glass under geological disposal conditions.

First, to understand the role of Al towards the initial dissolution rate, we calculated the activation energy for bond dissociation of Si and Al in silicate and aluminosilicate glass structures using the PMF method. It was shown that adding Al strengthens the local bonds around Si; as a result, the durability of glass against the water is increased. Simultaneously, it is also observed that reformation of Si with Al as second neighbor is much easier than Si-O-Si bond reformation. Therefore, adding Al to the silicate glass increases the durability by increasing the bond dissociation barrier and decreasing the reformation energy.

We can propose an explanation for this observation considering the increase in number of degrees of freedom when Al_2O_3 is added to a silicate glass. Firstly, the bond length of Si-O is 1.59 - 1.61 Å, whereas the bond length of Al-O is 1.74 - 1.75 Å [Zirl and Garofalini, 1990]. Experimental studies observed that Al-O bond length could go upto 1.91 Å [Ishizawa et al., 1980]. Indeed, the bond angle distribution of O-Si-O is found to be narrow with the mean value of 108.2°. Whereas, O-Al-O bond angle distribution is much broader with lower intensity [Xiang et al., 2013] than the O-Si-O bond angle distribution. When we look into the intermediate range order of glass structure, increasing the Al/Si ratio in the glass increases the number of smaller-sized rings (5 or 6 membered rings) at the expense of large-sized rings (rings with 9 or more members) [Xiang et al., 2013]. Focusing on the mechanical properties, it was shown that Young's modulus, bulk modulus, and shear modulus are impacted by the concentration of Al_2O_3 in the glass. It was concluded that Al_2O_3 in the glass tends to increase its elastic properties. We can imagine that when one or more Al atoms surround a Si atom, local chemical disorder might increase due to more degrees of freedom; as a result, an additional energy will be necessary for a local dissociation event to occur. This could be at the origin of the Al strengthening effect.

However, we observed that the activation energy required to dissociate bonds around Al is 0.49 eV (less than half of the activation energy needed to dissociate the bonds around Si in pure silicate glass). Therefore, if adding small to medium concentrations of Al_2O_3

into the glass strengthens the bonds around Si, the bonds around Al remain weak. The contribution of Al strengthening Si becomes dominant to increase the durability of glass against water. On the other hand, as Al dissolves preferentially from the glasses, a large concentration of Al in the glass makes it less durable because the structure collapses after the release of Al. This theory was supported by experimental results. ICP-OES and ToF-SIMS analysis on glasses containing a large amount of Al_2O_3 confirmed the preferential release of Al, followed by weakening of the glass silicate network, that in turn, affects the durability of glass.

7.2 Why a so large distribution of activation energies is observed?

It is also important to notice that distributions of activation energies for dissociating the bonds around Si in pure silicate and aluminosilicate glasses are wide, ranging from 0.25 to 2.15 eV. It is believed that activation energy for dissociating the siloxane bond is influenced by many factors that could be associated with the simulation method (surface models) or with physical reasons like the glass disorder [Rimsza et al., 2016] etc. Indeed, location of the target Si plays an important role. For instance, one Si atom located on a concave glass surface has higher activation energy than a Si atom located on a flat surface [Kagan et al., 2014]. Also in PMF calculations [Damodaran et al., 2022], we observed the influence of the number of Al as second neighbors and the number of bridged oxygen. These structural characteristics also significantly impact the determination of the activation energies. ReaxFF calculations revealed that water molecule explores multiple pathways before choosing one to progressively approach the Si atom and dissociate the bonds around it. In some other cases, the orientation of the water molecule is inverted with respect to the target atom. These water molecules have to rotate towards the target atom before approaching progressively for the bond dissociation. It means that not only the disorder of the glass structure, but also the disorder of the solution plays a role in the activation energy distribution. Similarly, Si connected to three-bridged oxygen might have higher activation energy when its non-bridged oxygen is oriented perpendicular to the water molecule. Jabraoui et al., observed that reaction between the glass and water is different if only a single water molecule or a collection of water molecules are considered for the chemical reaction [Jabraoui et al., 2021]. ReaxFF calculations performed in our study explain the presence of multiple water molecules are hiding the trajectory of the "active" water molecule. As a result, the activation energy calculated with a single water molecule will differ from that of several water molecules. Therefore, we observed that multiple factors could influence the activation energy leading to the broader distribution of energies.

7.3 Role of Al on gel properties

To understand the role of Al towards the residual alteration rate, we designed 6 Na-aluminoborosilicate glasses with varying concentrations of Al_2O_3 up to 9.6 wt%. The 6-month glass powder alteration in distilled water with a high SA/V ratio revealed two dissolution trends that depend on Al_2O_3 concentration. Glasses with Al_2O_3 up to 1.6 wt% (SBNA1, SBNA4, and SBNA5) quickly released Si from glass into the solution to saturate it. Immediately, the glass starts building a gel on its surface, which significantly limits the release of B and Na into the solution. Our PMF results show that the presence of Al_2O_3 strengthens the bonds around Si and allows easier reformation of the bonds. Therefore these glasses with a low amount of Al_2O_3 released Si quickly. Among them, it seems that glasses with a larger Na_2O content allow faster diffusion of water to release more Si. On the other hand, glasses with a Al_2O_3 content $\geq$ 5.6 wt% (SBNA2, SBNA3 and SBNA6) released Si slowly due to the strengthening effect of Al. As a result, the development of the aluminosilicate gel is slower and less efficient to slow down B and Na release from the glass into the solution. Consequently, the alteration rate of the high Al content glasses diminishes more slowly than for the other glasses.

It is unclear why the release of B and Na into the solution is dropped quickly for glasses with less Al_2O_3, whereas it drops after a long time in the residual regime for glasses with $\geq$ 5.6 wt% of Al_2O_3. It is validated that CJ2 (SBNA2 of this study) type of glasses will develop the gel through local reorganization [Gin et al., 2020b]. Therefore, we suspected that glasses with less Al_2O_3 might follow dissolution/reprecipitation mechanism to develop the gel (like CJ1 [Gin et al., 2020b] = SBNA1 of this study), since the residual regime of SBNA4 and SBNA5 matches with the SBNA1. However, investigating the SBNA4 with ToF-SIMS showed that glasses with low Al_2O_3 developed gel through local reorganization, without exchanging with ^{29}Si from the solution. Surprisingly, we observed that SBNA4 retained B in the gel, which is not common for young gel that was developed only by 1 month. It suggests that glasses with low Al_2O_3 (SBNA1, SBNA4 and SBNA5) might retain B in the gel soon after entering the residual regime. Therefore, these glasses cannot be reproduced by the present MC code since we don't know the mechanism behind the B retention in gel. We then investigated the other glasses with MC to understand the morphology of gel towards the retention of B. MC can reproduce these glasses with more Al_2O_3, since the limiting of B and Na release for these glasses are delayed.

To understand this process in atomic resolution, three MC parameters were optimized to reproduce the release of Si and B in long-term alteration for SBNA2, SBNA3 and SBNA6. Upon gel formation, it is observed that SBNA2 developed a thick silica enriched zone without pores on the gel's surface, close to the solution but the large thickness of this layer is probably due to an artifact of the calculation. In fact, a temporary exceeding quantity of Si is released in solution before being redeposited at the gel's surface. But such an external layer, with low thickness, has also been observed for the SBNA3 and SBNA6 glasses. So we propose this layer really exists, which might be dependent on the Al_2O_3 concentration. The fact that Cailleteau et al., [Cailleteau et al., 2008] and Gin et al.,

[Gin et al., 2020b] also observed experimentally similar dense layer on the surface of gel strengthens this conclusion. Cailleteau et al., [Cailleteau et al., 2008] proposed that this dense layer can reduce the diffusion of water across the gel. This explanation is probably not the good one because, later, Gin et al., [Gin et al., 2018] observed experimentally that diffusion of water across the mature gel is not limited. Nevertheless, in our case, we clearly observed, for glasses containing less Al_2O_3, that very rapidly stops the release of B atoms. In parallel, our Monte Carlo results suggest that an external layer enriched with Si can be formed on the gel surface. We propose that such an external layer can participate to the slowing down of the alteration for the SBNA1, SBNA4 and SBNA5 glasses.

7.4 Some considerations about water diffusion

The MC parameters have been optimized to reproduce at best the experimental release of Si and B in long-term alteration for three glasses (SBNA2, SBNA3, SBNA6). While achieving this, we observed a correlation between the MC parameters and the glass composition. Glasses with high quantity of B and Na allows faster water diffusion. This could be because of the channels opened by the organization of the Na atoms inside the glass and/or because of the network formed by the weak bonds around the B atoms [Taron, 2022]. In addition, the diffusion of water increases with decreasing quantity of Al in the glass. The silicate-reticulated network's strength also seems to have an impact on water diffusion.

7.5 A global synthesis of what we have learned from experiments and Monte Carlo simulations

One important phenomenon observed in SBNA4 is retention of B in the young gel through ToF-SIMS analysis. Similarly, Gin et al., [Gin et al., 2020a] observed the retention of B and Ca in the gel when altering the ISG coupon for 6 years. To understand the impact of retaining these elements in the gel, we saturated the solution with B, Ca, Na and Si and altered ISG coupons for 21 days. We observed that alteration rate of glass decreased by $\approx$ 50 times compared to the alteration in Si saturated solution. To investigate which element is preponderant, we altered ISG coupons in two solutions with the same composition but removed B from one solution and Ca from the other. ToF-SIMS analysis performed on these coupons revealed that the presence of both B and Ca in the solution is important for decreasing the alteration during residual regime. The two elements enter the gel and modify its transport properties. Tracing experiments with $H_2{}^{18}O$ showed that water diffusion through the gel is not significantly impacted by this incorporation of B and Ca in the gel. The main reason remains to be deciphered. Regarding B retention in the gel, we performed B sorption experiments on silica gel and mesoporous aluminosilicate

(MCM-41) as reference materials. It demonstrated that sorption process alone cannot account for the high retention capacity of ISG gels.

The experimental results show that in glasses with small amount of Al, more Si is quickly released into the solution. Also these glasses allow the gel to reorganize quickly, which favors the retention of B in gel. Indeed, we evidenced a strong correlation between B retention in the gel and a slow residual rate. On the other hand, glasses with a larger Al content releases a lower quantity of Si into the solution. The MC calculations show that systematically an external layer enriched with Si is formed at the gel's surface that is expected to further reduce the alteration rate. A global scheme begins to emerge to explain the change of the alteration rate versus time. Depending on the Al_2O_3 quantity in the glass, and on the quantity of Si released in solution, an external and dense layer can form more or less quickly. The consequence is that B atoms begin to be retained in the gel, which contributes in turn to slowing down the alteration. This scheme doesn't consider a possible aging effect of the gel that can also participate to the dynamics of the alteration.

To further validate these mechanisms and to take into account the role of gel aging, we need to improve the present Monte-Carlo code by introducing B diffusion inside the alteration layer. These modifications will have to be supported by new experiments, whose details are discussed in perspectives 7.6.

7.6 Perspectives

In Chapter 3.1, we demonstrated the correlation between the structural features of glass with their activation energy to dissociate the bonds around Si or Al through classical MD simulations. Since several structural features influence the activation energy for one chemical reaction, we tried to deepen this correlation by training with more advanced machine learning models like Multiple linear regression, Support vector machine, K-neighbor regressor, Adaboost, Neural network, Random forest, Gradient Boosting. We observed that Random forest was found to be the best among all these algorithms (almost 70% efficiency). The results are given in Section B.1. However, still the algorithm is far from perfect to perform the prediction, as the model stammers to tackle the non-linear role of Al towards hydrolysis energies around Si. A previous study by Krishnan et al., [Anoop Krishnan et al., 2018] has investigated multiple machine learning models to predict the initial dissolution rate from the glass composition. They observed that Artificial Neural Network (ANN) has the potential to handle the non-linear correlation of glass and its dissolution rate. Random forest performs 2nd best. In our study, we tried several algorithms including Random forest, but not ANN. So, training a predictive model through ANN could be a possibility to improve the existing models.

It is also important to notice that the models we developed in the study attempts to correlate simple structural features like bond angle, number of bridged oxygen, local

chemical environment, hydrostatic pressure and local shear towards the activation energy. However, more complex structural descriptors to represent the local environments through Dscribe python package [Himanen et al., 2020] will have to be tried to improve the efficiency of the predictive models. Therefore, applying ANN model with the structural descriptors shall make it possible to develop a good predictive model.

In Chapter 5.1, we tested a new MC model to reproduce the residual rates of three SBNA glasses. However, there are some mechanisms that need to be implemented to improve the model.

1. In the current MC model, the gel forms by complete release of Si into the solution and then redeposition on the glass surface. Based on many experimental evidences, at least on aluminosilicate glasses, local reorganization around Si needs to be implemented to better represent the gel formation mechanism for glasses containing Al_2O_3.

2. In current MC model, when the water molecule dissociates the four bonds around one B atom, the B atom is directly put into the bulk solution. However, without including the diffusion mechanism of B across the gel, it is difficult to reproduce the decreasing release of B with time. The diffusion coefficient of B at pH9, 90°C is 10^{-18} [Gin et al., 2020a]. Implementing B diffusion inside the alteration layer is an important challenge. Aertsens and coworkers initially developed an MC code with diffusion of elements to release into the solution [Aertsens and Van Iseghem, 1995]. But, the calculation becomes intensively heavy, which limited the size of the system they can consider. Nevertheless, according to the experiments presented in Chapter 6.1, an order of magnitude of the diffusion coefficient of B at pH9 across the gel has been obtained. Therefore, based on the current position and local environment of B inside the gel, we could implement a scheme to represent more precisely B diffusion inside the alteration layer. This mechanism will help us to reproduce the complete curve of the B release in solution.

3. Current MC does not have long-term aging of the gel. Introducing the Ostwald ripening mechanism to better reproduce the change of the pore size distribution with time will help to investigate the impact of the gel aging at long-term. Experimental pore size distributions can be estimated through the procedure of Gin et al [Gin et al., 2020b].

4. Kerisit et al., is attempting to perform MC simulation with MD simulation generated glass structure instead of representing them by ordered networks [Kerisit and Du, 2019]. Dissolution probabilities used in their study is kept constant. However, Chapter 3.1 and Chapter 4.1 shows that activation energy to dissociate the bond is highly influenced by the glass structural features. So succeeding the development of AI model to predict the activation energy for bond dissociation through glass structural features (as discussed previously), we can make the dissolution probabilities of MC model to be dynamic. Such MC model will be more realistic to represent the glass alteration.

5. Current MC code is not yet parallelized (works only with 1 core processor). Parallelizing the MC code will allow us to simulate faster glass alteration.

To investigate if the Si dense layer has contribution for B retention in the gel, we need experimental support. We propose to focus on glasses SBNA4 and SBNA6. Glass powders could be altered at high SA/V in distilled water (same procedure as in the Section 5.2.1) along with some glass coupons. We will take out 1 coupon after 3 months and another one after 6 months duration. Then ToF-SIMS will be performed to monitor the B retention and TEM will be performed to investigate if a dense layer has formed on the gel surface. This will clarify if the formation of a Si dense layer has a contribution for the retention of B in the gel.

Besides the formation of a Si-dense layer, we believe that the dynamics of the gel could have an important role on B retention. So far, several MC calculations have proposed that presence of insoluble elements like Al, Zr in the gel slows down the dynamics of reorganization [Cailleteau et al., 2008, Ledieu et al., 2005]. However, the experimental validation has not been performed yet. Gin et al., [Gin et al., 2018] developed a protocol to investigate the dynamics of the gel (young and mature gel). The same protocol could be used to test the dynamics of the gel formed on glasses with different Al_2O_3 concentration. (For instance: SBNA4 and SBNA6 of this study).

Finally, in Chapter 6.1, we have investigated the behavior of B across the gels prepared in two different pH conditions. However, a question remains open on whether the behavior of B is mostly influenced by the solution chemistry (acidic solution/basic solution) or by the gel structure developed in a particular pH. It would be important to test the protective characteristics of gel developed in basic pH under different conditions, to know its full potential towards B behavior. To answer this question, gel has to be developed in basic pH and acidic pH in the same way as shown in Section 2.5.2. While putting the coupons in a tracing solution containing ^{10}B, we could switch the solutions (for instance, the gel developed in basic pH will incubate in the acidic tracing solution). This will help us to understand the properties of the gel and the solution chemistry. Our hypothesis is that the solution chemistry will influence the diffusion speed of B across the gel. But morphology of the gel (developed at particular pH) could solely be responsible for the retention of B in it.

Summary of the contribution from this study

1. Addition of Al_2O_3 (approximately < 11 wt %) into silicate glass increases the strength of the bonds around the Si atoms to improve its durability during initial dissolution regime. Similarly, Al decreases the energy barrier for bond reformation around Si.

2. Incorporation of large amount of Al_2O_3 (approximately > 20 wt %) will lead to the preferential dissolution of Al, which will significantly affect the durability during initial dissolution regime. This strengthening role of Al on the bonds around Si is the preponderant limiting step during the initial dissolution regime of glasses with low Al_2O_3.

3. It has not been possible to correlate the local hydrolysis energies to the classical structural characteristics. A work using Machine Learning and larger structural feature database has to be developed in the future.

4. The energy difference between dissociating the bonds around Si in pure silicate vs aluminosilicate observed through PMF calculations were qualitatively reproduced with ReaxFF calculations.

5. During residual regime, glasses with no to small quantity of Al_2O_3 allows easier dissociation and reorganization of Si in the gel, which allows the formation of an external silica enriched layer at the interface between glass and solution.

6. On the other hand, in glasses with Al_2O_3 between 5 wt % to 9.6 wt % it takes a longer time to develop this external layer enriched in silica because the Si dissolution is more difficult.

7. This external silica enriched layer, probably associated to the aging mechanism of gel, plays an important role to retain the B. In consequence, further alteration of glass becomes very slow during the residual regime. This process might be an important rate limiting step during the residual regime.

Bibliography

[CTD,] Ctdp, common thermodynamic database project, http://ctdp.ensmp.fr/.

[Acocella et al., 1984] Acocella, J., Tomozawa, M., and Watson, E. (1984). The nature of dissolved water in sodium silicate glasses and its effect on various properties. *Journal of Non-Crystalline Solids*, 65(2-3):355–372.

[Aertsens and Ghaleb, 2001] Aertsens, M. and Ghaleb, D. (2001). New techniques for modelling glass dissolution. *Journal of nuclear materials*, 298(1-2):37–46.

[Aertsens and Van Iseghem, 1995] Aertsens, M. and Van Iseghem, P. (1995). Modelling glass dissolution with a monte carlo technique. *MRS Online Proceedings Library (OPL)*, 412.

[Anoop Krishnan et al., 2018] Anoop Krishnan, N., Mangalathu, S., Smedskjaer, M. M., Tandia, A., Burton, H., and Bauchy, M. (2018). Predicting the dissolution kinetics of silicate glasses using machine learning. *Journal of Non-Crystalline Solids*, 487:37–45.

[Aréna et al., 2019] Aréna, H., Rébiscoul, D., Garcès, E., and Godon, N. (2019). Comparative effect of alkaline elements and calcium on alteration of International Simple Glass. *npj Materials Degradation*, 3(1):10.

[Baral et al., 2019] Baral, K., Li, A., and Ching, W.-Y. (2019). Ab initio molecular dynamics simulation of na-doped aluminosilicate glasses and glass-water interaction. *AIP Advances*, 9(7):075218.

[Barkatt et al., 1993] Barkatt, A., Sang, J. C., Jakubik, R. F., and Saad, E. E. (1993). Oscillations in the dissolution kinetics of silicate glass in tris-buffered aqueous media. *Journal of non-crystalline solids*, 155(2):141–148.

[Bartholomew et al., 1980] Bartholomew, R., Butler, B., Hoover, H., and Wu, C. (1980). Infrared spectra of a water-containing glass. *Journal of the American Ceramic Society*, 63(9-10):481–485.

[Berendsen et al., 1987] Berendsen, H. J. C., Grigera, J. R., and Straatsma, T. P. (1987). The missing term in effective pair potentials. *The Journal of Physical Chemistry*, 91(24):6269–6271.

[Bisbrouck et al., 2022] Bisbrouck, N., Micoulaut, M., Delaye, J., Gin, S., and Angeli, F. (2022). Structure–property relationship and chemical durability of magnesium-containing borosilicate glasses with insight from topological constraints. *npj Materials Degradation*, 6(1):1–11.

[Bouyer et al., 2010a] Bouyer, F., Geneste, G., Ispas, S., Kob, W., and Ganster, P. (2010a). Water solubility in calcium aluminosilicate glasses investigated by first principles techniques. *Journal of Solid State Chemistry*, 183(12):2786–2796.

[Bouyer et al., 2010b] Bouyer, F., Geneste, G., Ispas, S., Kob, W., and Ganster, P. (2010b). Water solubility in calcium aluminosilicate glasses investigated by first principles techniques. *Journal of Solid State Chemistry*, 183(12):2786–2796.

[Cailleteau et al., 2008] Cailleteau, C., Angeli, F., Devreux, F., Gin, S., Jestin, J., Jollivet, P., and Spalla, O. (2008). Insight into silicate-glass corrosion mechanisms. *Nature Materials*, 7(12):978–983.

[Caurant and Majérus, 2021] Caurant, D. and Majérus, O. (2021). Glasses and Glass-Ceramics for Nuclear Waste Immobilization. In *Encyclopedia of Materials: Technical Ceramics and Glasses*, pages 762–789. Elsevier.

[Charpentier et al., 2018] Charpentier, T., Okhotnikov, K., Novikov, A. N., Hennet, L., Fischer, H. E., Neuville, D. R., and Florian, P. (2018). Structure of Strontium Aluminosilicate Glasses from Molecular Dynamics Simulation, Neutron Diffraction, and Nuclear Magnetic Resonance Studies. *The Journal of Physical Chemistry B*, 122(41):9567–9583.

[Chave et al., 2011] Chave, T., Frugier, P., Gin, S., and Ayral, A. (2011). Glass–water interphase reactivity with calcium rich solutions. *Geochimica et Cosmochimica Acta*, page 15.

[Collin et al., 2018a] Collin, M., Fournier, M., Frugier, P., Charpentier, T., Moskura, M., Deng, L., Ren, M., Du, J., and Gin, S. (2018a). Structure of International Simple Glass and properties of passivating layer formed in circumneutral pH conditions. *npj Materials Degradation*, 2(1):4.

[Collin et al., 2018b] Collin, M., Gin, S., Dazas, B., Mahadevan, T., Du, J., and Bourg, I. C. (2018b). Molecular Dynamics Simulations of Water Structure and Diffusion in a 1 nm Diameter Silica Nanopore as a Function of Surface Charge and Alkali Metal Counterion Identity. *The Journal of Physical Chemistry C*, 122(31):17764–17776.

[Collin et al., 2019] Collin, M., Gin, S., Jollivet, P., Dupuy, L., Dauvois, V., and Duffours, L. (2019). ToF-SIMS depth profiling of altered glass. *npj Materials Degradation*, 3(1):14.

[Criscenti et al., 2006a] Criscenti, L. J., Kubicki, J. D., and Brantley, S. L. (2006a). Silicate Glass and Mineral Dissolution: Calculated Reaction Paths and Activation Energies for Hydrolysis of a Q^3 Si by H_3O^+ Using Ab Initio Methods. *The Journal of Physical Chemistry A*, 110(1):198–206.

[Criscenti et al., 2006b] Criscenti, L. J., Kubicki, J. D., and Brantley, S. L. (2006b). Silicate glass and mineral dissolution: calculated reaction paths and activation energies for hydrolysis of a q3 si by h3o+ using ab initio methods. *The Journal of Physical Chemistry A*, 110(1):198–206.

[Damodaran et al., 2022] Damodaran, K., Delaye, J.-M., Kalinichev, A. G., and Gin, S. (2022). Deciphering the non-linear impact of Al on chemical durability of silicate glass. *Acta Materialia*, 225:117478.

[Del Bene et al., 2003] Del Bene, J. E., Runge, K., and Bartlett, R. J. (2003). A quantum chemical mechanism for the water-initiated decomposition of silica. *Computational Materials Science*, 27(1-2):102–108.

[Dell et al., 1983] Dell, W., Bray, P., and Xiao, S. (1983). 11b nmr studies and structural modeling of na2o b2o3 sio2 glasses of high soda content. *Journal of Non-Crystalline Solids*, 58(1):1–16.

[Demontis et al., 2001] Demontis, P., Spanu, S., and Suffritti, G. B. (2001). Application of the wolf method for the evaluation of coulombic interactions to complex condensed matter systems: Aluminosilicates and water. *The Journal of Chemical Physics*, 114(18):7980–7988.

[Deng et al., 2020] Deng, L., Urata, S., Takimoto, Y., Miyajima, T., Hahn, S. H., van Duin, A. C., and Du, J. (2020). Structural features of sodium silicate glasses from reactive force field-based molecular dynamics simulations. *Journal of the American Ceramic Society*, 103(3):1600–1614.

[Devreux and Barboux, 2001] Devreux, F. and Barboux, P. (2001). Numerical modelling of glass dissolution: gel layer morphology. *Journal of nuclear materials*, 298(1-2):145–149.

[Devreux et al., 2004] Devreux, F., Ledieu, A., Barboux, P., and Minet, Y. (2004). Leaching of borosilicate glasses. ii. model and monte-carlo simulations. *Journal of non-crystalline solids*, 343(1-3):13–25.

[Du and Cormack, 2005] Du, J. and Cormack, A. N. (2005). Molecular dynamics simulation of the structure and hydroxylation of silica glass surfaces. *Journal of the American Ceramic Society*, 88(9):2532–2539.

[Du et al., 2021] Du, J., Lu, X., Gin, S., Delaye, J.-M., Deng, L., Taron, M., Bisbrouck, N., Bauchy, M., and Vienna, J. D. (2021). Predicting the dissolution rate of borosilicate glasses using qspr analysis based on molecular dynamics simulations. *Journal of the American Ceramic Society*, 104(9):4445–4458.

[Du and de Leeuw, 2006] Du, Z. and de Leeuw, N. H. (2006). Molecular dynamics simulations of hydration, dissolution and nucleation processes at the α-quartz (0001) surface in liquid water. *Dalton Transactions*, (22):2623–2634.

[Dupuis et al., 2019] Dupuis, R., Béland, L. K., and Pellenq, R. J.-M. (2019). Molecular simulation of silica gels: Formation, dilution, and drying. *Physical Review Materials*, 3(7):075603.

[Dupuis et al., 2018] Dupuis, R., Dolado, J. S., Surga, J., and Ayuela, A. (2018). Doping as a Way To Protect Silicate Chains in Calcium Silicate Hydrates. *ACS Sustainable Chemistry & Engineering*, 6(11):15015–15021.

[Dupuis et al., 2020] Dupuis, R., Pellenq, R., Champenois, J.-B., and Poulesquen, A. (2020). Dissociation Mechanisms of Dissolved Alkali Silicates in Sodium Hydroxide. *The Journal of Physical Chemistry C*, 124(15):8288–8294.

[Ebert, 1993] Ebert, W. (1993). The effects of leachate ph and the ratio of glass surface area to leachant volume on glass reaction. *Phys. Chem. Glasses*, 34(2):58–65.

[Ebert et al., 1992] Ebert, W. L., Bates, J. K., Buck, E., and Bradley, C. (1992). Accelerated glass reaction under pct conditions. *MRS Online Proceedings Library (OPL)*, 294.

[Ewing et al., 2016] Ewing, R. C., Whittleston, R. A., and Yardley, B. W. (2016). Geological disposal of nuclear waste: a primer. *Elements*, 12(4):233–237.

[Farid et al., 2019] Farid, O., Ojovan, M., Massoud, A., and Abdel Rahman, R. (2019). An Assessment of Initial Leaching Characteristics of Alkali-Borosilicate Glasses for Nuclear Waste Immobilization. *Materials*, 12(9):1462.

[Feuston and Garofalini, 1990a] Feuston, B. and Garofalini, S. (1990a). Oligomerization in silica sols. *Journal of Physical Chemistry*, 94(13):5351–5356.

[Feuston and Garofalini, 1990b] Feuston, B. and Garofalini, S. H. (1990b). Water-induced relaxation of the vitreous silica surface. *Journal of applied physics*, 68(9):4830–4836.

[Fogarty et al., 2010] Fogarty, J. C., Aktulga, H. M., Grama, A. Y., Van Duin, A. C., and Pandit, S. A. (2010). A reactive molecular dynamics simulation of the silica-water interface. *The Journal of chemical physics*, 132(17):174704.

[Fournier et al., 2019] Fournier, M., Ducasse, T., Pérez, A., Barchouchi, A., Daval, D., and Gin, S. (2019). Effect of pH on the stability of passivating gel layers formed on International Simple Glass. *Journal of Nuclear Materials*, 524:21–38.

[Fournier et al., 2018] Fournier, M., Frugier, P., and Gin, S. (2018). Application of graal model to the resumption of international simple glass alteration. *npj Materials Degradation*, 2(1):1–9.

[Fournier et al., 2014] Fournier, M., Gin, S., and Frugier, P. (2014). Resumption of nuclear glass alteration: state of the art. *Journal of Nuclear Materials*, 448(1-3):348–363.

[Fournier et al., 2016] Fournier, M., Ull, A., Nicoleau, E., Inagaki, Y., Odorico, M., Frugier, P., and Gin, S. (2016). Glass dissolution rate measurement and calculation revisited. *Journal of Nuclear Materials*, 476:140–154.

[Frankel, 2018] Frankel, G. S. (2018). A comparative review of the aqueous corrosion of glasses, crystalline ceramics, and metals. *npj Materials Degradation*, page 17.

[Frankel et al., 2021] Frankel, G. S., Vienna, J. D., Lian, J., Guo, X., Gin, S., Kim, S. H., Du, J., Ryan, J. V., Wang, J., Windl, W., Taylor, C. D., and Scully, J. R. (2021). Recent Advances in Corrosion Science Applicable To Disposal of High-Level Nuclear Waste. *Chemical Reviews*, page acs.chemrev.0c00990.

[Frugier et al., 2005] Frugier, P., Martin, C., Ribet, I., Advocat, T., and Gin, S. (2005). The effect of composition on the leaching of three nuclear waste glasses: R7T7, AVM and VRZ. *Journal of Nuclear Materials*, 346(2-3):194–207.

[Frugier et al., 2018] Frugier, P., Minet, Y., Rajmohan, N., Godon, N., and Gin, S. (2018). Modeling glass corrosion with graal. *npj Materials Degradation*, 2(1):1–13.

[Ganster et al., 2004] Ganster, P., Benoit, M., Kob, W., and Delaye, J.-M. (2004). Structural properties of a calcium aluminosilicate glass from molecular-dynamics simulations: A finite size effects study. *The Journal of chemical physics*, 120(21):10172–10181.

[Garofalini and Martin, 1994] Garofalini, S. H. and Martin, G. (1994). Molecular simulations of the polymerization of silicic acid molecules and network formation. *The Journal of Physical Chemistry*, 98(4):1311–1316.

[Gdoutos et al., 2010] Gdoutos, E. E., Agrawal, R., and Espinosa, H. D. (2010). Comparison of the ewald and wolf methods for modeling electrostatic interactions in nanowires. *International Journal for Numerical Methods in Engineering*, 84(13):1541–1551.

[Geisler et al., 2010] Geisler, T., Janssen, A., Scheiter, D., Stephan, T., Berndt, J., and Putnis, A. (2010). Aqueous corrosion of borosilicate glass under acidic conditions: a new corrosion mechanism. *Journal of Non-Crystalline Solids*, 356(28-30):1458–1465.

[Geisler et al., 2015] Geisler, T., Nagel, T., Kilburn, M. R., Janssen, A., Icenhower, J. P., Fonseca, R. O., Grange, M., and Nemchin, A. A. (2015). The mechanism of borosilicate glass corrosion revisited. *Geochimica et Cosmochimica Acta*, 158:112–129.

[Gin et al., 2013] Gin, S., Abdelouas, A., Criscenti, L., Ebert, W., Ferrand, K., Geisler, T., Harrison, M., Inagaki, Y., Mitsui, S., Mueller, K., Marra, J., Pantano, C., Pierce, E., Ryan, J., Schofield, J., Steefel, C., and Vienna, J. (2013). An international initiative on long-term behavior of high-level nuclear waste glass. *Materials Today*, 16(6):243–248.

[Gin et al., 2012] Gin, S., Beaudoux, X., Angéli, F., Jégou, C., and Godon, N. (2012). Effect of composition on the short-term and long-term dissolution rates of ten borosilicate glasses of increasing complexity from 3 to 30 oxides. *Journal of Non-Crystalline Solids*, 358(18-19):2559–2570.

[Gin et al., 2018] Gin, S., Collin, M., Jollivet, P., Fournier, M., Minet, Y., Dupuy, L., Mahadevan, T., Kerisit, S., and Du, J. (2018). Dynamics of self-reorganization explains passivation of silicate glasses. *Nature Communications*, 9(1):2169.

[Gin et al., 2021a] Gin, S., Delaye, J.-M., Angeli, F., and Schuller, S. (2021a). Aqueous alteration of silicate glass: state of knowledge and perspectives. *npj Materials Degradation*, 5(1):42.

[Gin et al., 2021b] Gin, S., Delaye, J.-M., Angeli, F., and Schuller, S. (2021b). Aqueous alteration of silicate glass: state of knowledge and perspectives. *npj Materials Degradation*, 5(1):1–20.

[Gin et al., 2004] Gin, S., Godon, N., Ribet, I., Jollivet, P., Minet, Y., Frugier, P., Vernaz, E., Cavedon, J., Bonin, B., and Do Quang, R. (2004). Long-term behavior of r7t7-type nuclear glass: current state of knowledge and outlook. *MRS Online Proceedings Library (OPL)*, 824.

[Gin et al., 2020a] Gin, S., Guo, X., Delaye, J.-M., Angeli, F., Damodaran, K., Testud, V., Du, J., Kerisit, S., and Kim, S. H. (2020a). Insights into the mechanisms controlling the residual corrosion rate of borosilicate glasses. *npj Materials Degradation*, 4(1):41.

[Gin et al., 2017a] Gin, S., Jollivet, P., Barba Rossa, G., Tribet, M., Mougnaud, S., Collin, M., Fournier, M., Cadel, E., Cabie, M., and Dupuy, L. (2017a). Atom-Probe Tomography, TEM and ToF-SIMS study of borosilicate glass alteration rim: A multi-scale approach to investigating rate-limiting mechanisms. *Geochimica et Cosmochimica Acta*, 202:57–76.

[Gin et al., 2015] Gin, S., Jollivet, P., Fournier, M., Angeli, F., Frugier, P., and Charpentier, T. (2015). Origin and consequences of silicate glass passivation by surface layers. *Nature Communications*, 6(1):6360.

[Gin et al., 2017b] Gin, S., Jollivet, P., Tribet, M., Peuget, S., and Schuller, S. (2017b). Radionuclides containment in nuclear glasses: an overview. *Radiochimica Acta*, 105(11):927–959.

[Gin et al., 2020b] Gin, S., Mir, A., Jan, A., Delaye, J., Chauvet, E., De Puydt, Y., Gourgiotis, A., and Kerisit, S. (2020b). A General Mechanism for Gel Layer Formation on Borosilicate Glass under Aqueous Corrosion. *The Journal of Physical Chemistry C*, 124(9):5132–5144.

[Gin et al., 2016] Gin, S., Neill, L., Fournier, M., Frugier, P., Ducasse, T., Tribet, M., Abdelouas, A., Parruzot, B., Neeway, J., and Wall, N. (2016). The controversial role of inter-diffusion in glass alteration. *Chemical Geology*, 440:115–123.

[Grambow, 1984] Grambow, B. (1984). A general rate equation for nuclear waste glass corrosion. *MRS Online Proceedings Library (OPL)*, 44.

[Grambow, 2006] Grambow, B. (2006). Nuclear Waste Glasses - How Durable? *Elements*, 2(6):357–364.

[Grandjean et al., 2007] Grandjean, A., Malki, M., Simonnet, C., Manara, D., and Penelon, B. (2007). Correlation between electrical conductivity, viscosity, and structure in borosilicate glass-forming melts. *Physical Review B*, 75(5):054112.

[Gratz et al., 1991] Gratz, A., Manne, S., and Hansma, P. (1991). Atomic force microscopy of atomic-scale ledges and etch pits formed during dissolution of quartz. *Science*, 251(4999):1343–1346.

[Greaves and Sen, 2007] Greaves, G. N. and Sen, S. (2007). Inorganic glasses, glass-forming liquids and amorphizing solids. *Advances in Physics*, 56(1):1–166.

[Greer, 1999] Greer, A. L. (1999). Through a glass, lightly. *Nature*, 402(6758):132–133.

[Guillot and Guissani, 2001] Guillot, B. and Guissani, Y. (2001). How to build a better pair potential for water. *The Journal of Chemical Physics*, 114(15):6720–6733.

[Guo et al., 2020] Guo, X., Gin, S., and Frankel, G. S. (2020). Review of corrosion interactions between different materials relevant to disposal of high-level nuclear waste. *npj Materials Degradation*, 4(1):34.

[Hahn et al., 2018] Hahn, S. H., Rimsza, J., Criscenti, L., Sun, W., Deng, L., Du, J., Liang, T., Sinnott, S. B., and Van Duin, A. C. (2018). Development of a reaxff reactive force field for nasio x/water systems and its application to sodium and proton self-diffusion. *The Journal of Physical Chemistry C*, 122(34):19613–19624.

[Hamilton, 1999] Hamilton, J. P. (1999). *Corrosion behavior of sodium aluminosilicate glasses and crystals*. The Pennsylvania State University.

[Hamilton et al., 2001] Hamilton, J. P., Brantley, S. L., Pantano, C. G., Criscenti, L. J., and Kubicki, J. D. (2001). Dissolution of nepheline, jadeite and albite glasses: toward better models for aluminosilicate dissolution. *Geochimica et Cosmochimica Acta*, 65(21):3683–3702.

[Hamilton et al., 2000] Hamilton, J. P., Pantano, C. G., and Brantley, S. L. (2000). Dissolution of albite glass and crystal. *Geochimica et Cosmochimica Acta*, 64(15):2603–2615.

[Han et al., 2020] Han, T., Stone-Weiss, N., Huang, J., Goel, A., and Kumar, A. (2020). Machine learning as a tool to design glasses with controlled dissolution for healthcare applications. *Acta Biomaterialia*, 107:286–298.

[Hand and Tadjiev, 2010] Hand, R. J. and Tadjiev, D. R. (2010). Mechanical properties of silicate glasses as a function of composition. *Journal of Non-Crystalline Solids*, 356(44-49):2417–2423.

[Hellmann et al., 2015a] Hellmann, R., Cotte, S., Cadel, E., Malladi, S., Karlsson, L. S., Lozano-Perez, S., Cabié, M., and Seyeux, A. (2015a). Nanometre-scale evidence for interfacial dissolution–reprecipitation control of silicate glass corrosion. *Nature materials*, 14(3):307–311.

[Hellmann et al., 2015b] Hellmann, R., Cotte, S., Cadel, E., Malladi, S., Karlsson, L. S., Lozano-Perez, S., Cabié, M., and Seyeux, A. (2015b). Nanometre-scale evidence for interfacial dissolution–reprecipitation control of silicate glass corrosion. *Nature Materials*, 14(3):307–311.

[Hiemstra and Van Riemsdijk, 1990] Hiemstra, T. and Van Riemsdijk, W. (1990). Multiple activated complex dissolution of metal (hydr) oxides: A thermodynamic approach applied to quartz. *Journal of colloid and interface science*, 136(1):132–150.

[Himanen et al., 2020] Himanen, L., Jäger, M. O. J., Morooka, E. V., Federici Canova, F., Ranawat, Y. S., Gao, D. Z., Rinke, P., and Foster, A. S. (2020). DScribe: Library of descriptors for machine learning in materials science. *Computer Physics Communications*, 247:106949.

[Huseyin Kaya et al.,] Huseyin Kaya, Gin, S., Bryan D. Vogt, and Kim, S. H. Impact of aqueous solution pH on network structure of corrosioninduced surface layers of boroaluminosilicate glass. *Journal of the American Ceramic Society*, Under Revision.

[Icenhower and Dove, 2000] Icenhower, J. P. and Dove, P. M. (2000). The dissolution kinetics of amorphous silica into sodium chloride solutions: effects of temperature and ionic strength. *Geochimica et Cosmochimica Acta*, 64(24):4193–4203.

[Ishizawa et al., 1980] Ishizawa, N., Miyata, T., Minato, I., Marumo, F., and Iwai, S. (1980). A structural investigation of α-al2o3 at 2170 k. *Acta Crystallographica Section B: Structural Crystallography and Crystal Chemistry*, 36(2):228–230.

[Izrailev et al., 1999] Izrailev, S., Stepaniants, S., Isralewitz, B., Kosztin, D., Lu, H., Molnar, F., Wriggers, W., and Schulten, K. (1999). Steered molecular dynamics. In *Computational molecular dynamics: challenges, methods, ideas*, pages 39–65. Springer.

[Jabraoui et al., 2021] Jabraoui, H., Charpentier, T., Gin, S., Delaye, J.-M., and Pollet, R. (2021). Atomic Insights into the Events Governing the Borosilicate Glass–Water Interface. *The Journal of Physical Chemistry C*, 125(14):7919–7931.

[Jan et al., 2019a] Jan, A., Delaye, J.-M., Gin, S., and Kerisit, S. (2019a). Molecular dynamics simulation of ballistic effects in simplified nuclear waste glasses. *Journal of Non-Crystalline Solids*, 505:188–201.

[Jan et al., 2019b] Jan, A., Delaye, J.-M., Gin, S., and Kerisit, S. (2019b). Monte carlo simulation of the corrosion of irradiated simplified nuclear waste glasses. *Journal of Non-Crystalline Solids*, 519:119449.

[Jantzen and Ojovan, 2019] Jantzen, C. M. and Ojovan, M. I. (2019). On Selection of Matrix (Wasteform) Material for Higher Activity Nuclear Waste Immobilization (Review). *Russian Journal of Inorganic Chemistry*, 64(13):1611–1624.

[Jégou et al., 2000] Jégou, C., Gin, S., and Larché, F. (2000). Alteration kinetics of a simplified nuclear glass in an aqueous medium: effects of solution chemistry and of protective gel properties on diminishing the alteration rate. *Journal of Nuclear Materials*, 280(2):216–229.

[Jollivet et al., 2008] Jollivet, P., Angeli, F., Cailleteau, C., Devreux, F., Frugier, P., and Gin, S. (2008). Investigation of gel porosity clogging during glass leaching. *Journal of Non-Crystalline Solids*, 354(45-46):4952–4958.

[Jollivet et al., 2012] Jollivet, P., Gin, S., and Schumacher, S. (2012). Forward dissolution rate of silicate glasses of nuclear interest in clay-equilibrated groundwater. *Chemical Geology*, 330-331:207–217.

[Kagan et al., 2014] Kagan, M., Lockwood, G. K., and Garofalini, S. H. (2014). Reactive simulations of the activation barrier to dissolution of amorphous silica in water. *Phys. Chem. Chem. Phys.*, 16(20):9294–9301.

[Kerisit and Du, 2019] Kerisit, S. and Du, J. (2019). Monte carlo simulation of borosilicate glass dissolution using molecular dynamics-generated glass structures. *Journal of Non-Crystalline Solids*, 522:119601.

[Kerisit and Pierce, 2011] Kerisit, S. and Pierce, E. M. (2011). Monte carlo simulations of the dissolution of borosilicate and aluminoborosilicate glasses in dilute aqueous solutions. *Geochimica Et Cosmochimica Acta*, 75(18):5296–5309.

[Kerisit and Pierce, 2012] Kerisit, S. and Pierce, E. M. (2012). Monte carlo simulations of the dissolution of borosilicate glasses in near-equilibrium conditions. *Journal of non-crystalline solids*, 358(10):1324–1332.

[Kim and Kirkpatrick, 2006] Kim, Y. and Kirkpatrick, R. J. (2006). 11b nmr investigation of boron interaction with mineral surfaces: Results for boehmite, silica gel and illite. *Geochimica et Cosmochimica Acta*, 70(13):3231–3238.

[Kraus and Drass, 2020] Kraus, M. A. and Drass, M. (2020). Artificial intelligence for structural glass engineering applications — overview, case studies and future potentials. *Glass Structures & Engineering*, 5(3):247–285.

[Krishnan et al., 2018] Krishnan, N. A., Mangalathu, S., Smedskjaer, M. M., Tandia, A., Burton, H., and Bauchy, M. (2018). Predicting the dissolution kinetics of silicate glasses using machine learning. *Journal of Non-Crystalline Solids*, 487:37–45.

[Krough-Moe, 1965] Krough-Moe, J. (1965). Interpretation of infrared spectra of boron oxide and alkali borate glasses. *Phys. Chem. Glasses*, 2:46.

[Laio and Parrinello, 2002] Laio, A. and Parrinello, M. (2002). Escaping free-energy minima. *Proceedings of the National Academy of Sciences*, 99(20):12562–12566.

[Ledieu et al., 2004] Ledieu, A., Devreux, F., and Barboux, P. (2004). Monte Carlo simulations of borosilicate glass corrosion: predictions for morphology and kinetics. *Journal of Non-Crystalline Solids*, 345-346:715–719.

[Ledieu et al., 2005] Ledieu, A., Devreux, F., and Barboux, P. (2005). The role of aluminium in the durability of alumino-borosilicate glasses. *Physics and Chemistry of Glasses*, 46(1):12–20.

[Lillington et al., 2020] Lillington, J. N., Goût, T. L., Harrison, M. T., and Farnan, I. (2020). Predicting radioactive waste glass dissolution with machine learning. *Journal of Non-Crystalline Solids*, 533:119852.

[Liu et al., 2021] Liu, H., Fu, Z., Yang, K., Xu, X., and Bauchy, M. (2021). Machine learning for glass science and engineering: A review. *Journal of Non-Crystalline Solids*, 557:119419.

[Liu et al., 2019] Liu, H., Zhang, T., Anoop Krishnan, N. M., Smedskjaer, M. M., Ryan, J. V., Gin, S., and Bauchy, M. (2019). Predicting the dissolution kinetics of silicate glasses by topology-informed machine learning. *npj Materials Degradation*, 3(1):32.

[Loewenstein, 1954] Loewenstein, W. (1954). The distribution of aluminum in the tetrahedra of silicates and aluminates. *American Mineralogist: Journal of Earth and Planetary Materials*, 39(1-2):92–96.

[Lu et al., 2021] Lu, X., Reiser, J. T., Parruzot, B., Deng, L., Gussev, I. M., Neuefeind, J. C., Graham, T. R., Liu, H., Ryan, J. V., Kim, S. H., Washton, N., Lang, M., Du, J., and Vienna, J. D. (2021). Effects of Al:Si and (Al + Na):Si ratios on the properties of the international simple glass, part II: Structure. *Journal of the American Ceramic Society*, 104(1):183–207.

[Mahadevan et al., 2022] Mahadevan, T., Baroni, A., Taron, M., Gin, S., Du, J., and Delaye, J.-M. (2022). Development of potentials for molecular dynamics simulations of dry and hydrated calcium aluminosilicate glasses by force matching and refinement. *Journal of Non-Crystalline Solids*, 592:121746.

[Mahadevan and Garofalini, 2007] Mahadevan, T. and Garofalini, S. (2007). Dissociative water potential for molecular dynamics simulations. *The Journal of Physical Chemistry B*, 111(30):8919–8927.

[Mahadevan and Du, 2018] Mahadevan, T. S. and Du, J. (2018). Evaluating Water Reactivity at Silica Surfaces Using Reactive Potentials. *The Journal of Physical Chemistry C*, 122(18):9875–9885.

[Mahadevan and Du, 2021] Mahadevan, T. S. and Du, J. (2021). Atomic and microstructure features of nanoporous aluminosilicate glasses from reactive molecular dynamics simulations. *Journal of the American Ceramic Society*, 104(1):229–242.

[Mahadevan and Garofalini, 2008] Mahadevan, T. S. and Garofalini, S. H. (2008). Dissociative Chemisorption of Water onto Silica Surfaces and Formation of Hydronium Ions. *The Journal of Physical Chemistry C*, 112(5):1507–1515.

[Mahadevan et al., 2019] Mahadevan, T. S., Sun, W., and Du, J. (2019). Development of Water Reactive Potentials for Sodium Silicate Glasses. *The Journal of Physical Chemistry B*, 123(20):4452–4461.

[Majérus et al., 2020] Majérus, O., Lehuédé, P., Biron, I., Alloteau, F., Narayanasamy, S., and Caurant, D. (2020). Glass alteration in atmospheric conditions: crossing perspectives from cultural heritage, glass industry, and nuclear waste management. *npj Materials Degradation*, 4(1):27.

[Manara et al., 2009] Manara, D., Grandjean, A., and Neuville, D. (2009). Advances in understanding the structure of borosilicate glasses: A raman spectroscopy study. *American Mineralogist*, 94(5-6):777–784.

[Mauro and Smedskjaer, 2014] Mauro, J. C. and Smedskjaer, M. M. (2014). Statistical mechanics of glass. *Journal of Non-Crystalline Solids*, 396-397:41–53.

[McKeown et al., 1984] McKeown, D., Galeener, F., and Brown Jr, G. (1984). Raman studies of al coordination in silica-rich sodium aluminosilicate glasses and some related minerals. *Journal of Non-Crystalline Solids*, 68(2-3):361–378.

[Mesmer et al., 1972] Mesmer, R. E., Baes, C. F., and Sweeton, F. H. (1972). Acidity measurements at elevated temperatures. VI. Boric acid equilibriums. *Inorganic Chemistry*, 11(3):537–543.

[Michalske and Freiman, 1983] Michalske, T. A. and Freiman, S. W. (1983). A molecular mechanism for stress corrosion in vitreous silica. *Journal of the American Ceramic Society*, 66(4):284–288.

[Mishra et al., 2019] Mishra, P., Pandey, C. M., Singh, U., Gupta, A., Sahu, C., and Keshri, A. (2019). Descriptive Statistics and Normality Tests for Statistical Data. *Annals of Cardiac Anaesthesia*, 22(1):67–72.

[Mohd Razali and Yap, 2011] Mohd Razali, N. and Yap, B. (2011). Power Comparisons of Shapiro-Wilk, Kolmogorov-Smirnov, Lilliefors and Anderson-Darling Tests. *J. Stat. Model. Analytics*, 2.

[Nangia and Garrison, 2008] Nangia, S. and Garrison, B. J. (2008). Reaction rates and dissolution mechanisms of quartz as a function of ph. *The Journal of Physical Chemistry A*, 112(10):2027–2033.

[Nangia and Garrison, 2010] Nangia, S. and Garrison, B. J. (2010). Role of intrasurface hydrogen bonding on silica dissolution. *The Journal of Physical Chemistry C*, 114(5):2267–2272.

[Neeway et al., 2011] Neeway, J., Abdelouas, A., Grambow, B., and Schumacher, S. (2011). Dissolution mechanism of the SON68 reference nuclear waste glass: New data in dynamic system in silica saturation conditions. *Journal of Nuclear Materials*, 415(1):31–37.

[Neeway et al., 2012] Neeway, J., Abdelouas, A., Grambow, B., Schumacher, S., Martin, C., Kogawa, M., Utsunomiya, S., Gin, S., and Frugier, P. (2012). Vapor hydration of son68 glass from 90 c to 200 c: a kinetic study and corrosion products investigation. *Journal of Non-Crystalline Solids*, 358(21):2894–2905.

[Ngo et al., 2020] Ngo, D., Liu, H., Chen, Z., Kaya, H., Zimudzi, T. J., Gin, S., Mahadevan, T., Du, J., and Kim, S. H. (2020). Hydrogen bonding interactions of H2O and SiOH on a boroaluminosilicate glass corroded in aqueous solution. *npj Materials Degradation*, 4(1):1.

[Nils Ingri, 1962] Nils Ingri (1962). Equilibrium Studies of Polyanions. 8. On the First Equilibrium Steps in the Hydrolysis of Boric Acid, a Comparison between Equilibria in 0.1 M and 3.0 M NaClO4. *Acta Chemica Scandinavica*, 16:439 – 448.

[Norris, 2019] Norris, S. (2019). Multiple roles of clays in radioactive waste confinement – introduction. *Geological Society, London, Special Publications*, 482(1):1–9.

[Ojovan and Lee, 2011] Ojovan, M. I. and Lee, W. E. (2011). Glassy Wasteforms for Nuclear Waste Immobilization. *Metallurgical and Materials Transactions A*, 42(4):837–851.

[Ojovan and Lee, 2014] Ojovan, M. I. and Lee, W. E. (2014). *An introduction to nuclear waste immobilisation*. Elsevier insights. Elsevier, Amsterdam, second edition edition.

[Onodera et al., 2020] Onodera, Y., Kohara, S., Salmon, P. S., Hirata, A., Nishiyama, N., Kitani, S., Zeidler, A., Shiga, M., Masuno, A., Inoue, H., et al. (2020). Structure and properties of densified silica glass: characterizing the order within disorder. *NPG Asia Materials*, 12(1):1–16.

[Parab and Bhalerao, 2010] Parab, S. and Bhalerao, S. (2010). Choosing statistical test. *International Journal of Ayurveda Research*, 1(3):187–191.

[Pegg, 2015] Pegg, I. L. (2015). Turning nuclear waste into glass. *Physics Today*, 68(2).

[Pelmenschikov et al., 2001] Pelmenschikov, A., Leszczynski, J., and Pettersson, L. G. (2001). Mechanism of dissolution of neutral silica surfaces: Including effect of self-healing. *The Journal of Physical Chemistry A*, 105(41):9528–9532.

[Pelmenschikov et al., 2000] Pelmenschikov, A., Strandh, H., Pettersson, L. G. M., and Leszczynski, J. (2000). Lattice Resistance to Hydrolysis of Si-O-Si Bonds of Silicate Minerals: Ab Initio Calculations of a Single Water Attack onto the (001) and (111) β-Cristobalite Surfaces. 104:5779–5783.

[Pierce and Bacon, 2009] Pierce, E. M. and Bacon, D. H. (2009). Accelerated weathering of waste glass at 90° c with the pressurized unsaturated flow (puf) apparatus: Implications for predicting glass corrosion with a reactive transport model. *Environmental Issues and Waste Management Technologies in the Materials and Nuclear Industries XII*, pages 141–153.

[Piovesan et al., 2018] Piovesan, V., Bardez-Giboire, I., Fournier, M., Frugier, P., Jollivet, P., Montouillout, V., Pellerin, N., and Gin, S. (2018). Chemical durability of peraluminous glasses for nuclear waste conditioning. *npj Materials Degradation*, 2(1):7.

[Plimpton, 1995] Plimpton, S. (1995). Fast parallel algorithms for short-range molecular dynamics. *Journal of computational physics*, 117(1):1–19.

[Puibasset and Pellenq, 2004] Puibasset, J. and Pellenq, R. J.-M. (2004). A comparison of water adsorption on ordered and disordered silica substrates. *Physical Chemistry Chemical Physics*, 6(8):1933–1937.

[Rahbari et al., 2019] Rahbari, A., Hens, R., Jamali, S., Ramdin, M., Dubbeldam, D., and Vlugt, T. (2019). Effect of truncating electrostatic interactions on predicting thermodynamic properties of water–methanol systems. *Molecular Simulation*, 45(4-5):336–350.

[Reiser et al., 2021] Reiser, J. T., Lu, X., Parruzot, B., Liu, H., Subramani, T., Kaya, H., Kissinger, R. M., Crum, J. V., Ryan, J. V., Navrotsky, A., Kim, S. H., and Vienna, J. D. (2021). Effects of Al:Si and (Al + Na):Si ratios on the properties of the international simple glass, part I: Physical properties. *Journal of the American Ceramic Society*, 104(1):167–182.

[Rieke et al., 2018] Rieke, P. C., Kerisit, S., Ryan, J. V., and Neeway, J. J. (2018). Adaptation of the graal model of glass reactivity to accommodate non-linear diffusivity. *Journal of Nuclear Materials*, 512:79–93.

[Rimsza et al., 2016] Rimsza, J., Yeon, J., Van Duin, A., and Du, J. (2016). Water interactions with nanoporous silica: comparison of reaxff and ab initio based molecular dynamics simulations. *The Journal of Physical Chemistry C*, 120(43):24803–24816.

[Sadeghifar et al., 2012] Sadeghifar, A., Dadvar, M., Karimi, S., and Ghobadi, A. F. (2012). The wolf method applied to the type i methane and carbon dioxide gas hydrates. *Journal of Molecular Graphics and Modelling*, 38:455–464.

[Saldi et al., 2021] Saldi, G. D., Louvat, P., Schott, J., and Gaillardet, J. (2021). The ph dependence of the isotopic composition of boron adsorbed on amorphous silica. *Geochimica et Cosmochimica Acta*, 308:1–20.

[Schott et al., 2014] Schott, J., Kretzschmar, J., Acker, M., Eidner, S., Kumke, M. U., Drobot, B., Barkleit, A., Taut, S., Brendler, V., and Stumpf, T. (2014). Formation of a Eu(iii) borate solid species from a weak Eu(iii) borate complex in aqueous solution. *Dalton Trans.*, 43(30):11516–11528.

[Senftle et al., 2016] Senftle, T. P., Hong, S., Islam, M. M., Kylasa, S. B., Zheng, Y., Shin, Y. K., Junkermeier, C., Engel-Herbert, R., Janik, M. J., Aktulga, H. M., et al. (2016). The reaxff reactive force-field: development, applications and future directions. *npj Computational Materials*, 2(1):1–14.

[Shelby, 2020] Shelby, J. E. (2020). *Introduction to glass science and technology*. Royal society of chemistry.

[Smedskjaer et al., 2012] Smedskjaer, M. M., Huang, L., Scannell, G., and Mauro, J. C. (2012). Elastic interpretation of the glass transition in aluminosilicate liquids. *Physical Review B*, 85(14):144203.

[Smets and Tholen, 1984] Smets, B. M. J. and Tholen, M. G. W. (1984). Leaching of Glasses with Molar Composition 20Na2O · 10RO · x Al2O3 · (70-x)SiO2. *Journal of the American Ceramic Society*, 67(4):281–284.

[Stolper, 1982] Stolper, E. (1982). Water in silicate glasses: an infrared spectroscopic study. *Contributions to Mineralogy and Petrology*, 81(1):1–17.

[Strachan, 2017] Strachan, D. (2017). Glass dissolution asa function of ph and its implications for understanding mechanisms and future experiments. *Geochimica et Cosmochimica Acta*, 219:111–123.

[Strachan et al., 2022] Strachan, D., Neeway, J. J., Pederson, L., Schreiber, D. K., Mitroshkov, A., Zhu, Z., and Ryan, J. V. (2022). On the dissolution of a borosilicate glass with the use of isotopic tracing – Insights into the mechanism for the long-term dissolution rate. *Geochimica et Cosmochimica Acta*, 318:213–229.

[Taron, 2022] Taron, M. (2022). Simulation à l'échelle nanoscopique du transport réactif : application à la dissolution des verres nucléaires. *University of Montpellier*.

[Tersoff, 1988] Tersoff, J. (1988). Empirical interatomic potential for silicon with improved elastic properties. *Physical Review B*, 38(14):9902.

[Thompson and Stebbins, 2012] Thompson, L. M. and Stebbins, J. F. (2012). Non-stoichiometric non-bridging oxygens and five-coordinated aluminum in alkaline earth aluminosilicate glasses: Effect of modifier cation size. *Journal of non-crystalline solids*, 358(15):1783–1789.

[Thorpe et al., 2021] Thorpe, C. L., Neeway, J. J., Pearce, C. I., Hand, R. J., Fisher, A. J., Walling, S. A., Hyatt, N. C., Kruger, A. A., Schweiger, M., Kosson, D. S., Arendt, C. L., Marcial, J., and Corkhill, C. L. (2021). Forty years of durability assessment of nuclear waste glass by standard methods. *npj Materials Degradation*, 5(1):61.

[Todorov et al., 2006] Todorov, I. T., Smith, W., Trachenko, K., and Dove, M. T. (2006). DL_poly_3: new dimensions in molecular dynamics simulations via massive parallelism. *Journal of Materials Chemistry*, 16(20):1911.

[Tomozawa, 1985] Tomozawa, M. (1985). Water in glass. *Journal of Non-Crystalline Solids*, 73(1-3):197–204.

[Van Der Lee et al., 2003] Van Der Lee, J., De Windt, L., Lagneau, V., and Goblet, P. (2003). Module-oriented modeling of reactive transport with hytec. *Computers & Geosciences*, 29(3):265–275.

[Van Duin et al., 2003] Van Duin, A. C., Strachan, A., Stewman, S., Zhang, Q., Xu, X., and Goddard, W. A. (2003). Reaxffsio reactive force field for silicon and silicon oxide systems. *The Journal of Physical Chemistry A*, 107(19):3803–3811.

[Vasudevan et al., 2019] Vasudevan, R. K., Choudhary, K., Mehta, A., Smith, R., Kusne, G., Tavazza, F., Vlcek, L., Ziatdinov, M., Kalinin, S. V., and Hattrick-Simpers, J. (2019). Materials science in the artificial intelligence age: high-throughput library generation, machine learning, and a pathway from correlations to the underpinning physics. *MRS Communications*, 9(3):821–838.

[Vernaz et al., 2001] Vernaz, E., Gin, S., Jégou, C., and Ribet, I. (2001). Present understanding of r7t7 glass alteration kinetics and their impact on long-term behavior modeling. *Journal of Nuclear Materials*, 298(1-2):27–36.

[Vernaz et al., 2012] Vernaz, E., Gin, S., and Veyer, C. (2012). 5.18–waste glass a2–konings. *Comprehensive Nuclear Materials*, page 451.

[Vienna and Crum, 2018] Vienna, J. D. and Crum, J. V. (2018). Non-linear effects of alumina concentration on Product Consistency Test response of waste glasses. *Journal of Nuclear Materials*, 511:396–405.

[Vienna et al., 2018] Vienna, J. D., Neeway, J. J., Ryan, J. V., and Kerisit, S. N. (2018). Impacts of glass composition, pH, and temperature on glass forward dissolution rate. *npj Materials Degradation*, 2(1):22.

[Vienna et al., 2013] Vienna, J. D., Ryan, J. V., Gin, S., and Inagaki, Y. (2013). Current understanding and remaining challenges in modeling long-term degradation of borosilicate nuclear waste glasses. *International Journal of Applied Glass Science*, 4(4):283–294.

[Weigel et al., 2008] Weigel, C., Calas, G., Cormier, L., Galoisy, L., and Henderson, G. S. (2008). High-resolution Al L $_{2,3}$ -edge x-ray absorption near edge structure spectra of Al-containing crystals and glasses: coordination number and bonding information from edge components. *Journal of Physics: Condensed Matter*, 20(13):135219.

[Wolf et al., 1999] Wolf, D., Keblinski, P., Phillpot, S. R., and Eggebrecht, J. (1999). Exact method for the simulation of Coulombic systems by spherically truncated, pairwise r1 summation. *The Journal of Chemical Physics*, 110(17):8254–8282.

[Wondraczek et al., 2011] Wondraczek, L., Mauro, J. C., Eckert, J., Kühn, U., Horbach, J., Deubener, J., and Rouxel, T. (2011). Towards Ultrastrong Glasses. *Advanced Materials*, 23(39):4578–4586.

[Xiang et al., 2013] Xiang, Y., Du, J., Smedskjaer, M. M., and Mauro, J. C. (2013). Structure and properties of sodium aluminosilicate glasses from molecular dynamics simulations. *The Journal of Chemical Physics*, 139(4):044507.

[Xiao and Lasaga, 1994] Xiao, Y. and Lasaga, A. C. (1994). Ab initio quantum mechanical studies of the kinetics and mechanisms of silicate dissolution: H +(H30 ') catalysis. *Geochimica et Cosmochimica Acta*, 58(24):5379–5400.

[Xu and Van Deventer, 2000] Xu, H. and Van Deventer, J. (2000). Ab initio calculations on the five-membered alumino-silicate framework rings model: implications for dissolution in alkaline solutions. *Computers & Chemistry*, 24(3-4):391–404.

[Xu et al., 2016] Xu, K., Hrma, P., Rice, J. A., Schweiger, M. J., Riley, B. J., Overman, N. R., and Kruger, A. A. (2016). Conversion of Nuclear Waste to Molten Glass: Cold-Cap Reactions in Crucible Tests. *Journal of the American Ceramic Society*, 99(9):2964–2970.

[Yeon and Van Duin, 2016] Yeon, J. and Van Duin, A. C. (2016). Reaxff molecular dynamics simulations of hydroxylation kinetics for amorphous and nano-silica structure, and its relations with atomic strain energy. *The Journal of Physical Chemistry C*, 120(1):305–317.

[Yu et al., 2016] Yu, Y., Wang, B., Wang, M., Sant, G., and Bauchy, M. (2016). Revisiting silica with ReaxFF: Towards improved predictions of glass structure and properties via reactive molecular dynamics. *Journal of Non-Crystalline Solids*, 443:148–154.

[Yu et al., 2017] Yu, Y., Wang, B., Wang, M., Sant, G., and Bauchy, M. (2017). Reactive molecular dynamics simulations of sodium silicate glasses—toward an improved understanding of the structure. *International Journal of Applied Glass Science*, 8(3):276–284.

[Yun and Bray, 1978] Yun, Y. and Bray, P. (1978). Nuclear magnetic resonance studies of the glasses in the system na2o b2o3 sio2. *Journal of Non-Crystalline Solids*, 27(3):363–380.

[Zapol et al., 2013] Zapol, P., He, H., Kwon, K. D., and Criscenti, L. J. (2013). First-Principles Study of Hydrolysis Reaction Barriers in a Sodium Borosilicate Glass. *International Journal of Applied Glass Science*, 4(4):395–407.

[Zheng et al., 2012] Zheng, Q., Smedskjaer, M. M., Youngman, R. E., Potuzak, M., Mauro, J. C., and Yue, Y. (2012). Influence of aluminum speciation on the stability of aluminosilicate glasses against crystallization. *Applied Physics Letters*, 101(4):041906.

[Zhou, 2003] Zhou, M. (2003). A new look at the atomic level virial stress: on continuum-molecular system equivalence. *Proceedings of the Royal Society of London. Series A: Mathematical, Physical and Engineering Sciences*, 459(2037):2347–2392.

[Zimmerman et al., 2004] Zimmerman, J. A., WebbIII, E. B., Hoyt, J. J., Jones, R. E., Klein, P. A., and Bammann, D. J. (2004). Calculation of stress in atomistic simulation. *Modelling and Simulation in Materials Science and Engineering*, 12(4):S319–S332.

[Zirl and Garofalini, 1990] Zirl, D. M. and Garofalini, S. H. (1990). Structure of sodium aluminosilicate glasses. *Journal of the American Ceramic Society*, 73(10):2848–2856.

Appendix A

Supplementary Details: Deciphering the non-linear impact of Al on chemical durability of silicate glass

Atom type in glass	Type of test	P-Value	Type of distribution	Type of T-test selected	P-Value
Si in pure silicate	Kolmogorov-smirnov test	0.00	Not normal distribution	Reference	Reference
Si in aluminosilicate	Kolmogorov-smirnov test	0.00	Not normal distribution	Mann-whitney test	0.001
Al in aluminosilicate	Kolmogorov-smirnov test	0.00	Not normal distribution	Mann-whitney test	0.00

Table A.1: Statistical tests for the distribution of activation energies for bond dissociation of Si in pure silicate, Si and Al in aluminosilicate glass [Damodaran et al., 2022].

Type of coordination	Type of test	P-Value	Type of distribution	Type of T-test selected	P-Values
$Si\_4 \rightarrow Si\_3$	Kolmogorov-Smirnov test	0.00	Not normally distributed	Reference	Reference
$Si\_3 \rightarrow Si\_2$	Kolmogorov-Smirnov test	0.00	Not normally distributed	Mann-whitney test	0.034
$Si\_2 \rightarrow Si\_1$	Shapiro-Wilk test	0.696	Normally distributed	Mann-Whitney test	0.102

Table A.2: Statistical tests for the distribution of activation energies for dissociating Si in pure silicate glass based on the number of bridging oxygen atoms[Damodaran et al., 2022].

Type of coordination	Type of test	P-Value	Type of distribution	Type of T-test selected	P-Value
$Si\_4 \rightarrow Si\_3$	Kolmogorov-Smirnov test	0.00	Not normally distributed	Reference	Reference
$Si\_3 \rightarrow Si\_2$	Kolmogorov-Smirnov test	0.00	Not normally distributed	Mann-whitney test	0.393
$Si\_2 \rightarrow Si\_1$	Shapiro-Wilk test	0.1643	Normally distributed	Mann-Whitney test	0.288

Table A.3: Statistical tests for the distribution of activation energies for dissociating Si in aluminosilicate glass based on the number of bridging oxygen atoms[Damodaran et al., 2022].

Type of coordination	Type of test	P-Value	Type of distribution	Type of T-test selected	P-Value
$Al\_4 \rightarrow Al\_3$	Shapiro-Wilk test	0.107	Normally distributed	Reference	Reference
$Al\_3 \rightarrow Al\_2$	Shapiro-Wilk test	0.516	Normally distributed	Welch's t-test	0.882
$Al\_2 \rightarrow Al\_1$	Shapiro-Wilk test	0.748	Normally distributed	Welch's t-test	0.541

Table A.4: Statistical tests for the distribution of activation energies for dissociating Al in aluminosilicate glass based on the number of bridging oxygen atoms[Damodaran et al., 2022].

Type of coordination	Type of test	P-Value	Type of distribution	Type of T-test selected	P-Value
Al_0	Kolmogorov-Smirnov test	0.00	Not normally distributed	Reference	Reference
Al_1	Kolmogorov-Smirnov test	0.00	Not normally distributed	Mann-whitney test	0.03
Al_2	Shapiro-Wilk test	0.21	Normally distributed	Mann-whitney test	0.006
Al_3	Shapiro-Wilk test	0.811	Normally distributed	Mann-whitney test	0.016
Al_4	Shapiro-Wilk test	0.003	Not normally distributed	Mann-whitney test	0.027

Table A.5: Statistical tests for the distribution of activation energies for dissociating Si in aluminosilicate glass based on the position of Al as the second neighbour[Damodaran et al., 2022].

Type of coordination	Type of test	P-Value	Type of distribution	Type of T-test selected	P-Value
Si_4	Shapiro-Wilk test	0.304	Normally distributed	Reference	Reference
Si_3	Shapiro-Wilk test	0.508	Normally distributed	Welch's t-test	0.422
Si_2	Shapiro-Wilk test	0.97	Normally distributed	Welch's t-test	0.859

Table A.6: Statistical tests for the distribution of activation energies for dissociating Al in aluminosilicate glass based on the position of Si as the second neighbor[Damodaran et al., 2022].

Atom in Glass type	P-values for bond angle vs activation energy	P-Values for shear stress vs activation energy	P-values for hydrostatic pressure vs activation energy
Si in pure silicate	0.00	0.00	0.991
Si in aluminosilicate	0.028	0.0029	0.130
Al in aluminosilicate	0.02	0.9787	0.955

Table A.7: Statistical tests for the correlation of bond angle, shear stress and hydrostatic pressure with activation energy for Si in pure silicate, Si and Al in aluminosilicate glass[Damodaran et al., 2022].

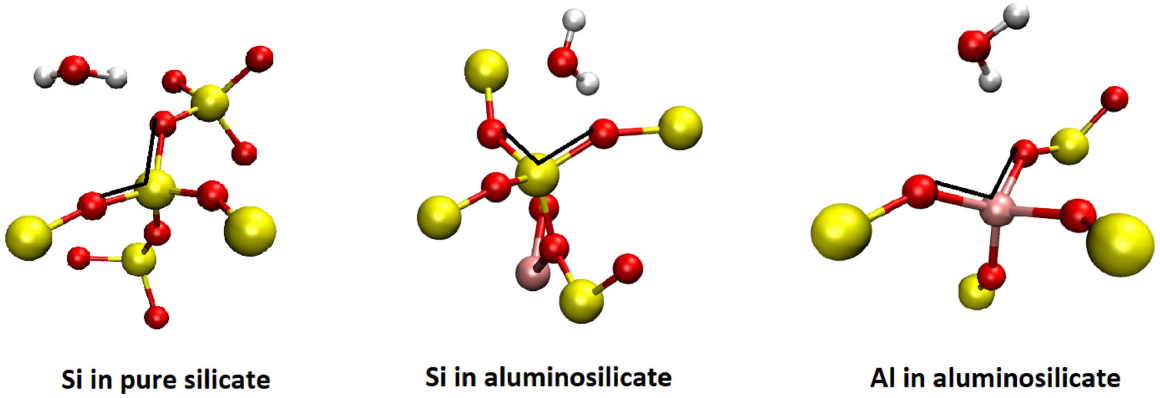

Figure A.1: Mechanism of dissociation of Si in pure silicate and Si, Al in aluminosilicate glass by water. O-Si-O and O-Al-O angles are widely open for providing way for the water molecule to interact and dissociate the bridge [Damodaran et al., 2022].

Appendix B

Supplementary Details: Classical MD to estimate Bond reformation energies, and ReaxFF calculations

B.1 Random forest algorithm to predict the bond dissociation energy of Si

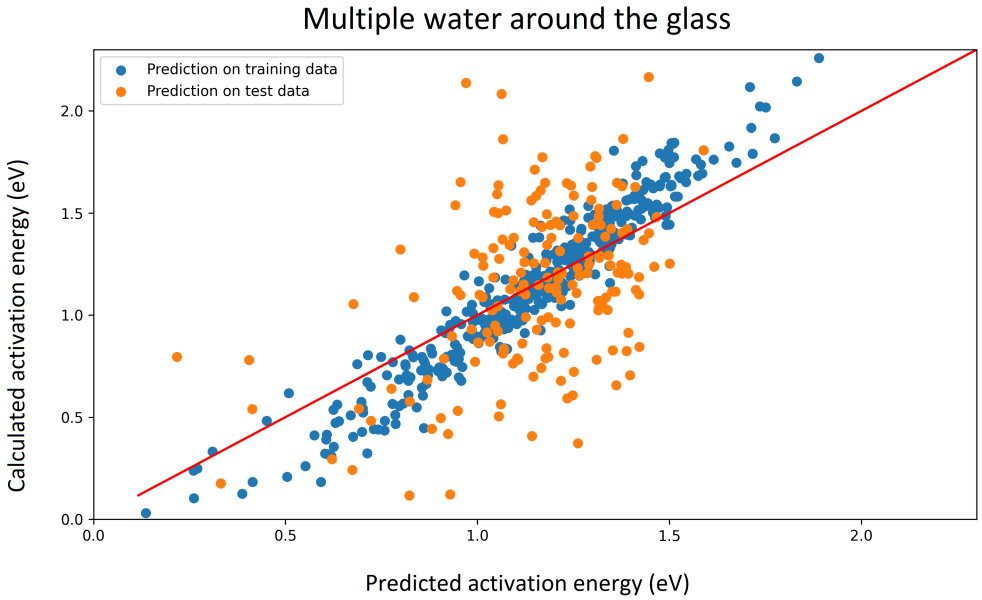

Figure B.1: Random forest method to predict the activation energy with multiple water. Color scheme: Blue - Prediction on training set data. Orange - Prediction on test set data.

PMF calculations in chapter 3.1 generated large statistical data of activation energy with the structural features of glass. We attempt to use these data to develop an artificial intelligence model to predict the activation energy based on structural features of glass

as input. The following structural features of glass are selected as input for the model: Si-O-Si bond angle, Number of bridged oxygen, Number of Si in environment, Number of Al in environment, Stress and Shear. We tried multiple machine learning algorithms like Multiple linear regression, Support vector machine, K-neighbor regressor, Adaboost, Neural network, Random forest, Gradient Boosting. We find that Random Forest Algorithm is better to predict the activation energy than others. However, lowest training set error the model could reach was 14.8% with the test set error of 37.04% as shown in the Supplementary figure B.1. The model faces large error on both the training set and test set.

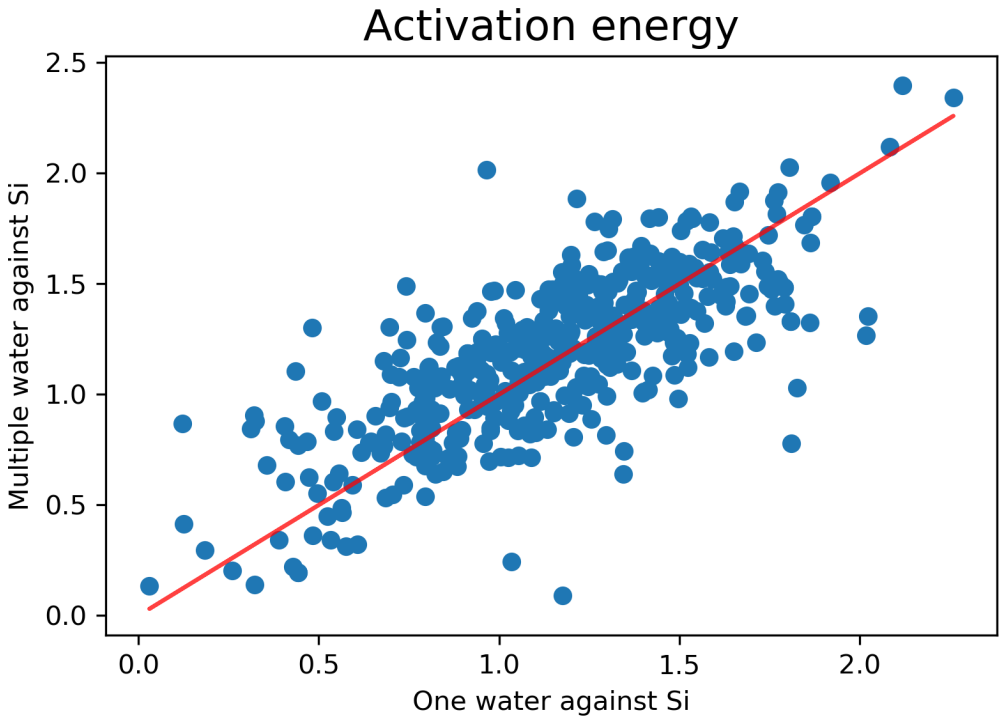

Figure B.2: Parameters to be optimized for the suitable nuclear waste glass[23].

Our ReaxFF calculations shown the influence of other water molecules might interfere the trajectory of water molecule attempting to dissociate the target Si. To avoid such interference biasing the activation energy, we performed simulations for the same set of glasses by removing all other water molecules and performed PMF for single water molecule to dissociate the target Si. We compared their activation energy with multiple water molecules as shown in supplementary figure B.2, and the average percentage of difference between them are 22.65%. Then repeated the random regression model to predict the activation energy based on data from single water molecule simulation. We observed improve in efficiency of the model where training set error was 9.39% and test set error was 27.6% as shown in the supplementary figure B.3.

Still the model's efficiency is not the best, and so we wanted to check if the initial position of the water molecule also has influence on their activation energy. So for the same set of glasses, we performed additional 10K relaxation before performing the PMF calculations. Even the bond angles are different for the simulations with 10K additional

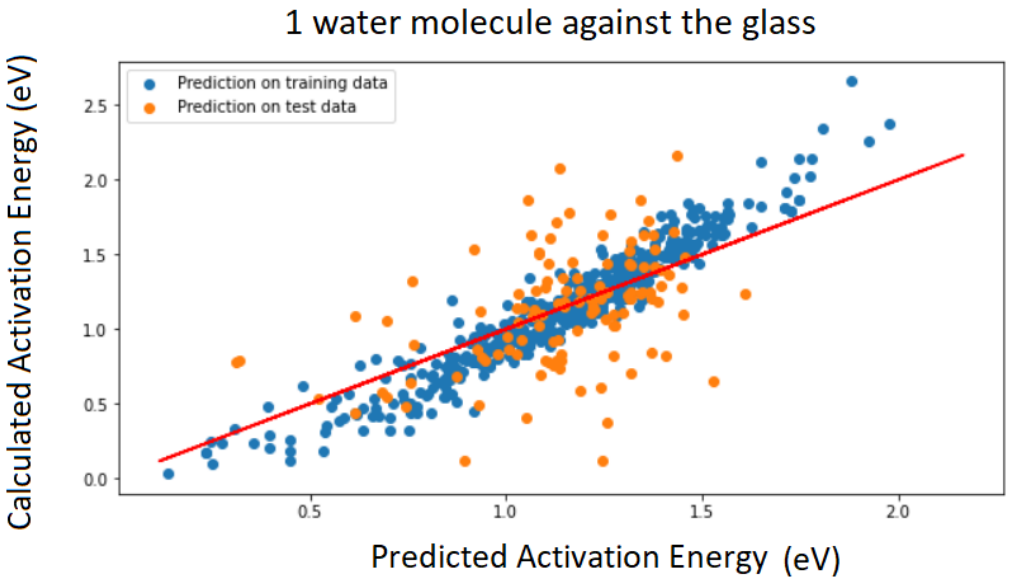

Figure B.3: Random forest method to predict the activation energy with single water. Color scheme: Blue - Prediction on training set data. Orange - Prediction on test set data.

relaxations as shown in supplementary figure B.4. Their activation energy is 27.71% different from the reference calculation, and their mean absolute difference in activation energy of 0.205 eV as shown in supplementary figure B.4. So finding a way to minimize this influence on activation energy will generate a clean dataset that can be used to develop a predictive model.

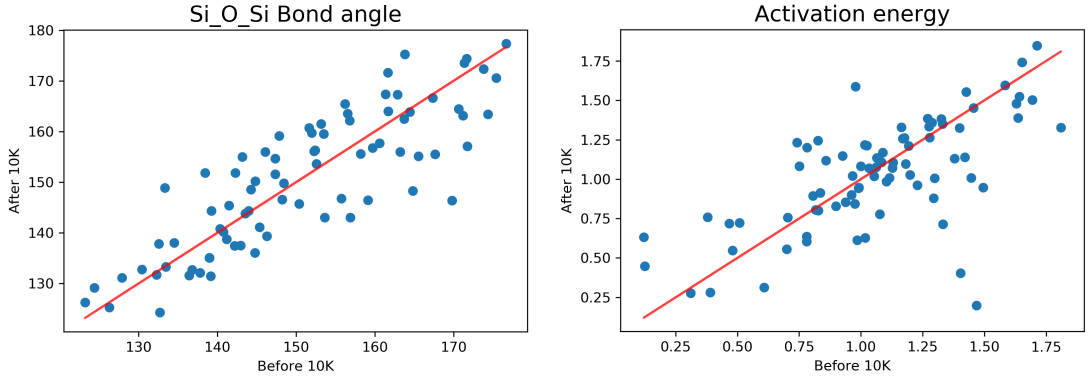

Figure B.4: Random Forest Method to predict the activation energy after 10K additional relaxation. (a) Si-O-Si bond angle is compared between the 10K additional relaxed simulation with reference. (b) Activation energy is compared between the 10K additional relaxed simulation with reference.

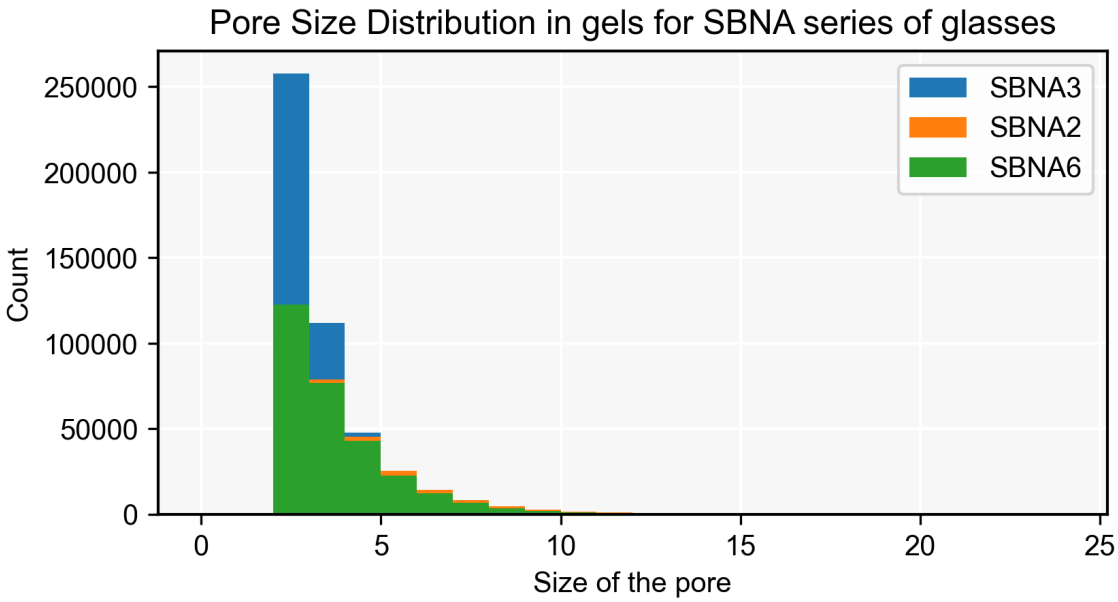

Figure B.5: Distribution of the pores for three glasses in gel region through MC simulation.

Appendix C

Supplementary Details: Long-term glass dissolution experiment and fitting with Monte-Carlo simulation method

Time	**SA/V**	**C(Si)**	**NL(Si)**	**EE(Si)**	**C(B)**	**NL(B)**	**EE(B)**	**C(Na)**	**NL(Na)**	**EE(Na)**	**pH**
0.0	50.0	0.0	0.00	0.0	0.0	0.00	0.0	0.0	0.00	0.0	9.12
1.3	50.1	346.5	0.23	90.2	322.9	1.03	410.9	551.9	1.05	418.1	9.1
2.8	51.2	390.3	0.25	100.4	415.4	1.30	521.7	679.8	1.27	508.5	9.05
4.0	53.1	384.9	0.24	96.4	434.9	1.33	531.1	676.5	1.23	492.6	
5.4	54.4	392.2	0.24	96.7	454.3	1.37	546.2	762.4	1.36	545.3	
6.8	56.1	412.4	0.25	99.7	489.5	1.44	576.3	824.9	1.44	577.8	
8.0	58.0	466.7	0.27	109.8	542.0	1.55	621.9	899.9	1.54	614.7	
8.9	60.4	432.7	0.25	99.4	577.3	1.60	641.8	900.6	1.49	598.0	
9.6	61.4	415.3	0.24	95.5	583.8	1.62	647.1	917.2	1.52	606.9	
10.5	62.4	423.8	0.24	96.9	605.0	1.67	666.7	939.8	1.55	618.7	
11.2	63.7	405.9	0.23	93.0	606.2	1.66	665.9	951.5	1.56	623.8	
11.8	64.8	417.6	0.24	95.0	631.7	1.72	688.6	974.1	1.59	634.9	
12.4	66.0	432.0	0.24	97.3	618.6	1.68	671.5	997.9	1.61	644.5	
13.0	67.2	436.8	0.24	97.9	643.7	1.73	693.6	1057.4	1.69	676.4	
13.4	68.5	430.6	0.24	96.4	656.2	1.76	702.7	1019.6	1.63	652.9	

Table C.1: Details about Long-Term alteration of SBNA1 glass powder in high surface area to volume ratio. Explanation of the column names and their units in table are: Time in $Day^{\frac{1}{2}}$; S/V - Surface area to volume ratio (cm^{-1}); C(Si) corr - Concentration of Si corrected (mg/l); NL(Si) - Normalized loss of Si (g/m^2); EE(Si) - Equivalent thickness of glass altered with respect to Si (nm); C(B) corr - Concentration of B corrected (mg/l); NL(B) - Normalized loss of B (g/m^2); EE(B) - Equivalent thickness of glass altered with respect to B (nm); C(Na) corr - Concentration of Na corrected (mg/l); NL(Na) - Normalized loss of Na (g/m^2); EE(Na) - Equivalent thickness of glass altered with respect to Na (nm);

Time	SA/V	C(Si)	NL(Si)	EE(Si)	C(B)	NL(B)	EE(B)	C(Na)	NL(Na)	EE(Na)	pH
0.0	50.0	0.0	0.00	0.0	0.0	0.00	0.0	0.0	0.00	0.0	9.12
1.3	50.1	118.9	0.08	33.2	97.1	0.33	132.0	89.9	0.18	72.7	8.9
2.8	51.5	140.2	0.10	38.4	231.5	0.77	308.0	224.1	0.44	177.3	8.85
4.0	53.3	153.2	0.10	41.0	354.9	1.15	458.9	397.6	0.76	305.3	
5.4	54.2	160.5	0.11	42.7	503.4	1.61	643.8	596.3	1.13	452.8	
6.8	55.6	169.5	0.11	44.2	670.9	2.09	837.6	720.0	1.34	534.8	
8.0	56.7	174.8	0.11	45.2	792.5	2.44	976.6	873.1	1.60	639.7	
8.9	85.1	256.5	0.11	44.8	1385.5	2.87	1146.3	1428.1	1.76	704.1	
9.6	61.9	197.1	0.12	48.0	1002.0	2.90	1161.3	1042.3	1.80	719.5	
10.5	63.0	200.3	0.12	48.4	1061.8	3.05	1219.8	1142.8	1.95	780.3	
11.2	64.1	202.6	0.12	48.6	1070.5	3.05	1221.7	1165.3	1.97	789.8	
11.8	65.1	210.7	0.13	50.3	1090.5	3.10	1240.2	1145.2	1.94	775.8	
12.4	66.6	213.0	0.13	50.4	1139.0	3.20	1280.8	1218.1	2.04	814.5	
13.0	67.7	213.3	0.13	50.3	1177.9	3.29	1314.5	1181.3	1.97	789.0	
13.4	69.0	219.9	0.13	51.4	1247.2	3.44	1377.7	1287.4	2.12	848.2	

Table C.2: Details about Long-Term alteration of SBNA2 glass powder in high surface area to volume ratio. Explanation of the column names and their units in table are: Time in $Day^{\frac{1}{2}}$; S/V - Surface area to volume ratio (cm^{-1}); C(Si) corr - Concentration of Si corrected (mg/l); NL(Si) - Normalized loss of Si (g/m^2); EE(Si) - Equivalent thickness of glass altered with respect to Si (nm); C(B) corr - Concentration of B corrected (mg/l); NL(B) - Normalized loss of B (g/m^2); EE(B) - Equivalent thickness of glass altered with respect to B (nm); C(Na) corr - Concentration of Na corrected (mg/l); NL(Na) - Normalized loss of Na (g/m^2); EE(Na) - Equivalent thickness of glass altered with respect to Na (nm);

Time	**SA/V**	**C(Si)**	**NL(Si)**	**EE(Si)**	**C(B)**	**NL(B)**	**EE(B)**	**C(Na)**	**NL(Na)**	**EE(Na)**	**pH**
0.0	52.1	0.0	0.00	0.0	0.0	0.00	0.0	0.0	0.00	0.0	9.12
1.3	52.4	66.5	0.05	19.0	167.0	0.47	187.4	211.5	0.35	140.4	8.95
2.8	53.2	186.7	0.13	53.4	842.5	2.34	937.8	1041.9	1.72	686.0	8.95
4.0	55.0	203.7	0.14	56.8	1068.5	2.90	1158.3	1337.4	2.14	857.4	
5.4	55.9	209.1	0.15	58.1	1234.3	3.32	1328.3	1445.8	2.30	921.5	
6.8	57.4	223.7	0.15	60.9	1383.2	3.65	1460.0	1700.8	2.65	1061.5	
8.0	58.6	229.9	0.15	61.9	1488.7	3.87	1549.6	1663.9	2.57	1027.8	
8.9	67.3	247.7	0.15	58.9	1730.3	3.96	1584.7	2042.3	2.77	1107.1	
9.6	61.2	232.1	0.15	61.3	1540.4	3.93	1572.9	1842.4	2.78	1112.6	
10.5	62.1	227.2	0.15	60.0	1535.4	3.91	1564.0	1837.4	2.77	1106.9	
11.2	63.1	225.4	0.15	59.4	1611.4	4.08	1631.6	1942.0	2.91	1162.2	
11.8	64.2	221.9	0.15	58.4	1594.6	4.03	1611.6	1934.3	2.89	1154.8	
12.4	65.3	230.5	0.15	60.2	1644.1	4.12	1649.9	2005.5	2.97	1188.1	
13.0	66.4	241.0	0.16	62.3	1602.8	4.02	1606.6	1905.4	2.83	1131.0	
13.4	67.7	247.9	0.16	63.7	1631.8	4.07	1628.2	2051.9	3.01	1203.7	

Table C.3: Details about Long-Term alteration of SBNA3 glass powder in high surface area to volume ratio. Explanation of the column names and their units in table are: Time in $Day^{\frac{1}{2}}$*; S/V - Surface area to volume ratio* (cm^{-1})*; C(Si) corr - Concentration of Si corrected (mg/l); NL(Si) - Normalized loss of Si* (g/m^2)*; EE(Si) - Equivalent thickness of glass altered with respect to Si (nm); C(B) corr - Concentration of B corrected (mg/l); NL(B) - Normalized loss of B* (g/m^2)*; EE(B) - Equivalent thickness of glass altered with respect to B (nm); C(Na) corr - Concentration of Na corrected (mg/l); NL(Na) - Normalized loss of Na* (g/m^2)*; EE(Na) - Equivalent thickness of glass altered with respect to Na (nm);*

Time	SA/V	C(Si)	NL(Si)	EE(Si)	C(B)	NL(B)	EE(B)	C(Na)	NL(Na)	EE(Na)	pH
0.0	46.6	0.0	0.00	0.0	0.0	0.00	0.0	0.0	0.00	0.0	9.12
1.3	46.8	377.9	0.29	114.3	514.3	1.70	680.6	913.7	1.54	614.7	9.23
2.8	48.6	448.3	0.33	131.8	588.5	1.89	757.2	1077.5	1.76	704.5	9.21
4.0	50.4	435.8	0.31	125.0	578.9	1.82	726.8	1055.5	1.68	673.5	
5.4	51.1	433.3	0.31	123.8	590.1	1.84	737.3	1079.6	1.71	685.4	
6.8	52.9	468.6	0.33	130.3	600.1	1.83	731.8	1117.6	1.73	692.1	
8.0	54.3	459.0	0.32	126.2	596.2	1.79	717.9	1084.7	1.66	664.0	
8.9	55.7	474.3	0.32	128.6	623.8	1.85	740.2	1139.2	1.72	687.1	
9.6	57.5	473.4	0.31	126.0	615.7	1.79	717.8	1133.6	1.68	671.3	
10.5	58.6	456.8	0.30	121.4	607.9	1.77	706.7	1120.5	1.65	661.6	
11.2	59.6	470.8	0.31	124.3	619.2	1.79	716.0	1144.6	1.68	671.9	
11.8	60.8	455.6	0.30	120.3	614.8	1.77	708.6	1130.4	1.65	661.9	
12.4	62.2	483.3	0.32	126.2	631.0	1.81	722.5	1176.9	1.71	683.3	
13.0	63.4	472.6	0.31	123.5	610.7	1.75	700.8	1121.9	1.64	654.3	
13.4	64.6	472.8	0.31	123.2	609.6	1.74	697.8	1144.2	1.66	663.4	

Table C.4: Details about Long-Term alteration of SBNA4 glass powder in high surface area to volume ratio. Explanation of the column names and their units in table are: Time in $Day^{\frac{1}{2}}$; S/V - Surface area to volume ratio (cm^{-1}); C(Si) corr - Concentration of Si corrected (mg/l); NL(Si) - Normalized loss of Si (g/m^2); EE(Si) - Equivalent thickness of glass altered with respect to Si (nm); C(B) corr - Concentration of B corrected (mg/l); NL(B) - Normalized loss of B (g/m^2); EE(B) - Equivalent thickness of glass altered with respect to B (nm); C(Na) corr - Concentration of Na corrected (mg/l); NL(Na) - Normalized loss of Na (g/m^2); EE(Na) - Equivalent thickness of glass altered with respect to Na (nm);

Time	SA/V	C(Si)	NL(Si)	EE(Si)	C(B)	NL(B)	EE(B)	C(Na)	NL(Na)	EE(Na)	pH
0.0	46.7	0.0	0.00	0.0	0.0	0.00	0.0	0.0	0.00	0.0	9.12
1.3	46.8	394.8	0.30	119.5	539.7	1.79	714.9	1001.6	1.69	674.3	9.22
2.8	48.2	439.4	0.33	130.2	638.3	2.07	827.3	1180.9	1.95	778.0	9.23
4.0	49.7	469.2	0.34	136.1	644.0	2.05	818.0	1237.6	2.00	798.5	
5.4	50.5	456.9	0.33	131.9	625.9	1.98	791.5	1211.5	1.94	778.0	
6.8	51.9	470.7	0.33	133.4	664.6	2.06	824.0	1207.8	1.91	762.4	
8.0	52.9	446.7	0.32	126.3	653.8	2.02	807.1	1184.4	1.86	744.5	
8.9	54.2	484.3	0.34	134.8	670.7	2.04	817.8	1224.5	1.90	759.8	
9.6	55.2	527.0	0.36	145.3	697.6	2.11	845.5	1280.7	1.97	789.6	
10.5	56.1	499.5	0.34	137.8	676.2	2.05	818.4	1227.3	1.89	756.4	
11.2	57.1	511.2	0.35	139.9	683.2	2.05	821.4	1243.9	1.90	761.4	
11.8	58.0	525.0	0.36	143.0	690.3	2.07	827.4	1295.5	1.97	787.9	
12.4	59.0	500.8	0.34	136.5	662.1	1.99	794.0	1213.8	1.85	740.6	
13.0	59.9	509.7	0.35	138.4	677.2	2.02	808.2	1275.7	1.93	771.9	
13.4	61.1	491.8	0.33	133.6	658.2	1.96	785.3	1195.9	1.82	727.3	

Table C.5: Details about Long-Term alteration of SBNA4R glass powder in high surface area to volume ratio. Explanation of the column names and their units in table are: Time in $Day^{\frac{1}{2}}$; S/V - Surface area to volume ratio (cm^{-1}); C(Si) corr - Concentration of Si corrected (mg/l); NL(Si) - Normalized loss of Si (g/m^2); EE(Si) - Equivalent thickness of glass altered with respect to Si (nm); C(B) corr - Concentration of B corrected (mg/l); NL(B) - Normalized loss of B (g/m^2); EE(B) - Equivalent thickness of glass altered with respect to B (nm); C(Na) corr - Concentration of Na corrected (mg/l); NL(Na) - Normalized loss of Na (g/m^2); EE(Na) - Equivalent thickness of glass altered with respect to Na (nm);

Time	SA/V	C(Si)	NL(Si)	EE(Si)	C(B)	NL(B)	EE(B)	C(Na)	NL(Na)	EE(Na)	pH
0.0	52.2	0.0	0.00	0.0	0.0	0.00	0.0	0.0	0.00	0.0	9.12
1.3	52.2	440.3	0.31	124.7	645.0	1.79	714.1	1162.6	1.65	660.1	9.2
2.8	53.4	451.7	0.32	126.3	667.2	1.82	729.0	1190.7	1.67	667.2	9.24
4.0	54.9	481.5	0.33	132.1	691.3	1.85	741.6	1260.3	1.73	693.2	
5.4	56.2	447.6	0.30	121.5	658.4	1.75	698.5	1236.0	1.68	671.7	
6.8	57.7	493.9	0.33	131.5	699.5	1.82	728.9	1251.3	1.67	669.2	
8.0	59.0	483.8	0.32	127.7	675.9	1.75	698.6	1238.4	1.64	656.1	
8.9	154.4	701.7	0.19	75.1	1699.0	1.70	680.4	3239.2	1.66	663.2	
9.6	64.0	502.0	0.31	125.7	733.6	1.81	724.0	1314.2	1.67	666.8	
10.5	65.2	479.3	0.30	119.7	733.5	1.80	719.3	1327.6	1.67	668.6	
11.2	66.3	517.6	0.32	128.1	770.1	1.88	750.1	1400.6	1.75	700.2	
11.8	67.7	506.1	0.31	124.7	737.9	1.79	717.8	1344.6	1.68	671.2	
12.4	68.9	517.1	0.32	126.6	761.1	1.84	734.4	1382.0	1.71	684.6	
13.0	70.1	509.4	0.31	124.7	749.9	1.81	723.5	1332.9	1.66	662.4	
13.4	71.7	525.1	0.32	127.2	756.7	1.81	725.0	1368.5	1.68	673.4	

Table C.6: Details about Long-Term alteration of SBNA5 glass powder in high surface area to volume ratio. Explanation of the column names and their units in table are: Time in $Day^{\frac{1}{2}}$; S/V - Surface area to volume ratio (cm^{-1}); C(Si) corr - Concentration of Si corrected (mg/l); NL(Si) - Normalized loss of Si (g/m^2); EE(Si) - Equivalent thickness of glass altered with respect to Si (nm); C(B) corr - Concentration of B corrected (mg/l); NL(B) - Normalized loss of B (g/m^2); EE(B) - Equivalent thickness of glass altered with respect to B (nm); C(Na) corr - Concentration of Na corrected (mg/l); NL(Na) - Normalized loss of Na (g/m^2); EE(Na) - Equivalent thickness of glass altered with respect to Na (nm);

Time	SA/V	C(Si)	NL(Si)	EE(Si)	C(B)	NL(B)	EE(B)	C(Na)	NL(Na)	EE(Na)	pH
0.0	56.5	0.0	0.00	0.0	0.0	0.00	0.0	0.0	0.00	0.0	9.12
1.3	56.6	39.2	0.02	9.5	40.0	0.13	52.9	39.0	0.09	34.1	8.9
2.8	58.4	65.7	0.04	15.5	109.7	0.35	141.2	98.3	0.21	83.7	8.75
4.0	61.2	75.3	0.04	17.1	181.1	0.56	223.7	144.1	0.29	117.9	8.95
5.4	61.9	76.3	0.04	17.4	270.4	0.83	331.3	193.8	0.39	157.5	
6.8	63.9	85.1	0.05	18.9	401.1	1.20	478.7	281.4	0.56	222.7	
8.0	64.9	91.0	0.05	20.1	521.2	1.54	615.3	359.0	0.70	281.0	
8.9	66.1	93.5	0.05	20.5	614.4	1.79	716.9	431.7	0.83	333.7	
9.6	67.2	92.1	0.05	20.1	660.1	1.91	764.9	429.8	0.83	331.0	
10.5	68.4	89.1	0.05	19.5	679.7	1.96	783.3	459.2	0.88	350.9	
11.2	69.5	93.2	0.05	20.2	736.5	2.10	841.5	465.3	0.88	353.9	
11.8	71.1	95.0	0.05	20.4	769.4	2.17	869.5	504.8	0.95	378.7	
12.4	72.0	94.7	0.05	20.3	791.1	2.23	891.8	554.2	1.03	412.6	
13.0	73.3	97.4	0.05	20.8	839.7	2.34	937.9	564.1	1.04	417.6	
13.4	74.6	96.8	0.05	20.6	850.0	2.36	944.8	573.4	1.06	422.3	

Table C.7: Details about Long-Term alteration of SBNA6 glass powder in high surface area to volume ratio. Explanation of the column names and their units in table are: Time in $Day^{\frac{1}{2}}$*; S/V - Surface area to volume ratio* (cm^{-1})*; C(Si) corr - Concentration of Si corrected (mg/l); NL(Si) - Normalized loss of Si* (g/m^2)*; EE(Si) - Equivalent thickness of glass altered with respect to Si (nm); C(B) corr - Concentration of B corrected (mg/l); NL(B) - Normalized loss of B* (g/m^2)*; EE(B) - Equivalent thickness of glass altered with respect to B (nm); C(Na) corr - Concentration of Na corrected (mg/l); NL(Na) - Normalized loss of Na* (g/m^2)*; EE(Na) - Equivalent thickness of glass altered with respect to Na (nm);*

Appendix D

Supplementary Details: Behavior of B in passivating gels formed on International Simple Glass in acid and basic pH

D.1 Supplementary methods

D.1.1 Extraction of the concentrations of ^{10}B in the gel from the raw ToF-SIMS data

Using the experimental conditions described in 2.5.2, gel were prepared in Si-saturated solution at 90°C then placed in a tracing solution containing 1000 ppm of ^{10}B for different contact time. ^{10}B entered into the gel for different contacting time was calculated using the 1 min contact time in tracing solution as a reference. For that, we assumed that no ^{10}B have entered into the gel from the solution in the 1 min contact time experiment. It is a reasonable assumption, according to the ^{10}B/^{11}B isotopic ratio recorded in this gel.

B is indicated as B_g and B_s to represent the B from the glass and solution, respectively. As usual, B isotopes are noted as ^{10}B and ^{11}B. * is used to indicate the multiplication in all the following equations.

$$RB = \frac{Raw\ intensity\ of\ ^{10}B}{Raw\ intensity\ of\ ^{11}B} \tag{D.1}$$

$$M = \frac{Mean\ intensity\ of\ ^{10}B\ in\ pristine\ glass}{Mean\ intensity\ of\ ^{11}B\ in\ pristine\ glass} \tag{D.2}$$

The abrupt transitions in the Na^+ profiles are used to determine the depth at which the gel ends and the pristine glass starts. The measured $^{10}B/^{11}B$ ratio, M, in the pristine glass was calculated using the average intensity for ^{10}B and ^{11}B in the glass region. There is a slight difference between the natural isotopic ratio (NIR) that is expected in the pristine glass and the measured ratio. We applied a correction to the measured data so that it fits the natural isotopic ratio of 0.205. The ratio of raw measured $^{10}B/^{11}B$ is called RB and the corrected $^{10}B/^{11}B$ ratio is called $C\frac{^{10}B}{^{11}B}$:

$$C\frac{^{10}B}{^{11}B} = RB(1 - \frac{M - NIR}{NIR}) \tag{D.3}$$

$$B_g = \frac{Mean\ normalized\ ^{11}B\ *\ Wt\%\ composition\ of\ B\ in\ glass}{Molar\ mass\ of\ B}\ *\ N_A \tag{D.4}$$

B_g is the amount of B coming from the glass, present in 100 grams of gel. In equation D.4, Wt% of B in ISG is 5.366, molar mass of B is 10.811 and NA is Avogadro number, 6.023x10^{23}. 1 min contacting time in tracing solution is used to calculate the B_g assuming that no ^{10}B entered into the gel from solution.

$$Volume\ (nm^3) = \frac{100\ g}{density\ of\ gel\ (\frac{g}{cm^3})}\ *\ 10^{21} \tag{D.5}$$

The volume (nm^3) of 100 grams of gel with a known density of 2.1 $\frac{g}{cm^3}$ is calculated. Since B_g represents the amount of B in 100 g of gel, dividing it with volume of 100 g of gel in (nm^3) provides the number of $\frac{B_g}{nm^3}$ for the two isotopes. These isotopes come from the glass.

$$^{10}B_g = \frac{B_g\ *\ 0.2}{Volume\ (nm^3)} \tag{D.6}$$

$$^{11}B_g = \frac{B_g\ *\ 0.8}{Volume\ (nm^3)} \tag{D.7}$$

Where 0.2 and 0.8 is the fraction of ^{10}B and ^{11}B in B_g, respectively.

Comparison between ToF-SIMS data for 1 min contact time with other contact time (OCT) is not possible without correction since there could be a slight difference in gel thickness between them. Moreover, the ToF-SIMS profiles are not provided with the same depth interval. To solve these issues, we normalized the gel thickness of OCT according to the 1 min ToF-SIMS profile and then interpolated the y-axis data of OCT according to the depth from 1 min. The normalized corrected $\frac{^{10}B}{^{11}B}$ ratio is called CNB.

As an experimental value, CNB takes into account the B from the solution and from the glass. Boron coming from the solution is noted as B_s. We used a tracing solution where the ratio $\frac{^{10}B}{^{11}B} = 99$.

$$CNB = \frac{^{10}B_s \ + \ ^{10}B_g}{^{11}B_s \ + \ ^{11}B_g} = \frac{^{10}B_s \ + \ ^{10}B_g}{\frac{^{10}B_s}{99} \ + \ ^{11}B_g} \tag{D.8}$$

$$^{10}B_s = \frac{99 \ * \ ^{10}B_g - (CNB \ * \ ^{11}B_g \ * \ 99)}{CNB \ - \ 99} \tag{D.9}$$

$$^{11}B_s = \frac{^{10}B_s}{99} \tag{D.10}$$

$^{10}B_s$ and $^{11}B_s$ are the amount of ^{10}B and ^{11}B entered into the gel from the tracing solution at a given contact time with reference to the 1 min contact time in tracing solution, respectively.

D.1.2 Calculation of the elemental composition from the ToF-SIMS results to compare with XPS values

To compare the elemental composition of gel obtained from ToF-SIMS with XPS, first element wise total number of atoms present in the 100 gram of gel are calculated from the ToF-SIMS intensity.

$$Num.\ of.\ X = N_A \ * \frac{Mean\ normalized\ intensity\ for\ X \ * \ wt\%\ of\ X\ in\ the\ glass}{M_X} \tag{D.11}$$

Where X is the element type (B, Na, Ca, Al, Zr, Si, Ca, O), and Num. of. X is element wise total number of atoms present in 100 gram of gel. M_X is the molar mass of the particular element, wt% of X in the glass is the concentration of X in glass in wt%, N_A is Avogadro number, 6.023 * 10^{23}.

$$Volume\ (nm^3) = \frac{100\ g}{density\ of\ gel\ (\frac{g}{cm^3})} \ * \ 10^{21} \tag{D.12}$$

The volume (nm^3) occupied by 100 grams of gel is calculated from Eqn. D.5. The number of X atom per nm^3 of gel is given by

$$X\ atom = \frac{Num.\ of.\ X}{Volume\ (nm)^3} \tag{D.13}$$

Gel composition is then obtained by normalization

$$X\ (\%) = \frac{Xatom}{\Sigma Xatom}\ *\ 100 \tag{D.14}$$

Where ΣX atom is summation of total number of atoms for all the elements in the gel.

D.1.3 Calculation for element normalization of ToF-SIMS profile

$$Mean\ Normalized = \frac{T_i}{MT_i} \tag{D.15}$$

Where T_i is the depth wise ToF-SIMS intensity of i element, MT_i is average ToF-SIMS intensity of element i in the pristine glass region.

$$Normalized\ with\ respect\ to\ Si = \frac{MN_i}{MN_{Si}} \tag{D.16}$$

Where MN_i is the depth wise Mean Normalized ToF-SIMS data of i element, MN_{Si} is the depth wise Mean Normalized ToF-SIMS data of Si.

D.2 Supplementary Figures

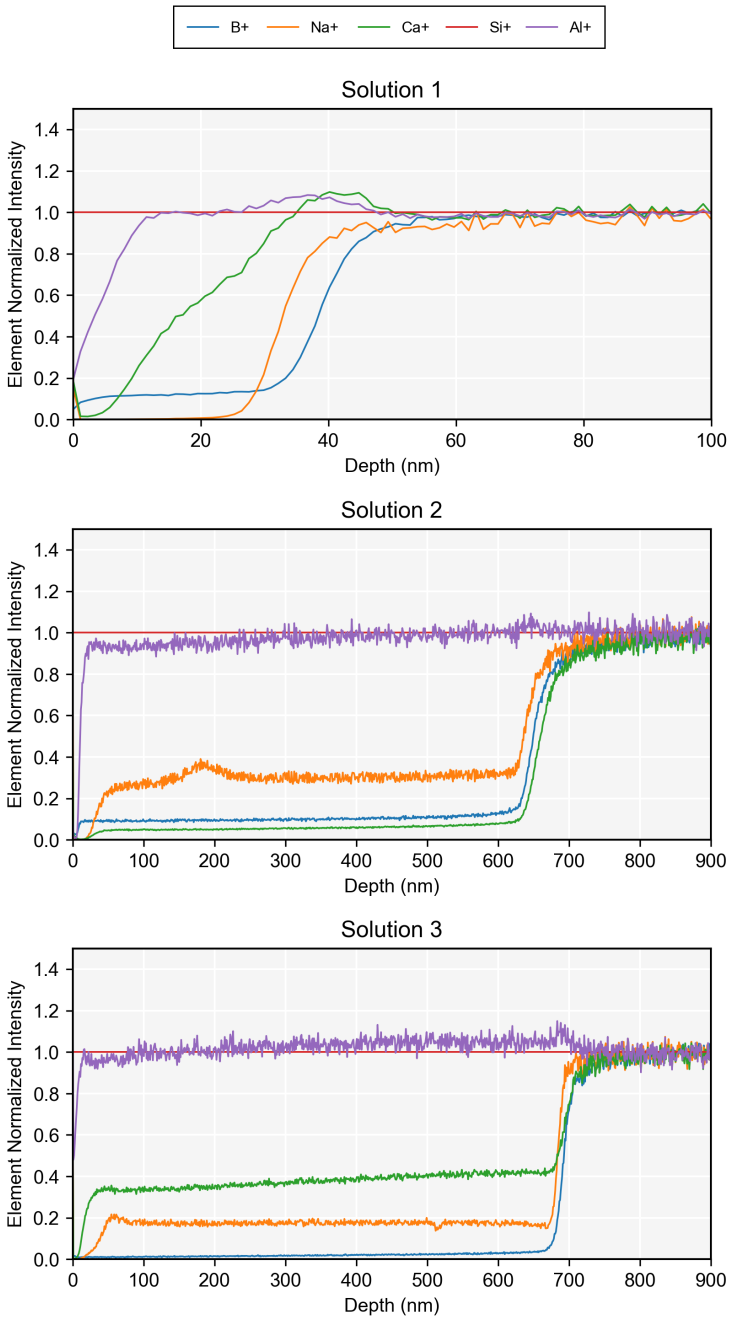

Figure D.1: ToF-SIMS analysis (positive mode) of ISG coupon altered for 21 days in pH7 90°C in three solutions: (A) Sol 1: Saturated with B, Ca, Na, Si; (B) Sol 2: Saturated with B, Na, Si; (C) Sol 3: Saturated with Ca, Na, and Si; Common for all three plots: All the elements are normalized with respect to the Si profile to eliminate the matrix dependency on other elements. Color scheme to represent each elements are consistently same on all three plots and its details are given at the top of Sol 1.

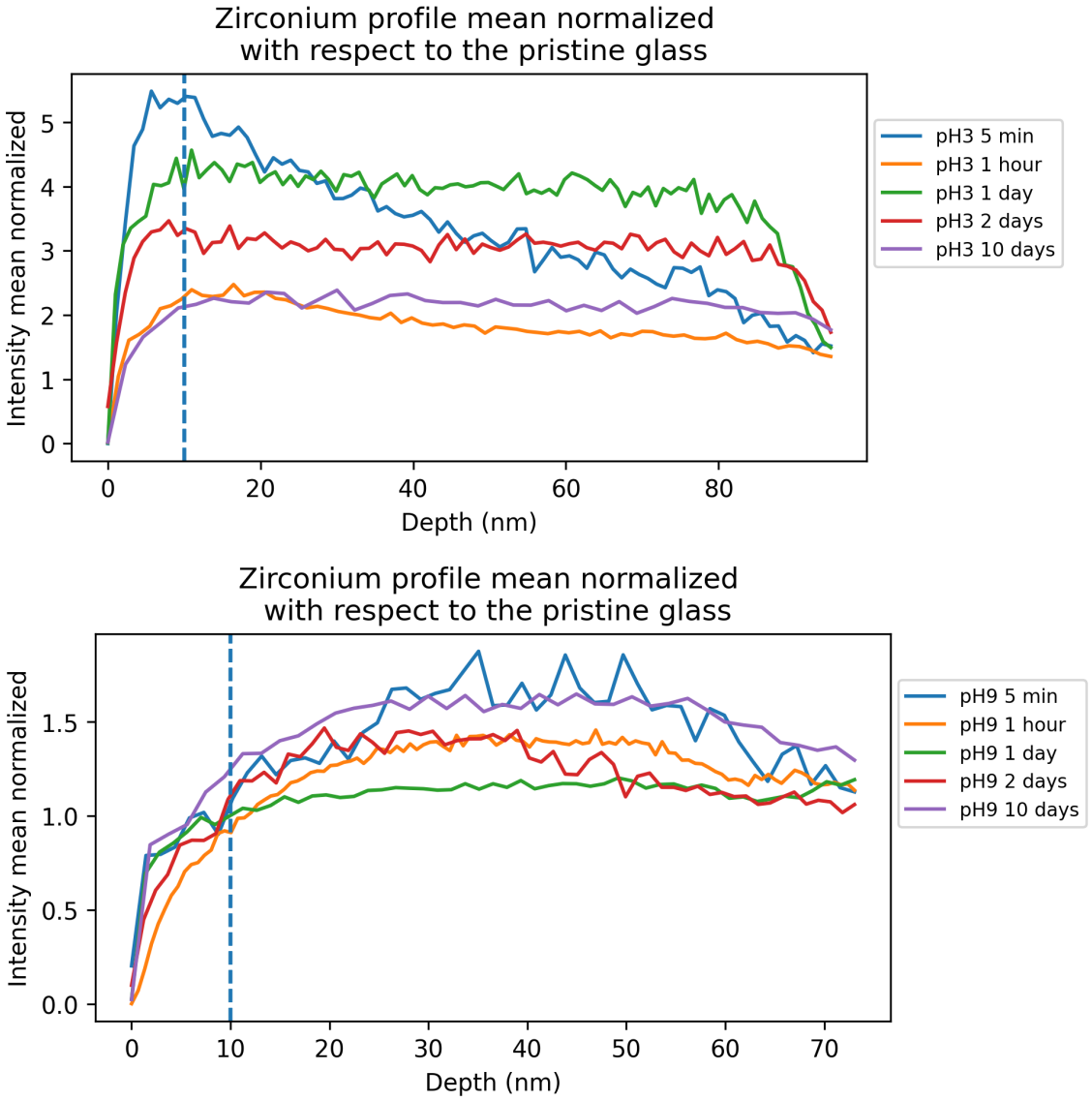

Figure D.2: ToF-SIMS Zr profile for ISG coupons altered in pH 3 (top) and pH 9 (bottom) and incubated for different contact time in the ^{10}B tracing solution. Gel starting region for both pH 3 and pH 9 are indicated with a vertical blue dotted line.

Appendix E

Details about scripts used in this thesis

All the python, fortran and shell scripts used during the thesis are available in the following Github link:

https://github.com/kamalesh-d/PhD-thesis

E.1 Scripts corresponding to the PMF work

Directory navigation: 1_pmf_calculations/pure_silicate
Filename: *automatic_glass_preparation.py*
This python file is pipeline, which will have multiple options to select for achieving the task. The chosen option has to be given in the "type_of_run" of this file. All the available options in the pipeline and its usage are follows:

Please note, whole pipeline is constructed to perform the MD simulations with DLpoly software package in ceres server. Need to modify the shell scripting, if interested to run in anyother server. All these following options are to be chosen at "type_of_run" in python file "automatic_glass_preparation.py". Below "type_of_run" in the same python file, there is an option "number_of_glasses_to_make", simply defining the number will perform all the following analysis for these many times.

1. glass_preparation - Set the glass composition in the FIELD file, and "config_aleatoire.f" fortran file present in the same folder. Then, choosing this "glass_preparation" as "type_of_run" will handle the (i) placing atoms randomly in simulation box, (ii) Starting the simulation at high temperature, (iii) Annealing to prepare the glass (iv) Relaxation with NVT, NPT and NVE ensemble to finally obtain the glass structure.

2. double_the_box - After preparing this glass, choosing this option will double the box along the z-axis, and relax the glass structure with NVT and NVE ensemble.

3. water_simulation - Choosing this option will prepare the same box size of (double_the_box) and relax the system with NVE and NVT ensembles.

4. add_glass_with_water - This option will combine the structure file of water and glass, and removes the water molecules in the glass region.

5. relax_glass_water - This option will relax the system containing Glass and Water with NVT and NVE ensembles. This will prepare the interface between them and also the potential is dissociative, some of the Si-O-Si bonds close to the water molecules will be broken during this run.

6. run_pmf - Choosing this option will automatically calculate the water molecules close in contact with glass < 3.5 Å distance. Then PMF will be performed between these selected water molecules against their target Si-O-Si bond.

7. result_analysis - This will option will try to compile the glass structure files and all other important results required to process for analysis.

8. aluminum_run_pmf - This option will compile all the scripts required to perform the PMF calculations for aluminosilicate glass. This is treated seperately because it needs to investigate Al and Si seperately in this case.

9. neural_network_input_preparation - Running this option will prepare a tab seperated txt file for each glass, which will contain all the glass structural features against their activation energy. This file will serve directly as an input to train the AI model for predicting the activation energy from glass structure.

10. neural_network_input_compiled - Previous option will generate a tab seperated txt file individiually for each glasses. This option will compile all those files and give their final output inside the folder "1_pmf_calculations/pure_silicate/6_analysis/bond_dissociation", and the filename is "neural_network_data_compiled".

E.2 Scripts corresponding to AI models predicting Activation Energy

Directory navigation:
2_artificial_intelligence_models/multiple_water_molecule_vs_activation_energy
Filename: *all_water_pure_silicate_glass.ipynb*
Jupyter notebook file with Random forest regression trained model. During simulation, multiple water molecules will present. 1 water molecule will be approached to attack the target Si, whose activation energy is used as training data.

Directory navigation:
2_artificial_intelligence_models/1_water_molecule_vs_activation_energy
Filename: *1_water_pure_silicate_glass.ipynb*
Jupyter notebook file with Random forest regression trained model. During simulation, single water molecule will present. That water molecule will be approached to attack the target Si, whose activation energy is used as training data. This is to eliminate influence of any other water molecule's presence.

Directory navigation:
2_artificial_intelligence_models/1_water_vs_all_water_comparison
Filename: *1_water_vs_all_water.ipynb*
Jupyter notebook file will involve in comparing the structural features of glass and activation energy for 1 water molecule simulation and multiple water molecule simulation.

E.3 Scripts corresponding to ToF-SIMS

Directory navigation: 4_ToF-SIMS_library
Filename: *Tof-SIMS_4.ipynb*
This jupyter notebook file is a library to process the ToF-SIMS data, even for a person without knowledge in python. User has multiple choices to set the options to process the ToF-SIMS data, and the script can process N number of ToF-SIMS file exactly in the same way in few seconds. Step-by-step instructions to use the jupyter notebook are guided in the Jupyter notebook file. All the features of this library are given below:

1. User has choice to define the list of elements to be investigated.
2. Possible analysis are: Raw point-to-point data visualization, Mean normalization with respect to the pristine glass, Zirconium or any element-based normalization. (Mean normalization and Zirconium normalization formula can be found in the article https://doi.org/10.1016/j.jnoncrysol.2022.121938).
3. Calculate the isotopic ratio for any elements of your choice. Optional to adjust the Tof-sims isotopic ratio with respect to the natural abundance.
4. User can define certain data to be displayed in the primary y-axis and remaining in the secondary y-axis. (For better display of data in the graph).
5. Most common customizations of the visualized data. (Like theme color, Grid properties, limits of the y-axis, line style, title, labeling etc). Publication quality images can be generated instantly.

6. If you are not satisfied with the available customization of the plot, It has an option to automatically export the processed data in csv format. From there, you can visualize directly with origin. (No need to do maths to process the mean normalization or element normalization or isotopic ratio).

7. The script also allows the data to be visualized in the interactive mode in the jupyter notebook. (You can directly move, play, zoom-in/out, display/hide some elements of your choice, etc). An example interactive visualization is given in the html format at "4_ToF-SIMS_library/Tof-SIMS.html".

8. Finally, after setting all the above parameters, I have a pilot mode, keeping this 'on' will automatically process all the tof-sims files in that particular directory, exactly with all the outputs you have requested from the script. (For example, 10 tof-sims files can be processed to get 10 plots in figure, with data in 10 different csv files etc).

All the above features can work independently, so user can customize the options to fit almost any project of their interest. The idea is to avoid spending time doing basic things, and focus really on what matters (Interpreting the sims data).